Synthesis of Well-Defined Star-Shaped and Multicyclic Block Copolyethers via *t*-Bu-P_4-Catalyzed Ring-Opening Polymerization of Glycidyl Ethers

A Dissertation for the Degree of Doctor of Philosophy

Yusuke Satoh

Hokkaido University

March, 2017

Table of Contents

Chapter 1

General Introduction

1.1 Macromolecular Architectures

1.1.1 Introduction of Macromolecular Architectures

Synthetic polymers exhibit a variety of physical and chemical properties depending on their chemical structures involving the main chain structure, side chain structure, tacticity, and molecular weight. In addition to such classical structural characteristics, macromolecular architectures have also been recognized as an important characteristic that affects the polymer properties. For example, star-shaped polymers show a lower glass transition temperature (T_g) value compared to that of the linear counterpart due to enhanced chain mobility originating from the branched main chain and chain ends.[1] In contrast, cyclic polymers show a higher T_g value than the linear counterpart due to the restricted chain mobility originating from the absence of chain ends.[2,3] Interestingly, both star-shaped and cyclic polymers show a lower intrinsic viscosity than that of the linear counterpart because of their reduced hydrodynamic volume.[1] In recent years, many types of polymers possessing nonlinear architectures, such as star-shaped, brush, cyclic, figure-eight-shaped, sun-shaped, and dendrimer-like star-branched polymers, have been reported with the development of a living polymerization system as well as highly efficient coupling reactions, which enabled researchers to investigate the relationship between the polymer properties and macromolecular architectures (**Figure 1-1**).[4–15] Such structure-property relationship studies should be of fundamental importance to provide novel guidelines for the creation of high

value-added polymeric materials with unprecedented performances that are unachievable by the linear polymers. Despite the significant efforts, the preparation of a series of macromolecular architectures with a fixed chemical composition, molecular weight, and dispersity still remains a challenging task, which limits the systematic investigation of the relationship between the macromolecular architectures and polymer properties. In particular, the structure-property relationship study for a block copolymer system is in the exploration stage simply due to the lack of a synthetic methodology for the block copolymers with various achitectures. Therefore, continuing efforts to develop precise synthetic methodologies for a series of architectural polymers with a well-controlled molecular weight and narrow dispersity is necessary to fully understand the essential effect of the macromolecular architectures on the polymer properties. Such a study is one of the central subjects in the field of current polymer chemistry. In this section, the general synthetic routes for the nonlinear homopolymers, i.e., star-shaped and cyclic homopolymers, will be reviewed. The current status of the research regarding the star-shaped and cyclic block copolymers will then be reviewed to clarify the remaining tasks to be addressed for the sustainable development of this research field.

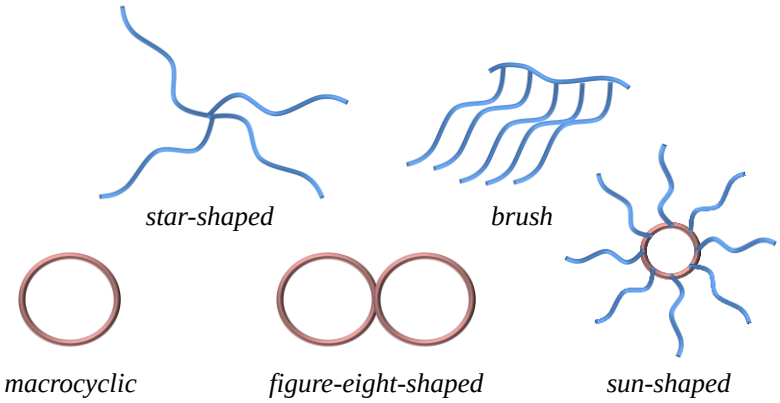

Figure 1-1. Schematic representation of macromolecular architectures.

1.1.2 Synthesis of Star-shaped Polymers

Star-shaped polymers are well-known to exhibit unique properties, like a lower T_g and viscosity than the linear counterpart due to their smaller hydrodynamic volume, and have received increased attention because their properties can be easily varied by changing the number of arms. The well-defined star-shaped polymers have been generally synthesized by two synthetic methods; (i) core-first method and (ii) coupling-onto method. The core-first method utilizes the polymerization of monomers using a core with a well-defined number of initiating sites.[16–20] For example, Matyjaszewski et al. demonstrated the synthesis of three and four-armed star-shaped polyacrylates by atom transfer radical polymerization (ATRP) using multifunctional core initiators (**Scheme 1-1a**).[21] Kim et al. synthesized three- and four-armed star-shaped polyethers by the anionic ring-opening polymerization of an epoxide using the pentaerythritol initiator.[22] On the other hand, the coupling-onto method utilizes the

coupling reactions of living or end-functionalized linear precursor polymers with a multifunctional coupling core.[23–26] For example, Ritchie et al. synthesized the four-armed star-shaped PEO, in which the hydroxyl-terminated PEO arms reacted with pentaerythritol tetrabromide (**Scheme 1-1b**).[15] The click coupling between the azido end-functionalized arm and multifunctional alkyne-containing agent was applied to the synthesis of various star-shaped polymers such as polystyrene.[27]

Scheme 1-1. Synthesis of star-shaped polymers by (a) core-first method and (b) coupling-onto method

(a) Core-first method

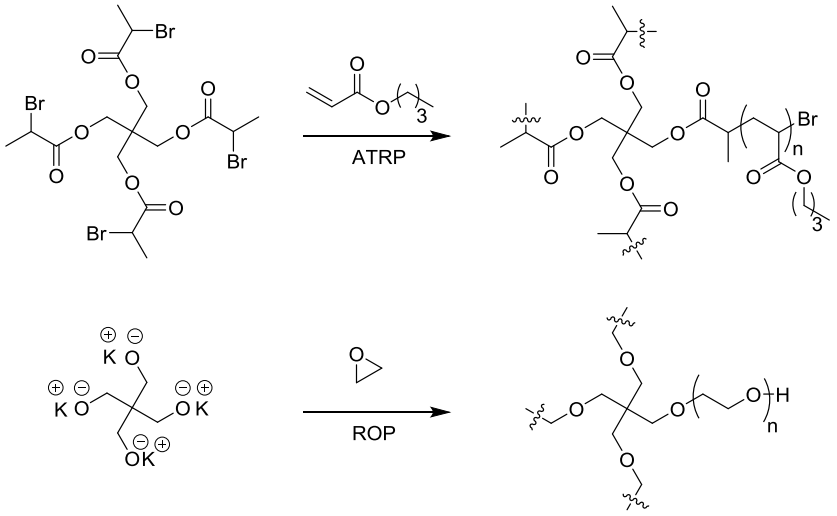

(b) Coupling-onto method

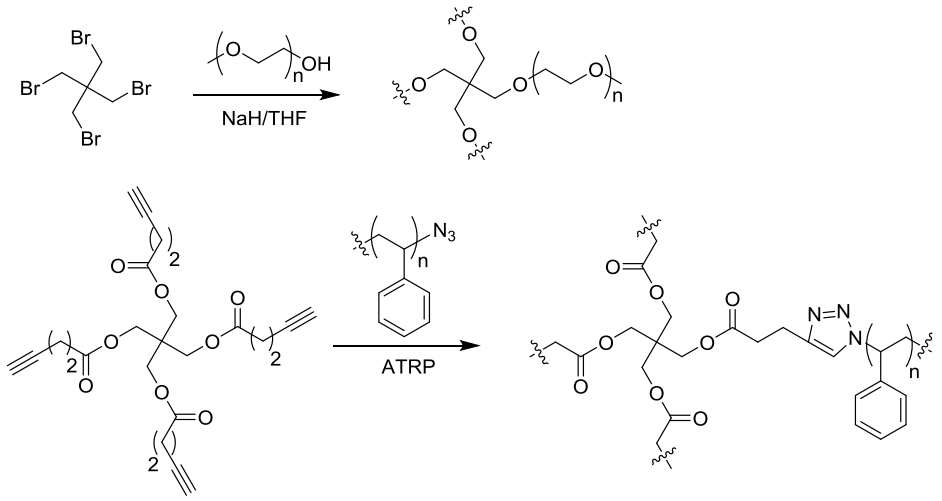

A huge number of synthetic studies for the star-shaped polymers has been performed based on the above-described methodologies, some of which served as the model polymer system for studying the effect of the branched architectures on the polymer properties and functions. However, in many cases of the core-first method, the synthesis of the appropriate

multifunctional initiators is required depending on the polymerization methods, and the homogeneous growth of each arm cannot be assured. In contrast, the coupling-onto method promises a uniform length of each arm in the resultant star-shaped polymer, though several steps are required to prepare the linear precursors and to remove the remaining linear precursors. Thus, the precise synthesis and characterization of well-defined star-shaped polymers still remains a challenging task.

1.1.3 Synthesis of Cyclic Polymers

Cyclic polymers are also gaining significant attention for their unique properties originating from the absence of the chain end. Several synthetic approaches for cyclic polymers have already been developed, which led to finding unprecedented physical and chemical properties of the cyclic polymers. In general, the synthetic approaches for cyclic polymers are classified into two types, i.e., “ring-expansion polymerization” and “ring-closure reaction”.

The “ring-expansion polymerization”provides cyclic polymers in one-pot, which involves the polymerization using a catalyst or initiator featuring a cyclic structure with an active bond for monomer insertion. For example, Grubbs et al. reported the synthesis of macrocyclic polyethylene by the ring-expansion metathesis polymerization of cyclooctene

using cyclic ruthenium complex catalysts (**Scheme 1-2a**).[28] Lee et al. synthesized macrocyclic polyesters using the cyclic tin oxide as an initiator (**Scheme 1-2b**).[29] Most recently, a novel organometallic catalyst was reported for synthesizing the conjugated cyclic polyacetylene having a high-purity and high molecular weight.[30] Although the ring-expansion polymerization approach allows the simple and easy synthesis of various cyclic polymers, tailor-made cyclic initiators or catalysts are required for the desired polymers. Furthermore, this methodology sometimes suffers from difficulties in controlling the molecular weight and removing the active species embedded in the cyclic polymer main chain.[31, 32]

Scheme 1-2. Synthesis of cyclic polymers by (a) ring-expansion metathesis polymerization, and (b) ring-expansion polymerization of cyclic esters using the cyclic tin oxide as an initiator

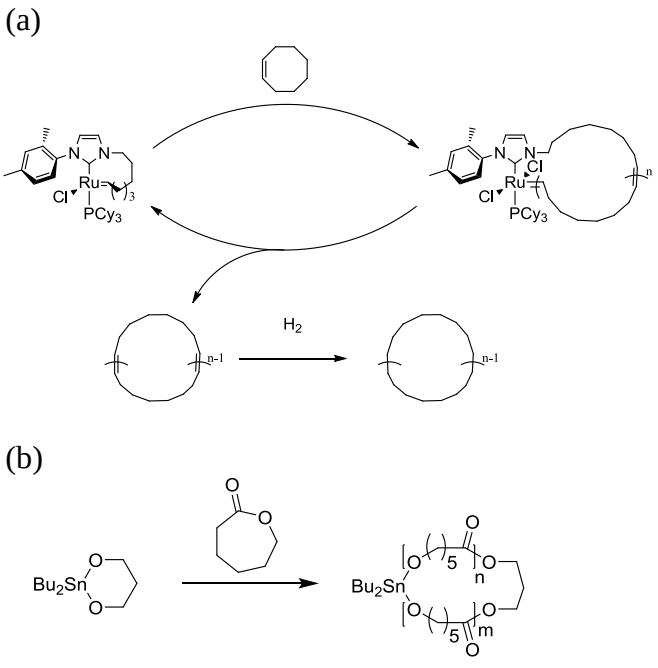

The "ring-closure reaction" has been recognized as the general route for the synthesis of cyclic polymers, which can be further classified into two types, i.e., "intramolecular cyclization" and "intermolecular cyclization". The intramolecular cyclization is based on the coupling reaction between complementary reactive functional groups at the α- and ω-chain ends.[33–39] For example, Deffieux et al. synthesized the cyclic poly(chloroethyl vinyl ether) using the heterodifunctional cyclization between the iodo and styrenic end groups.[40] Huang et al. also reported the synthesis of macrocyclic poly(ethylene oxide) (PEO) using the Glaser coupling of the α,ω-end ethynyl functionalized precursor (**Scheme 1-3a**).[41] For the cyclization reaction, the end groups of the linear precursor are required to be highly reactive in a selective manner.

The click reaction is well-known as an excellent reaction due to the qualitative yields and high selectivities.[42] In particular, the copper-catalyzed azido-ethynyl cycloaddition (CuAAC) is a typical click reaction.[43–45] Grayson et al. synthesized the macrocyclic polystyrenes (PSs) by intramolecular cyclization of the α-ethynyl-ω-azido end-functionalized linear PS based on the CuAAC (**Scheme 1-3b**).[9, 34] Pan et al. reported the synthesis of the figure-eight-shaped polystyrene via the CuAAC of the linear PS possessing two ethynyl groups at the chain center and two azido groups at the ω-ends (**Scheme 1-3c**).[46] In addition to this, many scientists have achieved the synthesis of cyclic polymers via the CuAAC.

Scheme 1-3. Synthesis of cyclic polymers by (a) Glaser coupling of linear precursor, and (b) intramolecular click cyclization of telechelic polystyrene

(a)

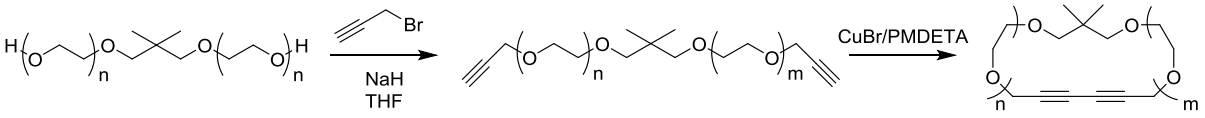

(b)

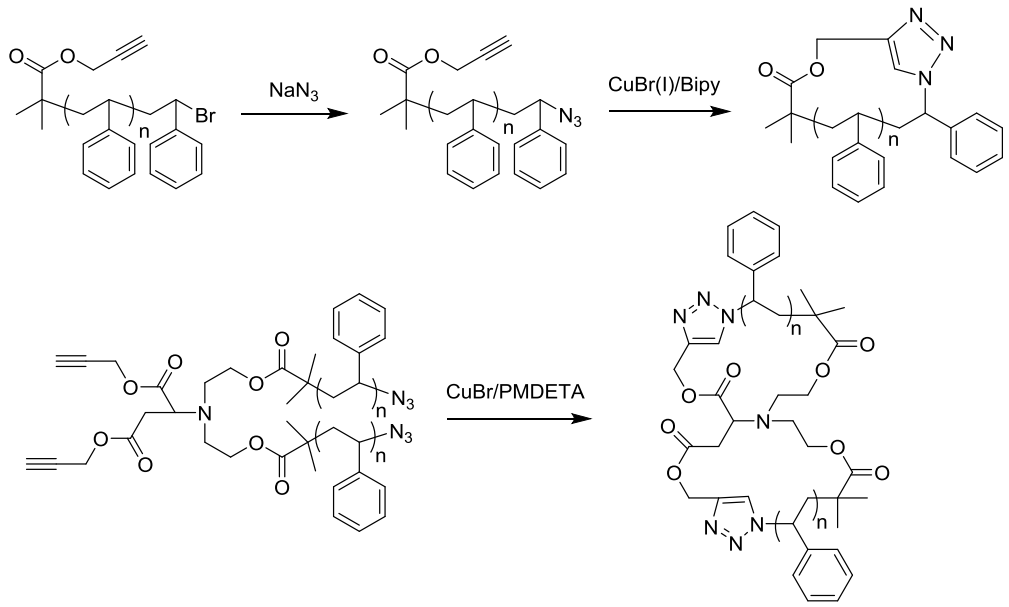

On the other hand, the intermolecular cyclization approach by a reaction between an end-functionalized polymer and a coupling agent was reported.[39, 47, 48] Tezuka et al. established a new synthetic method based on the "electrostatic self-assembly and covalent fixation (ESA-CF) process" using the telechelic polymer having a cyclic ammonium salt at the chain ends and the dicarboxylate linker (**Scheme 1-4a**).[49–51] This method enabled the synthesis of not only macrocyclic polymers, but also figure-eight-shaped, tadpole-shaped, theta-shaped, and more complex cyclic polymers. The CuAAC was also used for the

intermolecular cyclization approach to obtain complex cyclic polymers. Paik et al. achieved the synthesis of the figure-eight-shaped and the 4-armed cage-shaped PS via the click coupling of the ω-azido functionalized star-shaped PS and the ethynyl-functionalized linkers (**Scheme 1-4b**).[52]

Scheme 1-4. Synthesis of (a) the figure-eight shaped polytetrahydrofuran prepared by ESA-CF method, and (b) the figure-eight-shaped and the 4-armed cage-shaped polystyrenes via the click coupling

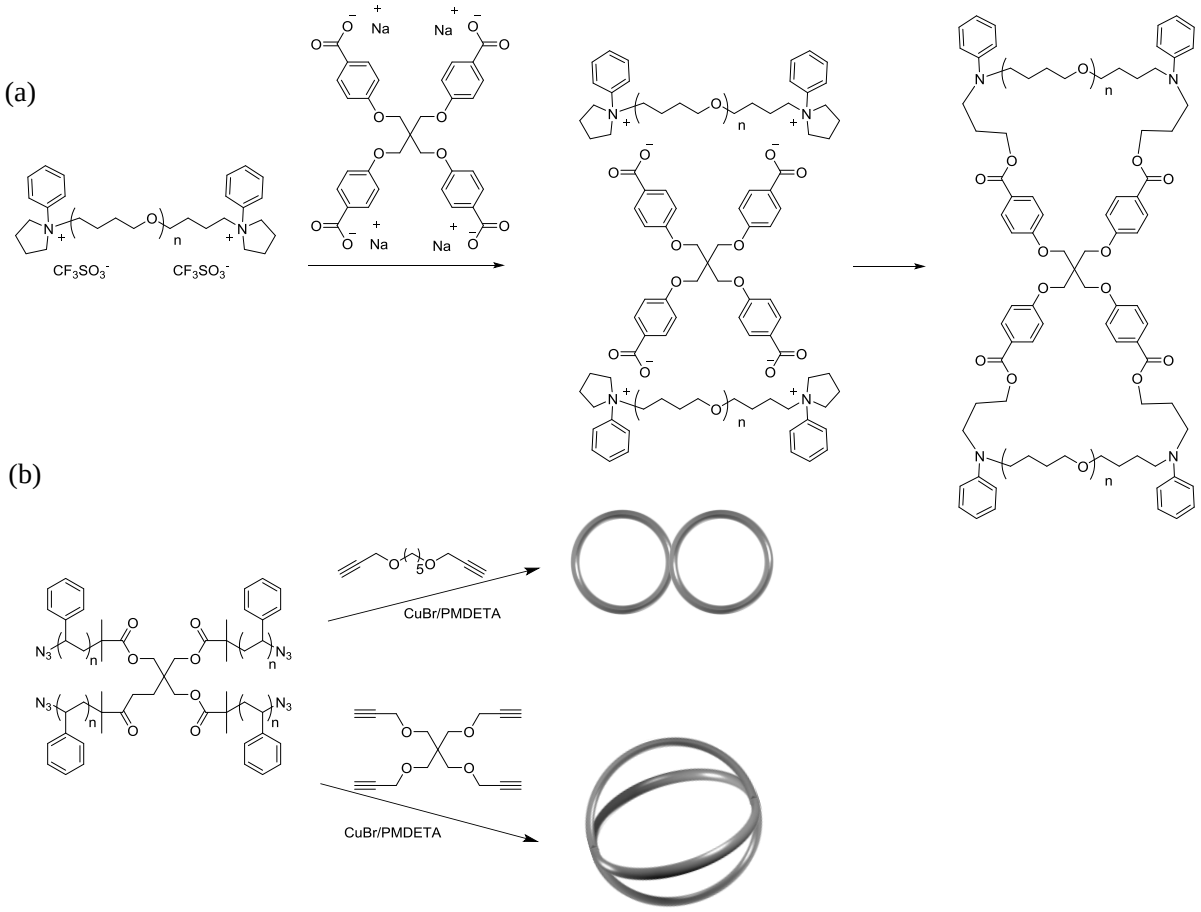

As already described, the ring-closure reaction is one of the successful methodologies to prepare many types of cyclic polymers. Among them, the CuAAC (click

cyclization) is particularly useful because the azido and ethynyl end-functionalized linear precursors can be easily prepared through controlled/living polymerizations. Despite the remarkable progress in the synthetic strategies for cyclic polymers, previous reports about the cyclic polymers had mainly focused on the vinyl polymer system. In addition, the preparation of a complehensive set of nonlinear polymers, including star, cyclic, multicyclic, and cages-shaped polymers, had never been achieved, in spite of its fundamental importance to fully understand the correlation between the macromolecular architecture and polymer properties/functions. Thus, a challenge still exists in developing novel synthetic strategies for a series of well-defined cyclic polymers which can be used as the model system for the structure-property relationship study.

1.2 Macromolecular Architectures in Block Copolymer System

1.2.1 Synthesis of Block Copolymers

Block copolymers consisting of more than two different polymer segments (or blocks) have attracted considerable attention as advanced functional materials because they exhibit chemical and physical properties different from their constitutional blocks. The most important characteristic of block copolymers is their self-assembly properties, such as microphase-separation and micellization.[53–56] For example, PS-*block*-poly(methyl methacrylate) (PS-*b*-PMMA) is well-known to show microphase separated structures.[57–59] PEO-containing block copolymers, such as PS-*b*-PEO,[60,61] PEO-*block*-poly(*ε*-caprolactone) (PEO-*b*-PCL),[62–64] and PEO-*block*-polyethylene (PEO-*b*-PE),[65–67] have also been used as the model system for the self-assembly study.

In general, block copolymers are synthesized by three strategies; (i) single-mode polymerization (sequential addition of monomers), (ii) coupling of complementary reactive functional polymers, and (iii) use of a dual initiator consisting of two distinct initiating sites (**Figure 1-2**). These methods basically require the controlled/living polymerization techniques, such as living radical polymerization (ATRP[68] and reversible additional-fragmentation[69]), ring-opening polymerization (ROP),[70, 71] ring-opening metathesis polymerization,[72, 73] and chain-growth polycondensation.[74, 75]

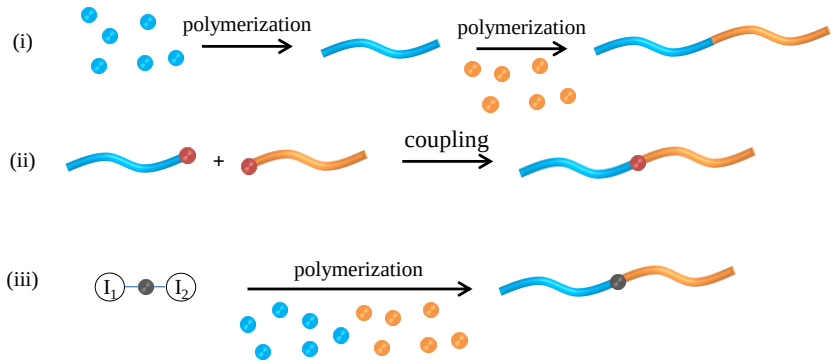

Figure 1-2. Schematic representation for synthetic method of block copolymer

Among the many types of block copolymers, amphiphilic block copolymers consisting of hydrophobic and hydrophilic segments are of significant interest because of their ability to self-assemble into ordered nanostructures in both the bulk and aqueous solution (**Figure 1-3**). In addition, the resultant self-assembled structures can be controlled by changing the molecular weights and hydrophilic/hydrophobic ratio of the block copolymer.[76] Therefore, the synthesis and characterization of various amphiphilic block copolymers are still an active area of research, which would provide useful information for designing drug delivery carriers,[77, 78] nanoreactors,[79] nanoporous materials, and nanoparticles.[80–82]

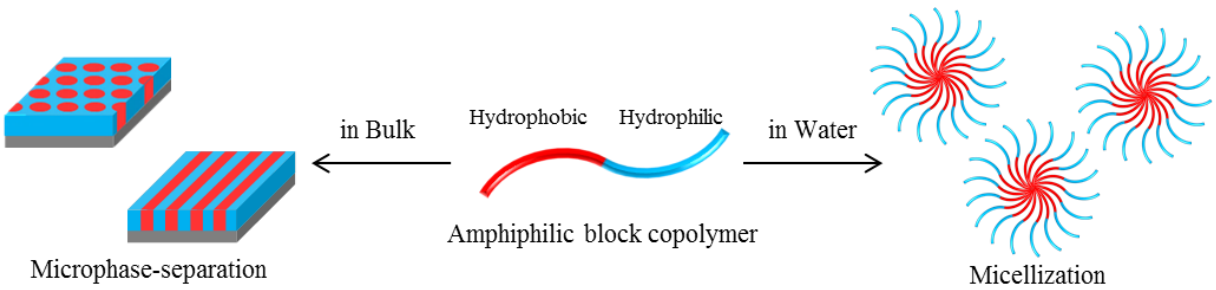

Figure 1-3. The self-assembled structures obtained from the amphiphilic block copolymer

1.2.2 Synthesis and Characteristics of Star-shaped Block Copolymers

The self-assembly behaviors of a block copolymer is basically determined by the molecular weight and volume fraction of each block. In addition, the macromolecular architectures and block arrangements also affect the self-assembly behavior of the amphiphilic block copolymers.[76] In this context, star-shaped block copolymers have received attention for a long time because their architecture can be easily varied by changing the number and length of their branching arms. Therefore, various star-shaped block copolymers, such as the star-block $(AB)_n$ and miktoarm A_nB_m types, as shown in **Figure 1-4**, have been attractive synthetic targets, some of which were employed to investigate the effect of the star-shaped architecture on the self-assembly behavior.[83–86]

The star-block copolymers are mainly synthesized by the core-first method. For example, Kim et al. synthesized the PEO-*b*-poly(L-lactide) and PEO-*b*-PCL amphiphilic star-block copolymers with varied arm numbers by the living ROP (**Scheme 1-5**).[87] Gnanou et al. achieved the synthesis of PEO-*b*-PS star-block copolymers via the ATRP of styrene using the star-shaped PEO as the macroinitiators (**Scheme 1-5**).[88] These synthetic studies provided new knowledge about the differences in the self-assembly behavior between the star-block copolymers and the corresponding *AB*- or *ABA*-type linear counterparts.[89, 90]

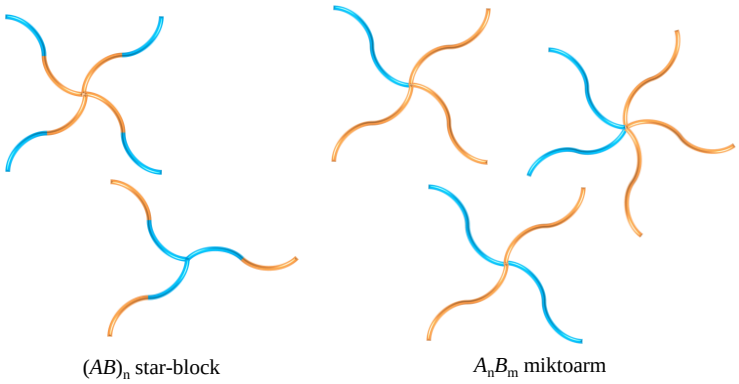

Figure 1-4. Schematic representation for $(AB)_n$ star-block and A_nB_m miktoarm types star-shaped block copolymers.

Scheme 1-5. Synthetic approaches for $(AB)_n$ star-block copolymers

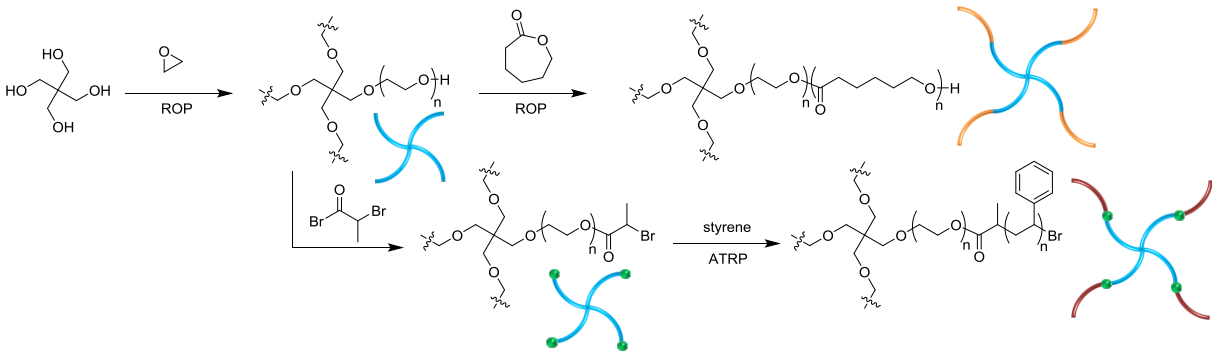

The miktoarm star polymers are synthesized by the combination of the core-first and coupling onto method. For example, two approaches were developed to synthesize A_2B or *ABC* miktoarm star polymers as shown in **Scheme 1-6**; one is the core-first method using specially-designed multifunctional initiators,[91–93] and the other one is the coupling between two or three types of functional polymers.[25, 94–96] Based on these approaches, several studies achieved the synthesis of a comprehensive set of amphiphilic miktoarm star polymers with comparable arm numbers and predicted molecular weights to investigate the effect of the branched architectures on the self-assembly behavior. For example, Faust et al. revealed that

the micellar properties, such as the critical micelle concentration (CMC) and the hydrodynamic radius (R_h) of micelles, were different among the *AB*-, A_2B-, and A_2B-type miktoarm star polymers.[97] Isono et al. succeeded in the synthesis of a series of miktoarm star copolymers, i.e., the *AB*, AB_2, AB_3, A_2B_2, A_2B, and A_3B type polymers, by the click coupling of the azido-functionalized PCLs and ethynyl-functionalized maltoheptaose (**Figure 1-5**).[98, 99] These ingenious studies have revealed that the microphase-separated structures and micellar morphologies are affected by the arm numbers and block arrangements. Although the synthetic methods for both the star-block and miktoarm star copolymers have been established, comprehensive studies of the self-assembly behaviors have rarely been carried out using a set of star-shaped block copolymers

Scheme 1-6. Synthetic approaches for miktoarm star polymers

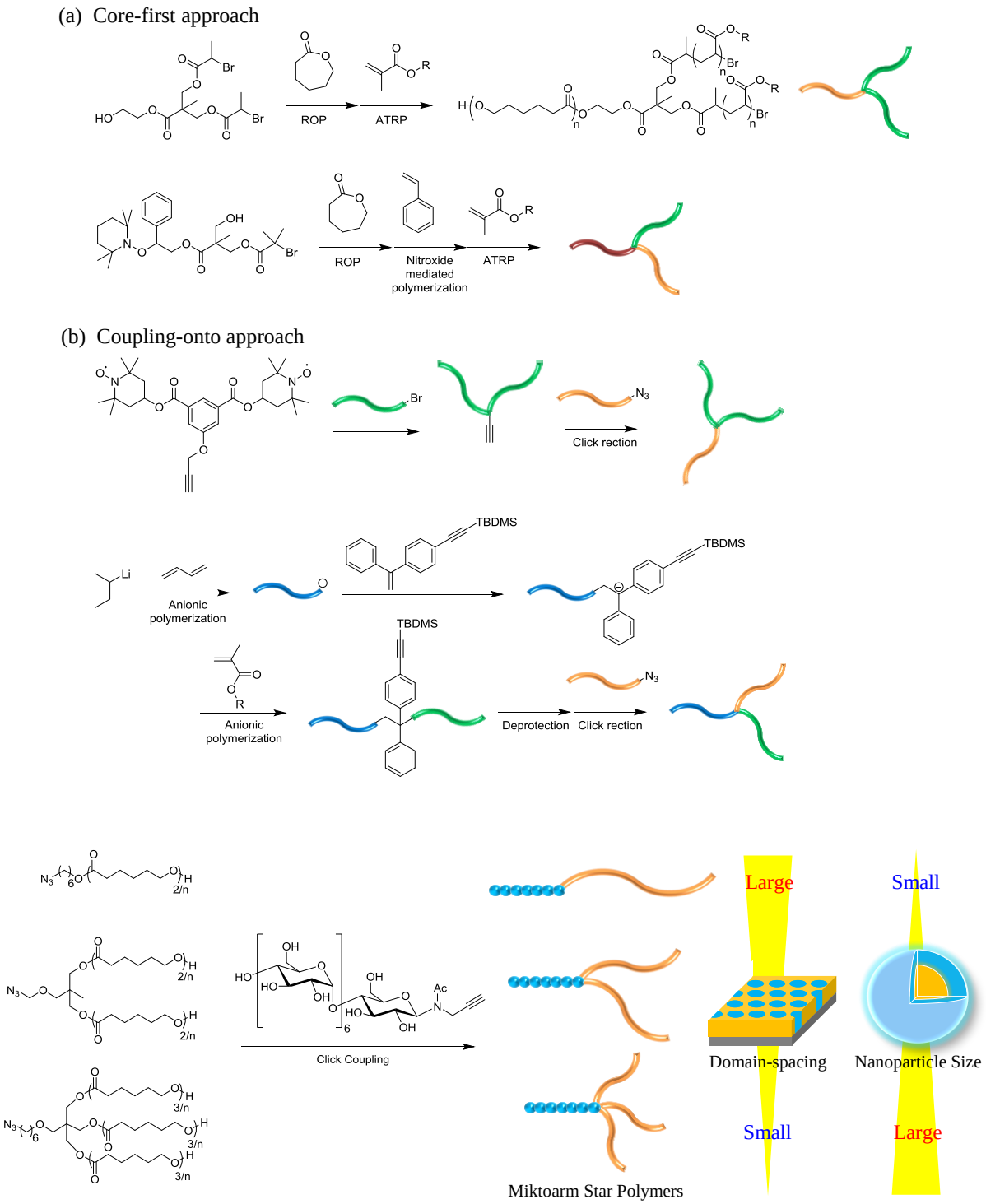

Figure 1-5. The synthesis and self-assembling behaviors of the maltoheptaose/PCL miktoarm star polymers.

1.2.3 Synthesis and Characteristics of Cyclic Block Copolymers

The cyclic block copolymers have also been synthesized to investigate their properties derived from the cyclized architecture. Indeed, several studies indicated that cyclic block copolymers display a unique self-assembly behavior.[100] For example, Tezuka et al. synthesized amphiphilic cyclic PEO-*b*-poly(butyl acrylate) and found that the structural stability of the micelles formed from the cyclic polymer was drastically increased as compared to the corresponding *ABA* linear counterpart (**Figure 1-6a**).[101] In addition, Hawker et al. revealed that the cyclic PS-*b*-PEO exhibited a phase-separated structure with a smaller domain-spacing in the thin film states as compared to that of the corresponding linear diblock copolymer (**Figure 1-6b**).[102] In contrast to the monocyclic polymers, Wu and Huang et al. reported that the amphiphilic figure-eight-shaped block copolymer formed larger and looser aggregates due to lower packing of the structures.[103, 104] In addition to these studies, there were several reports about the synthesis and characteristics of the cyclic-containing block copolymers, such as the tadpole-shaped[105–107] and jellyfish-structures.[108, 109]

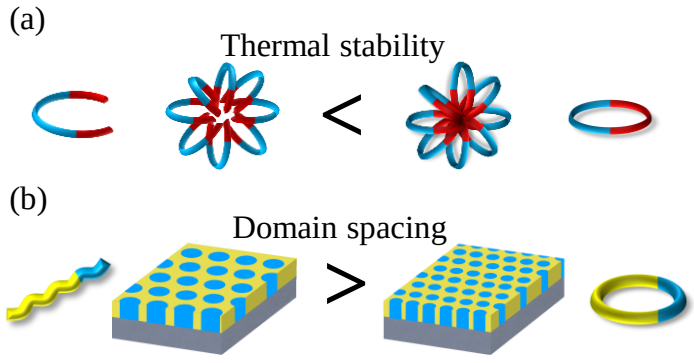

Figure 1-6. The self-assembled structures formed by linear and cyclic block copolymers (a) in the solution state, and (b) in the bulk state.

The cyclic block copolymers are generally synthesized by the ring-closure of the linear precursor. For example, a monocyclic diblock copolymer was obtained via the intramolecular or intermolecular click cyclization of end-functionalized linear precursors that were prepared by the living polymerization techniques. In a similar way, more complex cyclic-containing block copolymers, such as the figure-eight- and tadpole-shaped block copolymers, were synthesized via intermolecular and intramolecular coupling techniques (**Scheme 1-7a**). For example, Monteiro et al. established the synthetic approaches to produce amphiphilic tadpole-shaped block copolymers consisting of poly(acrylic acid) and PS.[107, 110] Tezuka et al. achieved the synthesis of a comprehensive set of cyclic-containing PEO-*b*-poly(THF) amphiphilic block copolymers by the combination of the ESA-CF technique and click reaction.[111] In addition, the intramolecular cyclization of star-shaped block copolymers was also reported as an effective method to produce the multicyclic block copolymers (**Scheme 1-7b**).[104, 112]

Scheme 1-7. Synthetic approaches for the cyclic containing block copolymers prepared from (a) linear precursors, and (b) star-shaped precursors

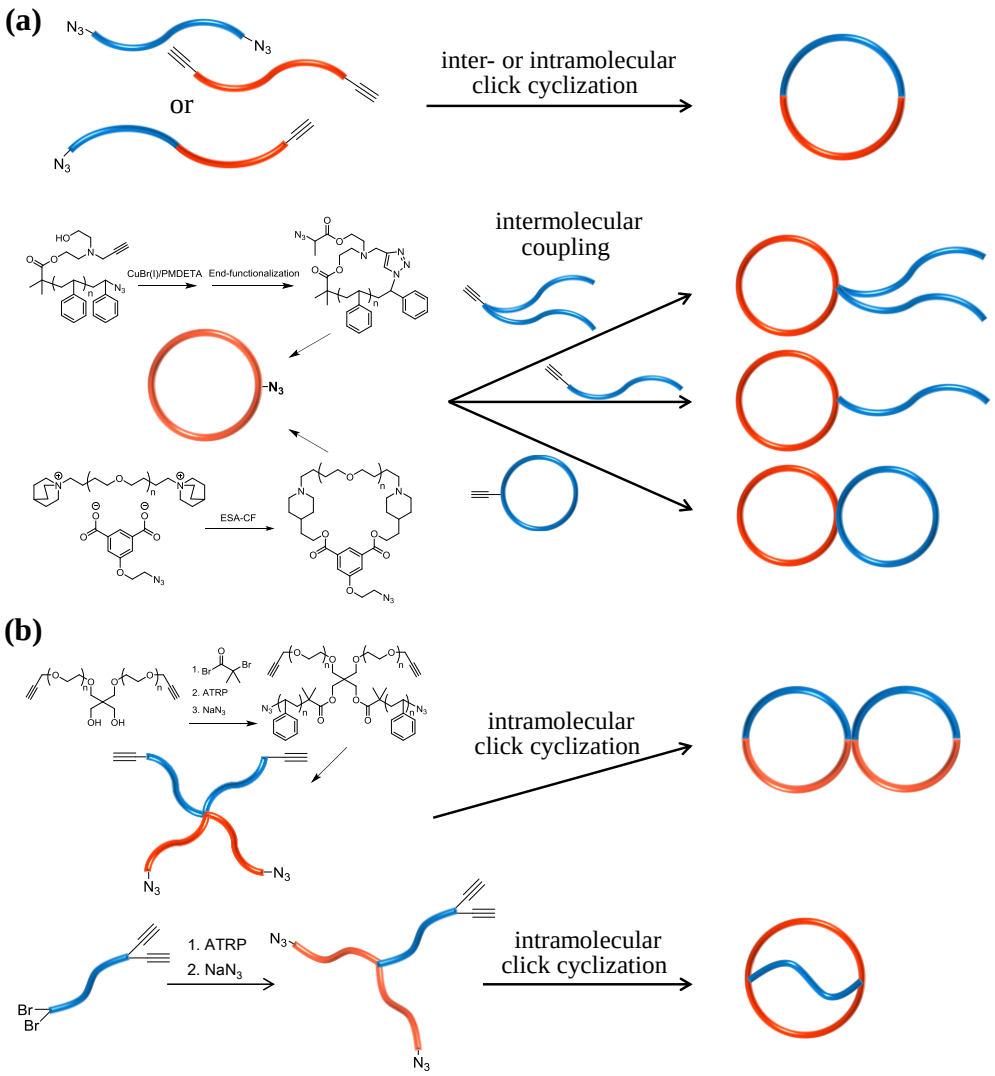

As already mentioned, the cyclic architectures affect the self-assembly behavior of amphiphilic block copolymers, leading to unprecedent and unique properties that are unattainable from the linear counterparts. Therefore, understanding the correlation between the cyclic architecture and self-assembly behavior would allow creation of high value-added materials based on the design of the macromolecular architecture. However, such

information is still unavailable because the inherent difficulty in the synthesis and purification has limited the access to a comprehensive set of cyclic-containing block copolymers with comparable molecular weights and monomer compositions. Therefore, concise and robust synthetic strategies are required for preparing the well-defined cyclic-containing block copolymers.

1.3 Polyether Based Polymer

1.3.1 Polyether Based Block Copolymers

Polyethers having a PEO backbone have been recognized as an important class of polymeric materials due to their nonionic character, chemical stability, low toxicity, and biocompatibility.[113–115] For example, PEO and poly(propylene oxide) (PPO), which are the representative examples of the polyethers, have indeed been used for a wide range of industrial applications such as nonionic surfactant agents, electrolytes of the lithium-polymer battery, medical agents, and soft segments of polyurethanes.[76, 116–119] In addition, polyether-based amphiphilic block copolymers (polyethers) are of particular importance in relation to their self-assembly properties to form micelles or microphase-separated structures. Due to such properties, the amphiphilic block copolyethers based on PEO and PPO have been commercialized with the brand name of Pluronic and been used for the applications involving carriers for drug delivery,[77, 120] nanoreactors,[79] template for nanoporous materials, and amphiphilic nanoparticles.[81, 82] Therefore, much effort is still being directed toward the development of new polyether-based block copolymer systems, such as poly(ethylene oxide)/poly(butylene oxide),[121] poly(glycidol)/poly(propylene oxide),[118] poly(ethoxyethyl glycidyl ether)/poly(propylene oxide) triblock copolymer,[122,123] poly(ethylene oxide)-*b*-poly(allyl glycidyl ether)-*b*-poly(*t*-butyl glycidyl ether),[124] poly(glycidol)-*b*-poly(glycidyl amine),[125] and poly(ethylene oxide)-*b*-poly(furfuryl glycidyl

ether)[126] (**Scheme 1-8**).

As described in Section 1.2, the self-assembly behavior of block copolymers is generally affected by their chemical compositions, hydrophilic/hydrophobic ratios, molecular weights, and dispersities. Considerable research efforts have revealed that the self-assembly behaviors of the block copolyethers are also affected by these characteristics.[127–129] In contrast, there are few reports related to the synthesis and characterization of the well-defined block copolyethers with various architectures, such as the star-shaped and cyclic-containing polyethers. Thus, the establishment of a synthetic approach for architecturally complex amphiphilic block copolyethers is desired for the development of advanced materials.

Scheme 1-8. The polyether-based amphiphilic block copolymers

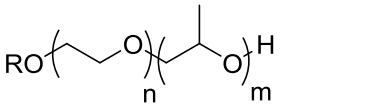

poly(ethylene oxide)/poly(propylene oxide)

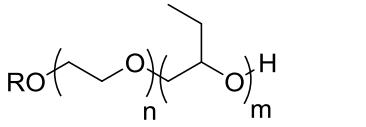

poly(ethylene oxide)/poly(butylene oxide)

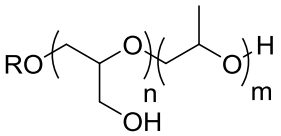

poly(glycidol)/poly(propylene oxide)

1.3.2 Synthesis of Polyether Derivative

For the synthesis of the well-defined block copolyethers, the anionic ROP of epoxide monomers is an effective method due to its living nature. The alkali-metal-mediated anionic ROP at high temperature is well-known as a general anionic ROP method of epoxides (**Scheme 1-9**). For example, Hawker et al. reported the living polymerization of allyl glycidyl ether using benzyl alcohol/potassium naphthalenide as an initiator.[130] Booth et al. also reported the polymerization of propylene oxide using potassium alkoxide and 18-crown-6-ether.[131] However, these alkoxide-mediated ROPs suffer from a chain transfer reaction to the monomer, and this could afford less control over the molecular weight, dispersity, and chain end functionality (**Scheme 1-10**).[132] Therefore, there have been many efforts to explore novel controlled/living polymerization systems for substituted epoxide monomers to reduce such side reactions.

Scheme 1-9. ROP of epoxides initiated by metal alkoxide

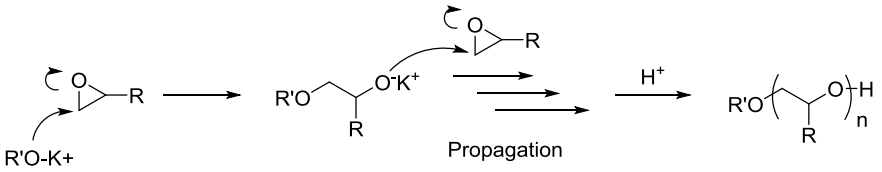

Scheme 1-10. Chain transfer reaction occurring during the polymerization of epoxides

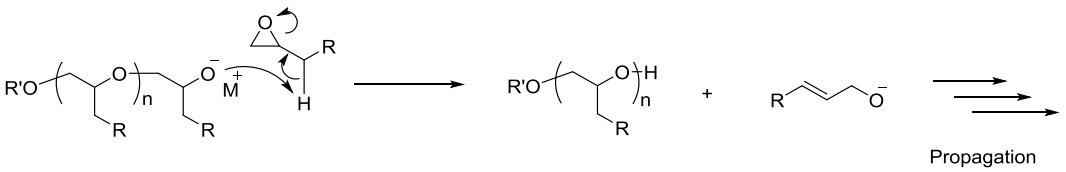

Recently, Misaka and coworkers reported that 1-*tert*-butyl-4,4,4-tris(dimethyl–amino)-2,2-bis[tris(dimethylamino)phosphoranylidenamino]-2Λ5,4Λ5-catenadi(phosphazene) (*t*-Bu-P_4) is an effective catalyst for the ROP of substituted epoxides.[133–135] *t*-Bu-P_4 was developed by Schwesinger et al., which has a high stability in air, high solubility in organic solvents, and strong basicity (p$K_{BH(MeCN)}$ = 42.7) similar to alkyl lithiums.[136] The positive charge in *t*-Bu-P_4 can be delocalized after protonation and the formed bulky cation of *t*-Bu-P_4H^+ made possible less aggregation with the alkoxide anion. These two factors endowed the counter anion with a high reactivity (**Figure 1-7**). Such specific features of *t*-Bu-P_4 produced a higher polymerization rate at room temperature than the alkali-metal-mediated anionic ROP, resulting in better control of the polymerization with minimal side reactions. The *t*-Bu-P_4-catalyzed ROP system made it possible to produce various α-end-functionalized polyethers with predictable molecular weights and narrow dispersities by using functional alcohol initiators (**Scheme 1-11**).

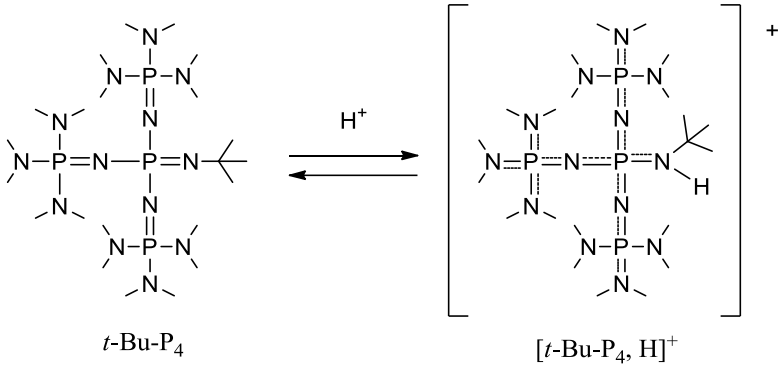

Figure 1-7. Phosphazene base "*t*-Bu-P_4" and protonated *t*-Bu-P_4.

Scheme 1-11. *t*-Bu-P_4-catalyzed ROP of epoxides using various alcohols as the initiator

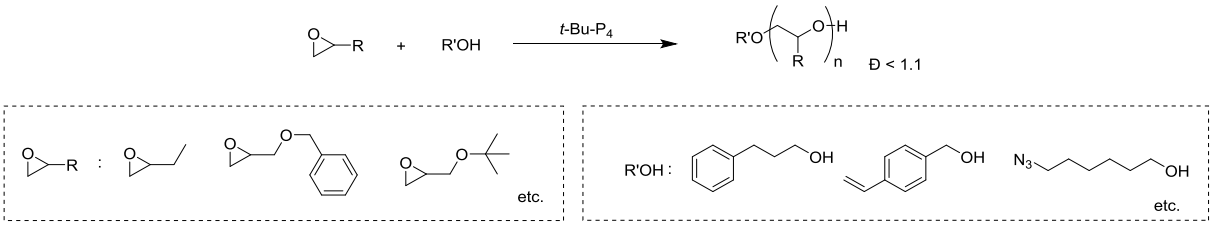

1.4 Objectives and Outline of the Thesis

As described in Section 1.1, the macromolecular architectures of polymers as well as their molecular weights, dispersities, and monomer compositions affect the polymer properties. In particular, the effect of the macromolecular architectures on the self-assembly behavior of amphiphilic block copolymers is of significant importance to create advanced materials, because the macromolecular architecture could be one of factors that affect the packing of polymer chains in the microphase-separated structures (Section 1.2). Although several reports have revealed the unique self-assembly properties of star-shaped and cyclic block copolymers, there are few reports about the systematic study of the relationship between polymer architectures and their self-assembly behavior. Generally, the construction of the block copolymers with complex macromolecular architectures, such as the star-block, miktoarm star, multicyclic, and tadpole-shaped, had been difficult due to the limitation of polymerization techniques as described in Section 1.2. Moreover, the difference in the molecular weights and monomer compositions have the potential to influence the self-assembly behavior. To reveal the essential topological effect on the self-assembly properties, it is necessary to prepare the architectural block copolymers with precisely controlled molecular weights, monomer compositions, and very narrow dispersities. Therefore, in this thesis, the author focused on the development of novel synthetic approaches for the well-defined architectural block copolymers, with a controllable molecular weight and

narrow dispersity, based on the combination of living polymerization techniques and efficient organic reactions.

As mentioned in Section 1.3, polyethers composed of a PEO backbone are an important class of polymers as well as vinyl polymers. In particular, amphiphilic block copolyethers have received much attention as surfactants in the medical and industrial fields. Thus, many types of polyether-based block copolymers were studied to create high-value-added materials based on their self-assembled structures. In addition, the investigation into the synthesis and properties of the amphiphilic block copolyethers with complex architectures would have a significant impact on the development of novel nanomaterials. However, the systematic characterization of the polyether-based block copolymers with various architectures has never been achieved, and the establishment of synthetic approaches providing well-defined block copolyethers is also a challenging issue.

Therefore, the objective of this thesis is to establish novel synthetic methodologies for a comprehensive set of well-defined amphiphilic block copolyethers possessing star-shaped, tadpole-shaped, and multicyclic architectures. The *t*-Bu-P_4-catalyzed ROP system and the CuAAC click reaction were used as the key steps in the synthetic approaches. The well-controlled living nature of the ROP and the highly efficient coupling reaction could enable the production of such polyethers with a highly-controlled molecular weight and narrow dispersity in high purity. As the second objective, the author investigated the

aqueous self-assembly properties of the amphiphilic block copolyethers with comparable molecular weights, monomer compositions, and narrow dispersities to reveal the essential effect of the macromolecular architectures.

The outline of this thesis is as follows:

Chapter 2 describes the synthesis of a comprehensive set of amphiphilic star-shaped block copolyethers with a fixed molecular weight and composition via the *t*-Bu-P_4-catalyzed ROP (**Figure 1-8**). The three- and four-armed star-block copolyethers, i.e., the $(AB)_3$-, $(BA)_3$-, $(AB)_4$-, and $(BA)_4$-type star-block copolyethers, where A and B represent hydrophobic and hydrophilic blocks, respectively, were synthesized by the sequential *t*-Bu-P_4-catalyzed block copolymerization using tri- and tetra-alcohol initiators, respectively, according to the core-first method. The homogeneous growth of each arm was confirmed by cleaving of the linkages between the initiator residue and polyether arms. The synthesis of the A_2B_2-, AB_2-, and A_2B-type miktoarm star copolyethers was achieved by the combination of the *t*-Bu-P_4-catalyzed ROP and azido-ethynyl click chemistry. The azido- and ethynyl-functionalized precursor polyethers with the predicted molecular weights were separately prepared by the *t*-Bu-P_4-catalyzed ROP with the aid of functional initiators as well as terminators. The intermolecular click reaction of the precursors provided the desired

miktoarm star copolyethers. All the obtained star-shaped block copolyethers had a comparable monomer composition (ratio in degree of polymerization = 50:50) and total molecular weight (ca. 22,200 g mol^{-1}) with a narrow dispersity (<1.05). The hydrodynamic diameter and the cloud point analyses for the aqueous micellar solution of the amphiphilic star-shaped block copolyethers revealed that the self-assembly properties were affected by the block arrangements and branched architectures of the amphiphilic polymers.

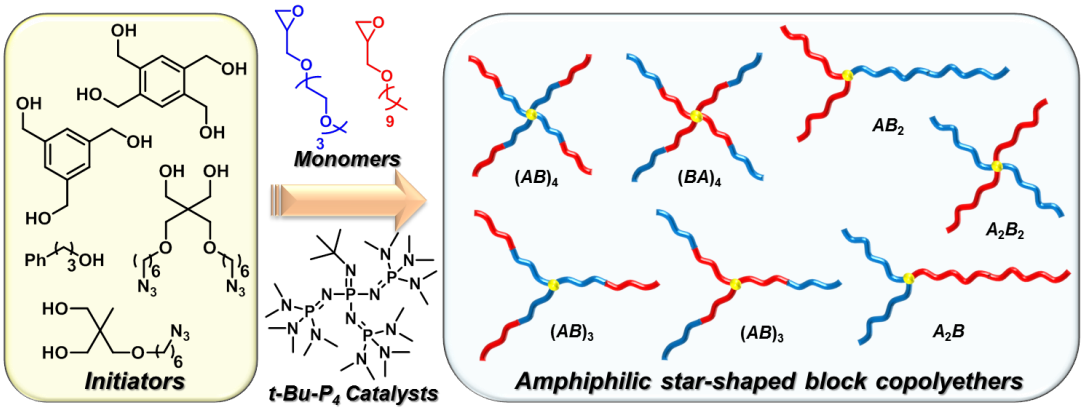

Figure 1-8. The synthesis of a comprehensive set of amphiphilic star-shaped block copolyethers with fixed molecular weights and compositions via the *t*-Bu-P_4-catalyzed ROP.

Chapter 3 describes the synthesis of systematic sets of figure-eight- and tadpole-shaped amphiphilic block copolyethers, together with the corresponding cyclic counterparts, via the combination of the *t*-Bu-P_4-catalyzed ROP and click cyclization (**Figure 1-9**). The clickable linear block copolyether precursors, with precisely controlled azido and ethynyl group placements as well as a fixed molecular weight and monomer composition

(degree of polymerization for each block was adjusted to be around 50) were prepared by the *t*-Bu-P_4-catalyzed ROP with the aid of functional initiators and terminators. The click cyclization of the precursors under highly diluted conditions produced a series of cyclic, figure-eight-, and tadpole-shaped block copolyethers with narrow dispersities of less than 1.06. Preliminary studies of the aqueous self-assembly behavior of the cyclic-containing block copolyethers revealed the significant variation in their cloud points depending on the block copolyether architecture, though there were small architectural effects on their critical micelle concentration and morphology of the aggregates.

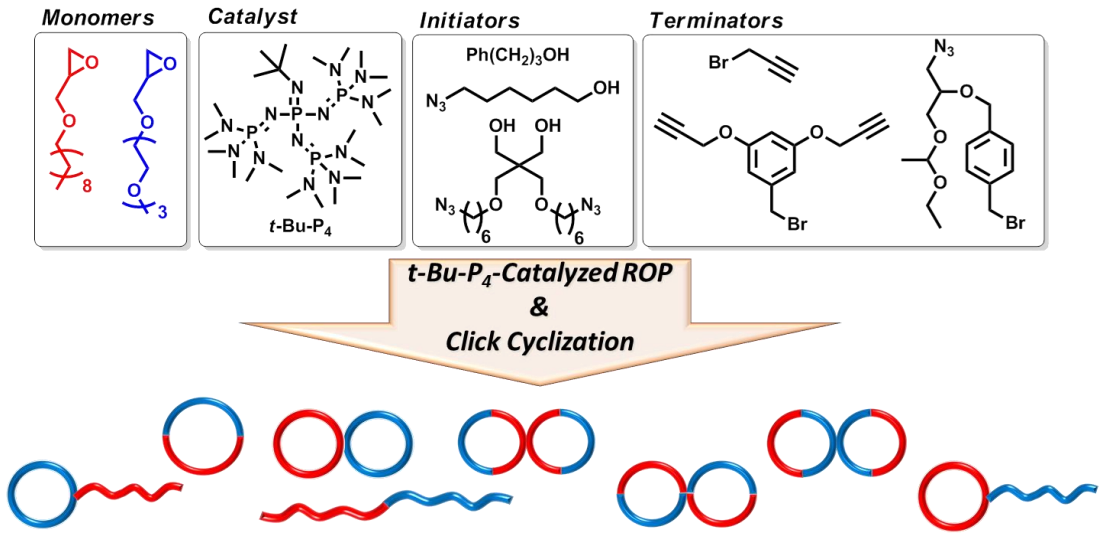

Figure 1-9. The synthesis of systematic sets of figure-eight- and tadpole-shaped amphiphilic block copolyethers, together with the corresponding cyclic counterparts.

Chapter 4 describes a novel synthetic approach for the three- and four-armed cage-shaped polyethers based on the topological conversion of the corresponding trefoil- and

quatrefoil-shaped precursors (**Figure 1-10**). The trefoil- and quatrefoil-shaped polyethers were synthesized by the following three reaction steps: (1) the *t*-Bu-P_4-catalyzed ring-opening polymerization of butylene oxide using multiple hydroxy- and azido-functionalized initiators to produce the three- or four-armed star-shaped polymers possessing three or four azido groups at the focal point, respectively, (2) the ω-end modification to install a propargyl group at each chain end, and (3) the intramolecular multiple click cyclization of the clickable star-shaped precursors. The topological conversion from the trefoil- and quatrefoil-shaped polyethers to the cage-shaped polyethers was achieved by the catalytic hydrogenolysis of the benzyl ether linkages that had been installed at the focal point. The amphiphilic cage-shaped block copolyethers together with the corresponding trefoil- and quatrefoil-shaped counterparts were also synthesized in a similar way using 2-(2-(2-methoxyethoxy)ethoxy)ethyl glycidyl ether as a hydrophilic monomer and decyl glycidyl ether as a hydrophobic monomer. Interestingly, significant changes in the critical micelle concentration and micellar morphology were observed for the amphiphilic block copolyethers upon the topological conversion from the trefoil- and quatrefoil-shaped to cage-shaped architectures.

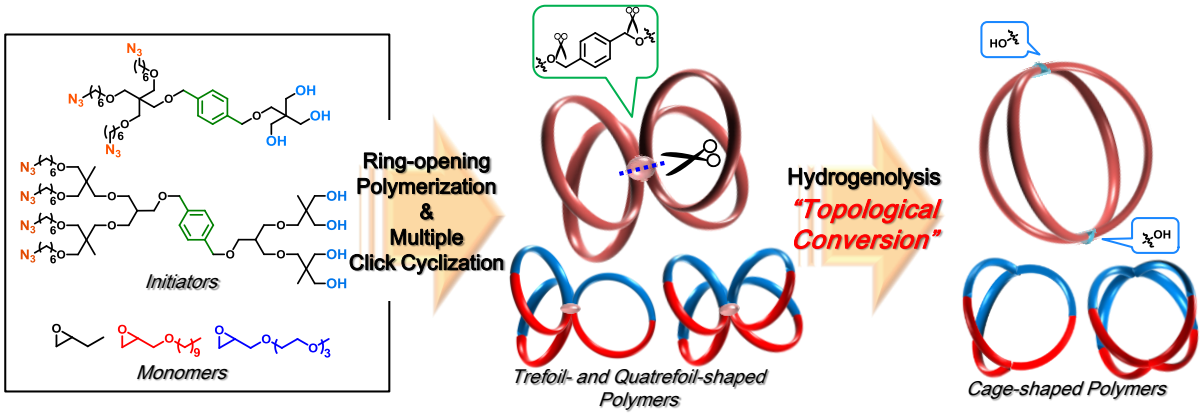

Figure 1-10. A novel synthetic approach for three- and four-armed cage-shaped polyethers based on the topological conversion of the corresponding trefoil- and quatrefoil-shaped precursors.

Chapter 5 summarizes the synthesis and self-assembling behavior of the well-defined star-shaped and multicyclic block copolyethers.

1.5 References and Notes

1. Mishra, M., Kobayashi, S., Eds.; *Star and Hyperbranched Polymers*; Marcel Dekker, Inc.: New York, **1999**.
2. Kricheldorf H. R. *J. Polym. Sci., Part A: Polym. Chem.* **2010**, *45*, 251–284.
3. Hogen-Esch, T. E. *J. Polym. Sci., Part A: Polym. Chem.* **2006**, *44*, 2139–2155.
4. Hadjichristidis, N.; Pitsikalis, M.; Pispas, S.; Iatrou, H. *Chem. Rev.* **2001**, *101*, 3747−3792.
5. Hadjichristidis, N.; Iatrou, H.; Pitsikalis, M.; Mays, J. *Prog. Polym. Sci.* **2006**, *31*, 1068−1132.
6. Pavlov, G. M.; Knop, K.; Okatova, O. V.; Schubert, U. S. *Macromolecules*, **2013**, *46*, 8671–8679.
7. Chen, Y. *Macromolecules*, **2012**, *45*, 2619–2631.
8. Yamamoto, T.; Tezuka, Y. *Polym. Chem.* **2011**, *2*, 1930–1941.
9. Laurent, B. A.; Grayson, S. M. *Chem. Soc. Rev.* **2009**, *38*, 2202–2213.
10. Hawker, C. J.; Bosman, A. W.; Harth, E. Chem. Rev. 2001, 101, 3661−3688.
11. Perrier, S.; Takolpuckdee, P. *J. Polym. Sci., Part A: Polym. Chem.* **2005**, *43*, 5347−5393.
12. Coessens, V.; Pintauer, T.; Matyjaszewski, K. *Prog. Polym. Sci.* **2001**, *26*, 337−377.
13. Akeroyd, N.; Klumperman, B. *Eur. Polym. J.* **2011**, *47*, 1207−1231.
14. Li, H.; Jérôme, R.; Lecomte, P. *Macromolecules*, **2008**, *41*, 650–654.
15. Sun, C.; Ritchie, J. E. *J. Phys. Chem. B* **2011**, *115*, 8381–8389.
16. Wang, J.-S.; Greszta, D.; Matyjaszewski, K. *Polym. Mater. Sci. Eng.* **1995**, *73*, 416–515.
17. Ueda, J.; Matsuyama, M.; Kamigaito, M.; Sawamoto, M. *Macromolecules***1998**, *31*, 557–562.
18. Angot, S.; Murthy, K. S.; Taton, D.; Gnanou, Y. *Macromolecules* **1998**, *31*, 7218–7225.
19. Matyjaszewski, K.; Miller, P. J.; Fossum, E.; Nakagawa, Y. *Appl. Organomet. Chem.* **1998**, *12*, 667–673.

20. Matyjaszewski, K. *Polym. Int.* **2003**, *52*, 1559–1565.
21. Matyjaszewski, K.; Miller, P. J.; Pyun, J.; Kickellbick, G.; Diamanti, S. *Macromolecules* **1999**, *32*, 6526-6535.
22. Choi, Y. K.; Bae, Y. H.; Kim, S. W. *Macromolecules* **1998,** *31,* 8766-8774.
23. Pozza, G. M. E; Crotty, S.; Rawiso, M.; Schubert, U. S.; Lutz, P. J. *J.Phys.Chem.B* **2015**, *119*, 1669−1680.
24. Whittaker, M. R.; Urbani, C. N.; Monteiro, M. J. *J. Am. Chem. Soc.* **2006**, *128*, 11360–11361.
25. Altintas, O.; Hizal, G.; Tunca, U. *J. Polym. Sci., Part A: Polym. Chem.* **2006**, *44*, 5699–5707.
26. Altintas, O.; Yankul, B.; Hizal, G.; Tunca, U. *J. Polym. Sci., Part A: Polym. Chem.* **2006**, *44*, 6458–6465.
27. Gao, H.; Matyjaszewski, K. *Macromolecules* **2006,** *39,* 4960-4965.
28. Bielawski, W. C.; Benitez, D.; Grubbs, H. R. *Science* **2002**, *297*, 2041-2044.
29. Kricheldorf, H. R.; Lee, S. *Macromolecules* **1995**, *28*, 6718-6725.
30. Christopher D. Roland, Hong Li, Khalil A. Abboud, Kenneth B. Wagener and Adam S. Veige *Nat. Chem.* **2016**, *8*, 791–796.
31. Shea, K. J.; Lee, S. Y.; Busch, B. B. *J. Org. Chem.* **1998**, *63*, 5746-5747.
32. Takeuchi, D.; Inoue, A.; Osakada, K.; Kobayashi, M.; Yamaguchi, K. *Organometallics* **2006**, *25*, 4062-4064.
33. Chen, F.; Liu, G.; Zhang, G. *J. Polym. Sci. Part A: Polym. Chem.* **2012**, *50*, 831–835.
34. Laurent, B. A.; Grayson, S. M. *J. Am. Chem. Soc.* **2006**, *128*, 4238–4239.
35. O’ Bryan, G.; Ningnuek, N.; Braslau, R. *Polymer* **2008**, *49*, 5241–5248.
36. Glassner, M.; Blinco, J. P.; Barner-Kowollik, C. *Macromol. Rapid Commun.* **2011**, *32*, 724–728.
37. Durmaz, H.; Dag, A.; Hizal, G.; Tunca, U. *J. Polym. Sci. Part A: Polym. Chem.* **2010**, *48*,

5083–5091.

38. Kubo, M.; Hayashi, T.; Kobayashi, H.; Tsuboi, K.; Itoh, T. *Macromolecules* **1997**, *30*, 2805–2807.
39. Lepoittevin, B.; Perrot, X.; Masure, M.; Hemery, P. *Macromolecules* **2001**, *34*, 425–429.
40. Schappacher, M. and Deffieux, A. *Macromolecules.* **1995**, *28*, 2629–2636.
41. Zhang, Y.; Wang, G.; Huang, J. *Macromolecules* **2010**, *43*, 10343–10347.
42. Kolb, H. C.; Finn, M. G.; Sharpless, K. B. *Angew. Chem. Int. Ed.* **2001**, *40*, 2004–2021
43. Huisgen, R; Szeimies, G.; Möbius, L. *Chem. Ber.* **1967**, *100*, 2494–2507.
44. Binder, W. H.; Sachsenhofer, R. *Macromol. Rapid Commun.* **2007**, *28*, 15–54.
45. Bock, V. D.; Hiemstra, H.; Maarseveen, J. H. V. *Eur. J. Org. Chem.* **2006**, 51–68.
46. Shi, G.; Pan, C. *Macromol. Rapid Commun.* **2008**, *29*, 1672–1678.
47. Jiang, H.; Chen, T.; Bo, S.; Xu, J. *Macromolecules* **1997**, *30*, 7345–7347.
48. Roovers, J.; Toporowski, P. M. *Macromolecules* **1983**, *16*, 843–849.
49. Oike, H.; Imaizumi, H.; Mouri, T.; Yoshioka, Y.; Uchibori, A.; Tezuka, Y. *J. Am. Chem. Soc.* **2000**, *122*, 9592–9599.
50. Tezuka, Y.; Oike, H. *Macromol. Rapid Commun.* **2001**, *22*, 1017–1029.
51. Tezuka, Y.; Oike, H. *Prog. Polym. Sci.* **2002**, *27*, 1069–1122.
52. Lee, T.; Oh, J.; Jeong, J.; June, H.; Chang,T.; Paik, H-j. *Macromolecules* **2016**, *49*, 3672–3680.
53. Hamely, I. W. *The physics of block copolymers*, Oxford Univerity Press, **1988**.
54. Kim, J. K.; Yang, S. Y.; Lee, Y.; Kim, Y. *Prog. Polym. Sci.* **2010**, *35*, 1325–1349.
55. Lodge. T. P. *Macromol. Chem. Phys.* **2003**, *204*, 265–273.
56. Luo, M.; EppsIII, T. H. *Macromolecules*, **2013**, *46*, 7567–7579.
57. Rubatat, L.; Li, C.; Dietsch, H.; Nykänen, A.; Ruokolainen, J.; Mezzenga, R. *Macromolecules* **2008**, *41*, 8130–8137.
58. Walheim, S.; Boltau, M.; Mlynek, J.; Krausch, G.; Steiner, U. *Macromolecules* **1997**, *30*,

4995–5003.

59. Zucchi, I. A.; Galante, M. J.; Williams, R. J. J. *Polymer* **2005**, *46*, 2603–2609.
60. Zhu, L.; Cheng, S. Z. D.; Calhoun, B. H.; Ge, Q.; Quirk, R. P.; Thomas, E. L.; Hsiao, B.S.; Yeh, F.; Lotz, B. *Polymer* **2001**, *42*, 5829–5839.
61. Huang, P.; Zhu, L.; Cheng, S. Z. D.; Ge, Q.; Quirk, R. P.; Thomas, E. L.; Lotz, B.; Hsiao, B. S.; Liu, L. Z.; Yeh, F. J. *Macromolecules* **2001**, *34*, 6649–6657.
62. Nojima, S.; Kiji, T.; Ohguma, Y. *Macromolecules* **2007**, *40*, 7566–7572.
63. Schuetz, P.; Greenall, M. J.; Bent, J.; Furzeland, S.; Atkins, D.; Butler, M. F.; McLeish, T. C. B.; Buzza, D. M. A. *Soft Matter* **2011**, *7*, 749–759.
64. Cohn, D.; Stern, T.; Gonzalez, M. F.; Epstein, *J. Journal of Biomedical Materials Research Part A* **2001**, *59*, 273–281.
65. Guilherme, L. A.; Borges, R. S.; Moraes, E. M. S.; Silva, G. G.; Pimenta, M. A.; Marletta, A.; Silva, R. A. *Electrochimica Acta* **2007**, *53*, 1503–1511.
66. Jannasch, P. *Chem. Mater* **2002**, *14*, 2718–2724.
67. Araujo, E. S.; Rieumont, J.; Nogueiras, C.; Oliveira, H. P. *European Polymer Journal* **2010**, *46*, 1854–1859.
68. Matyjaszewski, K. *Macromolecules* **2012**, *45*, 4015–4039.
69. Chiefari, J.; Chong, Y. K.; Ercole, F.; Krstina, J.; Jeffery, J.; Le, T. P. T.; Mayadunne, R. T. A.; Meijs, G. F.; Moad, C. L.; Moad, G.; Rizzardo, E.; Thang, S. H. *Macromolecules* **1998**, *31*, 5559–5562.
70. Kamber, N. E.; Jeong, W.; Waymouth, R. M.; Pratt, R. C.; Lohmeijer, B. G. G.; Hedrick, J. L. *Chem. Rev.* **2007**, *107*, 5813–5840.
71. Dechy-Cabaret, O.; Martin-Vaca, B.; Bourissou, D. *Chem. Rev.* **2004**, *104*, 6147–6176.
72. Schrock, R. R. *Acc. Chem. Res.* **1990**, *23*, 158–165.
73. Bielawski, C. W.; Grubbs, R. H. *Progress in Polymer Science* **2007**, *32*, 1–29.
74. Miyakoshi, R.; Yokoyama, A.; Yokozawa, T. *J. Am. Chem. Soc.* **2005**, *127*, 17542–17547.

75. Yokozawa, T.; Ogawa, M.; Sekino, A.; Sugi, R.; Yokoyama, A. *J. Am. Chem. Soc.* **2002**, *124*, 15158–15159.
76. Booth, C.; Attwood, D. *Macromol. Rapid Commun.* **2000**, *21*, 501–527.
77. Kim, S. Y.; Lee, Y. M. *Biomaterials* **2001**, *22*, 1697.
78. Kataoka, K.; Harada, A.; Nagasaki, Y. *Adv Drug Deliv Rev* **2001**,*47*, 113–131.
79. Riess, G. *Prog. Polym. Sci.* **2003**, *28*, 1107–1170.
80. Hartgerink, J. D.; Beniash, E.; Stupp, S. I. *Science* **2001**, *294*, 1684–1688.
81. Tang, C.; Qi, K.;Wooley, K. L.; Matyjaszewski, K.; Kowalewski, T. *Angew. Chem., Int. Ed.* **2004**, *43*, 2783–2787.
82. Bao, X. Y.; Zhao, X. S.; Li, X.; Chia, P. A.; Li, J.; *J. Phys. Chem. B* **2004**, *108*, 4684–4689.
83. Moughton, A. O.; Hillmyer, M. A.; Lodge, T. P. *Macromolecules* **2012**, *45*, 2–19.
84. Khanna, K.; Varshney, S.; Kakkar, A. *Polym. Chem.* **2010**, *1*, 1171–1185.
85. Hadjichristidis, N. *J. Polym. Sci. Part A: Polym. Chem.* **1999**, 37, 857–871.
86. Ishizu, K.; Uchida, S. *Prog. Polym. Sci.* **1999**, *24*, 1439–1480.
87. Choi, Y. K.; Bae, Y. H.; Kim, S. W. *Macromolecules* **1998**, *31*, 8766–8774.
88. Angot, S.; Taton, D.; Gnanou, Y. *Macromolecules* **2000**, *33*, 5418–5426.
89. Ishizu, K.; Uchida, S. *Prog. Polym. Sci.* **1999**, *24*, 1439–1480.
90. Francis, R.; Skolnik, A. M.; Carino, S. R.; Logan, J. L.; Underhill,R. S.; Angot, S.; Taton, D.; Gnanou, Y.; Duran, R. S. *Macromolecules* **2002**, *35*, 6483–6485.
91. Tunca, U.; Ozyurek, Z.; Erdogan, T.; Hizal, G. *J. Polym. Sci., Part: Polym. Chem.* **2004**, *42*, 4228–4236.
92. Heise, A.; Trollsas, M.; Magbitang, T.; Hedrick, J. L.; Frank, C. W.; Miller, R. D. *Macromolecules* **2001**, *34*, 2798–2804.
93. Gordin, C.; Delaite, C.; Medlej, H.; Josien-Lefebvre, D.; Hariri, K.; Rusu, M. *Polym. Bull.* **2009**, *63*, 789–801.

94. Whittaker, M. R.; Urbani, C. N.; Monteiro, M. J. *J. Am. Chem. Soc.* **2006**, *128*, 11360–11361.
95. Kulis, J.; Jia, Z.; Monteiro, M. J. *Macromolecules* **2012**, *45*, 5956–5966.
96. Hanisch, A.; Schmalz, H.; Müller, A. H. E. *Macromolecules* **2012**, *45*, 8300–8309.
97. Yun, J.; Faust, R. *Macromolecules* **2003,** *36*, 1717–1723.
98. Isono, T.; Otsuka, I.; Kondo, Y.; Halila, S.; Fort, S.; Rochas, C.; Satoh, T.; Borsali, R.; Kakuchi, T. *Macromolecules* **2013**, *46*, 1461–1469.
99. Isono, T.; Miyachi, K.; Satoh, Y.; Nakamura, R.; Zhang, Y.; Otsuka, I.; Tajima, K.; Kakuchi, T.; Borsali, R.; Satoh, T. *Macromolecules* **2016**, *49*, 4178−4194.
100. Williams, R. J.; Dove, A. P.; O'Reilly, R. K. *Polym. Chem* **2015**, *6*, 2998–3008.
101. Honda, S.; Yamamoto, T.; Tezuka, Y. *Nat. Commun*. **2013**, *5*, 1574.
102. Poelma, J. E.; Ono, K.; Miyama, D.; Aida, T.; Satoh, K.; Hawker, C. J. *ACS Nano* **2012**, *6*, 10845–10854.
103. Wang, X.; Li, L.; Ye, X.; Wu, C. *Macromolecules* **2014**, *47*, 2487–2495.
104. Fan, X.; Huang, B.; Wang, G.; Huang, J. *Macromolecules* **2012**, *45*, 3779–3786.
105. Wan, X.; Liu, T.; Liu, S. *Biomacromolecules* **2011**, *12*, 1146–1154.
106. Dong, Y.-Q.; Tong, Y.-Y.; Dong, B.-T.; Du, F.-S.; Li, Z.-C. *Macromolecules* **2009**, *42*, 2940–2948.
107. Lonsdale, D. E.; Monteiro, M. J. *J. Polym. Sci., Part A: Polym. Chem.* **2011**, *49*, 4603–4612.
108. Cai, T.; Yang, W. J.; Neoh, K.-G.; Kang, E.-T. *Polym. Chem.* **2012**, *3*, 1061–1068.
109. Schappacher, M; Deffieux, A. *Science* **2008**, *319*, 1512–1515.
110. Kulis, J.; Jia, Z; Monteiro, M. J. *Macromolecules* **2012**, *45*, 5956–5966.
111. Hatakeyama, F.; Yamamoto, T.; Tezuka, Y. *ACS Macro Lett.* **2013**, *2*, 427–431.
112. Shi, G.-Y.; Pan, C.-Y. *J. Polym. Sci., Part A: Polym. Chem.* **2009**, *47*, 2620–2630.
113. Mark, H. F.; Bikales, N. M.; Overberger, C. G.; Menges, G; Kroschwitz, J. I., Eds.

Encyclopedia of Polymer Science and Engineering, vol. 6; John Wiley & Sons, Inc., **1985**.

114. Schmolka, I. R. *J. Am. Oil Chem. Soc.* **1977**, *54*, 110–116.

115. Gupta, S.; Tyagi, R.; Parmar, V. S.; Sharma, S. K.; Haag, R. *Polymer* **2012**, *53*, 3053–3078.

116. Brocas, A.-L.; Gervais, M.; Carlotti, S.; Pispas, S. *Polym. Chem.* **2012**, *3*, 2148–2155.

117. Mai, S.-M.; Fairclough, J. P. A.; Terrill, N. J.; Turner, S. C.; Hamley, I. W.; Matsen, M. W.; Ryan, A. J.; Booth, C. *Macromolecules* **1998**, *31*, 8110–8116.

118. Halacheva, S.; Rangelov, S.; Tsvetanov, C. *Macromolecules* **2006**, *39*, 6845–6852.

119. Altinok, H.; Yu, G.-E.; Nixon, S. K.; Gorry, P. A.; Attwood, D.; Booth, C. *Langmuir* **1997**, *13*, 5837–5848.

120. Kataoka, K.; Harada, A.; Nagasaki, Y. *Adv Drug Deliv Rev* **2001**,*47*, 113–131.

121. Hartgerink, J. D.; Beniash, E.; Stupp, S. I. *Science* **2001**, *294*, 1684–1688.

122. Smart, T. P.; Ryan, A. J.; Howse, J. R.; Battaglia, G. *Langmuir* **2010**, *10*, 7425–7430.

123. Dimitrov, P.; Rangelov, S.; Dworak, A.; Tsvetanov, C. B. *Macromolecules*, **2004**, *37*, 1000–1008.

124. Barthel, M. J.; Babiuch, K.; Rudolph, T.; Vitz, J.; Hoeppener, S.; Gottschaldt, M.; Hager, M. D.; Schacher, F. H.; Schubert, U. S. *J. Polym. Sci., Part A: Polym. Chem.*, **2012**, *50*, 2914–2923.

125. Meyer, J.; Keul, H.; Möller. M. *Macromolecule*s **2011**, *44*, 4082–4091.

126. Barthel, M. J.; Rudolph, T.; Crotty, S.; Schacher, F. H.; Schubert, U, S. *J. Polym. Sci., Part A: Polym. Chem.* **2012**, *50*, 4958–4965.

127. Alexandridis, P.; Holzwarth, J. F.; Hatton, T. A. *Macromolecules* **1994**, *27*, 2414–2425.

128. Zhou, Z.-K.; Chu, B. *Macromolecules* **1994**, *27*, 2025–2033.

129. Yu, G.-E.; Garrett, C. A.; Mai, S.-M.; Altinok, H.; Attwood, D.; Price, C.; Booth, C. *Langmuir* **1998**, *14*, 2278–2285.

130. Lee, F. B.; Kade, J. M.; Chute, A. J.; Gupta, N.; Campos, M. L.; Fredrickson, H. G.;

Kramer, J. E.; Lynd, A. N.; Hawker, J. C. *J. Polym. Sci. Part A: Polym. Chem.* **2011**, *49*, 4498–4504.

131. Ding, J.; Price, C.; Booth, C. *Eur. Polym. J.* **1991**, *27*, 891–894.

132. Obermeier, B.; Wurm, F.; Frey, H. *Macromolecules* **2010**, *43*, 2244–2251.

133. Misaka, H.; Tamura, E.; Makiguchi, K.; Kamoshida, K.; Sakai, R.; Satoh, T.; Kakuchi, T. *J. Polym. Sci. Part A: Polym. Chem.* **2012**, *50*, 1941–1952.

134. Misaka, H.; Sakai, R.; Satoh, T.; Kakuchi, T. *Macromolecules* **2011**, *44*, 9099–9107.

135. Kwon, W.; Rho, Y.; Kamoshida, K.; Kwon, K.; Jeong, Y.; Kim, J.; Misaka, H.; Shin, T.; Kim, J.; Kim, K.; Jin, K.; Chang, T.; Kim, H.; Satoh, T; Kakuchi, T.; Ree, M. *Adv. Funct. Mater.* **2012**, *22*, 5194–5208.

136. Schwesinger, R.; Schlemper, H. *Angew. Chem. Int. Ed. Engl.* **1987**, *26*, 1167–1169.

Chapter 2

Synthesis of Well-Defined Star-block and Miktoarm Star Copolyethers

2.1 Introduction

The polyethers prepared from epoxy monomers are industrially important polymeric materials.[1–3] As described in Section 1.3, amphiphilic block copolymers consisting of hydrophilic and hydrophobic polyether segments are of particular interest due to their widespread applications.[4–8] The amphiphilic block copolyethers consisting of PEO and PPO with a wide variety of molecular weights and compositions are indeed commercially available under the brand name of Pluronic. In addition, the related families of amphiphilic block copolyethers have been synthesized by employing epoxy monomers with various substituents, such as butylene oxide,[4] styrene oxide,[9] allyl glycidyl ethers,[10] furfuryl glycidyl ether,[11] and ethoxyethyl glycidyl ether.[12] The most interesting aspect of these block copolyethers is the ability to self-assemble into a wide variety of nanostructures in both the solution and bulk states, which can be utilized for nanoreactors,[13] drug carriers,[14–15] and templates for porous material fabrication.[16–18] Thus, further investigations into the synthesis and self-assembly of novel amphiphilic block copolyether systems should be of fundamental importance for expanding their possible applications.

Over the past two decades, significant efforts have been made to understand the aqueous self-assembly behaviors of these amphiphilic block copolyethers, especially for the PEO/PPO system, which provided the main conclusion that the parameters influencing the resultant nanostructures were the total molecular weight and hydrophilic/hydrophobic ratio as

well as temperature and concentration.[5, 19] In addition, the polymer architecture involving the block arrangement and topological structure was also found to be an important variable that modulates the self-assembly behaviors. For example, Chu et al. reported that PEO-*b*-PPO-*b*-PEO triblock copolyethers showed a lower critical micelle concentration (CMC) and larger hydrodynamic radius (R_h) of the micelle than those of the PPO-*b*-PEO-*b*-PPOs.[20] Furthermore, Booth et al. investigated the effect of the cyclic architecture on the micellization properties using *cyclic*-PEO-*b*-PPO and *cyclic*-PEO-*b*-poly(butylene oxide), which proved that cyclic ones formed micelles with higher association numbers and larger radii as compared to the corresponding starting linear block copolyethers.[21]

Despite the interesting results for the linear and cyclic architectures, the amphiphilic star-shaped block copolyethers have received little attention in terms of both their synthesis and self-assembly. Star-shaped block copolymers can be basically classified into two types; i.e., the star-block copolymer and miktoarms star copolymer. As a consequence of the progress in the living polymerization techniques, a number of methodologies are now available for synthesizing a variety of star-block and miktoarm star copolymers with vinyl polymer backbones.[22–25] In sharp contrast, only a few examples of the amphiphilic star-shaped block copolyethers are known, e.g., (PEO-*b*-PPO)$_4$-type four-armed star-block copolyethers (Tetronic). Although several investigations into the self-assembly behavior of

Tetronic were reported,[26, 27] the synthesis and characterization of a comprehensive set of star-shaped amphiphilic block copolyethers have never been achieved. To understand the effect of the star-shaped architectures on the self-assembly behavior, robust and simple routes are desired for synthesizing the star-block and miktoarm star copolyethers with varied arm numbers as well as different block arrangements.

Star-shaped polyethers with a strictly defined arm number and predictable molecular weight can be obtained by the methodologies referred to as "core-first" and "coupling-onto" strategies (Section 1.1.2).[28,29] For the synthesis of the well-defined block copolyethers, the anionic ring-opening polymerization (ROP) of epoxide monomers should be the most effective method because of its living nature. Recently, Kakuchi and coworkers demonstrated that 1-*tert*-butyl-4,4,4-tris(dimethylamino)-2,2-bis[tris(dimethylamino)–phosphoranylidenamino]-2Λ5,4Λ5-catenadi(phosphazene) (*t*-Bu-P_4) effectively catalyzed the anionic ROP of various substituted epoxides to produce the corresponding polyethers with the predicted molecular weight and narrow dispersity.[30–36] The well-controlled nature of the *t*-Bu-P_4-catalyzed ROP system allowed the sequential block copolymerization, yielding narrowly-dispersed block copolyethers. Importantly, the alcohol initiator used in the ROP is quantitatively incorporated into the α-chain end of the resultant polyethers, which is of critical importance to synthesize well-defined star-shaped polyethers.

In this chapter, the author describes the synthesis of a comprehensive set of

amphiphilic star-shaped block copolyethers, i.e., the $(AB)_3$-, $(BA)_3$-, $(AB)_4$-, and $(BA)_4$-type star-block copolyethers and A_2B_2-, A_2B-, and AB_2-type miktoarm star copolyethers, where A and B represent the hydrophobic and hydrophilic blocks, respectively, via the *t*-Bu-P_4-catalyzed ROP of decyl glycidyl ether (**M1**) as a hydrophobic monomer and 2-(2-(2-methoxyethoxy)ethoxy)ethyl glycidyl ether (**M2**) as a hydrophilic monomer (**Scheme 2-1**). The $(AB)_3$-, $(BA)_3$-, $(AB)_4$-, and $(BA)_4$-type star-block copolyethers were synthesized in one step according to the "core-first method", in which 1,3,5-benzenetrimethanol and 1,2,4,5-benzenetetramethanol were used as the initiator. On the other hand, the author employed the "coupling-onto" approach to synthesize the A_2B_2-, A_2B-, and AB_2-type miktoarm star copolyethers. The azido- and ethynyl-functionalized prepolymers, which had been separately prepared via the *t*-Bu-P_4-catalyzed ROP, were coupled by the click reaction, producing the desired miktoarm star copolyethers. With a comprehensive set of the block copolyethers in hand, the critical micelle concentration, the morphology, and cloud point were evaluated in water to provide an insight into the correlation between the branched architecture and self-assembly properties.

Scheme 2-1. Synthesis of amphiphilic star-block and miktoarm star copolyethers via *t*-Bu-P_4-catalyzed ring-opening polymerization

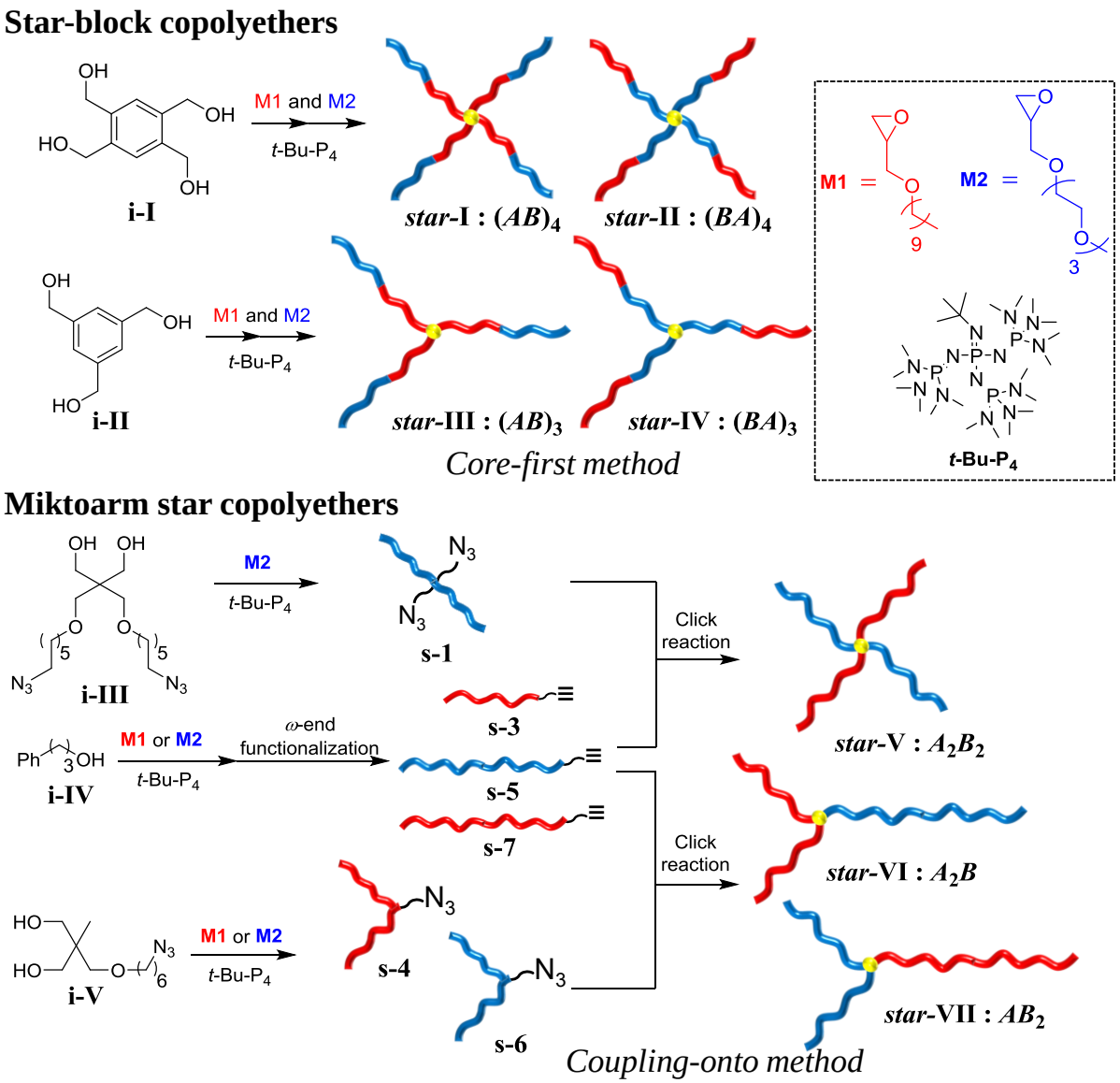

2.2 Results and Discussion

2.2.1 Synthesis of Four-Armed Star-Shaped Poly(butylene oxide)

The author first demonstrated the synthesis of the four-armed star-shaped poly(butylene oxide) (***star*-PBO**) to verify the synthetic strategy in this study based on the core-first approach. 1,2,4,5-benzenetetramethanol (**i-I**) was used as the tetraol initiator to obtaine the ***star*-PBO** because the linkage between a benzyloxy group in the core unit and a PBO arm was expected to be easily cleaved by a hydrogenolysis to confirm the homogeneous growth of each PBO arm during the polymerization (**Scheme 2-2**).

Scheme 2-2. Synthesis of four-armed star-shaped poly(butylene oxide)s (***star*-PBO**) by the *t*-Bu-P_4-catalyzed ROP of butylene oxide (BO).

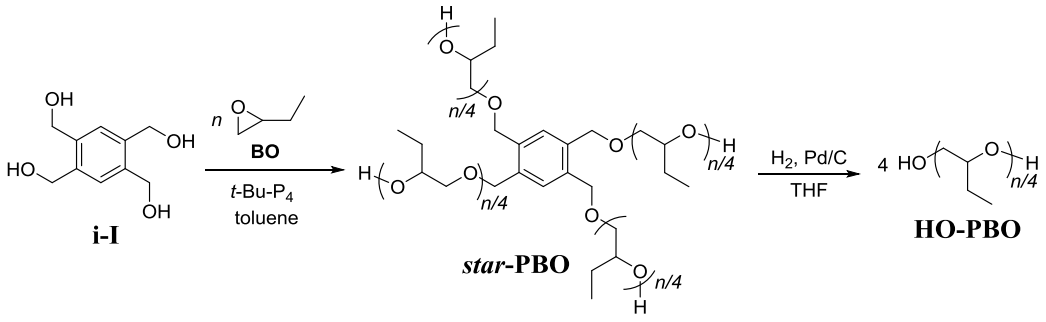

The *t*-Bu-P_4-catalyzed ROP of BO in toluene was carried out with the $[BO]_0/[\mathbf{i\text{-}I}]_0$ ratios of 60/1 at room temperature. The polymerization system was heterogeneous during the early stage and became homogeneous within ca. 1 h because the initiator was insoluble in toluene. The monomer conversion (conv.) reached >99% after 20 h, which was directly

determined from the ^{1}H NMR spectrum of the aliquots of the polymerization mixture in $CDCl_3$. The polymerization mixture was purified by passing through a pad of alumina to remove the catalyst residue, giving the product as a colorless viscous liquid in a 30.6% isolated yield. The SEC trace of the product exhibits a unimodal peak with a molecular weight distribution (*Đ*) of 1.03, as shown in **Figure 2-1**.

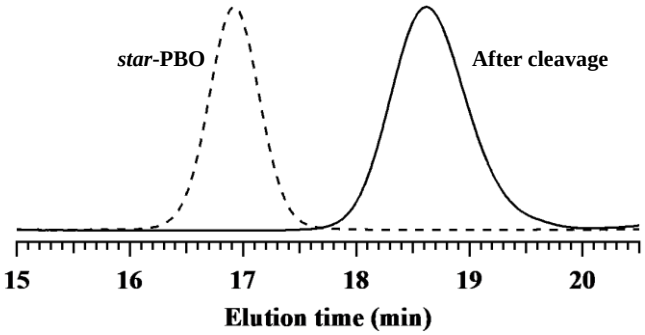

Figure 2-1. SEC traces of four-armed star-shaped poly(butylene oxide) (***star*-PBO**; $M_{n,NMR}$ = 4650 g mo^{-1}) and the cleaved PBO arm.

The ^{1}H NMR spectrum of the product shows signals in the ranges of 3.29 – 3.75, 1.36 – 1.69, and 0.75 – 1.05 ppm due to the protons of the PBO backbone (protons *b*, *c*, *d*, and *e*, respectively), while a minor signal due to the benzyl protons (proton *a*) is clearly observed at 4.52 ppm (**Figure 2-2a**). In addition, only one signal due to an aromatic proton was observed at 7.37 ppm, meaning that the four hydroxymethyl groups of **i-I** initiated the polymerization to give a four-armed star-shaped PBO. The number average molecular weight estimated by NMR ($M_{n,NMR}$) well agreed with that ($M_{n,calc}$) calculated by the monomer

conversion and the initial ratio of $[BO]_0/[\mathbf{i\text{-}I}]_0$; $M_{n,NMR}$ = 4,650 g mol^{-1} and $M_{n,calc}$ = 4,520 g mol^{-1}, indicating that the initiation efficiency of **i-I** was highly quantitative. The number average degree of polymerization (DP) was calculated to be 56. In addition, the MALDI-TOF MS spectrum of ***star*-PBO** shows only one set of peaks, which is assignable to the expected PBO structure having a benzenetetramethanol residue because the peak of the resultant polymer at *m*/*z* of 4,400.91 Da agreed with the 58-mer of PBO initiated from **i-I** (4,400.41 Da, calculated for $[M + Na]^+$) (**Figure 2-3a**). Thus, no side reactions, such as a chain transfer reaction to the monomer, occurred during the polymerization.

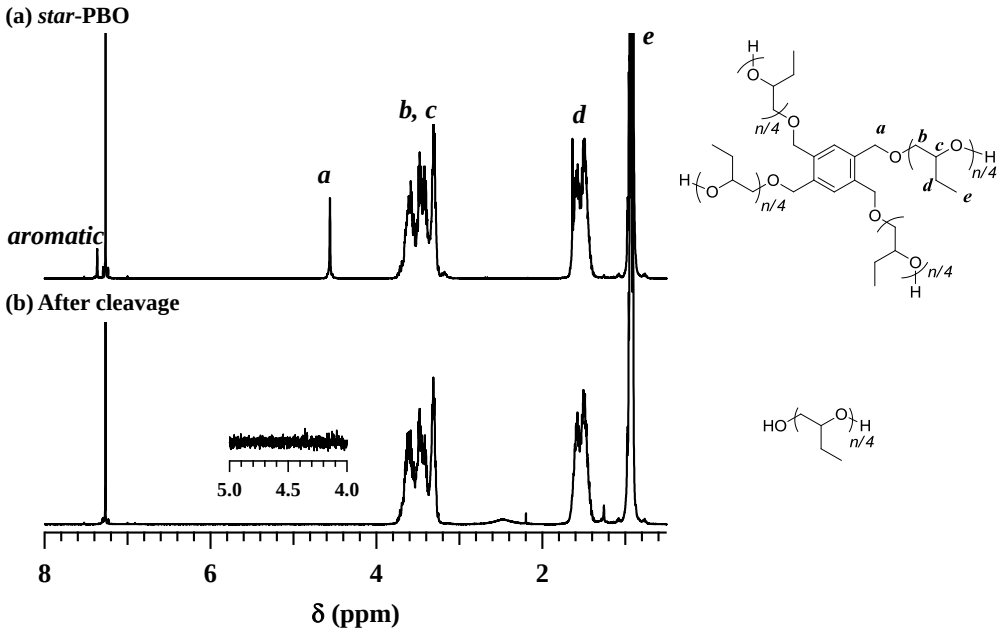

Figure 2-2. ^{1}H NMR spectra of (a) four-armed star-shaped poly(butylene oxide) (***star*-PBO**; $M_{n,NMR}$ = 4,650 g mol^{-1}) and (b) the cleaved poly(butylene oxide) arm in $CDCl_3$ (400 MHz). The inset shows the expanded ^{1}H NMR spectrum of the cleaved arm.

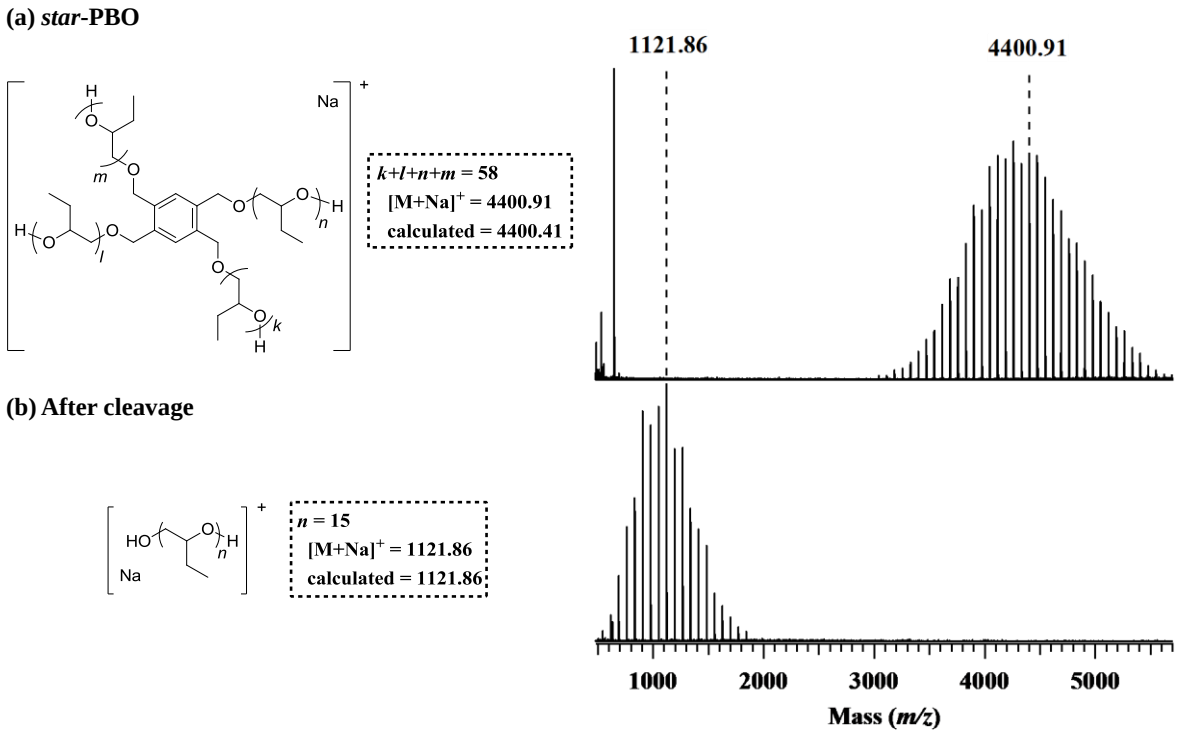

Figure 2-3. MALDI-TOF MS spectra of (a) four-armed star-shaped poly(butylene oxide) (***star*-PBO**; $M_{n,NMR}$ = 4,650 g mol^{-1}) and (b) the cleaved poly(butylene oxide) arm.

To provide an insight into the arm length and number of the star-shaped PBO, cleavage of the linkage between the initiator residue and PBO arms was performed. The cleavage experiment for ***star*-PBO** was carried out by catalytic hydrogenation using a Pd/C under a hydrogen atmosphere for 24 h, and the reaction product was obtained in an 83.0% isolated yield after removing the Pd/C. In the ^{1}H NMR spectrum of the cleaved PBO arm (**Figure 2-2b**), the signal due to the benzyl protons and aromatic protons completely disappeared, indicating that the hydrogenolysis of ***star*-PBO** perfectly occurred. **Figure 2-1** displays the SEC traces of ***star*-PBO** and the cleaved PBO arm. After the cleavage

experiment, the SEC trace shifted to the lower molecular weight region, and the SEC trace retained the unimodal dispersity with the $Đ$ value of 1.13. The MALDI-TOF MS measurement was employed to compare the absolute molecular weights of ***star*-PBO** and its cleaved arm (**Figure 2-3**). The MALDI-TOF MS spectrum of the cleaved arm from ***star*-PBO** shows one set of peaks, which is assignable to the structure of PBO with two hydroxyl groups at both the α- and ω-chain ends because the peak of the resultant polymer at m/z of 1,121.86 Da well agreed with the 15-mer of the cleaved PBO arm (1,121.86 Da, calculated for $[M + Na]^+$). The number average molecular weight calculated from the MALDI-TOF MS ($M_{n,MS}$) for the cleaved PBO arm was 1,104.93 g mol^{-1}, while that for ***star*-PBO** was 4,392.05 g mol^{-1}. Thus, the arm number of ***star*-PBO** was calculated to be 3.97 by dividing the $M_{n,MS}$ of ***star*-PBO** by that of the cleaved PBO arm. These results provided definitive evidence for the homogeneous growth of the PBO arms from each hydroxymethyl group of the initiator to afford the ***star*-PBO** with the desirable arm numbers and uniform arm length. Hence, the *t*-Bu-P_4-catalyzed ROP of the substituted epoxy monomer coupled with the initiator possessing multiple numbers of hydroxyl groups is one of the useful core-first methods for the precise synthesis of star-shaped polyethers.

2.2.2 Synthesis of Amphiphilic Linear and Star-block Copolyethers

2.2.2-1 Synthesis of Amphiphilic Linear block Copolyethers

Before the synthesis of star-shaped block copolyethers, the author confirmed the *t*-Bu-P_4-catalyzed ROP properties of decyl glycidyl ether (**M1**) and 2-(2-(2-methoxyethoxy)ethoxy)ethyl glycidyl ether (**M2**). The polymerizations of **M1** and **M2** were carried out using 3-phenyl-1-propanol (**i-IV**) as the initiator at the $[monomer]_0/[\textbf{i-IV}]_0/[t\text{-Bu-P}_4]_0$ ratio of 25/1/1 in toluene at room temperature (**Scheme 2-3**).

Scheme 2-3. (a) Homopolymerization and (b) block copolymerization for decyl glycidyl ether (**M1**) and 2-(2-(2-methoxyethoxy)ethoxy)ethyl glycidyl ether (**M2**)

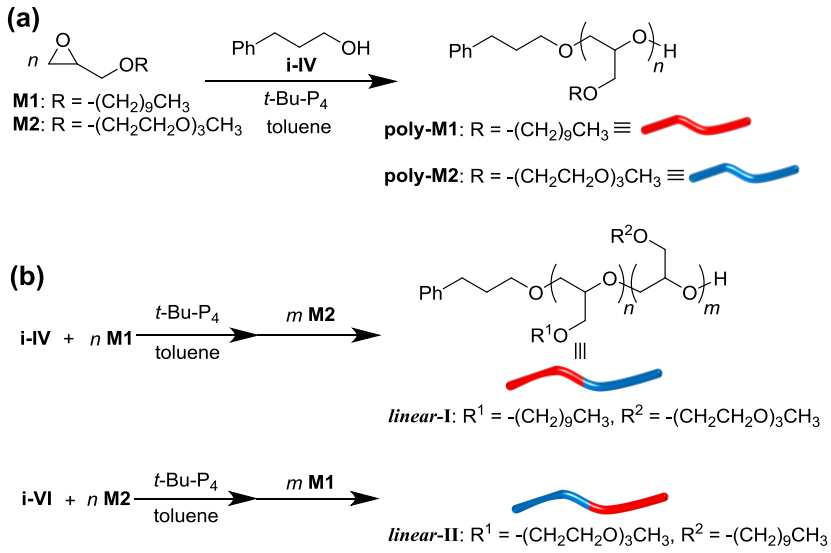

The monomer conversions of **M1** and **M2** reached >99% within 20 h to produce the narrowly dispersed **poly-M1** and **poly-M2** with the M_ns determined from the NMR of 5,710 and 5,750 g mol^{-1}, respectively. The $M_{n,calc}$s calculated from the initial monomer-to-initiator

ratio and monomer conversion matched with the $M_{n,NMR}$s of **poly-M1** and **poly-M2**, indicating the controlled nature of the *t*-Bu-P_4-catalyzed ROP systems. The NMR and matrix-assisted laser desorption/ionization mass spectral analyses of the obtained polymers revealed that the polymerizations of **poly-M1** and **poly-M2** proceeded without side reactions, such as the transfer reaction to the monomer (**Table 2-1**, **Figures 2-4** and **2-5**).

Table 2-1. The *t*-Bu-P_4-catalyzed ROP of **M1** and **M2**[a]

run	monomer (M)	$[M]_0/[\textbf{i-IV}]_0/[t\text{-Bu-P}_4]_0$	conv.[b] (%)	$M_{n,calc}$[b] (g mol^{-1})	$M_{n,NMR}$[b] (g mol^{-1})	$M_{n,SEC}$[c] (g mol^{-1})	$Đ$[c]
1	**M1**	25/1/1	>99	5,500	5,710	4,890	1.05
2		50/1/1	>99	10,900	10,200	8,730	1.03
3	**M2**	25/1/1	>99	5,640	5,750	4,440	1.05
4		50/1/1	>99	11,000	10,700	7,440	1.06

[a] Ar atmosphere; solvent, toluene; temperature, r.t.; polymerization time, 20 h; $[M]_0$ = 2.5 mol L^{-1}. [b] Estimated by ^{1}H NMR. [c] Estimated by SEC in THF using polystyrene standard.

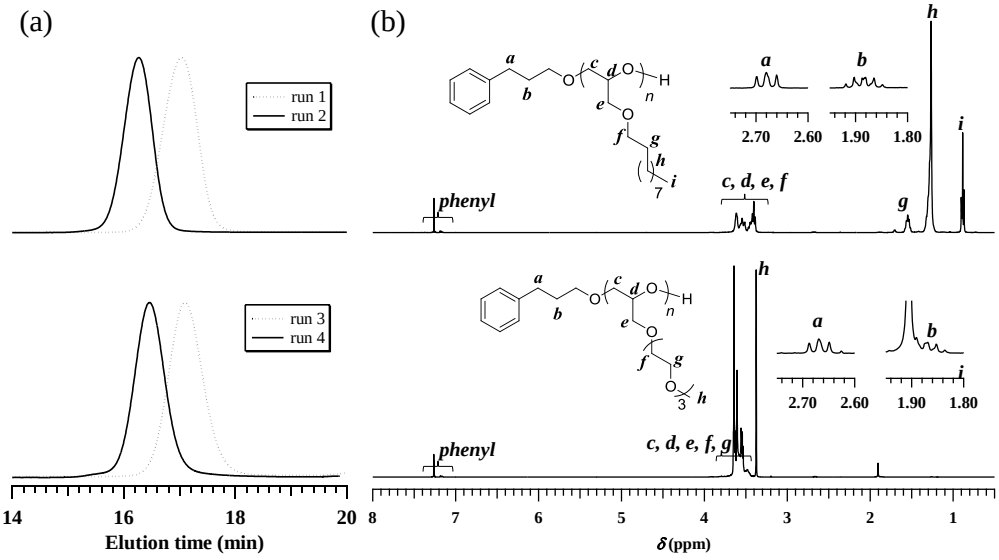

Figure 2-4. (a) SEC traces of **poly-M1** and **poly-M2**, (b) ^{1}H NMR spectra of **poly-M1** (run 2 in Table 2-1) and **poly-M2** (run 4) in $CDCl_3$ (400 MHz).

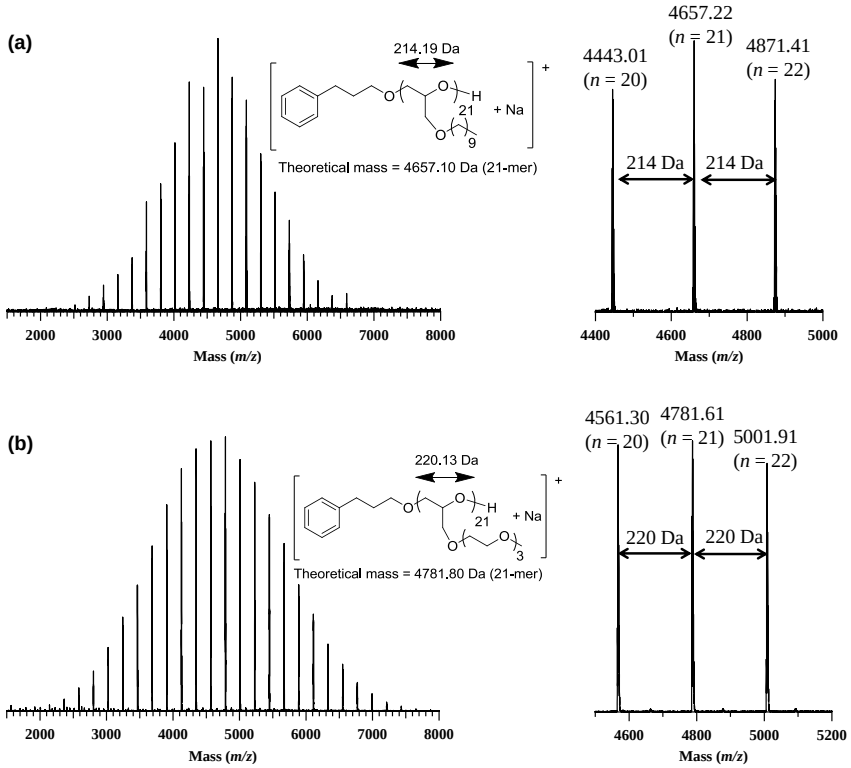

Figure 2-5. MALDI-TOF MS analysis of (a) **poly-M1** ($M_{n,NMR}$ = 5,710 g mol^{-1}) and (b) **poly-M2** ($M_{n,NMR}$ = 5,750g mol^{-1}). Both of the MALDI-TOF MS spectra showed one set of peaks, which is assignable to the expected structures of poly-**M1** and poly-**M2** with a 3-phenyl-1-propoxy group. For example, the peak observed in the spectrum (a) at *m*/*z* of 4657.22 Da well agreed with the theoretical mass of the 21-mer of poly-**M1** having a 3-phenyl-1-propoxy group (4,657.10 Da, calculated for [M + Na$^+$]). No peak assignable to the product coming from the side reactions was detected.

Based on these results, the linear amphiphilic diblock copolymers, ***linear*-I** and ***linear*-II**, were then synthesized via the sequential block copolymerization of **M1** and **M2**, as shown in **Scheme 2-3**. Unless otherwise noted, the number-average degree of polymerization (DP) of the targeted block cpolyether (poly-**M1**/poly-**M2**) is adjusted to be around 100 (50/50). A **poly-M1** with the $M_{n,NMR}$ of 10,800 g mol^{-1} and $Đ$ of 1.03 was first prepared by the *t*-Bu-P$_4$-catalyzed ROP of **M1** using **i-IV** as the initiator with the perfect

monomer conversion at the [**M1**]$_0$/[**i-IV**]$_0$/[*t*-Bu-P$_4$]$_0$ ratio of 50/1/1. The polymerization was further continued by the subsequent addition of 50 equivalents of **M2** with respect to **i-IV** to afford ***linear*-I** with the $M_{n,NMR}$ of 21,900 g mol^{-1} and $Đ$ of 1.04 in 90% yield. The SEC trace of **poly-M1** was completely shifted to the high molecular weight region after the subsequent polymerization of **M2**, indicating the successful block copolymerization of **M1** and **M2** (**Figure 2-6a**). The ^{1}H NMR spectrum of ***linear*-I** showed signals due to both the **poly-M1** and **poly-M2** along with the minor signals due to the 3-phenyl-1-propoxy group at 2.68 and 1.85 ppm, confirming that the obtained ***linear*-I** possesses an initiator moiety at the ω-chain end (**Figure 2-7**). Noteworthy is that the block copolymerization of **M1** and **M2** with the opposite monomer addition sequence also produced the corresponding block copolymer, ***linear*-II**, with the $M_{n,NMR}$ of 21,800 g mol^{-1} and $Đ$ of 1.05 (**Figure 2-6b**). Therefore, the *t*-Bu-P$_4$-catalyzed block copolymerizations of **M1** and **M2** were successful method to obtain the amphiphilic block copolyethers.

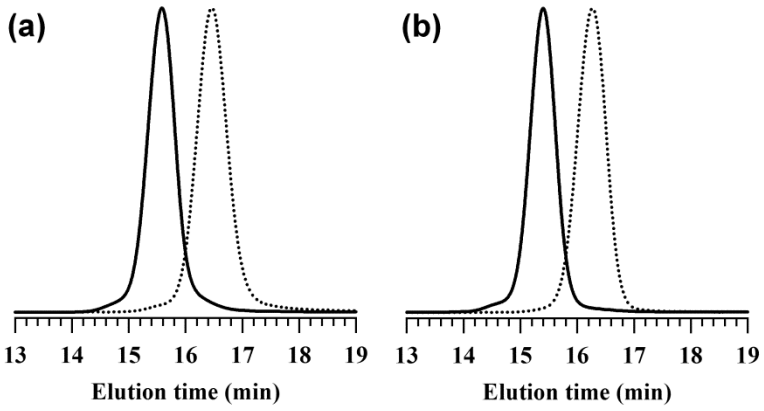

Figure 2-6. SEC traces of (a) ***linear*-I** and (b) ***linear*-II**. The dashed lines show the **poly-M1** and **poly-M2** obtained by the first polymerization.

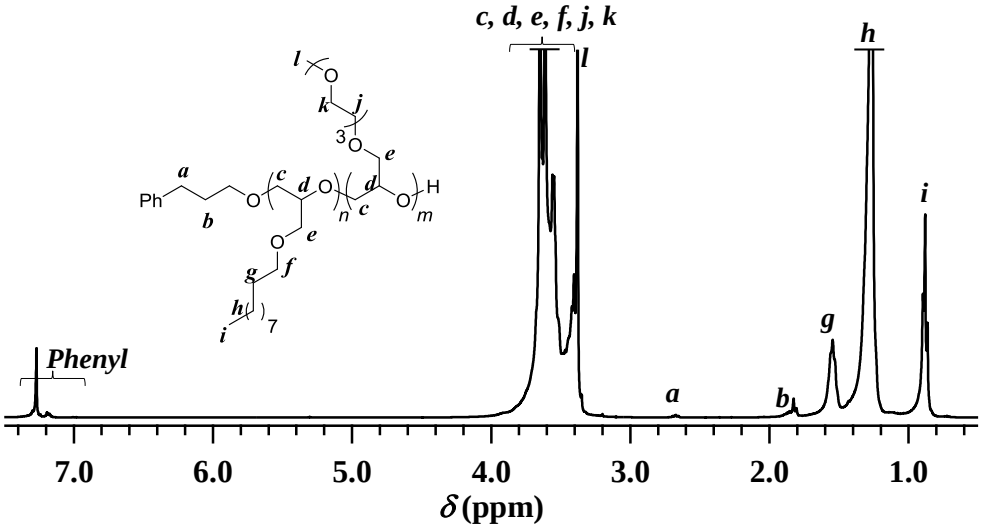

Figure 2-7. ^{1}H NMR spectrum of ***linear*-I** in $CDCl_3$ (400 MHz).

2.2.2-2 Synthesis of Amphiphilic Star-block Copolyethers

Next, the author applied the *t*-Bu-P_4-catalyzed ROP system to the synthesis of the amphiphilic $(AB)_4$- and $(BA)_4$-type star-block copolyethers (***star*-I** and ***star*-II**) by the sequential block copolymerization of **M1** followed by **M2** (and vice versa) using **i-I** as the tetraol initiator based on the core-first method (**Scheme 2-4**).

Scheme 2-4. Synthetic pathway for amphiphilic star-block copolyethers, ***star*-I**, ***star*-II**, ***star*-III**, and ***star*-IV** ($R^1 = –(CH_2)_9CH_3$, $R^2 = –(CH_2CH_2O)_3CH_3$)

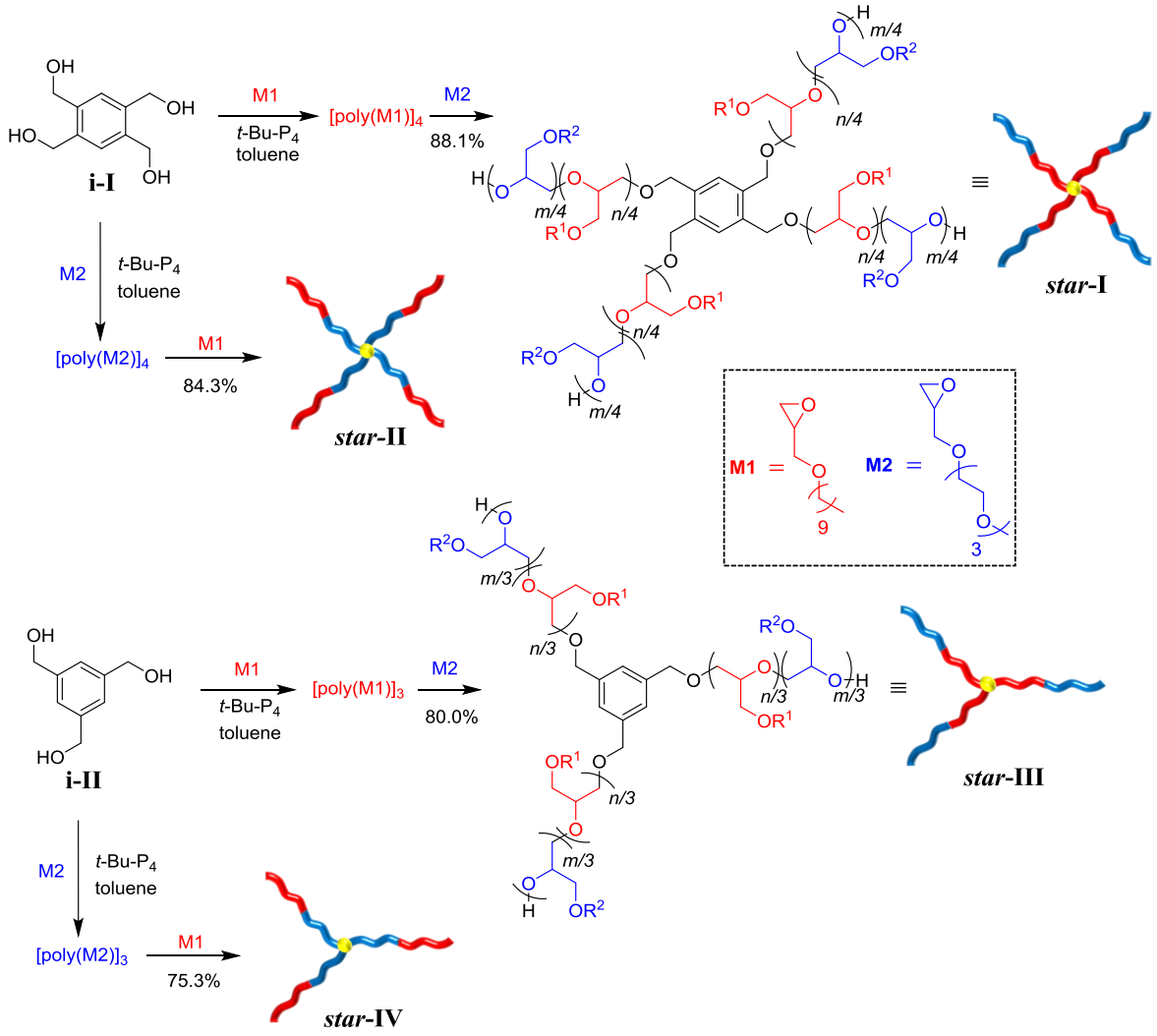

For the synthesis of ***star*-I**, **M1** was first polymerized with the $[\mathbf{M1}]_0/[\mathbf{i\text{-}1}]_0/[t\text{-BuP}_4]_0$ ratio of 50/1/1, and the monomer conversion of **M1** reached >99% after 20 h of polymerization to provide a four-armed star-shaped poly(**M1**) ($[\text{poly}(\mathbf{M1})]_4$). Subsequently, the polymerization was continued by the addition of 50 equiv. of **M2**, producing the desired ***star*-I** in 88.1% yield. The SEC trace of $[\text{poly}(\mathbf{M1})]_4$ obtained by the first polymerization ($M_{n,SEC}$ = 8,840 g mol^{-1}) clearly shifted toward the higher molecular weight region after the second polymerization ($M_{n,SEC}$ = 16,800 g mol^{-1}) while retaining the narrow $Đ$ of 1.03, which confirmed the success of the block copolymerization (**Figure 2-8a**). In the ^{1}H NMR spectrum of ***star*-I**, the signals assignable to the polyether backbone were observed along with a minor signal due to the benzyl protons of the corresponding initiator residue (4.50 ppm) (**Figures 2-8a** and **2-9a**). Based on the end group analysis by NMR, the DPs were calculated to be 51 for **M1** and 50 for **M2** (**Table 2-2**). In addition, the $M_{n,NMR}$ of ***star*-I** well agreed with the $M_{n,calc}$; $M_{n,NMR}$ = 22,200 g mol^{-1} and $M_{n,calc}$ = 21,900 g mol^{-1}. With this established procedure, the $(BA)_4$-type star-block copolyether ***star*-II** ($M_{n,NMR}$ = 22,200 g mol^{-1} and $Đ$ = 1.02) was also prepared by the sequential polymerization of **M2** (50 eq.) followed by **M1** (50 eq.) in 84.3% yield. The SEC traces of the obtained polymers from each polymerization stage strongly supported the successful synthesis of the well-defined ***star*-II** (**Figure 2-8b**). These results confirmed that the *t*-Bu-P_4-catalyzed ROP was an effective

method to produce the well-defined star-block copolyethers with a predictable molecular weight and narrow *Đ*.

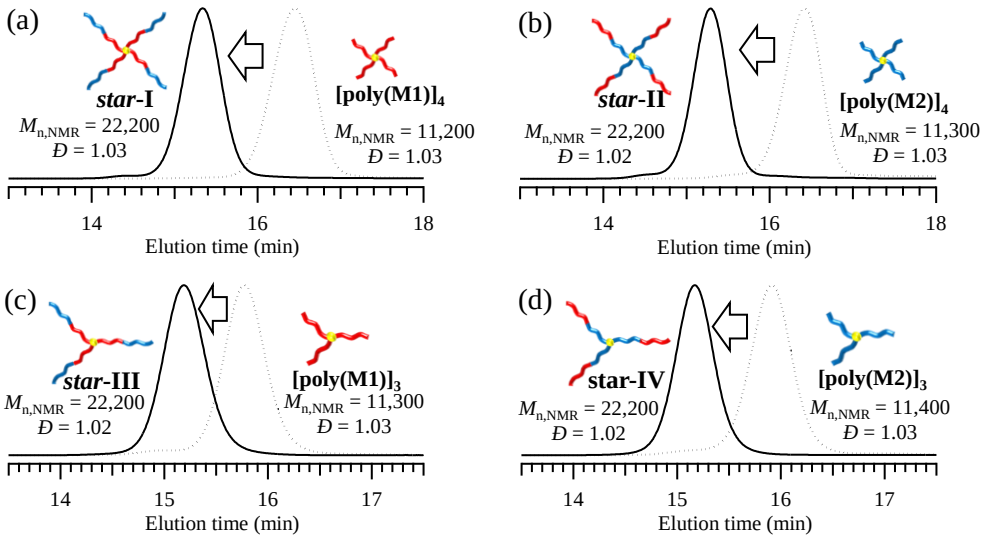

Figure 2-8. SEC traces of (a) ***star*-I**, (b) ***star*-II**, (c) ***star*-III**, and (d) ***star*-IV**. The dotted lines show the polymer obtained from the first polymerizations.

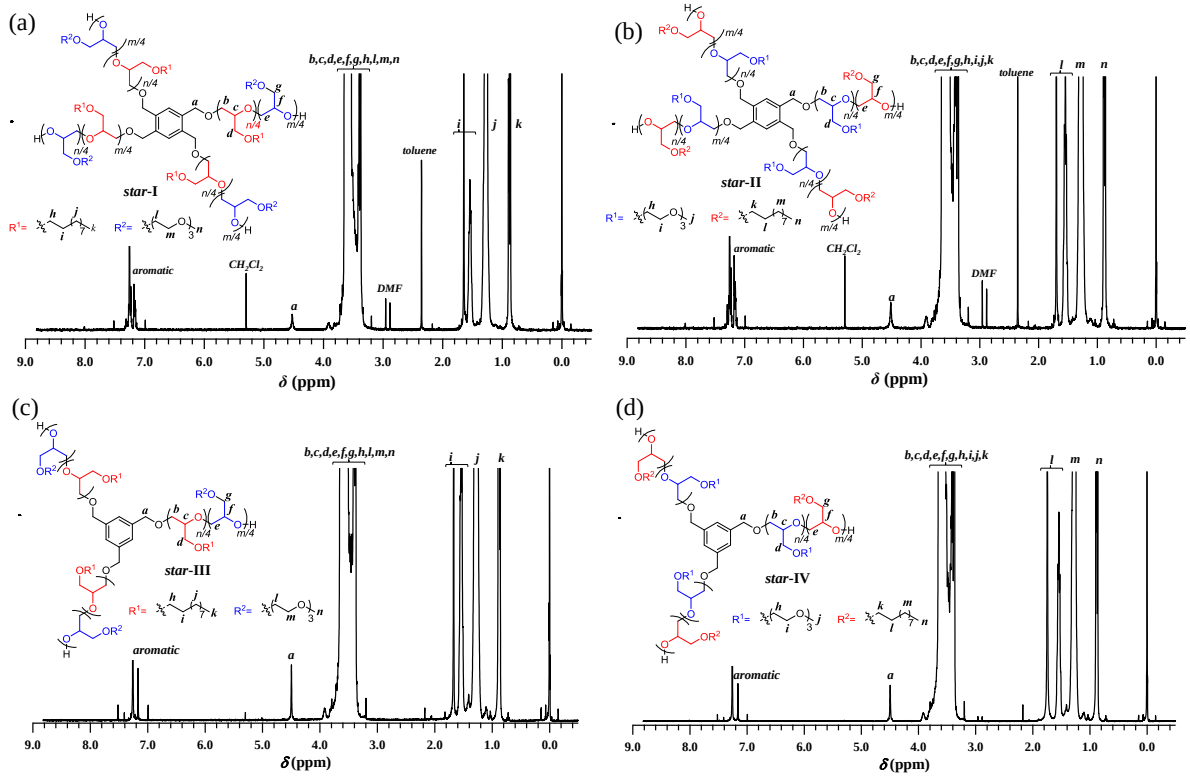

Figure 2-9. ^{1}H NMR spectrum of (a) ***star*-I**, (b) ***star*-II**, (c) ***star*-III**, and (d) ***star*-IV** in $CDCl_3$ (400 MHz).

Table 2-2. Synthesis of the Star-block Copolyethers via the *t*-Bu-P_4-catalyzed Block Copolymerization [a]

polymer	monomer		$[M]_0/[\mathbf{i\text{-}I}]_0/[t\text{-Bu-}P_4]_0$	DP [b]	$M_{n,calc}$ [b] [g mol^{-1}]	$M_{n,NMR}$ [b] [g mol^{-1}]	$M_{n,SEC}$ [c] [g mol^{-1}]	$Đ$ [c]
***star*-I**	1 st	**M1**	50/1/1	51	10,900	11,200	8,840	1.03
	2 nd	**M2**	50/1/1	50	21,900	22,200	16,800	1.03
***star*-II**	1 st	**M2**	50/1/1	50	11,200	11,300	9,100	1.03
	2 nd	**M1**	50/1/1	51	21,900	22,200	16,200	1.02
***star*-III**	1 st	**M1**	50/1/1	52	10,900	11,300	10,500	1.03
	2 nd	**M2**	50/1/1	50	21,900	22,200	15,600	1.02
***star*-IV**	1 st	**M2**	50/1/1	51	11,200	11,400	9,630	1.03
	2 nd	**M1**	50/1/1	51	21,900	22,200	15,900	1.02

[a] Ar atmosphere; solvent, toluene; temperature, r.t.; polymerization time, 20 h; $[M_{1st}]_0$ = 2.5 mol L^{-1}, $[M_{2nd}]_0$ = 1.25 mol L^{-1}. [b] Determined by ^{1}H NMR in $CDCl_3$. [c] Determined by SEC in THF using polystyrene standards.

In a similar manner, the amphiphilic $(AB)_3$- and $(BA)_3$-type star-block copolyethers (***star*-III** and ***star*-IV**) were also synthesized by the *t*-Bu-P_4 catalyzed ROP combined with 1,3,5-benzenetrimethanol (**i-II**) as the triol initiator. The block polymerizations were carried out at the $[\mathbf{M1}]_0/[\mathbf{M2}]_0/[\mathbf{i1}]_0/[t\text{-Bu-}P_4]_0$ ratio of 50/50/1/0.5 in toluene at room temperature to give ***star*-III** and ***star*-IV** in 80.0% and 75.3% yields, respectively (**Scheme 2-4**). The clear increase in the SEC elution volume by the second polymerization indicated the success of the block copolymerizations, and the obtained products were observed to have the narrow $Đ$ value of 1.02 (**Figures 2-8c** and **d**). The ^{1}H NMR spectra of ***star*-III** and ***star*-IV** showed signals due to the polyether backbone along with the minor signals due to the initiator residue

at 4.50 ppm (**Figures 2-9c** and **d**), and the $M_{n,NMR}$ values of ***star*-III** and ***star*-IV** (22,200 and 22,200 g mol^{-1}, respectively) well agreed with the $M_{n,calc}$s (21,900 g mol^{-1}) (**Table 2-2**).

The star-block copolyethers were also subjected the cleavage of the linkages between the polyether arms and the initiator residue to verify the arm length and number of the obtained star-block copolyethers. The cleavage reaction was performed on ***star*-II** by hydrogenolysis using Pd/C as a catalyst under a hydrogen atmosphere (**Scheme 2-5**).

Scheme 2-5. Hydrogenolysis of ***star*-II** and α,ω-end acetylation of poly(**M2**)-*b*-poly(**M1**)

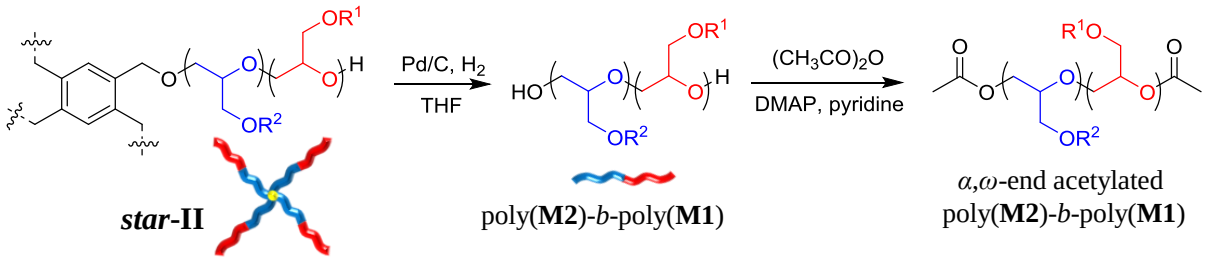

After the reaction for 48 h, the cleaved arm of ***star*-II** was isolated in 92.0% yield. In the ^{1}H NMR spectrum of the cleaved arm (**Figure 2-11b**), no signal due to the benzyl proton was observed, indicating that the linkages between the polyether arms and the initiator residue were perfectly cleaved. The SEC trace of the cleaved arms demonstrated a clean shift toward the lower molecular weight region ($M_{n,SEC}$ = 4,850 g mol^{-1}) as compared to ***star*-II** ($M_{n,SEC}$ = 16,200 g mol^{-1}), strongly supporting the complete cleavage of the four benzyl

positions on the initiator residue (**Figure 2-10a**). Importantly, the shape of the elution peak retained the unimodal and narrow $Đ$ of 1.04 during the cleavage reaction, which is an indication of the uniform arm length of ***star*-II**. The cleaved arm was treated with acetic anhydride in the presence of pyridine/DMAP to give the α,ω-end acetylated poly(**M2**)-*b*-poly(**M1**), which was used for determining the absolute molecular weight by end group analysis (**Scheme 2-5**). The signals due to the acetyl proton (*A*, 2.07 ppm), methylene proton at the α-chain end (*B*, 4.04 – 4.30 ppm), and methine proton at the ω-chain end (*C*, 5.09 ppm) were visible in the ^{1}H NMR spectrum of the product (**Figure 2-11c**), and the $M_{n,NMR}$ was determined to be 5,470 g mol^{-1}. Thus, the arm number of ***star*-II** was calculated to be 4.06 by dividing the $M_{n,NMR}$ of ***star*-II** by that of the cleaved arm. These results clearly demonstrated that the block copolymerization of **M1** and **M2** was initiated from each hydroxyl group on the initiator **i-I** to afford the amphiphilic four-armed star-block copolyethers with a uniform arm length.

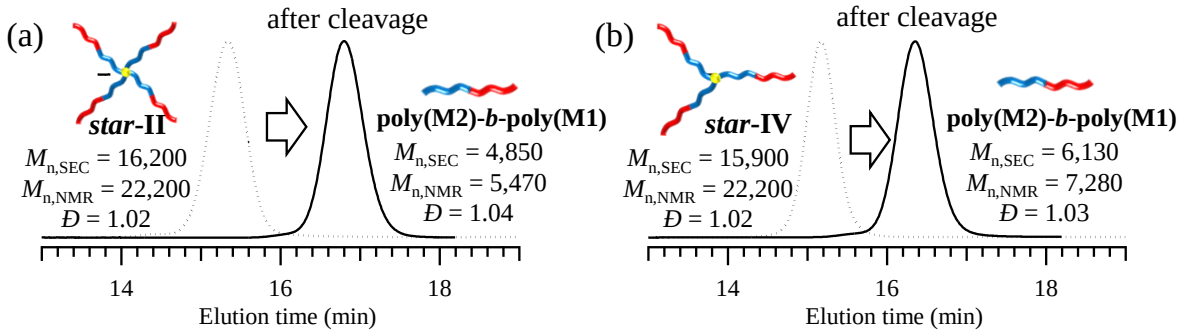

Figure 2-10. SEC traces of the star-block copolyethers (dotted line) and those of the cleaved arms (solid line).

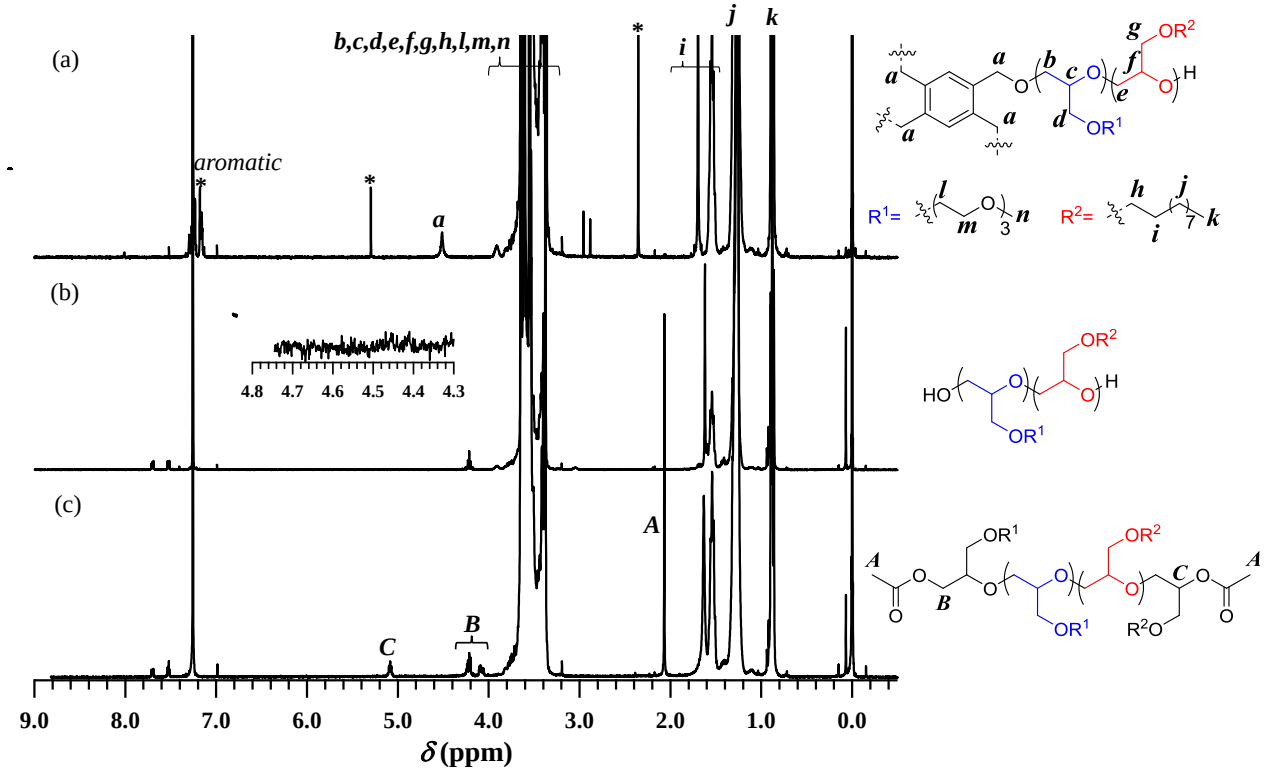

Figure 2-11. ^{1}H NMR spectra of (a) ***star*-II**, (b) the cleaved arm of ***star*-II**, and (c) the *α*,*ω*-end acetylated poly(**M2**)-*b*-poly(**M1**) in $CDCl_3$ (400 MHz). The inset shows the expanded ^{1}H NMR spectrum of (b). Asterisks mean residual solvent peak.

The cleavage reaction and *α*,*ω*-end acetylation of the cleaved arm were also performed on ***star*-IV**, which revealed that the three-armed star-block copolyethers with a uniform arm length had been obtained (**Figure 2-10b** and **Figure 2-12**). Thus, the author succeeded in producing a series of the amphiphilic star-block copolyethers with a fixed molecular weight and composition through the core-first approach combined with the *t*-Bu-P_4-catalyzed ROP.

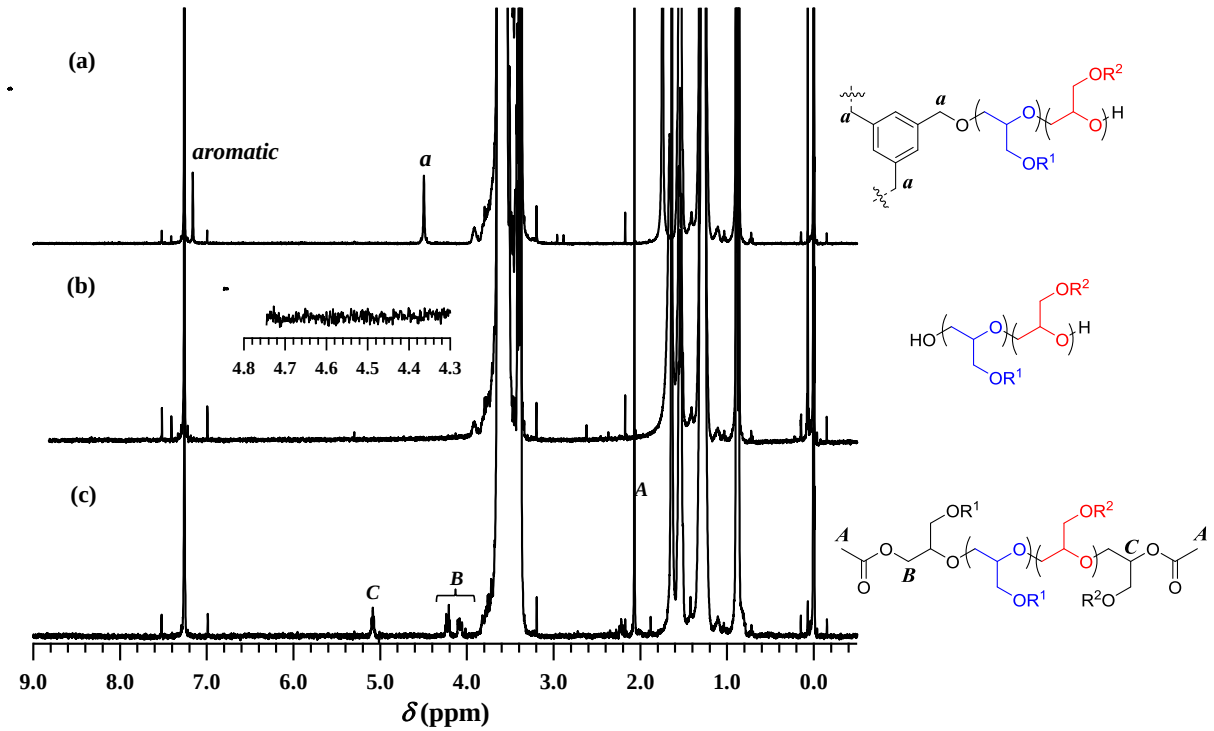

Figure 2-12. ^{1}H NMR spectra of (a) ***star*-IV**, (b) the cleaved arm of ***star*-IV**, and (c) the *α*,*ω*-end acetylated poly(**M2**)-*b*-poly(**M1**) in $CDCl_3$ (400 MHz). The inset shows the expanded ^{1}H NMR spectrum of (b). Asterisks mean residual solvent peak.

2.2.3 Synthesis of Amphiphilic Miktoarm Star Copolyethers

The author next investigated the synthesis of the amphiphilic miktoarm star copolyethers, i.e., the A_2B_2 (***star*-V**), A_2B (***star*-VI**), and AB_2-type miktoarm star copolyethers (***star*-VII**), in which the so-called coupling-onto method was employed as shown in **Scheme 2-6**.

Scheme 2-6. Synthetic pathway for amphiphilic miktoarm star copolyethers, ***star*-V**, ***star*-VI**, and ***star*-VII** ($R^1 = –(CH_2)_9CH_3$, $R^2 = –(CH_2CH_2O)_3CH_3$)

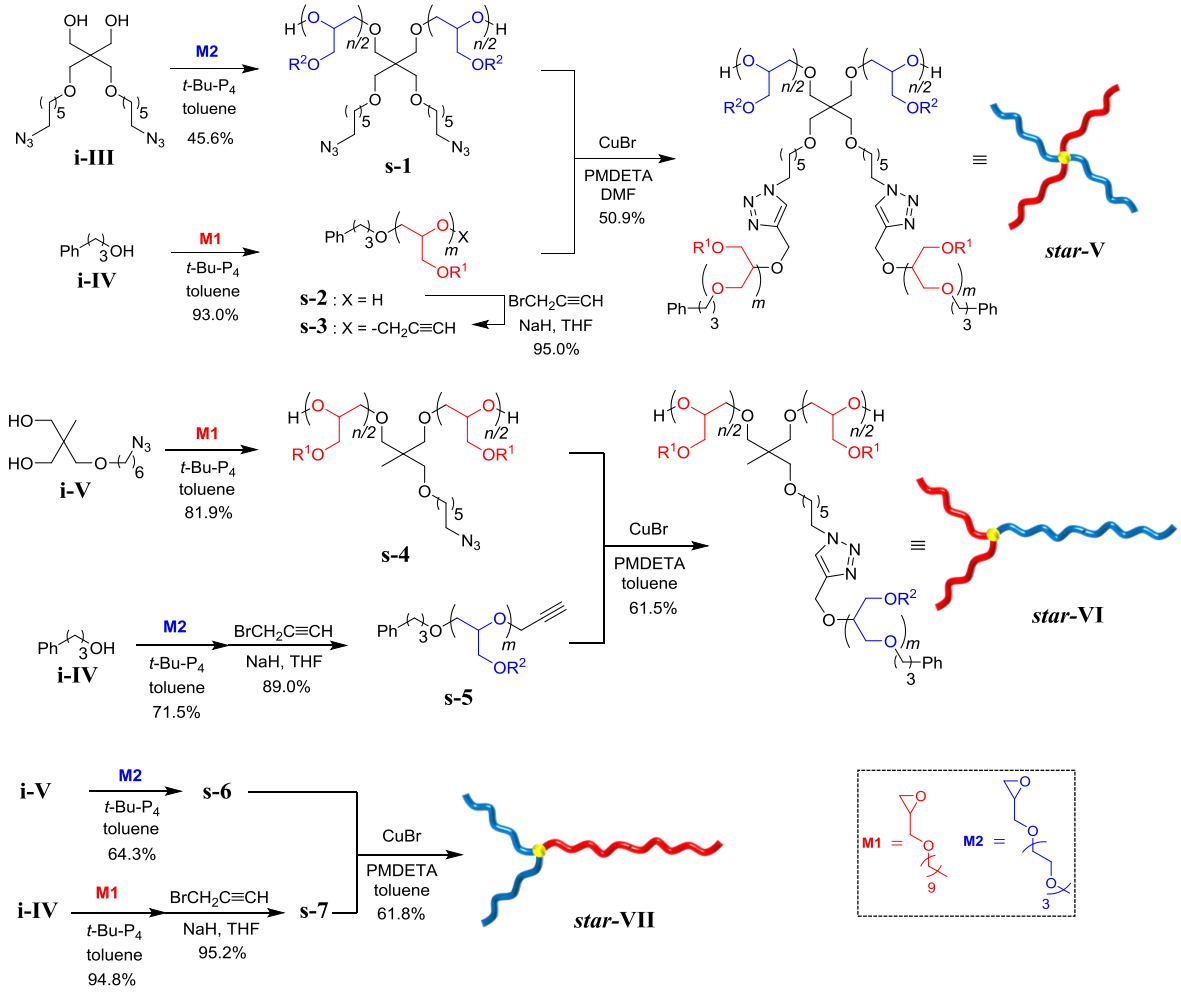

In order to synthesize ***star*-V**, two types of precursor polymers, i.e., a linear poly(**M2**) having two azido groups at the chain center (**s-1**) with the DP of ca. 50 and a poly(**M1**) having an ethynyl group at the ω-chain end with the DP of ca. 25 (**s-3**), were prepared (**Scheme 2-6**) . **s-1** was obtained in 45.6% yield by the *t*-Bu-P_4-catalyzed ROP using the [**M2**]$_0$/[**i-III**]$_0$/[*t*-Bu-P_4]$_0$ ratio of 50/1/1, and a monomodal and sharp elution peak with the $Đ$ value of 1.04 was observed in the SEC trace of the product (**Figure 2-13a**). In the ^{1}H NMR spectra of the product (**Figure 2-13b**), the signals assignable to the poly(**M2**) backbone were observed along with minor signals due to the methylene adjacent to the azido group of the initiator residues at 3.26 ppm (proton *A*), indicating that the polymerization of **M2** was initiated from the two hydroxyl groups on **i-III** to provide **s-1** ($M_{n,NMR}$ = 11,200 g mol^{-1}, $Đ$ = 1.04, DP = 49) with the predicted chemical structure. Next, **s-2** was prepared by the *t*-Bu-P_4-catalyzed ROP of **M1** with **i-IV** as the initiator, then the ω-end ethynylation of **s-2** was performed by treating with propargyl bromide in the presence of sodium hydride to give **s-3** ($M_{n,NMR}$ = 5,800 g mol^{-1}, $Đ$ = 1.05, DP = 25). The quantitative introduction of the ethynyl group at the ω-chain end was verified by comparing the integral values of the ^{1}H NMR signals due to the ethynyl group (proton *B* at 4.30 ppm and proton *C* at 2.50 ppm) and the initiator residue (proton *a'* at 2.68 ppm) (**Figure 2-13b**). The SEC trace of **s-3** also showed a unimodal peak with the $Đ$ value of 1.05 (**Figure 2-13a**). In addition, a matrix-assisted laser desorption ionization time-of-flight mass (MALDI-TOF MS) spectral

analysis provided detail information about the end group structures of **s-1** and **s-3** (**Figure 2-14, 2-15**). Thus, the NMR and MALDI-TOF MS results confirmed that the precursor polymers, **s-1** and **s-3**, with the expected structures had been produced.

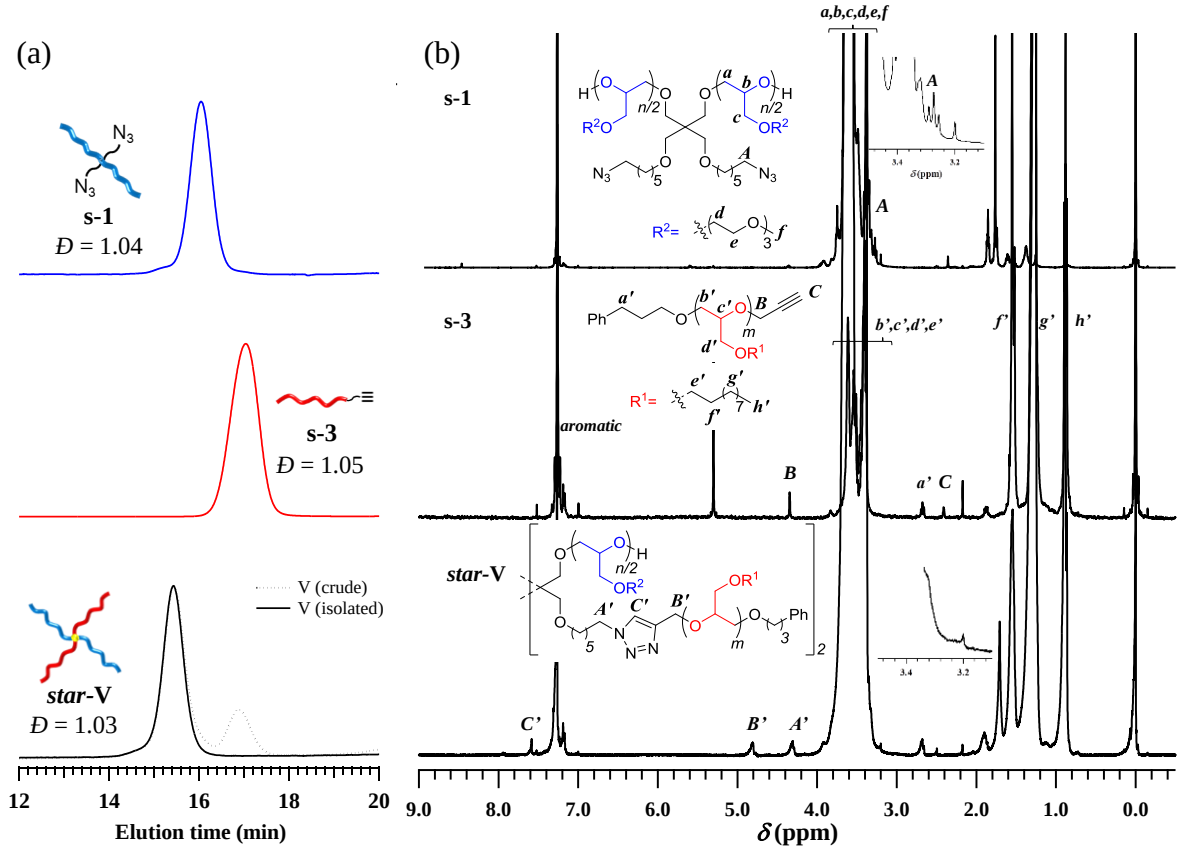

Figure 2-13. (a) SEC traces of **s-1**, **s-3**, and ***star*-V** (dotted line, before purification; solid line, after the purification using preparative SEC). (b) ^{1}H NMR spectra of **s-1**, **s-3**, and ***star*-V** in $CDCl_3$ (400 MHz). The insets show the expanded ^{1}H NMR spectra.

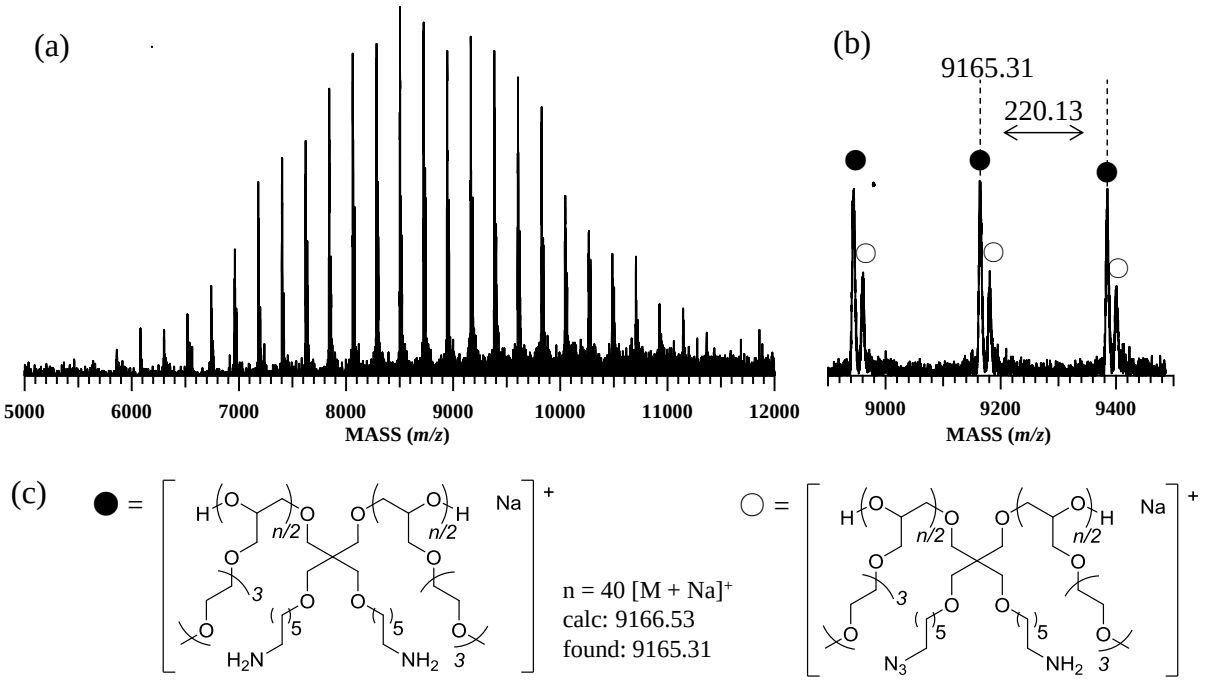

Figure 2-14. (a) MALDI-TOF MS spectrum of **s-1** ($M_{n,NMR}$ = 11,200 g mol^{-1}), (b) the expanded spectrum from 8900 to 9500 Da, and (c) the structure assignment. The MALDI-TOF MS spectrum of **s-1** showed two sets of peaks, which have a regular interval of 220.13 Da corresponding to the **M2** repeating unit. The major set of peaks denoted by the filled circle (●) was assigned to the poly(**M2**) having two amino groups at the chain center, and another set of peaks denoted by the open circle (○) was assigned to the poly(**M2**) having an amino group and an azido group at the chain center. It had been reported that the azido group decomposed into an amino group during the ionization process of the MALDI-TOF MS measurement,[37] thus the author concluded that the observed two species corresponded to the expected chemical structure of **s-1**.

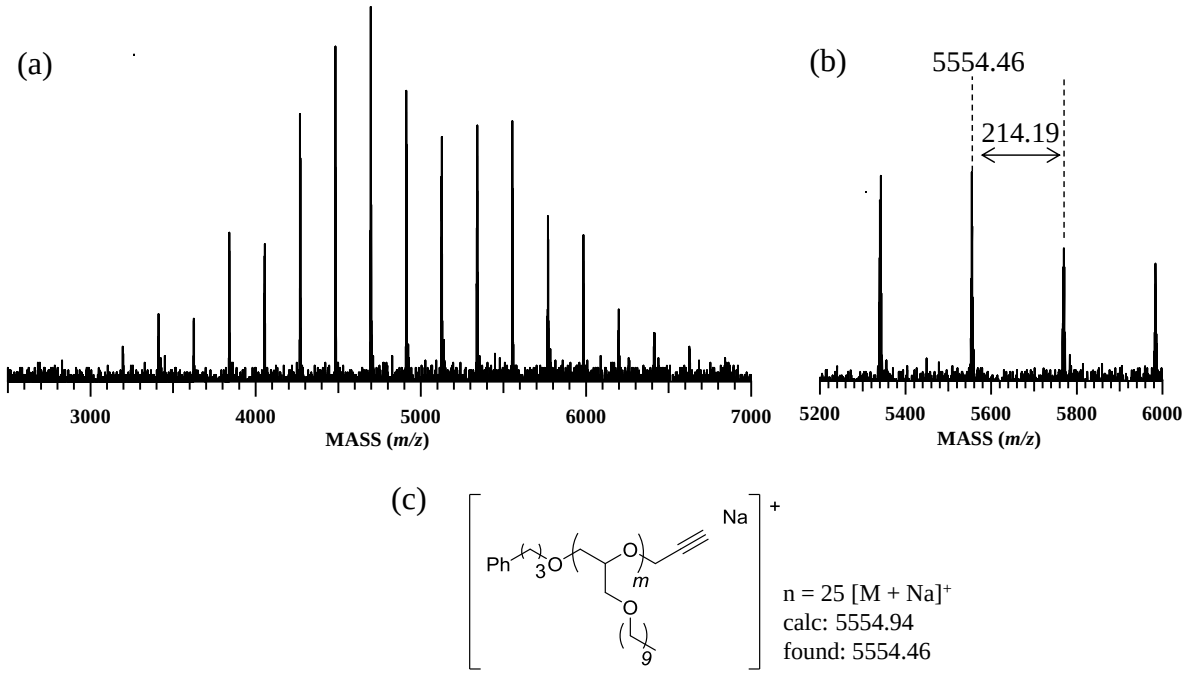

Figure 2-15. (a) MALDI-TOF MS spectrum of **s-3** ($M_{n,NMR}$ = 5,800 g mol^{-1}), (b) the expanded spectrum from 5200 to 6000 Da, and (c) the structure assignment. The MALDI-TOF MS spectrum of **s-3** showed only one set of peaks having a regular interval of 220.13 Da for the molar mass of the **M1** unit, and the peak at *m*/*z* of 5554.46 Da well agreed with the molar mass for the 25-mer of **s-3** with Na^+ (5554.94 Da).

The intermolecular click reaction of **s-1** and **s-3** was carried out using the CuBr/PMDETA catalyst system in DMF at 100 °C in which an excess amount of **s-3** was added with respect to **s-1**. The absence of the starting material **s-1** was confirmed by FT-IR analysis in which the absorption at 2098 cm^{-1} due to the azido groups completely disappeared (**Figure 2-16**). The obtained product was purified by removing the unreacted **s-3** using preparative SEC to give a light brown waxy solid in 50.9% yield. The SEC analysis revealed an increase in the molecular weight of the product when compared to the precursor polymers, **s-1** and **s-3** (**Figure 2-13a**). In addition, the dispersity value remained narrow ($Đ$ = 1.03). These

results indicated that the quantitative coupling of **s-1** and **s-3** had occurred to produce the A_2B_2-type miktoarm star copolyether ***star*-V**. The ^{1}H NMR spectra of the obtained product showed the new signals *A'* (4.26–4.40 ppm), *B'* (4.75–4.91 ppm), and *C'* (7.58–7.64 ppm) due to the newly formed triazole rings and it neighboring methylenes produced through the click reaction, while the signals due to the methylene adjacent to the azido group (*A*; 3.26 ppm) of **s-1** and the ethynyl group (*B*; 4.30 ppm, *C*; 2.39 ppm) of **s-3** completely disappeared (**Figure 2-13b**). In addition, the $M_{n,NMR}$ of 22,200 g mol^{-1} for the isolated ***star*-V** well agreed with the $M_{n,calc}$ of 22,400 g mol^{-1} (**Table 2-3**). These results definitely confirmed that the well-defined A_2B_2-type miktoarm star copolyether, ***star*-V**, was obtained with a sufficient purity.

Table 2-3. Synthesis of A_2B_2-type Miktoarm Star Copolyether (***star*-V**) and the Corresponding Precursors (**s-1** and **s-3**)

polymer	$M_{n,calc}$ [a] [g mol^{-1}]	$M_{n,NMR}$ [a] [g mol^{-1}]	$M_{n,SEC}$ [b] [g mol^{-1}]	$Đ$ [b]
s-1	11,400	11,200	9,420	1.04
s-3	5,530	5,800	4,900	1.05
***star*-V**	22,400	22,200	15,300	1.03

[a] Determined by ^{1}H NMR in $CDCl_3$. [b] Determined by SEC in THF using polystyrene standards.

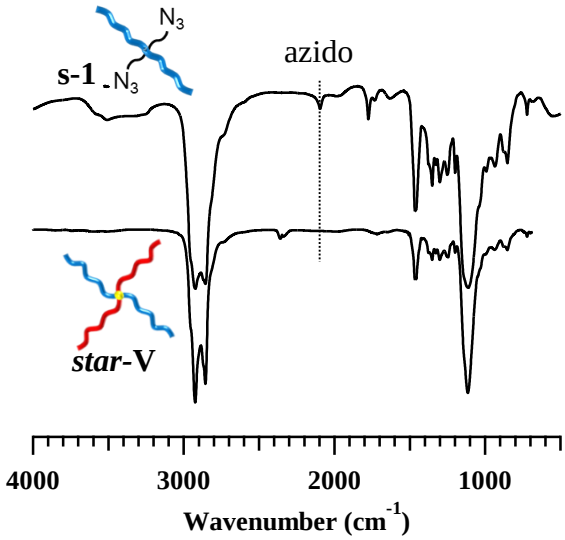

Figure 2-16. FT-IR spectra of **s-1** (upper) and ***star*-V** (lower).

The A_2B-type miktoarm star copolyether ***star*-VI** was also synthesized via the intermolecular click coupling strategy (**Scheme 2-6**). First, the *t*-Bu-P_4-catalyzed ROP of **M1** using **i-V** as an initiator was carried out at the [**M2**]$_0$/[**i-V**]$_0$/[*t*-Bu-P_4]$_0$ ratio of 50/1/1 to give the hydrophobic precursor polymer having an azido group at the chain center (**s-4**) in 81.9% ($M_{n,NMR}$ = 10,600 g mol^{-1}, $Đ$ = 1.03, DP = 49). The ^{1}H NMR spectrum of **s-4** showed the signals of the polyether backbone along with the minor signal at 3.26 ppm (proton A) due to the initiator residue (**Figure 2-17b**). In addition, the MALDI-TOF MS analysis definitely confirmed that **s-4** with the expected chemical structure was obtained (**Figure 2-18**). The hydrophilic precursor polymer having an ethynyl group at the ω-chain end (**s-5**; $M_{n,NMR}$ = 11,400 g mol^{-1}, $Đ$ = 1.04, DP = 50) was prepared by the ω-end ethynylation of the poly(**M2**) which was obtained by the *t*-Bu-P_4-catalyzed ROP of **M2** with **i-IV** as the initiator. The

intermolecular click reaction between **s-4** and **s-5** was carried out using the same condition as described for the reaction between **s-1** and **s-3**. The excess of **s-4** was removed by reacting with the propargyl-functionalized Wang resin (PSt-C≡CH), and the disappearance of **s-4** was confirmed by an FT-IR analysis (**Figure 2-19a**). The reacted mixture was then purified using an alumina column and preparative SEC to give a coupling product in 61.5% yield. The obtained polymer was identified to be the targeted miktoarm star copolymer ***star*-VI** by the ^{1}H NMR and SEC analyses. The ^{1}H NMR spectrum showed signals, *A'* (4.25–4.36 ppm), *B'* (4.74–4.84 ppm), and *C'* (7.59–7.62 ppm) due to the triazol ring and its neighboring methylenes, while the signals due to the ethynyl group (*B*; 4.33 ppm, *C*; 2.49 ppm) and the methylene adjacent to the azido group (*A*; 3.26 ppm) were not detected (**Figure 2-17b**). The $M_{n,NMR}$ (22,200 g mol^{-1}) of ***star*-VI** was well agreed with the predicted value (22,200 g mol^{-1}), and the *Đ* value was determined to be 1.05 by the SEC analysis (**Table 2-4**).

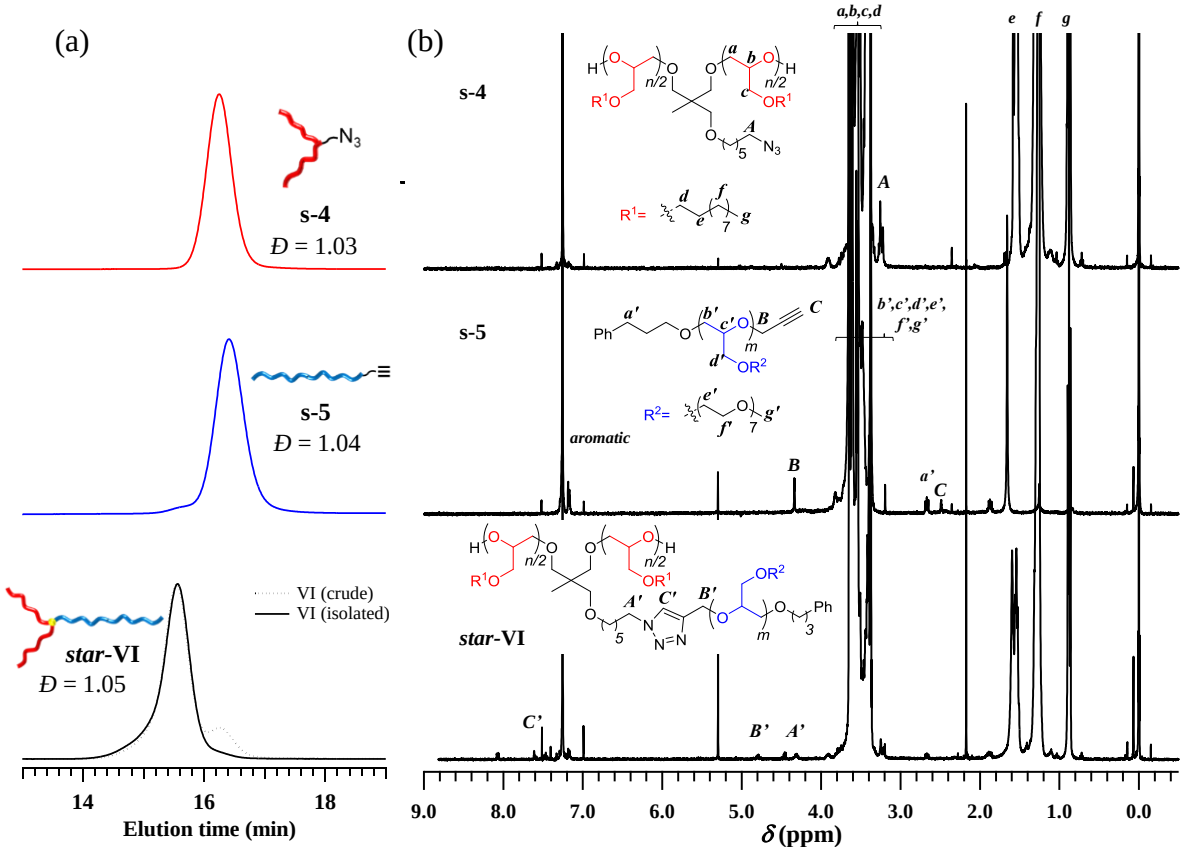

Figure 2-17. (a) SEC traces of **s-4**, **s-5**, and ***star*-VI** (dotted line, before purification; solid line, after the purification using preparative SEC). (b) ^{1}H NMR spectra of **s-4**, **s-5** and ***star*-VI** in $CDCl_3$ (400 MHz).

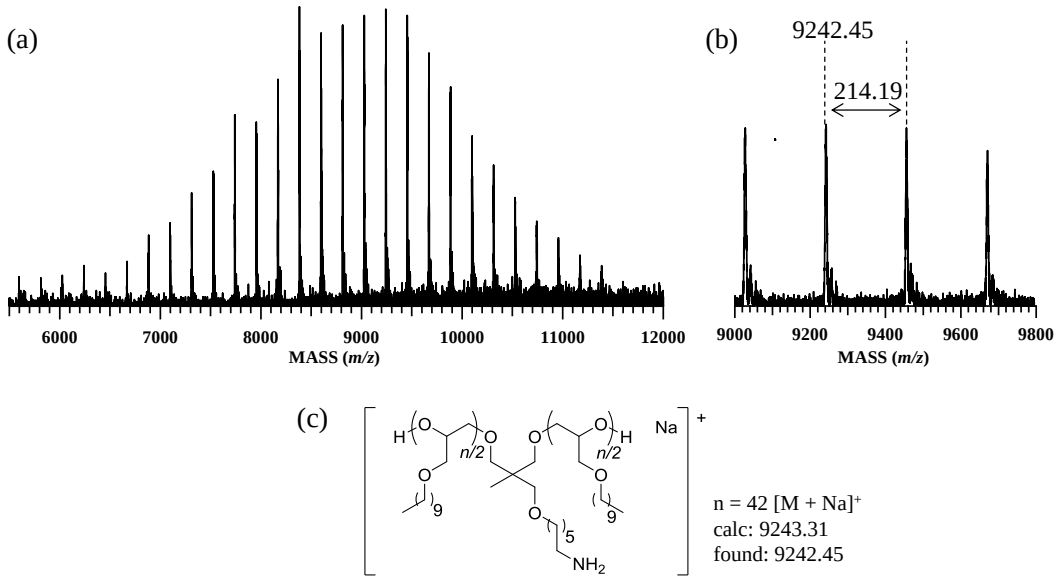

Figure 2-18. (a) MALDI-TOF MS spectrum of **s-4** ($M_{n,NMR}$ = 10,600 g mol^{-1}), (b) the expanded spectrum from 9000 to 9800 Da, and (c) the structure assignment.

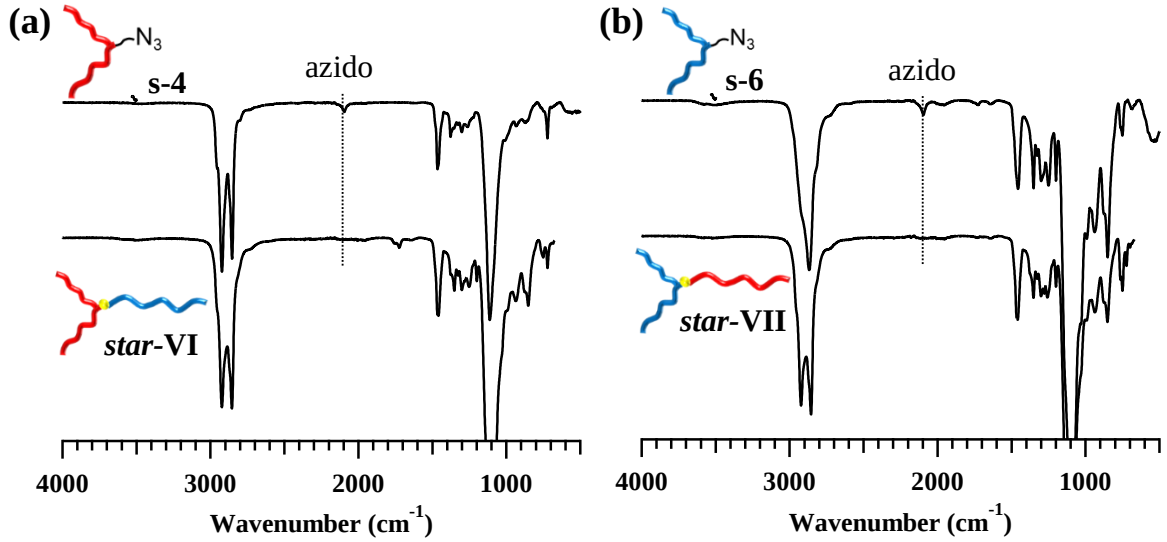

Figure 2-19. FT-IR spectra of the polymers. (a) **s-4** (upper) and ***star*-VI** (lower). (b) **s-6** (upper) and ***star*-VII** (lower).

In a similar fashion, the AB_2-type miktoarm star copolyether (***star*-VII**; $M_{n,NMR}$ = 22,300 g mol^{-1}, $Đ$ = 1.03) was obtained in 61.8% yield, starting from the hydrophilic precursor with an azido group at the chain center (**s-6**; $M_{n,NMR}$ = 11,500 g mol^{-1}, $Đ$ = 1.03, DP = 50) and the hydrophobic precursor with an ethynyl group at the ω-chain end (**s-7**; $M_{n,NMR}$ = 10,800 g mol^{-1}, $Đ$ = 1.03, DP = 50) (**Figure 2-20**). Thus, the coupling-onto method combined with the well-defined precursors prepared via the *t*-Bu-P_4-catalyzed ROP worked well to produce the miktoarm star copolyethers ***star*-V**, ***star*-VI**, and ***star*-VII**.

Table 2-4. Synthesis of A_2B- and AB_2-type Miktoarm Star Copolyethers (***star*-VI**, ***star*-VII**) and the Corresponding Precursors

polymer	$M_{n,calc}$ [a] [g mol^{-1}]	$M_{n,NMR}$ [a] [g mol^{-1}]	$M_{n,SEC}$ [b] [g mol^{-1}]	$Đ$ [b]
s-4	11,100	10,600	8,390	1.03
s-5	11,100	11,400	9,450	1.04
***star*-VI**	22,200	22,200	16,700	1.05
s-6	11,500	11,500	11,100	1.03
s-7	10,700	10,800	8,940	1.03
***star*-VII**	22,200	22,300	17,000	1.03

[a] Determined by ^{1}H NMR in $CDCl_3$. [b] Determined by SEC in THF using polystyrene standards

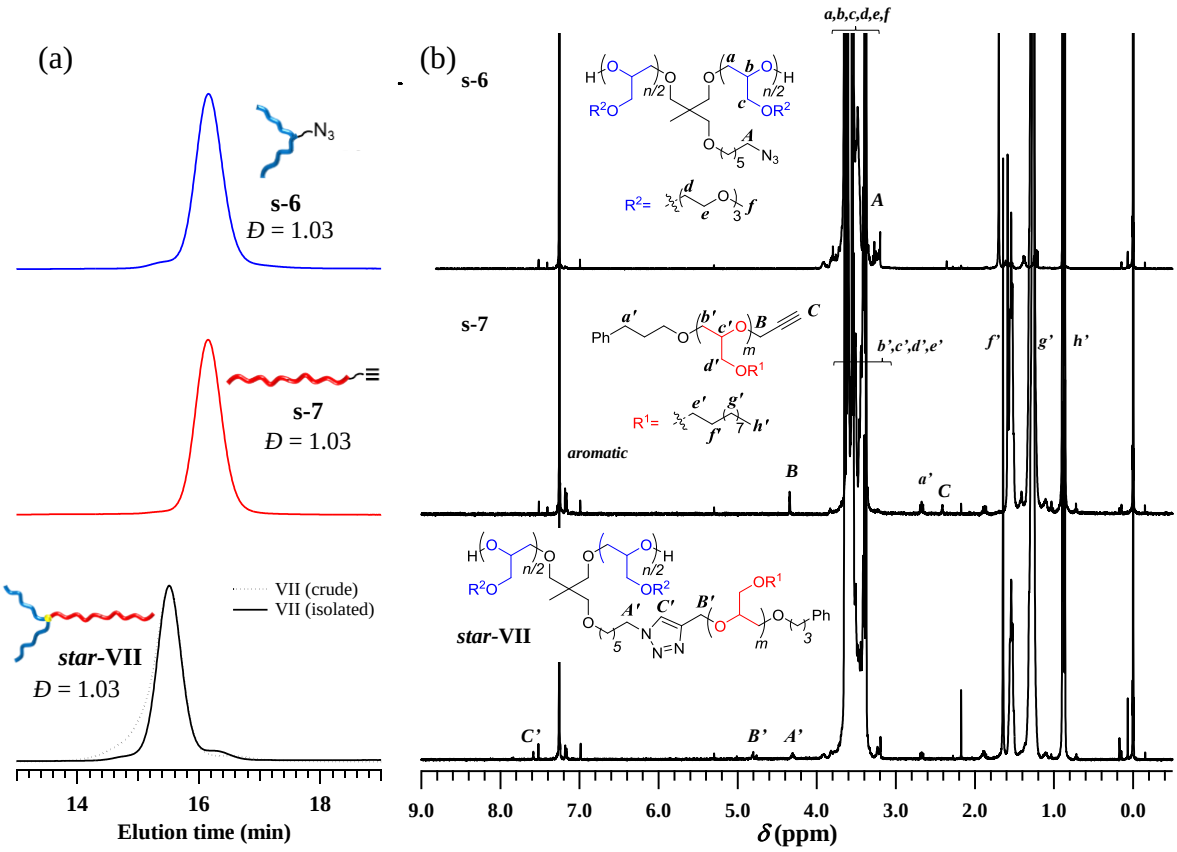

Figure 2-20. (a) SEC traces of **s-6**, **s-7**, and ***star*-VII** (dotted line, before purification; solid line, after the purification using preparative SEC). (b) ^{1}H NMR spectra of **s-6**, **s-7** and ***star*-VII** in $CDCl_3$ (400 MHz).

2.2.4 Self-assembly Properties of Amphiphilic Star-shaped Block Copolyethers in Water

In order to investigate the effect of the branched architecture on the self-assembly properties in water, the author determined the critical micelle concentration (CMC), the morphology of the aggregates, and the cloud point ($T_{c.d.}$) for the obtained star-shaped block copolyethers (***star*-I**, ***star*-II**, ***star*-III**, ***star*-IV**, ***star*-V**, ***star*-VI**, and ***star*-VII**) and linear diblock copolymer (***linear*-I**). Importantly, the samples used in this study have comparable total molecular weights (ca. 22,200 g mol^{-1}) and hydrophobic/hydrophilic ratios (ca. 50:50) (**Table 2-5**). Thus, the author can obtain information about the pure effect of the star-shaped architectures on the aqueous self-assembly behaviors. First, the author determined the CMC of the block copolyethers in pure water by a fluorescence technique using pyrene as the probe at room temperature. The CMC value of the block copolyethers were in the range of 1.3 to 5.2 mg L^{-1} (**Table 2-5** and **Figure 2-21)**, implying a minimal effect of the branched architecture on the CMC value.

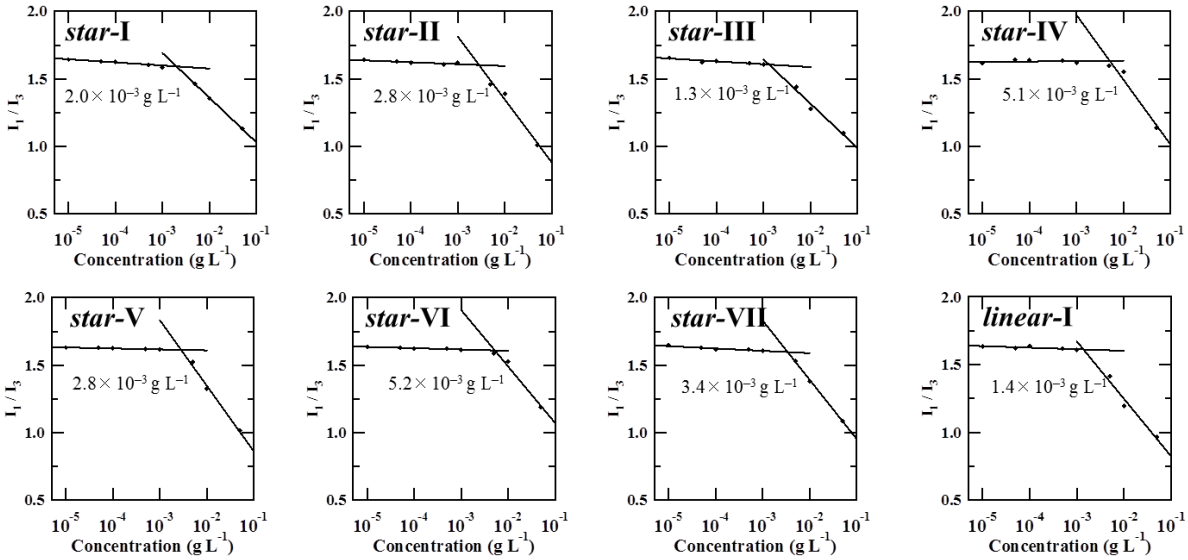

Figure 2-21. Variation in I_1/I_3 of pyrene emission spectra for ***star*-I**, ***star*-II**, ***star*-III**, ***star*-IV**, ***star*-V**, ***star*-VI**, and ***star*-VII** as a function of polymer concentrations (measured at 25 °C).

Table 2-5. Molecular Characteristics, Critical Micelle Concentrations (CMC), Hydrodynamic radii (R_h), and Cloud Points ($T_{c.d.}$) of the Amphiphilic Block Copolyethers

sample		$M_{n,NMR}$ [a] [g mol^{-1}]	$Đ$ [b]	DP_1/DP_2 [c]	CMC [d] [mg L^{-1}]	R_h [e] [nm]	$T_{c.d.}$ [f] [°C]
***star*-I**	$(AB)_4$	22,200	1.03	50/50	2.0	57	83
***star*-II**	$(BA)_4$	22,200	1.02	50/50	2.8	116	n.d. (<30) [g]
***star*-III**	$(AB)_3$	22,200	1.02	52/50	1.3	106	77
***star*-IV**	$(BA)_3$	22,200	1.02	51/51	5.1	102	n.d. (<30) [g]
***star*-V**	A_2B_2	22,200	1.03	50/50	2.8	43	96
***star*-VI**	A_2B	22,200	1.05	50/51	5.2	46	77
***star*-VII**	AB_2	22,300	1.03	50/50	3.4	18	92
***linear*-I**	AB	21,900	1.04	50/51	1.4	62	83

[a] Determined by ^{1}H NMR. [b] Determined by SEC in THF. [c] Number-average degree of polymerizations of 2-(2-(2-methoxyethoxy)ethoxy)ethyl glycidyl ether (DP_1) and decyl glycidyl ether (DP_2) in the copolymer were determined by ^{1}H NMR. [d] Determined by steady-state fluorescence method using pyrene as a probe at 25 °C. [e] Determined based on multi-angle DLS measurements (concentration, 0.50 g L^{-1}; temperature, 25 °C). [f] Determined by turbidimetric analysis (concentration, 0.50 g L^{-1}). $T_{c.d.}$ was defined by the temperature at which the transmittance of sample solution reached 50%. [g] The solution has already gotten clouded.

Next, the author investigated the micellar aggregate structures by dynamic light scattering (DLS) and transmission electron microscopy (TEM). The micellar solution was prepared by direct dissolution of the block copolyethers in pure water followed by filtration using a 0.45 μm PTFE membrane filter (the polymer concentration was adjusted to be 0.50 g L^{-1}). The dynamic light scattering (DLS) experiment was employed to investigate the size of the aggregates (**Figure 2-22**). The intensity-average size distribution of every block copolymer aqueous solution displayed a monomodal peak corresponding to the aggregates formed through the self-assembling process. Multi-angle DLS measurements for the solutions revealed the linear dependence of the relaxation frequency ($\Gamma = 1/\tau$) on the square of the wavevector (q^2), which clearly indicated the Brownian diffusive motion. The slope is equal to the diffusion coefficient (D) of the aggregates in water, from which the hydrodynamic radius (R_h) was calculated by the Stokes-Einstein relation and was in the range of 18 – 116 nm (**Table 2-5** and **Figure 2-22**). The actual morphology of the nanoparticles was then evaluated by TEM observations, which revealed the presence of spherical nanoparticles or agglomerates for every block copolyether sample (**Figure 2-23**). Given that the R_h value for the spherical nanoparticles of ***star*-I**, ***star*-II**, ***star*-III**, ***star*-IV**, ***star*-V**, ***star*-VI**, and ***linear*-I** were apparently higher than the fully-extended chain length of the block copolyether (the full-extended chain lengths of ***star*-I** and ***star*-VI** were calculated to be 18 nm and 27 nm, respectively, in which the DP and molecular length of the monomeric repeating

unit were assumed to be 100 and 0.358 nm, respectively), the resultant morphologies can be assigned to a large compound micelle. Meanwhile, the spherical nanoparticle of ***star*-VII** should be attributed to a regular spherical micelle due to the lower R_h value of 18 nm. Thus, the author found that the branched architecture of the block copolymer affected both the dimensions and inner structure of the self-assembled nanoparticle. Interestingly, the author found a tendency that the star-block copolyethers had larger micellar sizes than for the miktoarm star ones (**Figure 2-24a**). Among the star-block coplyethers, however, no clear correlation was observed between the micellar size and branched architecture. This should be due to the complicated chain packing structures around the interface between the hydrophobic core and hydrophilic shell regions. In contrast, the comparison of the micellar size among the miktoarm star copolyethers proved the tendency that the introduction of the branched hydrophilic block led to forming smaller micellar aggregates; ***star*-VI** (46 nm) > ***star*-V** (43 nm) >> ***star*-VII** (18 nm) (**Figure 2-24a**). The local growth in the shell region due to the branched hydrophilic block caused the increase in the curvature at the core-shell interface, which might led to forming a micellar aggregate with a smaller size (**Figure 2-24b**). On the other hand, ***linear*-I** showed larger micellar size than the miktoarm star ones, that was also explainable due to the longer chain length of hydrophilic and hydrophobic blocks.

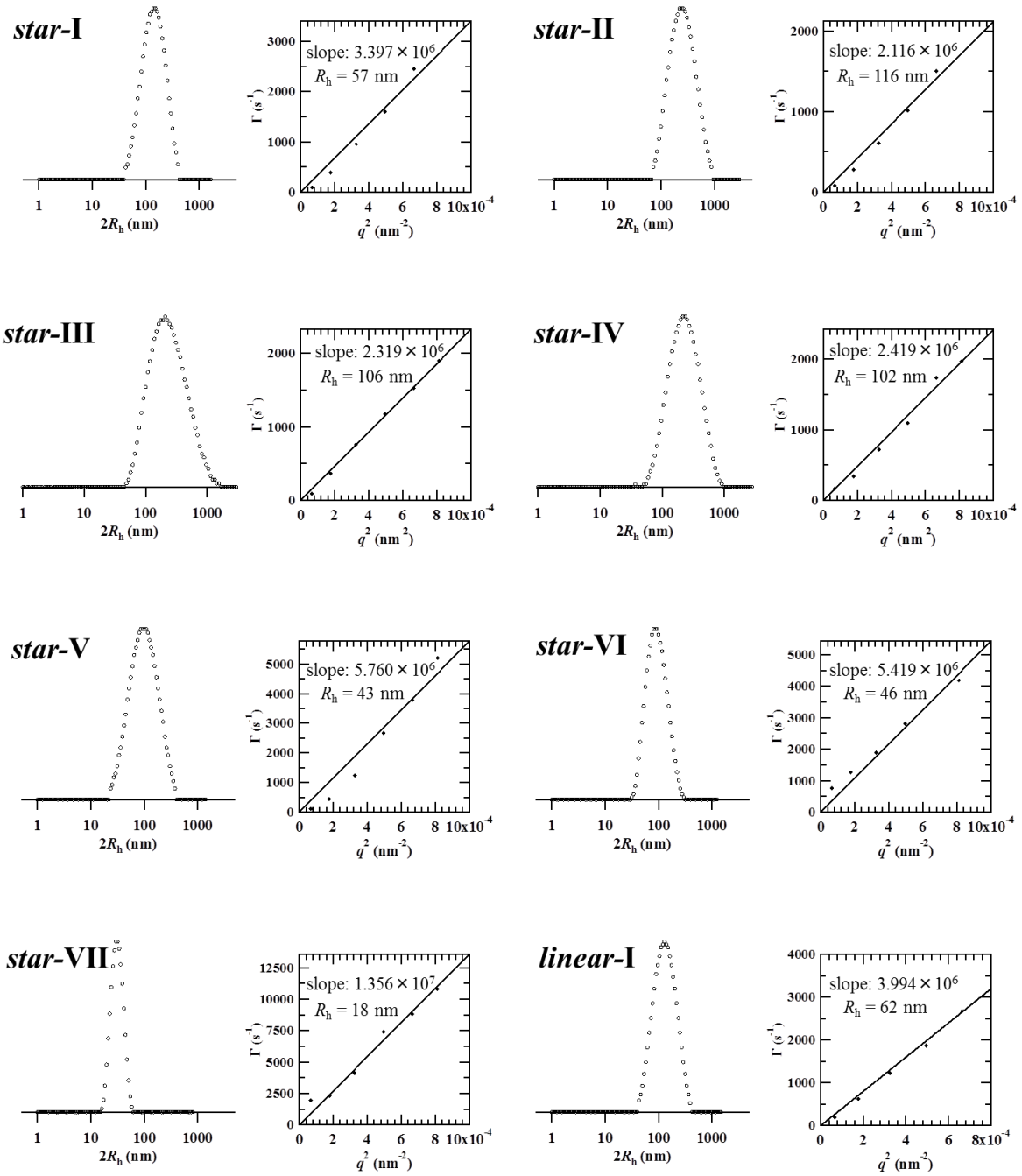

Figure 2-22. Particle size distribution (measured at the scattering angle of 90 °; left) and dependence of the relaxation frequency (Γ) on the squared wave vector (q^2) (right) for the micellar solutions of ***star*-I**, ***star*-II**, ***star*-III**, ***star*-IV**, ***star*-V**, ***star*-VI**, ***star*-VII**, and ***linear*-I** (0.50 g L^{-1}, 25 °C). The R_h value (hydrodynamic radius) was calculated based on the Stokes-Einstein relation using the slope of the Γ vs. q^2 plot.

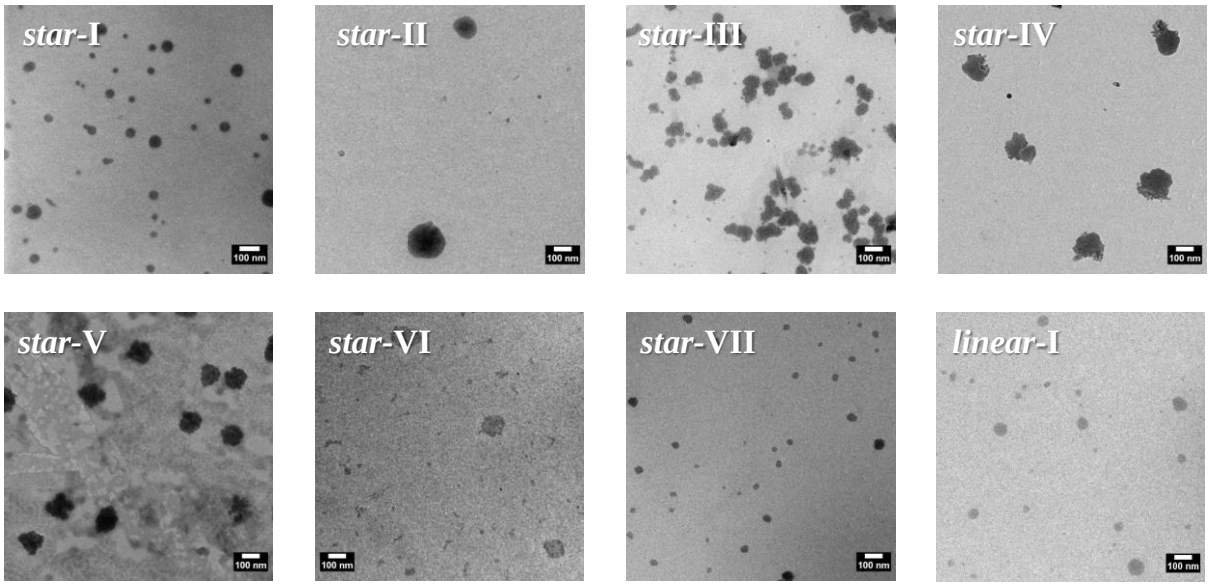

Figure 2-23. TEM images of micellar aggregates formed from ***star*-I**, ***star*-II**, ***star*-III**, ***star*-IV**, ***star*-V**, ***star*-VI**, and ***star*-VII** (polymer concentration, 0.50 g L^{-1}).

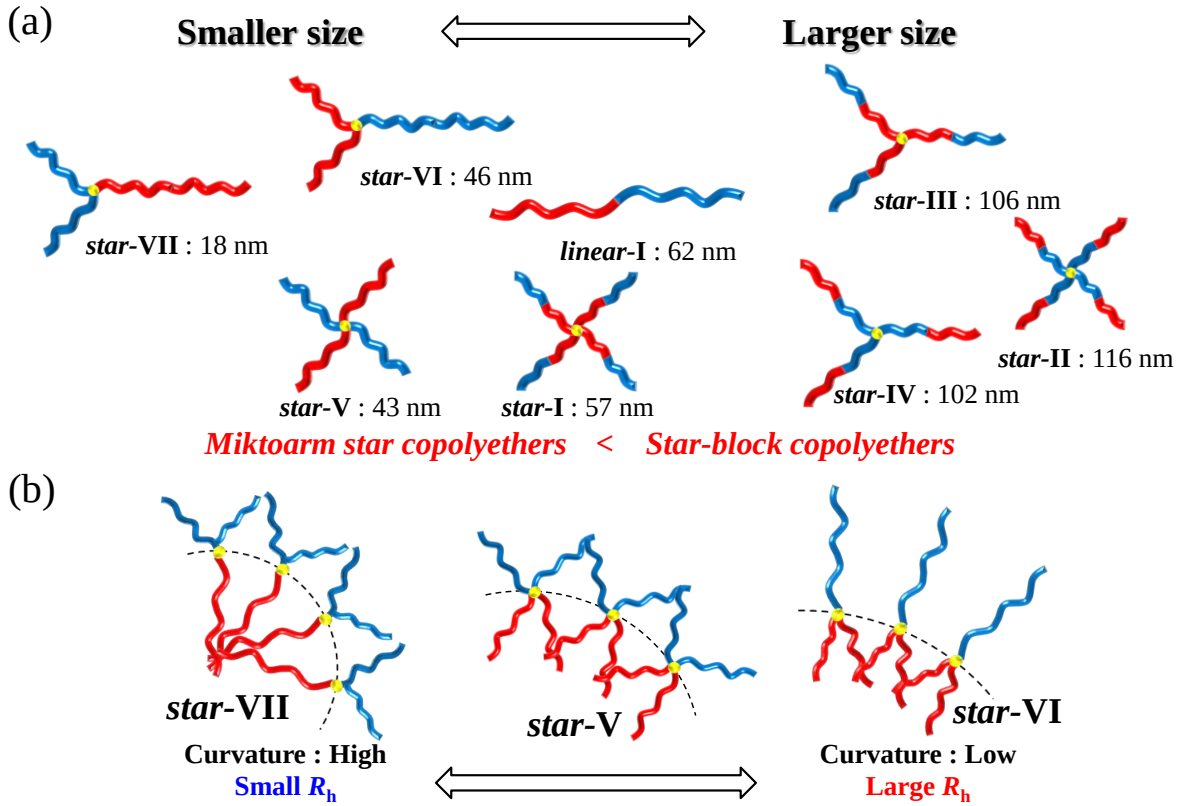

Figure 2-24. Schematic representation of (a) R_h values of the amphiphilic block copolyethers and (b) the proposed correlation between the branched architecture and R_h values of ***star*-V**, ***star*-VI**, and ***star*-VII**.

Finally, the author evaluated the cloud point ($T_{c.d.}$) of the block copolyether solution, which is one of the important specifications of nonionic surfactants. The $T_{c.d.}$ in water was evaluated based on a turbidimetric measurement and was defined as the temperature at which the transmittance of the block copolyether solution reached 50%. The $(AB)_4$- and $(AB)_3$-type star-block copolyethers, ***star*-I** and ***star*-III**, exhibited a $T_{c.d.}$ at 83 °C and 77 °C, respectively, while the $(BA)_4$- and $(BA)_3$- type star-block copolyethers, ***star*-II** and ***star*-IV**, had already clouded at room temperature (**Table 2-5**, **Figure 2-25**, and **Figure 2-26**). The significantly low $T_{c.d.}$ values of ***star*-II** and ***star*-IV** were attributed to the enhanced inter-micelle cross-linking through the hydrophobic end blocks.[38, 39] When compared with the $T_{c.d.}$ values among the miktoarm star copolyethers and the linear copolyether, the author found that the introduction of the branched hydrophilic block led to a higher $T_{c.d.}$ value; ***star*-V** (96 °C) ≈ ***star*-VII** (92 °C) > ***linear*-I** (83 °C) > ***star*-VI** (77 °C). These results suggested that the branched hydrophilic arm on the shell region would reduce the inter-micelle linkage due to its lower entanglement nature. From these results, the author can conclude that the star-shaped arhictectures as well as the block arrangement of the hydrophilic/hydrophobic parts play an important role in the aqueous self-assembly properties of the amphiphilic block copolyethers leading to various micellar morphologies, solubilities, and stabilities.

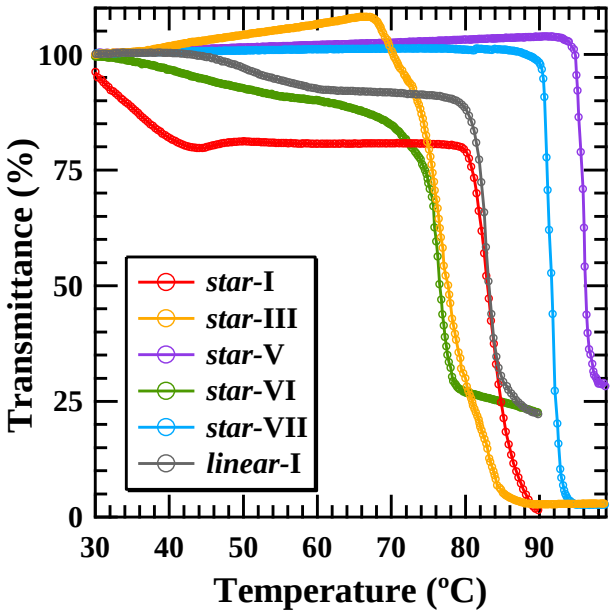

Figure 2-25. Temperature dependence of optical transmittance at 300 nm obtained for 0.50 g L^{-1} aqueous solution of star-shaped block copolyethers.

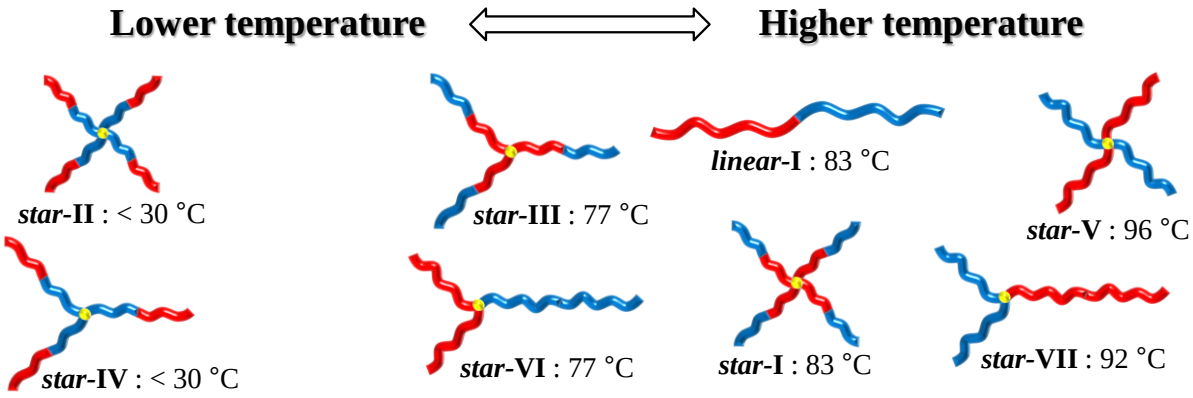

Figure 2-26. Schematic representation of $T_{c.d.}$ values of the amphiphilic star-shaped block copolyethers.

2.3 Conclusions

The author have demonstrated the synthesis of a comprehensive set of amphiphilic star-shaped block copolyethers, i.e., the $(AB)_3$-, $(BA)_3$-, $(AB)_4$-, and $(BA)_4$-type star-block copolyethers and the A_2B_2-, AB_2-, and A_2B-type miktoarm star copolyethers, via the *t*-Bu-P_4-catalyzed ROP combined with the core-first or the coupling-onto approaches. The well-controlled nature of the *t*-Bu-P_4-catalyzed ROP system made it possible to produce the narrowly-dispersed amphiphilic star-shaped block copolyethers with a comparable molecular weight and monomer composition. The presented synthetic route provided easy access to well-defined block copolyethers with various branched architectures, which might be useful as a model system for investigating the pure effect of the branched architecture on the self-assembly properties. The preliminary study of the aqueous self-assembly of the obtained amphiphilic block copolyethers revealed that the branched architecture affected the inner structure and size of the resultant micelles but did not affect the CMC values. In addition, the $T_{c.d.}$ value of the aqueous solution was also found to be dependent on the branched architecture.

2.4 Experimental Section

Materials. 6-Azido-1-hexanol,[40] Decyl glycidyl ether (**M1**)[41] and 2-(2-(2-Methoxyethoxy)ethoxy)ethyl glycidyl ether (**M1**)[42] were synthesized according to reported methods, purified by distillation under vacuum over calcium hydride, and stored under an argon atmosphere. 1,2,4,5-Benzenetetramethanol (**i-I**),[43] 2-[(6-azidohexyloxy)methyl]-2-methylpropane-1,3-diol (**i-V**),[44] 5,5-bis(bromomethyl)-2,2-dimethyl-1,3-dioxane,[45] and propargyl-functionalized Wang resin (PSt-C≡CH)[46] were prepared according to reported methods. 60% NaH, propargyl bromide, 1,3,5-benzenetrimethanol (**i-II**), palladium 10% on carbon (Pd/C; wetted with ca. 55% water), and *N,N,N',N'',N''*-pentamethyldiethylenetriamine (PMDETA) were purchased from Tokyo Chemical Industry Co., Ltd. (TCI) and used as received. 1,2-Butylene oxide (BO) and 3-Phenyl-1-propanol (**i-IV**) was purchased from TCI, and purified by distillation under vacuum over calcium hydride. *t*-Bu-P_4 (in *n*-hexane as 1.0 mol L^{-1} solution) and copper(I) bromide were purchased from Sigma-Aldrich Chemicals Co. and used as received. Dry dimethylformamide (DMF; >99.5%; water content, <0.005%), dry toluene (>99.5%; water content, <0.001%), and dry tetrahydrofuran (THF; >99.5%; water content, <0.001%) were purchased from Kanto Chemical Co., Inc., and used as received.

Instruments. The polymerization was carried out in an MBRAUN stainless steel glovebox equipped with a gas purification system (molecular sieves and copper catalyst) and

a dry argon atmosphere (H_2O, O_2 <1 ppm). The moisture and oxygen contents in the glovebox were monitored by an MB-MO-SE 1 moisture probe and an MB-OX-SE 1 oxygen probe, respectively. The solvent used for the polymerization (toluene) was purified using an MBRAUN solvent purification system (MB SPS COMPACT) consisting of an activated alumina column and an activated copper catalyst column. The number-average molecular weight ($M_{n,SEC}$) and dispersity ($Đ$) of the polymers were calculated on the basis of a polystyrene (PSt) calibration. The size exclusion chromatography (SEC) was performed at 40 °C in THF (flow rate, 1.0 mL min^{-1}) using a Shodex GPC-101 gel permeation chromatography system (Shodex DU-2130 dual pump, Shodex RI-71 reflective index detector, and Shodex ERC-3125SN degasser) equipped with a Shodex KF-G guard column (4.6 mm × 10 mm; particle size, 8 μm) and two Shodex KF-804L columns (linear, 8 mm × 300 mm). The preparative SEC was performed in $CHCl_3$ (3.5 mL min^{-1}) at 23 °C using a JAI LC-9201 equipped with a JAI JAIGEL-2H column (20 mm × 600 mm; exclusion limit, 5×10^3), a JAI JAIGEL-3H column (20 mm × 600 mm; exclusion limit, 7 × 104) and a JAI RI-50s refractive index detector. The intrinsic viscosity ([η]) of the polymer solution was determined by SEC in THF (flow rate, 1.0 mL min^{-1}) at 40 °C using an Agilent 1100 series instrument equipped with two Shodex KF-804L columns (linear, 8 mm × 300 mm) and a viscosity detector (Wyatt Technology). The ^1H (400 MHz) and ^{13}C NMR (100 MHz) spectra were recorded using a JEOL ECS400 instrument. The Fourier transform infrared spectroscopy (FT-IR) analysis was

carried out using a Perkin-Elmer Frontier MIR spectrometer equipped with a Single Reflection Diamond Universal Attenuated Total Reflection (ATR) accessory. Matrix-assisted laser desorption ionization time-of-flight mass spectrometry (MALDI-TOF MS) of the obtained polymers was performed using an Applied Biosystems Voyager-DE STR-H equipped with a 337-nm nitrogen laser (3-ns pulse width). Two hundred shots were accumulated for the spectra at a 20-kV acceleration voltage in the reflector mode and calibrated using polystyrene as the internal standard. Samples for the MALDI-TOF MS measurement were prepared by mixing the polymer (10 g L^{-1}, 100 μL, in THF), a matrix (dithranol, 20 g L^{-1}, 20 μL, in THF), and a cationizing agent (sodium trifluoroacetate, 10 g L^{-1}, 20 μL, in methanol).

Synthesis of 2,2-Bis((6-azidohexyloxy)methy)propane-1,3-diol (i-III). To a stirred solution of 6-azido-1-hexanol (5.67 g, 39.6 mmol) in dry DMF (50.0 mL) was added NaH (3.20 g, 80.0 mmol; 60% in mineral oil) and stirred under a nitrogen atmosphere at 50 °C for 30 min. After cooling to 0 °C, 5,5-bis(bromomethyl)-2,2-dimethyl-1,3-dioxane (4.00 g, 13.2 mmol) was added to the reaction mixture, and the entire mixture was stirred under a nitrogen atmosphere at 60 °C for 48 h. After removing the solvent by evaporation, the obtained residue was dissolved in diethyl ether and washed three times with water. The combined organic layer was dried over anhydrous Na_2SO_4 and then concentrated. The residue was purified by silica gel column chromatography (*n*-hexane/AcOEt = 3/2 (v/v), R_f = 0.62) to give 5,5-bis((6-azidohexyloxy)methy)-2,2-dimethyl-1,3-dioxane (2.69 g) as a

colorless liquid. Yield: 47.8%. ^{1}H NMR (400 MHz, $CDCl_3$): δ (ppm) 3.74 (s, 4H, $N_3(CH_2)_6OCH_2-$), 3.38 (m, 8H, $-C(CH_2O)_2C-$, $N_3(CH_2)_5CH_2-$), 3.26 (t, J = 8.00 Hz, 4H, N_3CH_2-), 1.41−1.59 (m, 16H, $N_3CH_2(CH_2)_4CH_2O-$), 1.26 (s, $-CH_3$). ^{13}C NMR (100 MHz, $CDCl_3$) δ (ppm): 98.0 ($(CH_3)_2C-$), 71.3 ($N_3(CH_2)_5CH_2O-$), 71.2 ($N_3(CH_2)_6OCH_2-$), 62.8 ($C(CH_2O-Acetal)_2$), 51.4 (N_3CH_2-), 39.3 ($-(CH_2)_2C(CH_2)_2-$), 29.6 ($N_3CH_2CH_2-$), 29.3 ($N_3(CH_2)_4CH_2-$), 27.0 ($N_3(CH_2)_2CH_2-$), 25.7 ($N_3(CH_2)_3CH_2-$), 23.75($-CH_3$).

To a stirred solution of 5,5-bis((6-azidohexyloxy)methy)-2,2-dimethyl-1,3-dioxane (2.69 g, 6.31 mmol) in methanol (50.0 mL) was added a cation exchange resin (DOWEX 50W-X2-200, 2.67 g), and the reaction mixture was stirred at room temperature for 24 h. The reaction mixture was filtered to remove the resin, and the filtrate was concentrated. The residue was purified by silica gel column chromatography (*n*-hexane/AcOEt = 1/2 (v/v), R_f = 0.56) to give **i-III** (987 mg) as a colorless liquid. Yield: 40.5%. ^{1}H NMR (400MHz, $CDCl_3$): δ (ppm) 3.64 (s, 4H, $-CH_2OH$), 3.49 (s, 4H, $N_3(CH_2)_6OCH_2-$), 3.43 (t, J = 4.00, 4H, $N_3(CH_2)_5CH_2O-$), 3.27 (t, J = 4.00, 4H, N_3CH_2-), 2.93 (s, 2H, $-OH$), 1.59 (m, 8H, $N_3(CH_2)_2CH_2-$, $N_3(CH_2)_3CH_2-$), 1.37 (m, 8H, $N_3CH_2CH_2-$, $N_3(CH_2)_4CH_2-$). ^{13}C NMR (100 MHz, $CDCl_3$): δ (ppm) 72.9 ($N_3(CH_2)_5CH_2O-$), 71.7 ($N_3(CH_2)_6OCH_2-$), 64.5 ($-CH_2OH$), 51.3 (N_3CH_2-), 44.5 ($-(CH_2O)_2C(CH_2OH)_2$), 29.3 ($N_3CH_2CH_2-$), 28.9 ($N_3(CH_2)_4CH_2-$), 26.4 ($N_3(CH_2)_2CH_2-$), 25.7 ($N_3(CH_2)_3CH_2-$). Anal. Calcd. for $C_{17}H_{34}N_6O_4$: C, 52.83; H, 8.87; N, 21.74. Found: C, 52.86; H, 8.94; N, 21.55.

Synthesis of Four-Armed Star-Shaped Poly(butylene oxide) (*star*-PBO). To a stirred suspension of **i-I** (19.0 mg, 95.9 μmol) and *t*-Bu-P_4 (95.9 μL as 1.0 mol·L^{-1} stock solution in *n*-hexane, 95.9 μmol) in toluene (536 μL) was added BO (500 μL, 5.76 mmol), and the mixture was stirred at room temperature for 20 h. An excess of benzoic acid was then added to the mixture to terminate the polymerization, and the polymer was purified by passing through a pad of alumina to give *star*-PBO as a colorless viscous liquid (132 mg). Yield: 30.6%. ^{1}H NMR (400 MHz, $CDCl_3$): δ (ppm) 7.30 (aromatic), 4.52 (Ph(CH_2O−PBO)$_4$), 3.29−3.75 (−OCH_2CH(CH_2CH_3)O−, −OCH_2CH(CH_2CH_3)O−), 1.36−1.69 (−OCH_2CH(C$H_2$$CH_3$)O−), 0.92 (−$OCH_2$CH($CH_2CH_3$)O−). $M_{n,NMR}$ = 4650 g mol^{-1}; $M_{n,SEC}$ = 5770 g mol^{-1}; $Đ$ = 1.03.

Hydrogenolysis of *star*-PBO. A mixture of *star*-PBO ($M_{n,NMR}$ = 4650 g mol^{-1}, 100 mg) and the Pd/C (100 mg) in THF (15 mL) was stirred under a hydrogen atmosphere at room temperature for 24 h. The reaction mixture was filtered to remove Pd/C, and the filtrate was evaporated to dryness to give the cleaved PBO (HO-PBO) as a colorless viscous liquid (83.0 mg). Yield: 83.0%. ^{1}H NMR (400 MHz, $CDCl_3$): δ (ppm) 3.29−3.75 (−OCH_2CH(CH_2CH_3)O−, −OCH_2CH(CH_2CH_3)O−), 1.36−1.69 (−OCH_2CH(C$H_2$$CH_3$)O−), 0.92 (−$OCH_2$CH($CH_2CH_3$)O−). $M_{n,SEC}$ = 1320 g mol^{-1}; $Đ$ = 1.13.

Synthesis of poly-M1. A typical polymerization procedure is as follows (Procedure A): **M1** (276 μL, 1.17 mmol) was added to a stirred solution of **i-IV** (46.7 μL as a 1.0 mol L^{-1}

stock solution in toluene, 46.7 μmol) and *t*-Bu-P_4 (46.7 μL as a 1.0 mol L^{-1} stock solution in *n*-hexane, 46.7 μmol) in toluene (97 μL), and the mixture was stirred at room temperature for 20 h. An excess of benzoic acid was then added to the mixture to terminate the polymerization, and the polymer was then purified by passing through a pad of alumina with THF to give **poly-M1** as a colorless viscous liquid (232 mg). Yield: 93.0%. ^{1}H NMR (400 MHz, $CDCl_3$): δ (ppm) 7.36, 7.17 (aromatic), 3.29−3.75 ($Ph(CH_2)_2CH_2OCH_2$−, −$OCH_2CH(CH_2OCH_2(CH_2)_8CH_3)O$−), 2.68 ($PhCH_2CH_2CH_2$−), 1.85 ($PhCH_2CH_2CH_2O$−), 1.10−1.69 (−$OCH_2CH(CH_2OCH_2CH_2(CH_2)_7CH_3)O$−), 0.78−0.95 (−$OCH_2CH(CH_2OCH_2(CH_2)_8CH_3)O$−). $M_{n,NMR}$ = 5710 g mol^{-1}; $M_{n,SEC}$ = 4890 g mol^{-1}; M_w/M_n = 1.05.

Synthesis of poly-M2. Procedure A was used for the polymerization of **M2** (234 μL, 1.14 mmol) with **i-IV** (45.4 μL as 1.0 mol L^{-1} stock solution in toluene, 45.4 μmol) and *t*-Bu-P_4 (45.4 μL as 1.0 mol L^{-1} stock solution in *n*-hexane, 45.4 μmol) in toluene (129 μL) to give **poly-M2** as a colorless viscous liquid (101 mg). Yield: 40.0%. ^{1}H NMR (400 MHz, $CDCl_3$): δ (ppm) 7.36, 7.17 (aromatic), 3.29−3.75 ($Ph(CH_2)_2CH_2OCH_2$−, −$OCH_2CH(CH_2O(CH_2CH_2O)_3CH_3)O$−), 2.68 ($PhCH_2CH_2CH_2$−), 1.85 ($PhCH_2CH_2CH_2O$−). $M_{n,NMR}$ = 5750 g mol^{-1}; $M_{n,SEC}$ = 4440 g mol^{-1}; M_w/M_n = 1.05.

Synthesis of *linear*-I. A typical block copolymerization procedure is as follows (Procedure B): **M1** (276 μL, 1.17 mmol, first monomer) was added to a stirred solution of

i-IV (23.3 μL as 1.0 mol L^{-1} stock solution in toluene, 23.3 μmol) and *t*-Bu-P_4 (23.3 μL as 1.0 mol L^{-1} stock solution in *n*-hexane, 23.3 μmol) in toluene (144 μL), then the mixture was stirred at room temperature for 20 h. **M2** (241 μL, 1.17 mmol, second moonmer) and toluene (226 μL) were added to the stirred mixture to further continue the polymerization. After stirring for 20 h at room temperature, an excess of benzoic acid was then added to the mixture to terminate the polymerization, and the polymer was purified by passage through a pad of alumina with THF to give ***linear*-I** as a colorless waxy solid (456 mg). Yield: 90.0%. ^{1}H NMR (400 MHz, $CDCl_3$): δ (ppm) 7.36, 7.17 (aromatic), 3.29−3.75 ($Ph(CH_2)_2CH_2OCH_2$−, −$OCH_2CH(CH_2OCH_2(CH_2)_8CH_3)O$−, −$OCH_2CH(CH_2O(CH_2CH_2O)_3CH_3)O$−), 2.68 ($PhCH_2CH_2CH_2$−), 1.10−1.69 ($PhCH_2CH_2CH_2O$−, −$OCH_2CH(CH_2OCH_2CH_2(CH_2)_7CH_3)O$−), 0.78−0.95 (−$OCH_2CH(CH_2OCH_2(CH_2)_8CH_3)O$−). $M_{n,NMR}$ = 21900 g mol^{-1}; $M_{n,SEC}$ = 15900 g mol^{-1}; M_w/M_n = 1.04.

Synthesis of *linear*-II. Procedure B was used for the polymerization of **M2** (234 μL, 1.14 mmol, first monomer), and **M1** (269 μL, 1.14 mmol, second moonmer) with **i-IV** (22.7 μL as 1.0 mol L^{-1} stock solution in toluene, 22.7 μmol) and *t*-Bu-P_4 (22.7 μL as 1.0 mol L^{-1} stock solution in *n*-hexane, 22.7 μmol) in toluene (360 μL) to give ***linear*-II** as a colorless waxy solid (457 mg). Yield: 93.0%. ^{1}H NMR (400 MHz, $CDCl_3$): δ (ppm) 7.36, 7.17 (aromatic), 3.29−3.75 ($Ph(CH_2)_2CH_2OCH_2$−, −$OCH_2CH(CH_2OCH_2(CH_2)_8CH_3)O$−, −$OCH_2CH(CH_2O(CH_2CH_2O)_3CH_3)O$−), 2.68 ($PhCH_2CH_2CH_2$−), 1.10−1.69

(PhCH$_2$C*H*$_2$CH$_2$O−, −OCH$_2$CH(CH$_2$OCH$_2$C*H*$_2$(C*H*$_2$)$_7$CH$_3$)O−), 0.78−0.95 (−OCH$_2$CH(CH$_2$OCH$_2$(CH$_2$)$_8$C*H*$_3$)O−). $M_{n,NMR}$ = 21800 g mol^{-1}; $M_{n,SEC}$ = 13800 g mol^{-1}; M_w/M_n = 1.05.

Synthesis of (*AB*)$_4$-type star-block copolyether (*star*-I). Procedure B was used for the diblock polymerization of **M1** (553 µL, 2.33 mmol, first monomer, polymerization time = 20 h) and **M2** (482 µL, 2.33 mmol, second monomer, polymerization time = 20 h) with **i-I** (9.3 mg, 47 µmol) and *t*-Bu-P$_4$ (23.3 µL as 1.0 mol L^{-1} stock solution in *n*-hexane, 23.3 µmol) in toluene (809 µL) to give ***star*-I** as a colorless waxy solid (893 mg). Yield: 88.1%. ^{1}H NMR (400 MHz, CDCl$_3$): δ (ppm) 7.17 (aromatic), 4.55 (–PhC*H*$_2$O–), 3.29−3.75 (−OC*H*$_2$C*H*(C*H*$_2$OC*H*$_2$(CH$_2$)$_8$CH$_3$)O−, −OC*H*$_2$C*H*(C*H*$_2$O(C*H*$_2$C*H*$_2$O)$_3$C*H*$_3$)O−), 1.10−1.69 (−OCH$_2$CH(CH$_2$OCH$_2$C*H*$_2$(C*H*$_2$)$_7$CH$_3$)O−), 0.78−0.95 (−OCH$_2$CH(CH$_2$OCH$_2$(CH$_2$)$_8$C*H*$_3$)O−). $M_{n,NMR}$ = 22,200 g mol^{-1}; $M_{n,SEC}$ = 16,800 g mol^{-1}; *Đ* = 1.03.

Synthesis of (*BA*)$_4$-type Star-Block Copolyether (*star*-II). Procedure B was used for the diblock polymerization of **M2** (467 µL, 2.27 mmol, first monomer, polymerization time = 20 h) and **M1** (538 µL, 2.27 mmol, second monomer, polymerization time = 20 h) with **i-I** (9.0 mg, 45 µmol) and *t*-Bu-P$_4$ (22.7 µL as 1.0 mol L^{-1} stock solution in *n*-hexane, 22.7 µmol) in toluene (809 µL) to give ***star*-II** as a colorless waxy solid (832 mg). Yield: 84.3%. ^{1}H NMR (400 MHz, CDCl$_3$): δ (ppm) 7.17 (aromatic), 4.55 (–PhC*H*$_2$O–), 3.29−3.75 (−OC*H*$_2$C*H*(C*H*$_2$OC*H*$_2$(CH$_2$)$_8$CH$_3$)O−, −OC*H*$_2$C*H*(C*H*$_2$O(C*H*$_2$C*H*$_2$O)$_3$C*H*$_3$)O−), 1.10−1.69

(−$OCH_2CH(CH_2OCH_2CH_2(CH_2)_7CH_3)O$−), 0.78−0.95 (−$OCH_2CH(CH_2OCH_2(CH_2)_8CH_3)O$−). $M_{n,NMR}$ = 22,200 g mol^{-1}; $M_{n,SEC}$ = 16,200 g mol^{-1}; $Đ$ = 1.02.

Hydrogenolysis of *star*-II. Pd/C (450 mg) was added to a stirred solution of ***star*-II** (150 mg) in THF (3.0 mL), then the mixture was stirred under a hydrogen atmosphere at room temperature for 48 h. After removing the Pd/C by filtration, the cleaved poly(**M2**)-*b*-poly(**M1**) arm was obtained as a colorless viscous liquid (138 mg). Yield: 92.0%. ^{1}H NMR (400 MHz, $CDCl_3$): δ (ppm) 3.29−3.75 (−$OCH_2CH(CH_2OCH_2(CH_2)_8CH_3)O$−, −$OCH_2CH(CH_2O(CH_2CH_2O)_3CH_3)O$−), 1.10−1.69 (−$OCH_2CH(CH_2OCH_2CH_2(CH_2)_7CH_3)O$−), 0.78−0.95 (−$OCH_2CH(CH_2OCH_2(CH_2)_8CH_3)O$−). $M_{n,SEC}$ = 4,850 g mol^{-1}; $Đ$ = 1.04.

***α,ω*-End acetylation of Cleaved Poly(M2)-*b*-poly(M1).** The cleaved poly(**M2**)-*b*-poly(**M1**) arm (50 mg) and acetic anhydride (20.4 mg, 200 μmol) were added to a solution of 4-dimethylaminopyridine (2.4 mg, 20 μmol) in pyridine (3.0 mL), then the mixture was stirred at room temperature for 24 h. The reaction mixture was diluted with EtOAc and washed three times with a $CuSO_4$ aqueous solution. The organic layer was concentrated, and the residue was purified by dialysis against MeOH to give *α,ω*-end-acetylated poly(**M2**)-*b*-poly(**M1**) as a colorless viscous liquid (47.6 mg). Yield: 95.2%. ^{1}H NMR (400 MHz, $CDCl_3$): δ (ppm) 5.09 ($CH_3COOCH(CH_2O(CH_2)_9CH_3)CH_2O$–), 4.04–4.12 ($CH_3COOCH_2CH(CH_2O(CH_2CH_2O)_3CH_3)O$–), 3.29−3.75

(−OCH_2CH(CH_2OCH_2(CH_2)$_8$CH_3)O−, −OCH_2CH(CH_2O(CH_2CH_2O)$_3$CH_3)O−), 2.07 (CH_3COO–), 1.10−1.69 (−OCH$_2$CH(CH$_2$OCH$_2$CH_2(CH_2)$_7$CH$_3$)O−), 0.78−0.95 (−OCH$_2$CH(CH$_2$OCH$_2$(CH$_2$)$_8$CH_3)O−). $M_{n,NMR}$ = 5,470 g mol^{-1}; $M_{n,SEC}$ = 5,460 g mol^{-1}; $Đ$ = 1.04.

Synthesis of (*AB*)$_3$-type star-block copolyether (*star*-III). Procedure B was used for the block copolymerization of **M1** (553 μL, 2.33 mmol, first monomer, polymerization time = 20 h) and **M2** (482 μL, 2.33 mmol, second monomer, polymerization time = 20 h) with **i-II** (7.9 mg, 47 μmol) and *t*-Bu-P$_4$ (23.3 μL as 1.0 mol L^{-1} stock solution in *n*-hexane, 23.3 μmol) in toluene (1.21 mL) to give ***star*-III** as a colorless waxy solid (811 mg). Yield: 80.0%. ^{1}H NMR (400 MHz, $CDCl_3$): δ (ppm) 7.17 (aromatic), 4.50 (–PhCH_2O–), 3.29−3.75 (−OCH_2CH(CH_2OCH_2(CH_2)$_8$CH_3)O−, −OCH_2CH(CH_2O(CH_2CH_2O)$_3$CH_3)O−), 1.10−1.69 (−OCH$_2$CH(CH$_2$OCH$_2$CH_2(CH_2)$_7$CH$_3$)O−), 0.78−0.95 (−OCH$_2$CH(CH$_2$OCH$_2$(CH$_2$)$_8$CH_3)O−). $M_{n,NMR}$ = 22,200 g mol^{-1}; $M_{n,SEC}$ = 15,600 g mol^{-1}; $Đ$ = 1.02.

Synthesis of (*BA*)$_3$-type star-block copolyethers (*star*-IV). Procedure B was used for the diblock polymerization of **M2** (467 μL, 2.27 mmol, first monomer, polymerization time = 20 h) and **M1** (538 μL, 2.27 mmol, second monomer, polymerization time = 20 h) with **i-II** (7.6 mg, 45 μmol) and *t*-Bu-P$_4$ (22.7 μL as 1.0 mol L^{-1} stock solution in *n*-hexane, 22.7 μmol) in toluene (1.17 mL) to give ***star*-IV** as a colorless waxy solid (743 mg). Yield: 75.3%. ^{1}H NMR (400 MHz, $CDCl_3$): δ (ppm) 7.16 (aromatic), 4.50 (–PhCH_2O–), 3.29−3.75

(−OC*H*$_2$C*H*(C*H*$_2$OC*H*$_2$(CH$_2$)$_8$CH$_3$)O−, −OC*H*$_2$C*H*(C*H*$_2$O(C*H*$_2$C*H*$_2$O)$_3$C*H*$_3$)O−), 1.10−1.69 (−OCH$_2$CH(CH$_2$OCH$_2$C*H*$_2$(C*H*$_2$)$_7$CH$_3$)O−), 0.78−0.95 (−OCH$_2$CH(CH$_2$OCH$_2$(CH$_2$)$_8$C*H*$_3$)O−). $M_{n,NMR}$ = 22,200 g mol^{-1}; $M_{n,SEC}$ = 15,900 g mol^{-1}; $Đ$ = 1.02.

Hydrogenolysis of *star*-IV and *α,ω*-End acetylation of the cleaved poly(M2)-*b*-poly(M1). Pd/C (300 mg) was added to a stirred solution of ***star*-IV** (100 mg) in THF (3.0 ml), and the mixture was stirred under a hydrogen atmosphere at room temperature for 48 h. After removing Pd/C by filtration, the cleaved poly(**M2**)-*b*-poly(**M1**) arm was obtained as a colorless viscous liquid (89 mg). Yield: 89.0%. ^{1}H NMR (400 MHz, $CDCl_3$): δ (ppm) 3.29−3.86 (−OC*H*$_2$C*H*(C*H*$_2$OC*H*$_2$(CH$_2$)$_8$CH$_3$)O−, −OC*H*$_2$C*H*(C*H*$_2$O(C*H*$_2$C*H*$_2$O)$_3$C*H*$_3$)O−), 1.16−1.77 (−OCH$_2$CH(CH$_2$OCH$_2$C*H*$_2$(C*H*$_2$)$_7$CH$_3$)O−), 0.78−0.95 (−OCH$_2$CH(CH$_2$OCH$_2$(CH$_2$)$_8$C*H*$_3$)O−). $M_{n,SEC}$ = 6,130 g mol^{-1}; $Đ$ = 1.03.

The cleaved poly(**M2**)-*b*-poly(**M1**) arm (50 mg) and acetic anhydride (14.0 mg, 137 μmol) were added to a solution of 4-dimethylaminopyridine (1.7 mg, 14 μmol) in pyridine (3 mL), and the mixture was stirred at room temperature for 24 h. The reaction mixture was diluted with EtOAc, then washed three times with a $CuSO_4$ aqueous solution. The organic layer was concentrated, and the residue was purified by dialysis against MeOH to give the *α,ω*-end-acetylated poly(**M2**)-*b*-poly(**M1**) as a colorless viscous liquid (42.2 mg). Yield: 84.4%. ^{1}H NMR (400 MHz, $CDCl_3$): δ (ppm) 5.08 (CH$_3$COOC*H*(CH$_2$O(CH$_2$)$_9$CH$_3$)CH$_2$O–),

4.04–4.27 ($CH_3COOCH_2CH(CH_2O(CH_2CH_2O)_3CH_3)O$–), 3.29−3.85 (−$OCH_2CH(CH_2OCH_2(CH_2)_8CH_3)O$−, −$OCH_2CH(CH_2O(CH_2CH_2O)_3CH_3)O$−), 2.07 ($CH_3COO$–), 1.05−1.69 (−$OCH_2CH(CH_2OCH_2CH_2(CH_2)_7CH_3)O$−), 0.78−0.95 (−$OCH_2CH(CH_2OCH_2(CH_2)_8CH_3)O$−). $M_{n,NMR}$ = 7,280 g mol^{-1}; $M_{n,SEC}$ = 6,770 g mol^{-1}; $Đ$ = 1.03.

Synthesis of Poly(M2) with Two Azido Groups at Chain Center (s-1). The typical homopolymerization procedure is as follows (Procedure A): **M2** (234 μL, 1.14 mmol) was added to a stirred solution of **i-III** (22.7 μL as 1.0 mol L^{-1} stock solution in toluene, 22.7 μmol) and *t*-Bu-P_4 (22.7 μL as 1.0 mol L^{-1} stock solution in *n*-hexane, 22.7 μmol) in toluene (174 μL), then the mixture was stirred at room temperature for 20 h. After the polymerization, an excess of benzoic acid was then added to the mixture to terminate the polymerization, and the polymer was purified by passage through a pad of alumina with THF to give **s-1** as a colorless viscous liquid (114 mg). Yield: 45.6%. ^{1}H NMR (400 MHz, $CDCl_3$): δ (ppm) 3.29–3.75 ($N_3(CH_2)_5CH_2OCH_2$−, −$OCH_2CH(CH_2OCH_2(CH_2)_8CH_3)O$−, −$OCH_2CH(CH_2O(CH_2CH_2O)_3CH_3)O$−), 3.26 ($N_3CH_2$–), 1.10−1.69 ($N_3CH_2(CH_2)_4CH_2O$−). $M_{n,NMR}$ = 11,200 g mol^{-1}; $M_{n,SEC}$ = 9,420 g mol^{-1}; $Đ$ = 1.04.

Synthesis of Poly(M1) with an *ω*-End Hydroxyl Group (s-2). Procedure A was used for the polymerization of **M1** (276 μL, 1.17 mmol) with **i-IV** (46.7 μL as 1.0 mol L^{-1} stock solution in toluene, 46.7 μmol) and *t*-Bu-P_4 (46.7 μL as 1.0 mol L^{-1} stock solution in

n-hexane, 46.7 μmol) in toluene (97 μL) to give **s-2** as a colorless viscous liquid (232 mg). Yield: 93.0%. ^{1}H NMR (400 MHz, $CDCl_3$): δ (ppm) 7.36, 7.17 (aromatic), 3.29−3.75 (Ph$(CH_2)_2CH_2OCH_2$−, −$OCH_2CH(CH_2OCH_2(CH_2)_8CH_3)$O−), 2.68 (Ph$CH_2CH_2CH_2$−), 1.85 (Ph$CH_2CH_2CH_2$O−), 1.10−1.69 (−$OCH_2CH(CH_2OCH_2CH_2(CH_2)_7CH_3)$O−), 0.78−0.95 (−$OCH_2CH(CH_2OCH_2(CH_2)_8CH_3)$O−). $M_{n,NMR}$ = 5,710 g mol^{-1}; $M_{n,SEC}$ = 4,890 g mol^{-1}; $Đ$ = 1.05.

Synthesis of Poly(M1) with an ω-End Ethynyl Group (s-3). The typical procedure for the ω-chain end ethynylation is as follows (Procedure C): NaH (14.0 mg, 350 μmol; 60% in mineral oil) was added to a stirred solution of **s-2** (200 mg, 35.0 μmol) in THF (9.0 ml), then the solution was stirred at 40 ºC for 30 min. After cooling to room temperature, propargyl bromide (26.2 μL, 350 μmol) was then added to the solution, and the entire mixture was stirred at room temperature for 48 h. The polymer was purified by passage through a pad of alumina to give **s-3** as a pale yellow waxy solid (190 mg). Yield: 95.0%. ^{1}H NMR (400 MHz, $CDCl_3$): δ (ppm) 7.36, 7.17 (aromatic), 4.30 (–$OCH_2C{\equiv}CH$), 3.29−3.75 (Ph$(CH_2)_2CH_2OCH_2$−, −$OCH_2CH(CH_2OCH_2(CH_2)_8CH_3)$O−), 2.68 (Ph$CH_2CH_2CH_2$−), 2.39 (–C≡C*H*), 1.85 (Ph$CH_2CH_2CH_2$O−), 1.10−1.69 (−$OCH_2CH(CH_2OCH_2CH_2(CH_2)_7CH_3)$O−), 0.78−0.95 (−$OCH_2CH(CH_2OCH_2(CH_2)_8CH_3)$O−). $M_{n,NMR}$ = 5,800 g mol^{-1}; $M_{n,SEC}$ = 4,900 g mol^{-1}; $Đ$ = 1.05.

Synthesis of A_2B_2-type miktoarm star copolyether (*star*-V). CuBr (10.1 mg, 70.2 μmol) and PMDETA (29.3 μL, 140 μmol) were added to a stirred solution of **s-1** (114 mg, 10.2 μmol) and **s-3** (161 mg, 28.1 μmol) in degassed DMF (2.63 mL). The mixture was stirred at 100 ºC for 24 h. After cooling to room temperature, the solvent of the mixture was removed by evaporation, and the residue was purified by passage through a pad of alumina followed by preparative SEC to give ***star*-V** a light brown waxy solid (140 mg). Yield: 50.9%. ^{1}H NMR (400 MHz, $CDCl_3$): δ (ppm) 7.56 (triazole methine), 7.17 (aromatic), 4.79 (–OC*H*$_2$−triazole ring), 4.33 (triazole ring−C*H*$_2$(CH$_2$)$_5$O−), 3.29−3.75 (triazole ring−(CH$_2$)$_5$C*H*$_2$OC*H*$_2$−, Ph(CH$_2$)$_2$C*H*$_2$OC*H*$_2$−, −OC*H*$_2$C*H*(C*H*$_2$OC*H*$_2$(CH$_2$)$_8$CH$_3$)O−, −OC*H*$_2$C*H*(C*H*$_2$O(C*H*$_2$C*H*$_2$O)$_3$C*H*$_3$)O−), 2.68 (PhC*H*$_2$CH$_2$CH$_2$−), 1.85 (PhCH$_2$C*H*$_2$CH$_2$O−), 1.10−1.69 (triazole ring−CH$_2$(C*H*$_2$)$_4$CH$_2$O−, −OCH$_2$CH(CH$_2$OCH$_2$C*H*$_2$(C*H*$_2$)$_7$CH$_3$)O−), 0.78−0.95 (−OCH$_2$CH(CH$_2$OCH$_2$(CH$_2$)$_8$C*H*$_3$)O−). $M_{n,NMR}$ = 22,200 g mol^{-1}; $M_{n,SEC}$ = 15,300 g mol^{-1}; $Đ$ = 1.03.

Synthesis of Poly(M1) with an azido group at chain center (s-4). Procedure A was used for the polymerization of **M1** (773 μL, 3.26 mmol) with **i-V** (16.0 mg, 65.3 μmol) and *t*-Bu-P$_4$ (65.3 μL as 1.0 mol L^{-1} stock solution in *n*-hexane, 65.3 μmol) in toluene (467 μL) to give **s-4** as a colorless viscous liquid (573 mg). Yield: 81.9%. ^{1}H NMR (400 MHz, $CDCl_3$): δ (ppm) 3.29–3.80 (N$_3$(CH$_2$)$_5$C*H*$_2$OC*H*$_2$−, −C(CH$_3$)C*H*$_2$O−, −OC*H*$_2$C*H*(C*H*$_2$OC*H*$_2$(CH$_2$)$_8$CH$_3$)O−), 3.26 (N$_3$C*H*$_2$–), 1.10−1.69 (N$_3$CH$_2$(C*H*$_2$)$_4$CH$_2$O−,

−$OCH_2CH(CH_2OCH_2CH_2(CH_2)_7CH_3)O$−), 0.78−0.98 (−$OCH_2CH(CH_2OCH_2(CH_2)_8CH_3)O$−, −$C(CH_3)CH_2O$−). $M_{n,NMR}$ = 10,600 g mol^{-1}; $M_{n,SEC}$ = 8,390 g mol^{-1}; $Đ$ = 1.03.

Synthesis of Poly(M2) with an *ω*-end ethynyl group (s-5). Procedure A was used for the polymerization of **M2** (937 μL, 4.54 mmol) with **i-IV** (90.8 μL as 1.0 mol L^{-1} stock solution in toluene, 90.8 μmol) and *t*-Bu-P_4 (90.8 μL as 1.0 mol L^{-1} stock solution in *n*-hexane, 90.8 μmol) in toluene (697 μL) to give poly(**M2**) as a colorless viscous liquid (715 mg). Yield: 71.5%. ^{1}H NMR (400 MHz, $CDCl_3$): δ (ppm) 7.28, 7.18 (aromatic), 3.29−3.80 ($Ph(CH_2)_2CH_2OCH_2$−, −$OCH_2CH(CH_2O(CH_2CH_2O)_3CH_3)O$−), 2.67 ($PhCH_2CH_2CH_2$−), 1.87 ($PhCH_2CH_2CH_2O$−). $M_{n,NMR}$ = 11,000 g mol^{-1}; $M_{n,SEC}$ = 9,580 g mol^{-1}; $Đ$ = 1.03.

Procedure C was used for the propargylation of poly(**M2**) (710 mg) with NaH (44.7 mg, 644 μmol; 60% in mineral oil) and propargyl bromide (48.3 μL, 644 μmol) in THF (5.0 mL) to give **s-5** as a pale yellow viscous liquid (632 mg). Yield: 89.0%. ^{1}H NMR (400 MHz, $CDCl_3$): δ (ppm) 7.28, 7.18 (aromatic), 4.33 (–$OCH_2C{\equiv}CH$), 3.29−3.80 ($Ph(CH_2)_2CH_2OCH_2$−, −$OCH_2CH(CH_2O(CH_2CH_2O)_3CH_3)O$−), 2.67 ($PhCH_2CH_2CH_2$−), 2.49 (–C≡C*H*), 1.87 ($PhCH_2CH_2CH_2O$−). $M_{n,NMR}$ = 11,400 g mol^{-1}; $M_{n,SEC}$ = 9,450 g mol^{-1}; $Đ$ = 1.04.

Synthesis of A_2B-type miktoarm star copolyether (*star*-VI). To a stirred solution of **s-4** (153 mg, 14.4 μmol) in degassed toluene (5.0 mL) were added **s-5** (150 mg, 13.1 μmol), CuBr (18.8 mg, 131 μmol), and PMDETA (54.7 μL, 262 μmol). The mixture was stirred at 70 ºC for 24 h. PSt-C≡CH (100 mg) was then added to the reaction mixture, and the entire

mixture was stirred at 70 ºC for 24 h. After cooling to room temperature, the solvent of the mixture was removed by evaporation, and the residue was purified by passage through a pad of alumina followed by preparative SEC to give ***star*-VI** as a light brown waxy solid (178 mg). Yield: 61.5%. ^{1}H NMR (400 MHz, $CDCl_3$): δ (ppm) 7.60 (triazole methine), 7.16 (aromatic), 4.79 (–OCH_2−triazole ring), 4.30 (triazole ring−CH_2(CH$_2$)$_5$O−), 3.29−3.80 (triazole ring−(CH$_2$)$_5$CH_2OCH_2−, Ph(CH$_2$)$_2$CH_2OCH_2−, −C(CH$_3$)CH_2O−, −OCH_2CH(CH_2OCH_2(CH$_2$)$_8$CH$_3$)O−, −OCH_2CH(CH_2O(CH_2CH_2O)$_3$CH_3)O−), 2.70 (PhCH_2CH$_2$CH$_2$−), 1.89 (PhCH$_2$CH_2CH$_2$O−), 1.10−1.69 (triazole ring−CH$_2$(CH_2)$_4$CH$_2$O−, −OCH$_2$CH(CH$_2$OCH$_2$CH_2(CH_2)$_7$CH$_3$)O−), 0.78−0.96 (−OCH$_2$CH(CH$_2$OCH$_2$(CH$_2$)$_8$CH_3)O−, −C(CH_3)CH$_2$O−). $M_{n,NMR}$ = 22,200 g mol^{-1}; $M_{n,SEC}$ = 16,700 g mol^{-1}; $Đ$ = 1.05.

Synthesis of poly(M2) with an azido group at chain center (s-6). Procedure A was used for the polymerization of **M2** (522 µL, 2.53 mmol) with **i-V** (12.4 mg, 50.6 µmol) and *t*-Bu-P$_4$ (50.6 µL as 1.0 mol L^{-1} stock solution in *n*-hexane, 50.6 µmol) in toluene (439 µL) to give **s-6** as a colorless viscous liquid (358 mg). Yield: 64.3%. ^{1}H NMR (400 MHz, $CDCl_3$): δ (ppm) 3.29–3.75 (N$_3$(CH$_2$)$_5$CH_2OCH_2−, −C(CH$_3$)CH_2O−, −OCH_2CH(CH_2O(CH_2CH_2O)$_3$CH_3)O−), 3.26 (N$_3$CH_2–), 1.10−1.69 (N$_3$CH$_2$(CH_2)$_4$CH$_2$O−), 0.82 (−C(CH_3)CH$_2$O−). $M_{n,NMR}$ = 11,500 g mol^{-1}; $M_{n,SEC}$ = 11,100 g mol^{-1}; $Đ$ = 1.03.

Synthesis of Poly(M1) with an ω-end ethynyl group (s-7). Procedure A was used for the polymerization of **M1** (1.11 mL, 4.67 mmol) with **i-IV** (93.3 µL as 1.0 mol L^{-1} stock

solution in toluene, 93.3 μmol) and *t*-Bu-P_4 (93.3 μL as 1.0 mol L^{-1} stock solution in *n*-hexane, 93.3 μmol) in toluene (575 μL) to give poly(**M1**) as a colorless viscous liquid (952 mg). Yield: 94.8%. ^{1}H NMR (400 MHz, $CDCl_3$): δ (ppm) 7.26, 7.18 (aromatic), 3.29−3.75 ($Ph(CH_2)_2CH_2OCH_2$−, $-OCH_2CH(CH_2OCH_2(CH_2)_8CH_3)O-$), 2.67 ($PhCH_2CH_2CH_2-$), 1.86 ($PhCH_2CH_2CH_2O-$), 1.10−1.65 ($-OCH_2CH(CH_2OCH_2CH_2(CH_2)_7CH_3)O-$), 0.78−0.95 ($-OCH_2CH(CH_2OCH_2(CH_2)_8CH_3)O-$). $M_{n,NMR}$ = 10,600 g mol^{-1}; $M_{n,SEC}$ = 9,100 g mol^{-1}; $Đ$ = 1.03.

Procedure C was used for the propargylation of poly(**M1**) (500 mg) with NaH (18.8 mg, 470 μmol; 60% in mineral oil) and propargyl bromide (35.3 μL, 470 μmol) in THF (4.0 mL) to give **s-7** as a pale yellow viscous liquid (476 mg). Yield: 95.2%. ^{1}H NMR (400 MHz, $CDCl_3$): δ (ppm) 7.26, 7.18 (aromatic), 4.33 ($-OCH_2C\equiv CH$), 3.29−3.75 ($Ph(CH_2)_2CH_2OCH_2$−, $-OCH_2CH(CH_2OCH_2(CH_2)_8CH_3)O-$), 2.67 ($PhCH_2CH_2CH_2-$), 2.41 ($-C\equiv CH$), 1.86 ($PhCH_2CH_2CH_2O-$), 1.10−1.65 ($-OCH_2CH(CH_2OCH_2CH_2(CH_2)_7CH_3)O-$), 0.78−0.95 ($-OCH_2CH(CH_2OCH_2(CH_2)_8CH_3)O-$). $M_{n,NMR}$ = 10,800 g mol^{-1}; $M_{n,SEC}$ = 8,940 g mol^{-1}; $Đ$ = 1.03.

Synthesis of *A*B_2-type miktoarm star copolyether (*star*-VII). To a stirred solution of **s-6** (175 mg, 15.2 μmol) in degassed toluene (5.0 mL) were added **s-7** (150 mg, 13.8 μmol), CuBr (19.8 mg, 138 μmol), and PMDETA (57.6 μL, 276 μmol). The mixture was stirred at 70 ºC for 24 h. PSt-C≡CH (100 mg) was added to the reaction mixture, then

the mixture was stirred at 70 ºC for 24h. After cooling to room temperature, the solvent of the mixture was removed by evaporation, and the residue was purified by passage through a pad of alumina followed by preparative SEC to give a light brown waxy solid (191 mg). Yield: 61.8%. ^{1}H NMR (400 MHz, $CDCl_3$): δ (ppm) 7.58 (triazole methine), 7.18 (aromatic), 4.80 (–OCH_2−triazole ring), 4.31 (triazole ring−CH_2(CH$_2$)$_5$O−), 3.29−3.80 (triazole ring−(CH$_2$)$_5$CH_2OCH_2−, Ph(CH$_2$)$_2$CH_2OCH_2−, −C(CH$_3$)CH_2O−, −OCH_2CH(CH_2OCH_2(CH$_2$)$_8$CH$_3$)O−, −OCH_2CH(CH_2O(CH_2CH_2O)$_3$CH_3)O−), 2.67 (PhCH_2CH$_2$CH$_2$−), 1.86 (PhCH$_2$CH_2CH$_2$O−), 1.10−1.69 (triazole ring−CH$_2$(CH_2)$_4$CH$_2$O−, −OCH$_2$CH(CH$_2$OCH$_2$CH_2(CH_2)$_7$CH$_3$)O−), 0.78−0.96 (−OCH$_2$CH(CH$_2$OCH$_2$(CH$_2$)$_8$CH_3)O−, −C(CH_3)CH$_2$O−). $M_{n,NMR}$ = 22,300 g mol^{-1}; $M_{n,SEC}$ = 17,000 g mol^{-1}; $Đ$ = 1.03.

Determination of Critical Micelle Concentration (CMC). The CMC of the block copolyether was determined by fluorescence spectroscopy using pyrene as a fluorescence probe. 100 µL of the pyrene solution in acetone (1.0×10^{-4} mol L^{-1}) was placed in different vials, and the solvent was evaporated. The aqueous micellar solution of the block copolyether (0.50 g L^{-1}) was added to the vial containing pyrene. The final volume was adjusted with deionized water to obtain a series of solutions with a constant pyrene concentration (1.0×10^{-6} mol L^{-1}) and varying polymer concentrations (0.05 g L^{-1} to 10^{-5} g L^{-1}). Each solution was sonicated for 30 min and allowed to equilibrate for 24 h. The emission spectrum was recorded by a JASCO FP-6300 spectrofluorometer equipped with a

Jasco STR-313 temperature controller (λ_{ex} = 337 nm, excitation bandwidth 2.0 nm and emission bandwidth 2.0 nm). The ratio of the emission intensities of I_1 (at 373 nm) and I_3 (at 384 nm) was plotted versus the polymer concentrations and the CMC was determined from the inflection point of the graph.

Dynamic Light Scattering (DLS) Measurement. The block copolyether sample (5.0 mg) was dissolved in deionized water (10 mL) and sonicated at room temperature for 1 h, followed by equilibration for 24 h. Before the DLS measurement, the sample solution was passed through a 0.45 μm PTFE membrane filter. The DLS measurements were performed using an Otsuka Electronics FDLS-300 light scattering spectrometer with an Otsuka Electronics NM-454L temperature controller. The sample solutions were maintained at 25 °C in all experiments. The relaxation-time (τ) distribution and particle size distribution were obtained by the CONTIN analysis using the autocorrelation function. The apparent diffusion coefficient (D) was calculated using the following equation:

$$\left.\frac{\Gamma}{q^2}\right|_{q \to 0} = D$$

where Γ is the relaxation frequency ($\Gamma = \tau^{-1}$) and q is the wave vector defined by the following equation:

$$q = \frac{4\pi n}{\lambda} \sin\left(\frac{\theta}{2}\right)$$

where λ is the wavelength of the laser beam (532 nm), θ is the scattering angle, and n is the refractive index of the medium. Consequently, the hydrodynamic radius (R_h) was calculated from the Stokes-Einstein relation as follows:

$$R_h = \frac{k_B T}{6\pi\eta\Gamma} q^2 = \frac{k_B T}{6\pi\eta D}$$

where k_B is the Boltzmann constant, T is the temperature, and η is the viscosity of the medium.

Transmission Electron Microscopic (TEM) Measurement. A drop of the aqueous micellar solution (0.50 g L^{-1}) was placed on a copper grid coated with carbon, then the grid was air-dried for 24 h before the experiment was performed. No staining was required. TEM measurements were carried out using a JEM-2000FX microscope operating at an accelerating voltage of 80 kV.

Determination of Cloud Point ($T_{c.d.}$). The transmittance of the aqueous micellar solution (0.50 g L^{-1}) was measured at 300 nm by a Jasco V-550 spectrophotometer equipped of the Jasco ETC-505T temperature controller with a heating rate of 1 ºC min^{-1}. The $T_{c.d.}$ was defined as the temperature at which the transmittance of the sample solution reached 50%.

2.5 References and Notes

1. Mark, H. F.; Bikales, N. M.; Overberger, C. G.; Menges, G; Kroschwitz, J. I., Eds. *Encyclopedia of Polymer Science and Engineering*, vol. 6; John Wiley & Sons, Inc., **1985**.
2. Schmolka, I. R. *J. Am. Oil Chem. Soc.* **1977**, *54*, 110–116.
3. Gupta, S.; Tyagi, R.; Parmar, V. S.; Sharma, S. K.; Haag, R. *Polymer* **2012**, *53*, 3053–3078.
4. Booth, C.; Attwood, D. *Macromol. Rapid Commun.* **2000**, *21*, 501–527.
5. Brocas, A.-L.; Gervais, M.; Carlotti, S.; Pispas, S. *Polym. Chem.* **2012**, *3*, 2148–2155.
6. Mai, S.-M.; Fairclough, J. P. A.; Terrill, N. J.; Turner, S. C.; Hamley, I. W.; Matsen, M. W.; Ryan, A. J.; Booth, C. *Macromolecules* **1998**, *31*, 8110–8116.
7. Halacheva, S.; Rangelov, S.; Tsvetanov, C. *Macromolecules* **2006**, *39*, 6845–6852.
8. Altinok, H.; Yu, G.-E.; Nixon, S. K.; Gorry, P. A.; Attwood, D.; Booth, C. *Langmuir* **1997**, *13*, 5837–5848.
9. Mai, S.-M.; Booth, C.; Kelarakis, A.; Havredaki, V.; Ryan, A. J. *Langmuir* **2000**, *16*, 1681–1688.
10. Barthel, M. J.; Babiuch, K.; Rudolph, T.; Vitz, J.; Hoeppener, S.; Gottschaldt, M.; Hager, M. D.; Schacher, F. H.; Schubert, U. S. *J. Polym. Sci. Part A: Polym. Chem.*, **2012**, *50*, 2914–2923.
11. Barthel, M. J.; Rudolph, T.; Crotty, S.; Schacher, F. H.; Schubert, U. S.; *J. Polym. Sci. Part A: Polym. Chem.* **2012**, *50*, 4958–4965.
12. Dimitrov, P.; Rangelov, S.; Dworak, A.; Tsvetanov, C. B. *Macromolecules*, **2004**, *37*, 1000–1008.
13. Riess, G. *Prog. Polym. Sci.* **2003**, *28*, 1107–1170.
14. Kim, S. Y.; Lee, Y. M. *Biomaterials* **2001**, *22*, 1697–1704.
15. Kataoka, K.; Harada, A.; Nagasaki, Y. *Adv. Drug Delivery Rev.* **2001**,*47*, 113–131.

16. Hartgerink, J. D.; Beniash, E.; Stupp, S. I. *Science* **2001**, *294*,1684–1688.
17. Tang, C.; Qi, K.;Wooley, K. L.; Matyjaszewski, K.; Kowalewski, T. *Angew. Chem., Int. Ed.* **2004**, *43*, 2783–2787.
18. Bao, X. Y.; Zhao, X. S.; Li, X.; Chia, P. A.; Li, J. *J. Phys. Chem. B* **2004**, *108*, 4684–4689.
19. Alexandridis, P.; Holzwarth, J. F.; Hatton, T. A. *Macromolecules* **1994**, *27*, 2414–2425.
20. Zhou, Z.-K.; Chu, B. *Macromolecules* **1994**, *27*, 2025–2033.
21. Yu, G.-E.; Garrett, C. A.; Mai, S.-M.; Altinok, H.; Attwood, D.; Price, C.; Booth, C. *Langmuir* **1998**, *14*, 2278–2285.
22. Heise, A.; Hedrick, J. L.; Frank, C. W.; Miller, R. D. *J. Am. Chem. Soc.* **1999**, *121*, 8647–8648.
23. Pispas, S.; Hadjichristidis, N.; Potemkin, I.; Khokhlov, A. *Macromolecules* **2000**, *33*, 1741–1746.
24. Ishizu, K.; Uchida, S. *Prog. Polym. Sci.* **1999**, *24*, 1439–1480.
25. Hadjichristidis, N.; Pitsikalis, M.; Pispas, S.; Iatrou, H. *Chem. Rev.* **2001**, *101*, 3747–3792.
26. Larraneta, E.; Isasi, J. R. *Langmuir* **2013**, *29*, 1045−1053.
27. Hurter, P. N.; Hatton, T. A. *Langmuir* **1992**, *8*, 1291–1299.
28. Choi, Y. K.; Bae, Y. H.; Kim, S. W. *Macromolecules* **1998**, *31*, 8766–8774.
29. Sun, C.; Ritchie, J. E. *J. Phys. Chem. B* **2011**, *115*, 8381–8389.
30. Misaka, H.; Sakai, R.; Satoh, T.; Kakuchi, T. *Macromolecules* **2011**, *44*, 9099−9107.
31. Misaka, H.; Tamura, E.; Makiguchi, K.; Kamoshida, K.; Sakai, R.; Satoh, T.; Kakuchi, T. *J. Polym. Sci. Part A: Polym. Chem.* **2012**, *50*, 1941−1952.
32. Kwon, W.; Roh, Y.; Kamoshida, K.; Kwon, K. H.; Jeong, Y. C.; Kim, J.; Misaka, H.; Shin, T. J.; Kim, J.; Kim, K.-W.; Jin, K. S.; Chang, T.; Kim, H.; Satoh, T.; Kakuchi, T.; Ree, M. *Adv. Funct. Mater.* **2012**, *22*, 5194−5208.

33. Engler, A. C.; Chan, J. M. W.; Fukushima, K.; Coady, D. J.; Yang, Y. Y.; Hedrick, J. L. *ACS Macro Lett.* **2013**, *2*, 332–336.
34. Isono, T.; Asai, S.; Satoh, Y.; Takaoka, T.; Tajima K.; Kakuchi, T.; Satoh, T. *Macromolecules* **2013**, *46*, 3841−3849.
35. Zhao, J.; Pahovnik, D.; Gnanou, Y.; Hadjichristidis, N. *Macromolecules*, **2014**, *47*, 3814–3822.
36. Zhao, J.; Pahovnik, D.; Gnanou, Y.; Hadjichristidis, N. *Macromolecules*, **2014**, *47*, 1693–1698.
37. Hiki,S.; Kataoka, K. *Bioconjugate Chem.* **2007**, *18*, 2191−2196.
38. Lee, S. H.; Lee, Y.; Lee, S.-W.; Ji, H.-Y.; Lee, J.-H.; Lee, D. S.; Park, T. G. *Acta Biomaterialia* **2011**, *7*, 1468–1476.
39. Honda, S.; Yamamoto, T.; Tezuka, Y. *J. Am. Chem. Soc.* **2010**, *132*, 10251−10253.
40. Malkoch, M.; Schleicher, K.; Drockenmuller, E.; Hawker, C. J.; Russell, T. P.; Wu, P.; Fokin, V. V. *Macromolecules* **2005**, *38*, 3663−3678.
41. Karuna, M. S. L.; Devi, B. L. A. P.; Prasad, P. S. S.; Prasad, R. B. N. *J. Surfact. Deterg.* **2009**, *12*, 117–123.
42. Diaz-Quijada, G. A.; Farrahi, S.; Clarke, J.; Tonary, A. M.; Pezacki, J. P. *J. Biomater. Appl.* **2007**, *21*, 235–249.
43. An, H.; Bradshaw, J. S.; Krakowiak, K. E.; Tarbet, B. J.; Dalley, N. K. *J. Org. Chem.* **1993**, *58*, 7694–7699.
44. Isono, T.; Otsuka, I.; Kondo, Y.; Halila, S.; Fort, S.; Rochas, C.; Satoh, T.; Borsali, R.; Kakuchi, T. *Macromolecules* **2013**, *46*, 1461–1469.
45. Li, X.-M.; Fan, F.; Lu, J.-S.; Xue, S.-F.; Zhang, Y.-Q.; Zhu, Q.-J.; Tao, Z.; Lawrance, G. A.; Wei, G. *New J. Chem.* **2011**, *35*, 1088−1095.
46. Rao, J.; Zhang, Y.; Zhang, J.; Liu, S. *Biomacromolecules* **2008**, *9*, 2586−2593.

Chapter 3

Synthesis of Well-Defined Cyclic, Figure-Eight-Shaped, and Tadpole-Shaped Block Copolyethers

3.1 Introduction

Macromolecules possessing cyclic architectures, such as cyclic, figure-eight-shaped, and tadpole-shaped polymers, are of great interest due to the endless nature of the cyclic chain, which endowed them with an increased glass transition temperature, lower viscosity, and smaller hydrodynamic volume.[1-6] In addition, the cyclic block copolymers provided special properties in relation to self-assembly as described in Section 1.2, which are typically not attainable with the corresponding linear counterparts.[7-15] Although many synthetic approaches for cyclic block copolymers have been established,[16–23] the synthesis of cyclic-containing block copolymers, such as figure-eight- and tadpole-shaped block copolymers, is still a remaining and challenging task. Moreover, the synthesis of a comprehensive set of such block copolymers, i.e., linear, cyclic, figure-eight-shaped, and tadpole-shaped block copolymers, possessing comparable chemical structures, monomer compositions, and molecular weights have been never achieved. To provide a fundamental insight into the relationship between the cyclic-containing topology and self-assembling property, a concise and robust strategy is required for preparing figure-eight- and tadpole-shaped block copolymers possessing varied block arrangements.

Among the wide range of block copolymer systems, polyether-based amphiphilic block copolymers have been recognized as the most traditional but important class of block copolymer materials as described in Section 1.3.[24-26] Indeed, there has been considerable

efforts to investigate the self-assembly of polyether-based block copolymers in both bulk and solution states during the past several decades.[25,27-34] However, there is less information available about the topological effects on the self-assembly. The synthesis of polyether-based block copolymers possessing a macrocyclic architecture was achieved by the acetalization of PEO-*b*-PPO-*b*-PEO or PEO-*b*-PBO-*b*-PEO triblock copolymers through the reaction of a hydroxyl end group with dichloromethane under Williamson conditions and high dilution.[33,34] Although this methodology is hard to use for the synthesis of polyether-based block copolymers with figure-eight- and tadpole-shaped architectures, the other approaches based on the intramolecular click reactions of α-azido-ω-ethynyl- (or α-ethynyl-ω-azido-) functionalized precursors have emerged as a powerful method for constructing cyclic polymers and cyclic block copolymers.[35,36] Such a highly efficient method should be expandable for the synthesis of polyether-based block copolymers with figure-eight- and tadpole-shaped architectures by combining the appropriately designed precursor block copolymers with precisely controlled azido and ethynyl group placements as well as a fixed molecular weight and monomer composition.

This chapter describes a novel approach to provide systematic sets of cyclic, figure-eight- and tadpole-shaped amphiphilic block copolymers via the intramolecular click reaction of linear block copolymer precursors bearing azido and ethynyl functionalities at designed positions, together with the corresponding figure-eight-shaped homo polymer, as

shown in **Scheme 3-1**. The clickable linear block copolymer precursors were precisely synthesized based on the *t*-Bu-P_4-catalyzed ROP of decyl glycidyl ether (**M1**) as a hydrophobic monomer and 2-(2-(2-methoxyethoxy)ethoxy)ethyl glycidyl ether (**M2**) as a hydrophilic monomer with the combination of functional initiators and terminators. The intramolecular click reaction of *α*-azido-*ω*-ethynyl-functionalized poly-**M1**-*block*-poly-**M2** was then examined to produce the cyclic block copolymer and to provide fundamental insight into the cyclization conditions. Finally, the combination of the *t*-Bu-P_4-catalyzed ROP and intramolecular click cyclization was applied to clickable linear precursors with various di-, tri-, and penta-block sequences for producing figure-eight-shaped block copolymers with four different block arrangements and tadpole-shaped block copolymers with two different block arrangements. A preliminary study of the self-assembling properties in water was performed using the obtained linear, cyclic, figure-eight-shaped, and tadpole-shaped block copolymers.

Scheme 3-1. Synthesis of cyclic, figure-eight-shaped, and tadpole-shaped amphiphilic block copolyethers by combining the *t*-Bu-P_4-catalyzed ring-opening polymerization (ROP) and intramolecular click cyclization

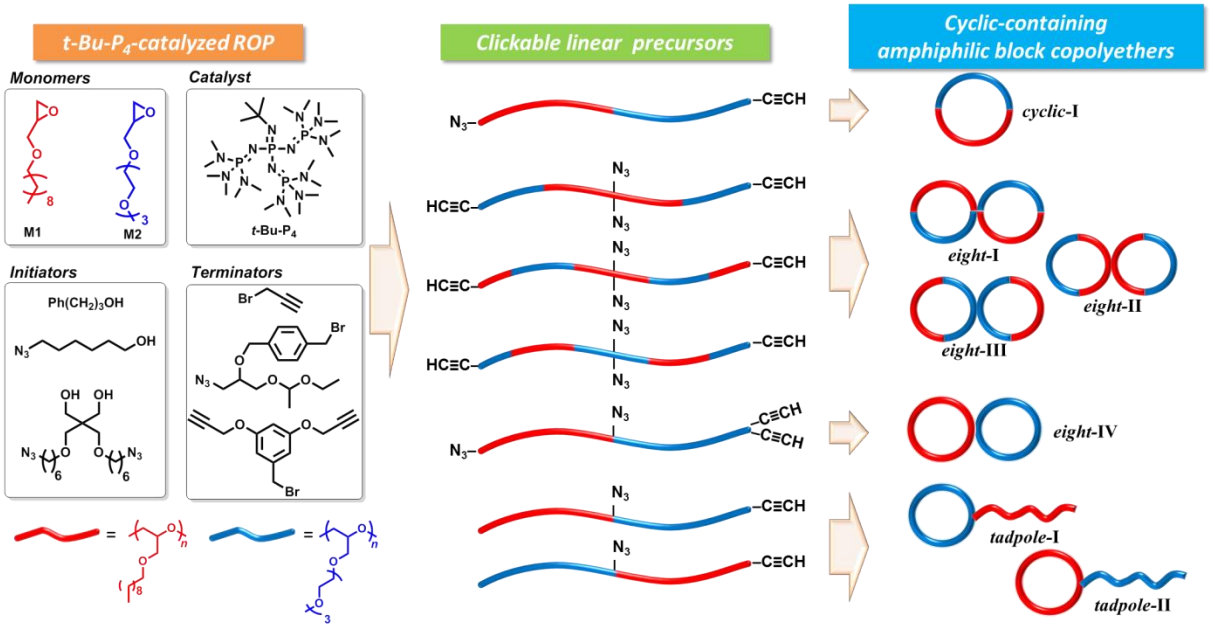

3.2 Results and Discussion

3.2.1 Synthesis of Figure-Eight-Shaped Poly(butylene oxide)

The author first demonstrated the synthesis of the figure-eight-shaped poly(butylene oxide) (*eight*-PBO) to verify the synthetic strategy based on the intramolecular click cyclization. The intramolecular click cyclization of azido and ethynyl end-functionalized polymers is one of the most reliable methods for the synthesis of cyclic polyethers,[37–40] and Pan et al. used the click cyclization method for producing a figure-eight-shaped polystyrene.[41] Our synthetic strategy for the figure-eight-shaped PBO (*eight*-PBO) involves (1) the preparation of a PBO with two azido groups at the chain center ($(N_3)_2$-$(PBO)_2$), (2) the preparation of a PBO with two azido groups and two ethynyl groups ($(N_3)_2$-$(PBO\text{-}C{\equiv}CH)_2$) by modification of $(N_3)_2$-$(PBO)_2$ with propargyl bromide, and (3) the intramolecular double click cyclization of $(N_3)_2$-$(PBO\text{-}C{\equiv}CH)_2$, as shown in **Scheme 3-2**.

Scheme 3-2. Synthesis of figure-eight-shaped poly(butylene oxide) (***eight*-PBO**) by the *t*-Bu-P_4-catalyzed ROP of butylene oxide (BO)

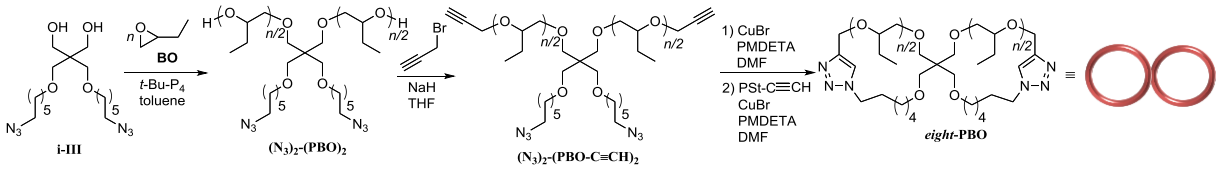

To obtain the $(N_3)_2$-$(PBO)_2$, the *t*-Bu-P_4-catalyzed ROP of BO was performed using 2,2-bis((6-azidohexyloxy)methyl)propane-1,3-diol (**i-III**) as the initiator in toluene at the

$[BO]_0/[\textbf{i-III}]_0/[t\text{-Bu-P}_4]_0$ ratio of 30/1/0.5. The SEC trace of the product shows a unimodal peak with dispersity (*Đ*) of 1.06. In the ^{1}H NMR spectrum of the product, the signals assigned to the protons of the PBO backbone and a minor signal due to the methylene proton adjacent to the azido group (proton *a*). The number average molecular weight determined from ^{1}H NMR ($M_{n,NMR}$) of $(N_3)_2$-$(PBO)_2$ was calculated to be 2,480 g mol^{-1}, which well agreed with the number average molecular weight calculated from monomer conversion ($M_{n,calc}$) of 2,550 g mol^{-1} (**Table 3-1**)

Table 3-1. Synthesis of Figure-eight-shaped Poly(butylene oxide) (*eight*-PBO) and the Precursor Polymers

Polymer	$M_{n,calc}$ [a] [g mol^{-1}]	$M_{n,NMR}$ [a] [g mol^{-1}]	$M_{n,SEC}$ [b] [g mol^{-1}]	$\langle G \rangle$	*Đ* [b]
$(N_3)_2$-$(PBO)_2$	2,550	2,480	3,020	0.83	1.06
$(N_3)_2$-$(PBO\text{-}C{\equiv}CH)_2$	2,620	2,560	2,800		1.07
eight-PBO	2,620	6,700	2,330		1.06

[a] Determined by ^{1}H NMR spectrum in $CHCl_3$. [b] Determined by SEC in THF using polystyrene standards.

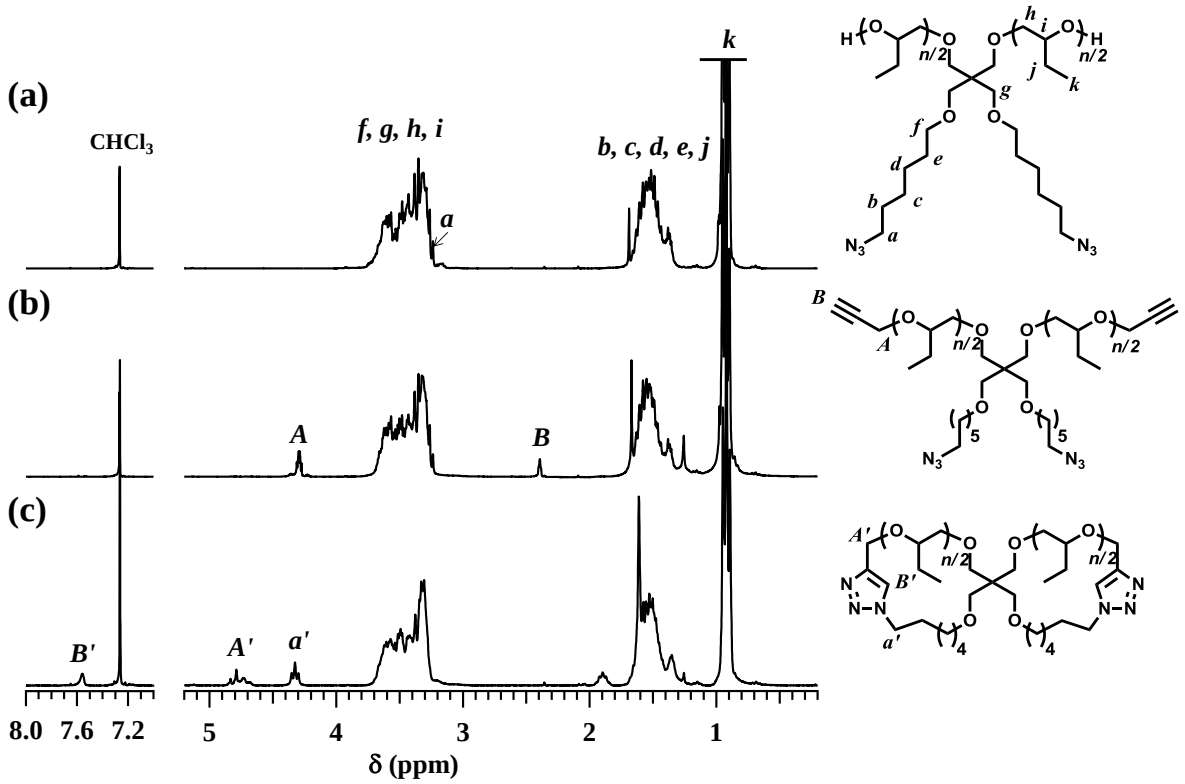

Figure 3-1. ^{1}H NMR spectra of (a) poly(butylene oxide) (PBO) with two azido groups at chain center (**$(N_3)_2$-$(PBO)_2$**) (b) ω,ω'-diethynyl PBO with two azido groups (**$(N_3)_2$-(PBO-C≡CH)$_2$**), and (c) figure-eight-shaped PBO (***eight*-PBO**) in $CDCl_3$ (400 MHz).

The obtained $(N_3)_2$-$(PBO)_2$ was treated with a three-fold excess of propargyl bromide using NaH in THF to give $(N_3)_2$-$(PBO\text{-}C{\equiv}CH)_2$ as a pale yellow viscous liquid in 94.8% isolated yield. The ^{1}H NMR spectrum of the resultant polymer shows new signals due to the protons of the propargyl group at the ω-chain ends (protons A, 4.30 ppm; proton B, 2.39 ppm), as shown in **Figure 3-1b**, and the $M_{n,NMR}$ of 2,560 g mol^{-1} firmly agreed with the $M_{n,calc}$ of 2,560 g mol^{-1} for the $(N_3)_2$-$(PBO\text{-}C{\equiv}CH)_2$. These results definitely concluded that the propargyl group was quantitatively introduced on the ω-chain ends. Furthermore, the

MALDI-TOF MS measurement result confirmed the 100% conversion from $(N_3)_2$-$(PBO)_2$ into the desired $(N_3)_2$-$(PBO\text{-}C{\equiv}CH)_2$ (**Figure 3-2**).

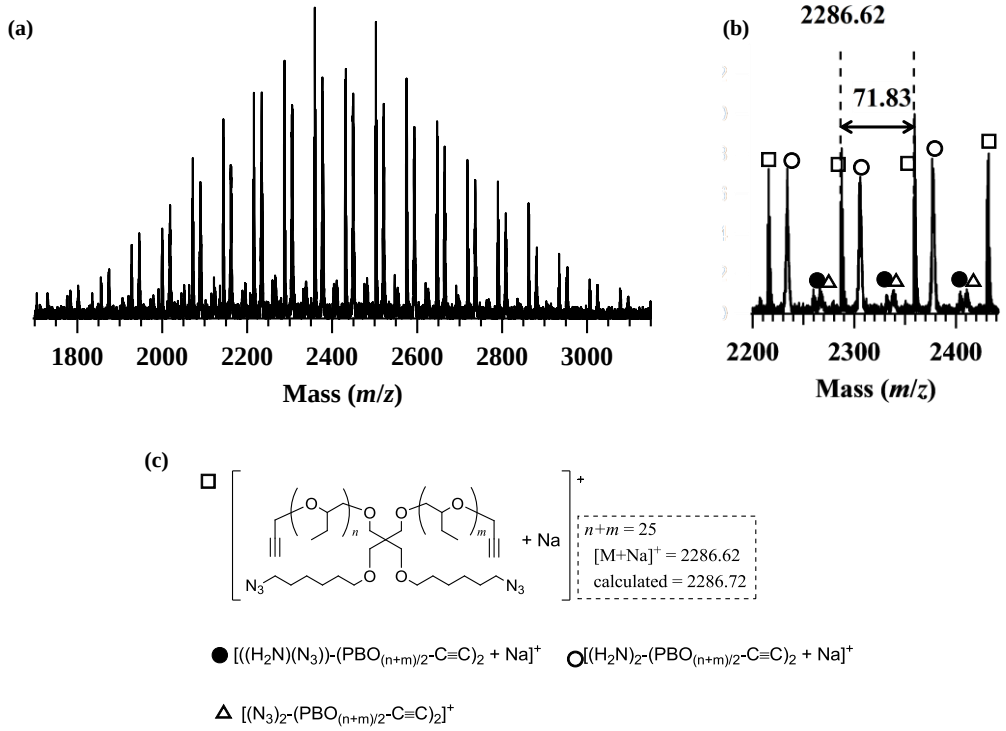

Figure 3-2. (a) MALDI-TOF MS spectrum of $(N_3)_2$-$(PBO\text{-}C{\equiv}CH)_2$, (b) the expanded spectrum from 2,200 to 2,450 Da, and (c) the structural assignment.

Finally, the double click cyclization of $(N_3)_2$-$(PBO\text{-}C{\equiv}CH)_2$ was carried out using CuBr/*N*,*N*,*N*',*N*'',*N*''-pentamethyldiethylenetriamine (PMDETA) in DMF at 100 °C under a highly diluted condition. The polymer solution was added to the catalyst solution using a syringe pump over 26 h, thus ensuring the highly diluted condition. To remove the unreacted $(N_3)_2$-$(PBO\text{-}C{\equiv}CH)_2$, the ethynyl-functionalized Wang resin (PSt-C≡CH) was added to the reacting mixture. After completing the reaction, the mixture was purified by

passing it through a pad of alumina followed by preparative SEC to give the product as a light brown viscous liquid in 74.4% isolated yield. **Figure 3-3** shows a comparison of the SEC traces between $(N_3)_2$-(PBO-C≡CH)$_2$ and the resultant product. The SEC trace of the product before purification using preparative SEC shows two peaks, in which no elution peak of the starting materials ($M_{n,SEC}$ = 2,800 g mol^{-1}) is observed. Although ca. 9% of a by-product was observed in the higher molecular weight region ($M_{n,SEC}$ = 5,120 g mol^{-1}), it was completely removed using preparative SEC. The isolated lower molecular weight fraction ($M_{n,SEC}$ = 2,330 g mol^{-1}) should be the desired *eight*-PBO because the ⟨*G*⟩ value (⟨*G*⟩ = $M_{n,SEC}$ (*eight*-PBO)/$M_{n,SEC}$ ($(N_3)_2$-(PBO-C≡CH)$_2$)) of 0.83 was comparable to the reported values for the figure-eight-shaped polymers.[41,42] In the ^{1}H NMR spectrum of the isolated product (**Figure 3-1c**), the signals due to the terminal acetylene protons (proton *B*, 2.39 ppm) and the methylene protons adjacent to the azido group (proton *a*, 3.27 ppm) completely disappeared, while the signals assignable to the methine protons in the triazole rings (proton *B'*, 7.56 ppm) and methylene protons adjacent to the triazole rings (proton *A'*, 4.79 ppm; proton *a'*, 4.33 ppm) are observed. The $M_{n,NMR}$ and DP were calculated to be 2,700 g mol^{-1} and 31, respectively. The complete disappearance of the azido group in the isolated product was also confirmed from the FT-IR analysis (**Figure 3-4**). These results suggested that there was no unreacted azido group in the product, and the azido group was converted into the triazole ring. Finally, the chemical structure of the product was identified by the MALDI-TOF MS

measurement (**Figure 3-5**); the peak at 2,286.77 Da completely agreed with the calculated molar mass for the 25-mer of *eight*-PBO (2,286.72 Da, calcd. for $[M + Na]^+$).

Thus, the intramolecular double click cyclization turned out to be a useful method to produce the figure-eight-shaped polyether, in which the suitable design of the initiator is necessary for the *t*-Bu-P_4-catalyzed ROP of epoxy monomers leading to the polyether precursor with two azido groups and two ethynyl end-functional groups.

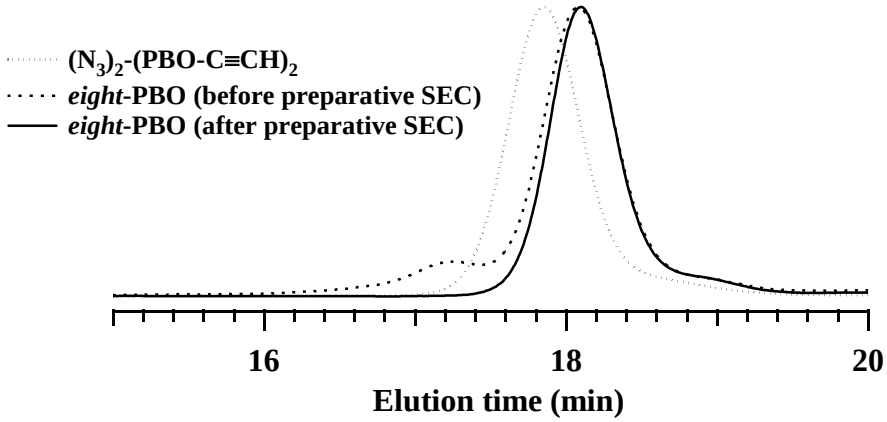

Figure 3-3. SEC traces of $(N_3)_2$-(PBO-C≡CH)$_2$ (dashed line), and *eight*-PBO before preparative SEC (dotted line), and *eight*-PBO after preparative SEC (solid line).

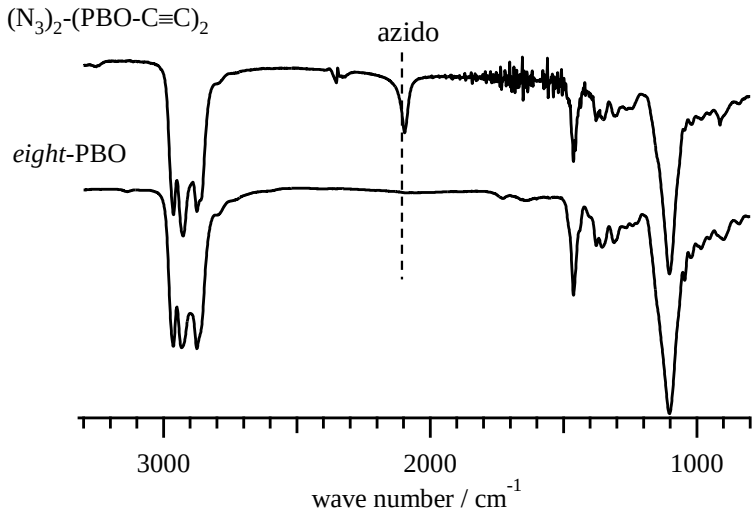

Figure 3-4. FT-IR spectra of $(N_3)_2$-(PBO-C≡CH)$_2$ and *eight*-PBO.

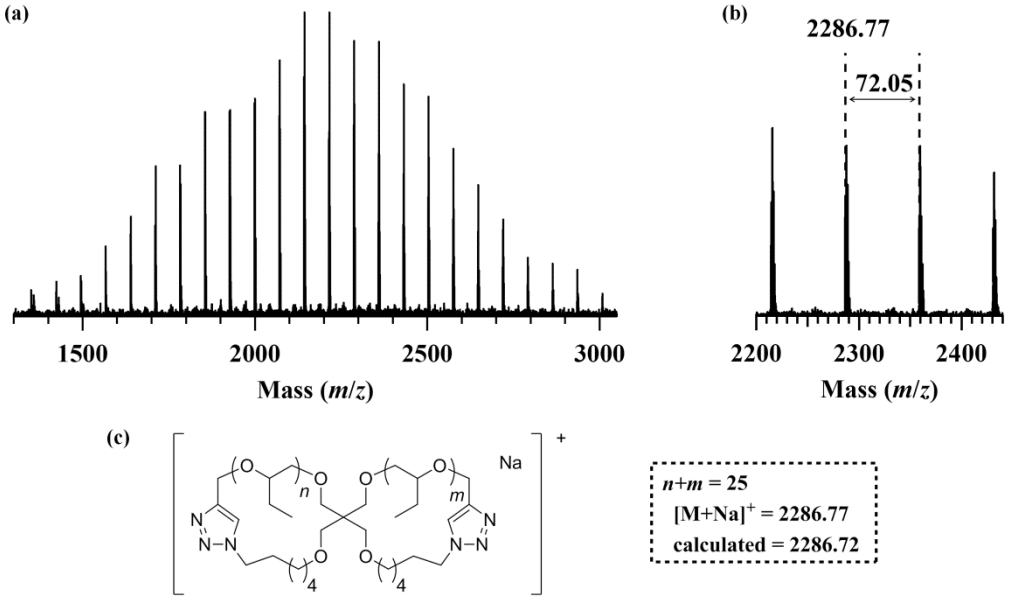

Figure 3-5. (a) MALDI-TOF MS spectrum of *eight*-PBO, (b) the expanded spectrum from 2200 to 2450 Da, and (c) the structural assignment.

3.2.2 Synthesis of Cyclic and Figure-Eight-Shaped Block Copolyethers

3.2.2-1 Synthesis of Cyclic Block Copolyether

Utilizing the *t*-Bu-P_4-catalyzed ROP and click cyclization procedure, the author firstly synthesized the cyclic amphiphilic block copolymer, ***cyclic*-I**, through three reaction steps as shown in **Scheme 3-3**: (1) the block copolymerization of **M1** and **M2** initiated from 6-azido-1-hexanol (**i-VI**) to form the *α*-azido-functionalized poly-**M1**-*block*-poly-**M2** (**c-1**), (2) the modification of the terminal hydroxyl group into the propargyl group to form the *α*-azido-*ω*-ethynyl-functionalized poly-**M1**-*block*-poly-**M2** (**c-2**), and (3) the intramolecular click cyclization.

Scheme 3-3. Synthesis of cyclic amphiphilic block copolyether

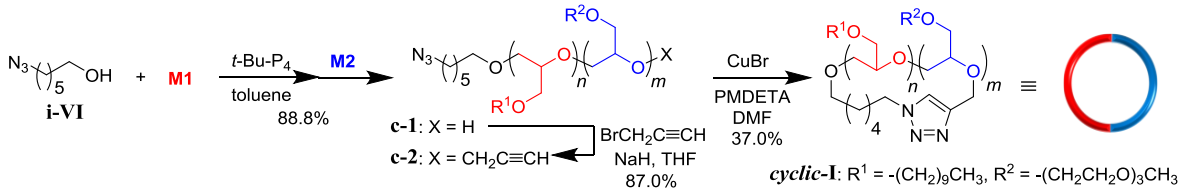

The *t*-Bu-P_4-catalyzed ROP of **M1** using 6-azido-1-hexanol (**i-VI**) as the initiator was performed with the $[\mathbf{M1}]_0/[\mathbf{i\text{-}VI}]_0/[t\text{-Bu-P}_4]_0$ ratio of 50/1/1 and the monomer conversion of **M1** reached >99% after 20 h of polymerization. The NMR and SEC measurements for the aliquot sample verified the formation of the *α*-azido-functionalized poly-**M1** with the $M_{n,NMR}$ of 11,000 g mol^{-1} and $Đ$ value of 1.05. The subsequent addition of 50 equiv. of **M2** (with respect to **i-VI**) to the polymerization mixture allowed the block copolymerization to produce **c-1** with $M_{n,NMR}$ of 22,000 g mol^{-1}. The SEC trace of **c-1** was completely shifted to the

higher molecular weight region as compared to that of the poly-**M1** obtained by the first polymerization while retaining the narrow $Đ$ of 1.05 (**Figure 3-6a**). The hydroxyl ω-chain end of **c-1** was then treated with propargyl bromide in the presence of sodium hydride to produce **c-2** ($M_{n,NMR}$ = 21,900 g mol^{-1}, $Đ$ = 1.04). The quantitative introduction of the propargyl group was verified by comparing the integration ratio of the signals due to the methylene adjacent to the azido group (proton *a* in **Figure 3-6b**) at 3.26 ppm and the methylene adjacent to the ethynyl group (proton *A*) at 4.40 ppm.

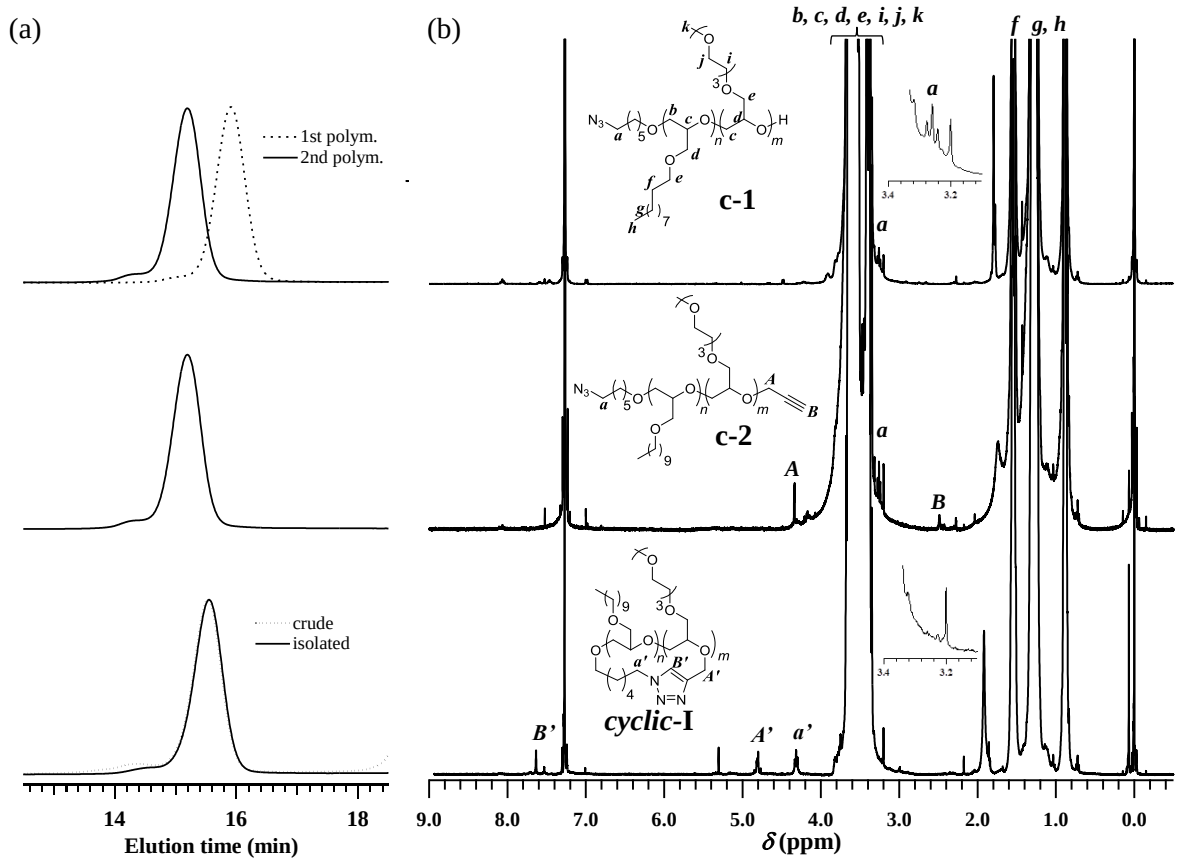

Figure 3-6. (a) SEC traces of **c-1** (dashed line, poly-**M1** obtained by the first polymerization; solid line, **c-1** obtained by the second polymerization), **c-2**, and ***cyclic*-I** (dashed line, before purification; solid line, after the purification using preparative SEC). (b) ^{1}H NMR spectra of **c-1**, **c-2**, and ***cyclic*-I** in $CDCl_3$ (400 MHz). The insets show the expanded ^{1}H NMR spectra.

The *α*-azido-*ω*-ethynyl-functionalized linear precursor, **c-2**, was subjected to the intramolecular click cyclization with the CuBr/*N,N,N',N'',N''*-pentamethyldiethylenetriamine (PMDETA) catalyst system in DMF at 120 °C. To ensure highly diluted conditions, the DMF solution of **c-2** (40 g L^{-1}) was slowly (0.3 mL h^{-1}) added to the catalyst solution in DMF (27.5 mL). After completing the addition, propargyl-functionalized Wang resin (PSt-C≡CH) was added to the reaction mixture to completely remove the unreacted **c-2**, and the absence of the starting material **c-2** after the reaction was confirmed by an FT-IR analysis, in which the absorption at 2100 cm^{-1} due to the azido group completely disappeared (**Figure 3-7**). Although *ca*. 7% of a high molecular weight elution peak due to byproducts formed by intermolecular click reaction was observed in the SEC trace, the cyclic diblock copolymer, ***cyclic*-I** ($M_{n,NMR}$ = 22,300 g mol^{-1}), was isolated after the purification using preparative SEC as a light brown waxy solid in 37.0% yield. The cyclized product ***cyclic*-I** displayed a unimodal elution peak with the $Đ$ value of 1.04 (**Figure 3-6a**). A decrease in the elution volume was observed from the starting materials **c-2** to ***cyclic*-I**, indicating the formation of a cyclic product having a hydrodynamic volume smaller than the linear precursor. The ratio between the $M_{n,SEC}$s at the peak top of ***cyclic*-I** and **c-2**, i.e., $M_{p,sec(cyclic)}/M_{p,sec(linear)} = \langle G \rangle$, was determined to be 0.80 (**Table 3-2**), which was in good agreement with the reported value for the monocyclic polymer ($\langle G \rangle$ = 0.69 – 0.81). This is strong evidence for the intramolecular cyclization to form the cyclic polymer. Furthermore, the shrinking factor, *g*', based on the

intrinsic viscosities of ***cyclic*-I** ($[\eta]_{cyclic}$ = 8.0 mL g^{-1}) and **c-2** ($[\eta]_{linear}$ = 13.1 mL g^{-1}), i.e. g' = $[\eta]_{cyclic}/[\eta]_{linear}$ = 0.61 (**Table 3-2**), also supported the decrease in the hydrodynamic volume due to cyclization. The ^{1}H NMR comparison of **c-2** and ***cyclic*-I** confirmed that the signals due to the methylene adjacent to the azido group (proton *a*; 3.26 ppm), ethynyl proton (proton *B*; 2.50 ppm), and methylene adjacent to the ethynyl group (proton *A*; 4.40 ppm) of **c-2** were replaced after the click reaction by a methine proton of the newly formed triazole ring (proton *B'*; 7.60 ppm) and two methylene protons adjacent to the triazole ring (protons *a'* and *A'*; 4.33 and 4.80 ppm). Thus, the desired cyclic block copolyether, ***cyclic*-I**, was obtained by the intramolecular click cyclization of the *α*-azido-*ω*-ethynyl-functionalized linear precursor.

Table 3-2. Molecular Characteristics and Intrinsic Viscosities ($[\eta]$) of the Cyclic Block Copolyether and the Precursors

sample	$M_{n,NMR}$ [a] [g mol^{-1}]	$M_{p,sec}$ [b] [g mol^{-1}]	$\langle G \rangle$	$Đ$ [c]	DP_1/DP_2 [d]	$[\eta]$ [e] [mL g^{-1}]	g'	yield [%]
c-1	22,000	–		1.05		–		88.8
c-2	21,900	16,100	0.80	1.04	51/50	13.1	0.61	87.0
***cyclic*-I**	22,300	12,800		1.04		8.0		37.0

[a] Determined by ^{1}H NMR. [b] Determined by the peak top of SEC trace in THF using polystyrene standerds. [c] Determined by SEC in THF. [d] Number-average degree of polymerizations of decyl glycidyl ether (DP_1) and 2-(2-(2-methoxyethoxy)ethoxy)ethyl glycidyl ether (DP_2) in the copolymer were determined by ^{1}H NMR. [e] Determined by SEC-MALS in THF (0.3 mg mL^{-1}).

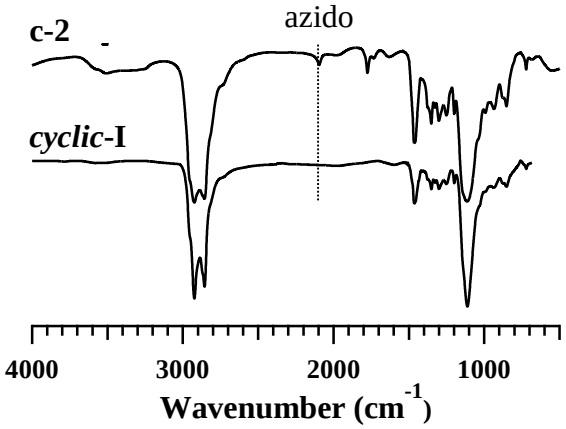

Figure 3-7. FT-IR spectra of **c-2** (upper) and ***cyclic*-I** (lower).

3.2.2-2 Synthesis of Figure-eight-shaped Block Copolyethers

The intramolecular click cyclization was further applied to produce four types of figure-eight-shaped block copolymers using the appropriate linear precursors with azido and ethynyl functionalities, as depicted in **Scheme 3-4** and **Scheme 3-5**. First, a triblock copolymer bearing two azido groups at the chain center, **e-1**, was prepared by the *t*-Bu-P_4-catalyzed sequential block copolymerization of **M1** (50 equiv.) and following **M2** (50 equiv.) using **i-III** as the initiator. The progress of the block copolymerization was followed by SEC measurements, and the elution peak of the polymer obtained by the first polymerization of **M1** shifted to a higher molecular weight region by the second polymerization of **M2** while retaining a narrow dispersity (**Figure 3-8a**). The presence of the initiator moiety was confirmed by the signal due to the methylene proton adjacent to the azido group (proton *a* in **Figure 3-8b**). In a similar fashion, the pentablock copolymers, **e-3**

and **e-5**, were prepared by the sequential block copolymerizations using **i-III** as the initiator with the following monomer addition sequence: 25 equiv. of **M1** → 50 equiv. of **M2** → 25 equiv. of **M1** for **e-3** and 25 equiv. of **M2** → 50 equiv. of **M1** → 25 equiv. of **M2** for **e-5**. The SEC results clearly demonstrated the progress of the sequential block copolymerizations (**Figure 3-9a**, **3-10a**).

Scheme 3-4. Synthesis of figure-eight-shaped amphiphilic block copolyethers consisting of the same two cyclic units

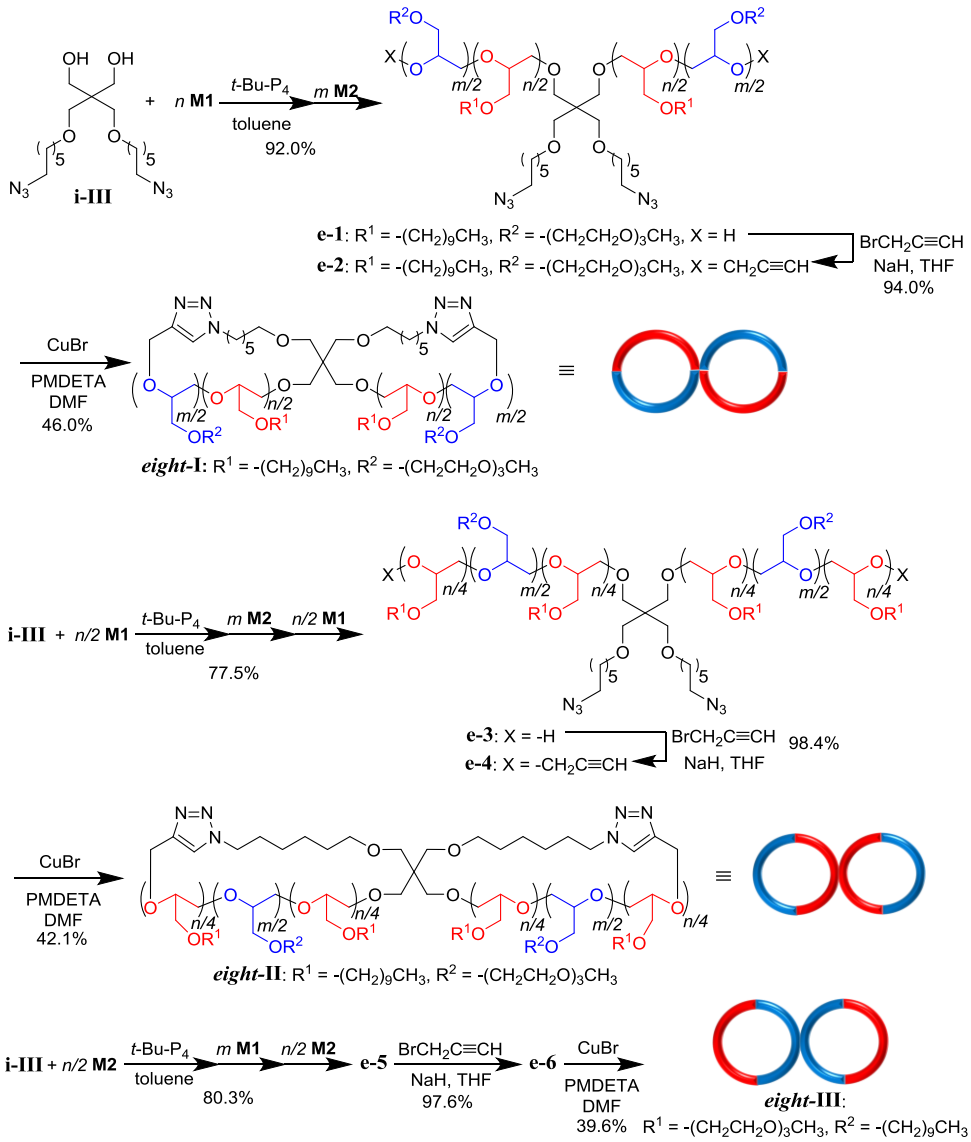

For all the block copolymerizations, the full conversion of the monomer was ensured by the NMR measurement of the aliquot of the reacting mixture before adding the next monomer. The $M_{n,NMR}$ values of **e-1**, **e-3**, and **e-5** (21800, 22100, and 22000 g mol^{-1} for **e-1**, **e-3**, and **e-5**, respectively) well agreed with the predicted value (22,100 g mol^{-1}), and the $Đ$ values were in the range of 1.04 – 1.08. The treatment of **e-1**, **e-3**, and **e-5** with propargyl bromide in the presence of sodium hydride produced **e-2**, **e-4**, and **e-6**, which was confirmed by the signals due to the ethynyl proton (proton *B* in **Figure 3-8b**, **3-9b**, **3-10b**) and methylene proton adjacent to the ethynyl group (proton *A*). The *α*,*α*'-diazido-*ω*,*ω*'-diethynyl linear block copolymer precursors **e-2**, **e-4**, and **e-6**, were then subjected to the click cyclization using the same conditions for the synthesis of ***cyclic*-I**. The figure-eight-shaped block copolymers, ***eight*-I** ($M_{n,NMR}$ = 21,800 g mol^{-1}, $Đ$ = 1.06), ***eight*-II** ($M_{n,NMR}$ = 22,300 g mol^{-1}, $Đ$ = 1.03), and ***eight*-III** ($M_{n,NMR}$ = 22,200 g mol^{-1}, $Đ$ = 1.03), were obtained as a light brown waxy solid by purification using an alumina column and preparative SEC in 39.6 – 46.0% yields (**Table 3-3**). In the SEC traces of the crude products, *ca.* 14%, 16%, and 21% of high molecular weight byproducts were detected for the click cyclization of **e-2**, **e-4**, and **e-6**, respectively. The ^{1}H NMR analyses of the isolated figure-eight-shaped block copolymers confirmed the absence of the azido and ethynyl groups as well as the formation of triazole rings (**Figure 3-8b**, **3-9b**, **3-10b**). For example, the ^{1}H NMR spectrum of ***eight*-I** exhibited a signal due to the triazol methine (proton *B'*) at 7.56 ppm and methylenes adjacent to the triazole ring

(proton *a'* and *A'*) at 4.33 and 4.79 ppm, while the signals due to the propargyl group and methylene adjacent to the azido group disappeared (**Figure 3-8b**). The FT-IR analysis also confirmed the absence of the azido group in the isolated products (**Figure 3-11**). Moreover, the cyclized structures for the obtained block copolymers were established by the lower molecular weight region in the SEC trace as compared to the linear precursors as well as the decrease in the intrinsic viscosity. For example, the SEC trace shifted to the lower molecular weight region after the click reaction of **e-2** to form ***eight*-I** (**Figure 3-8a**), and the $\langle G \rangle$ value was calculated to be 0.80 (**Table 3-3**), which was in good agreement with that of the figure-eight-shaped poly(butylene oxide) ($\langle G \rangle$ = 0.83). The *g*' values of ***eight*-I**, ***eight*-II**, and ***eight*-III** were in the range of 0.46 – 0.56 (**Table 3-3**) and were lower than that of ***cyclic*-I**, indicating the more compact conformations of ***eight*-I**, ***eight*-II**, and ***eight*-III** than the ***cyclic*-I**. Thus, the three types of figure-eight-shaped block copolymers with different distributions of hydrophilic and hydrophobic blocks were obtained by the double click cyclization of the multiblock type precursors having two ethynyl groups at the ω-chain ends and two azido groups at the chain center.

Table 3-3. Molecular Characteristics and Intrinsic Viscosities ([η]) of the Figure-eight-shaped Block Copolyether and the Precursors

sample	$M_{n,NMR}$ [a] [g mol^{-1}]	$M_{p,sec}$ [b] [g mol^{-1}]	$\langle G \rangle$	$Đ$ [c]	DP_1/DP_2 [d]	$[\eta]$ [e] [mL g^{-1}]	g'	yield [%]
e-2	21,900	14,100	0.80	1.04	50/48	12.2	0.46	46.0
***eight*-I**	21,800	11,300		1.06		5.6		
e-4	22,100	15,400	0.86	1.06	52/48	14.0	0.47	42.1
***eight*-II**	22,300	13,300		1.03		6.6		
e-6	22,100	15,300	0.90	1.08	50/50	14.7	0.56	39.6
***eight*-III**	22,200	13,700		1.03		8.2		
e-11	22,100	16,500	0.75	1.05	50/50	10.3	0.60	38.7
***eight*-IV**	22,200	12,400		1.04		6.2		

[a] Determined by ^{1}H NMR. [b] Determined by the peak top of SEC trace in THF using polystyrene standerds. [c] Determined by SEC in THF. [d] Number-average degree of polymerizations of decyl glycidyl ether (DP_1) and 2-(2-(2-methoxyethoxy)ethoxy)ethyl glycidyl ether (DP_2) in the copolymer were determined by ^{1}H NMR. [e] Determined by SEC-MALS in THF (0.3 mg mL^{-1}).

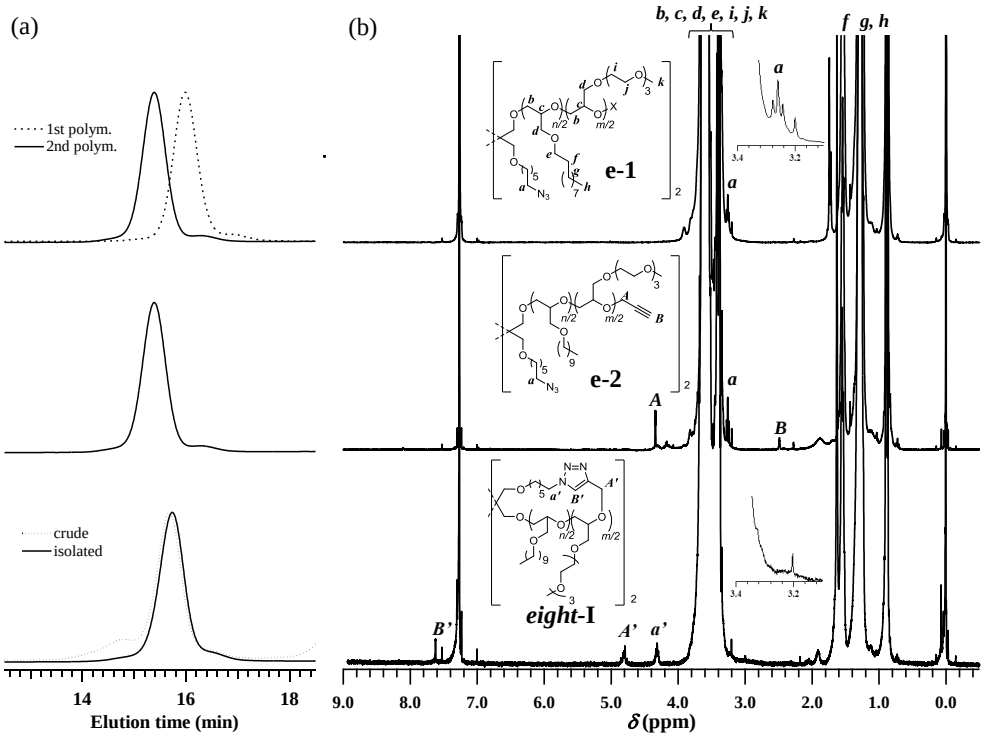

Figure 3-8. (a) SEC traces of **e-1** (dashed line, poly-**M1** obtained by the first polymerization; solid line, **e-1** obtained by the second polymerization), **e-2**, and ***eight*-I**

(dashed line, before purification; solid line, after the purification by preparative SEC). (b) ^{1}H NMR spectra of **e-1**, **e-2**, and ***eight*-I** in $CDCl_3$ (400 MHz).

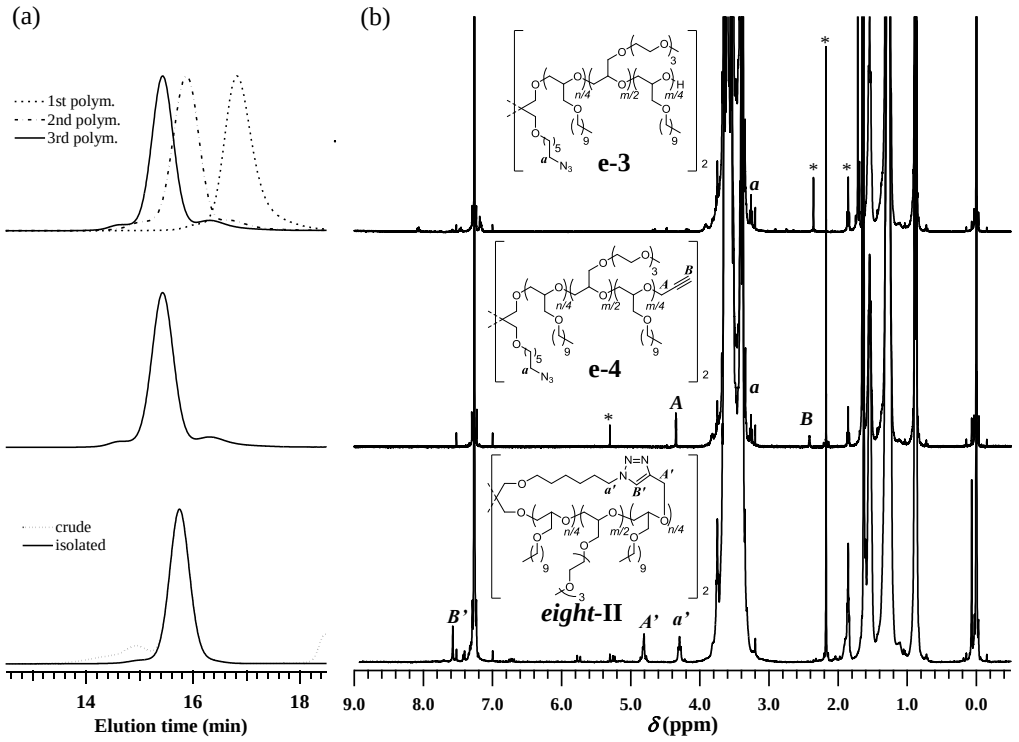

Figure 3-9. (a) SEC traces and (b) ^{1}H NMR spectra in $CDCl_3$ (400 MHz) of **e-3**, **e-4**, and ***eight*-II**. The asterisk means solvent peaks.

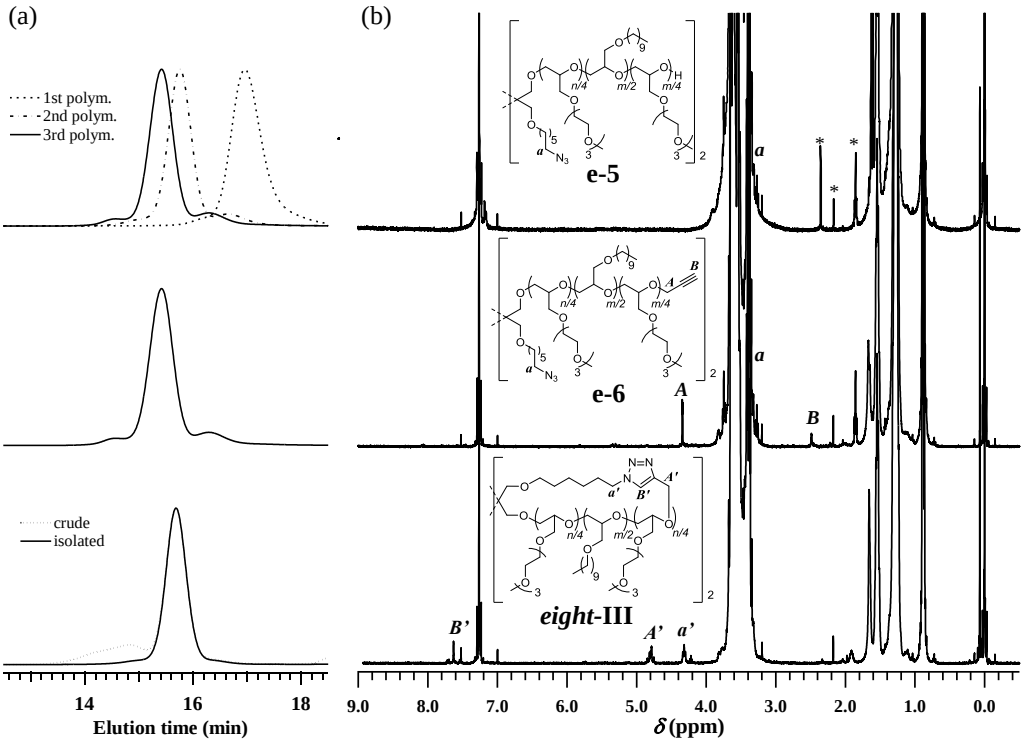

Figure 3-10. (a) SEC traces and (b) ^{1}H NMR spectra in $CDCl_3$ (400 MHz) of **e-5**, **e-6**, and ***eight*-III**. The asterisk means solvent peaks.

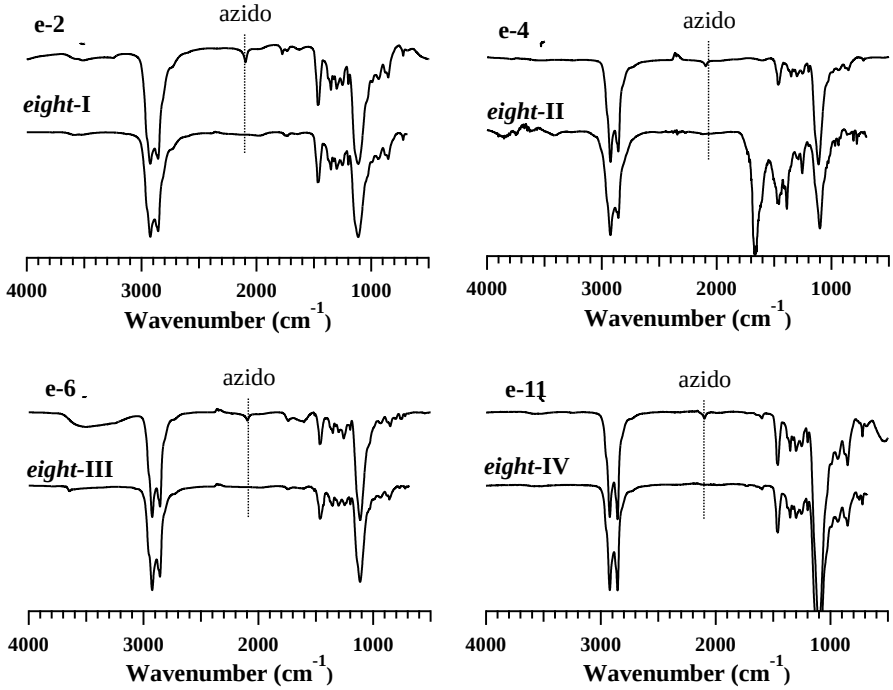

Figure 3-11. FT-IR spectra of **e-2**, **e-4**, **e-6**, **e-11**, ***eight*-I**, ***eight*-II**, ***eight*-III** and ***eight*-IV**.

The next target is the figure-eight-shaped block copolymer consisting of two different cyclic units, ***eight*-IV**, which is in contrast to the above-prepared figure-eight-shaped block copolymers having the same two cyclic units. Our synthetic strategy for ***eight*-IV** is based on the double click cyclization of a linear diblock copolymer of **M1** and **M2** bearing two ethynyl groups at the ω-chain end and two azido groups at the α-chain end and the chain center (**e-11**), as shown in **Scheme 3-5**. To synthesize the diblock copolymer having two azido groups at the α-chain end and the chain center (**e-10**), the author first prepared the α,ω-diazido-ω-hydroxyl poly-**M1** (**e-8**), in which the hydroxyl group would be used as the

initiation site for the subsequent chain extension. The author newly designed and synthesized

1-(((1-azido-3-(1-ethoxyethoxy)propan-2-yl)oxy)methyl)-4-(bromomethyl)benzene (**t-I**) as the terminator for introducing both the azido and hydroxyl groups at the ω-chain end. **t-I** was prepared by the ring-opening of ethoxyethyl glycidyl ether using sodium azide in the presence of ammonium chloride followed by the treatment with an excess amount of α,α-dibromo-*p*-xylene, as shown in **Scheme 3-5b**.

Scheme 3-5. Synthesis of figure-eight-shaped amphiphilic block copolyethers consisting of two different cyclic units

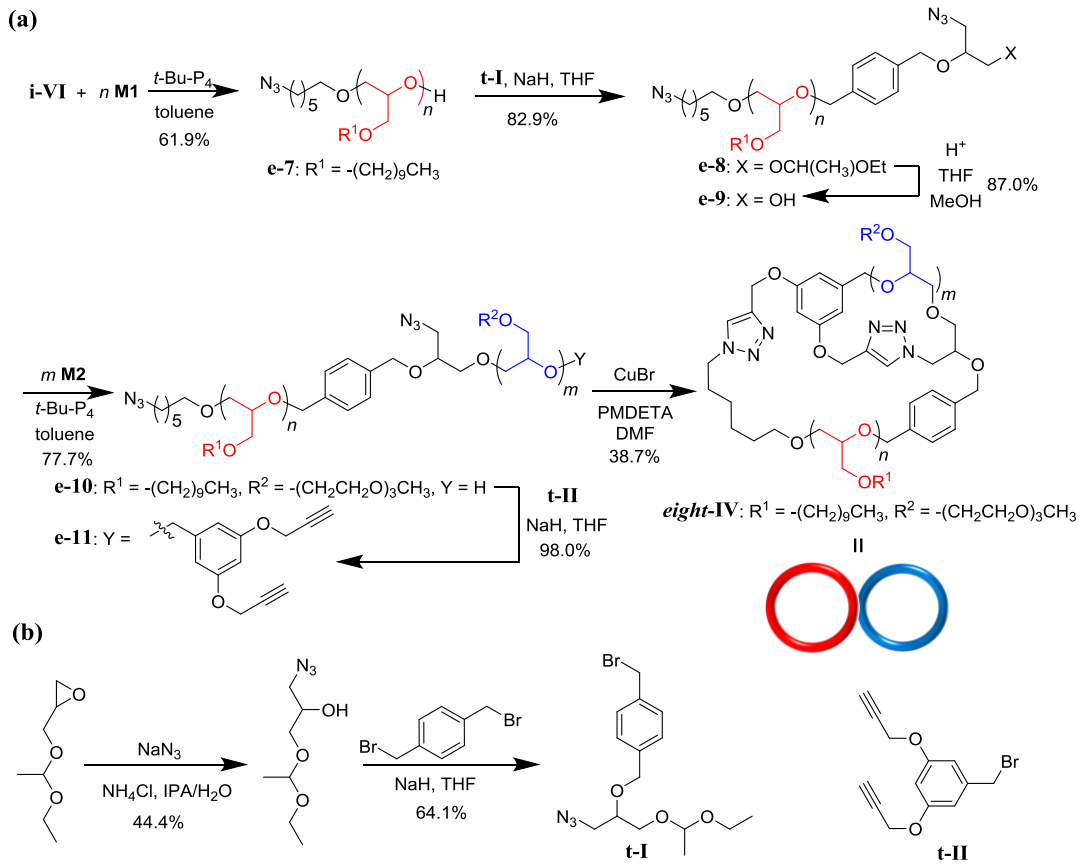

An α-azido end-functionalized poly-**M1** (**e-7**, $M_{n,NMR}$ = 10900, $Đ$ = 1.02) was treated with **t-I** in the presence of sodium hydride, and the ethoxyethyl group was then deprotected under acidic conditions to give **e-9**. The ^{1}H NMR spectrum of **e-9** showed the signals due to the benzyl protons (protons *A* and *D* in **Figure 3-12b**) at 4.70 ppm as well as methylene protons adjacent to the azido group (protons *a*) at 3.26 ppm, from which the quantitative introduction of an azido and a hydroxyl group at the ω-chain end was verified. After a rigorous dehydration, **e-9** was utilized as a macroinitiator for the synthesis of a diblock copolymer of **M1** and **M2** with two azido groups at the α-chain end and the junction point of the two blocks, **e-10**. The polymerization was carried out at the $[\mathbf{M2}]_0/[\mathbf{e\text{-}9}]_0/[t\text{-Bu-P}_4]_0$ ratio of 50/1/1 to give **e-10** in 77.7% yield. The SEC trace of **e-9** shifted to the higher molecular weight region after the polymerization (**Figure 3-12a**), which confirmed that the polymerization was initiated from the hydroxyl group of **e-9**. The $M_{n,NMR}$ and $Đ$ of the isolated **e-10** were determined to be 22000 g mol^{-1} and 1.06, respectively. **e-10** was then further converted to the requisite linear precursor, **e-11** ($M_{n,NMR}$ = 22100 g mol^{-1}, $Đ$ = 1.05), by the treatment with 1-bromomethyl-3,5-bis(2-propynyloxy)benzene (**t-II**) in the presence of sodium hydride. The double click cyclization of **e-11** and SEC fractionation led to the desired ***eight*-IV** with the $M_{n,NMR}$ and $Đ$ of 22,200 g mol^{-1} and 1.04, respectively, in 38.7% isolated yield. Here, *ca*. 38% of high molecular weight byproducts formed through the intermolecular click reaction were detected in the SEC trace of the crude product. The ^{1}H NMR and IR spectroscopic

analyses proved that there were no unreacted azido and ethynyl groups (**Figures 3-12b** and **3-11**), implying that the obtained product should have a doubly cyclized structure. In addition, the ^{1}H NMR spectrum of ***eight*-IV** showed two signals due to the triazole methine protons (proton *J'* in **Figure 3-12b**) at 7.76 and 7.64 ppm. The increase in the SEC elution volume (**Figure 3-12a**; $\langle G \rangle$ = 0.75) as well as decrease in the intrinsic viscosity (g' = 0.60) also provided evidence of the doubly cyclized architecture of the product (**Table 3-3**). Therefore, the synthesis of a series of figure-eight-shaped amphiphilic block copolymers with four different types of hydrophobic/hydrophilic orientations has been achieved via the double click cyclization of diazido-diethynyl-functionalized linear precursors.

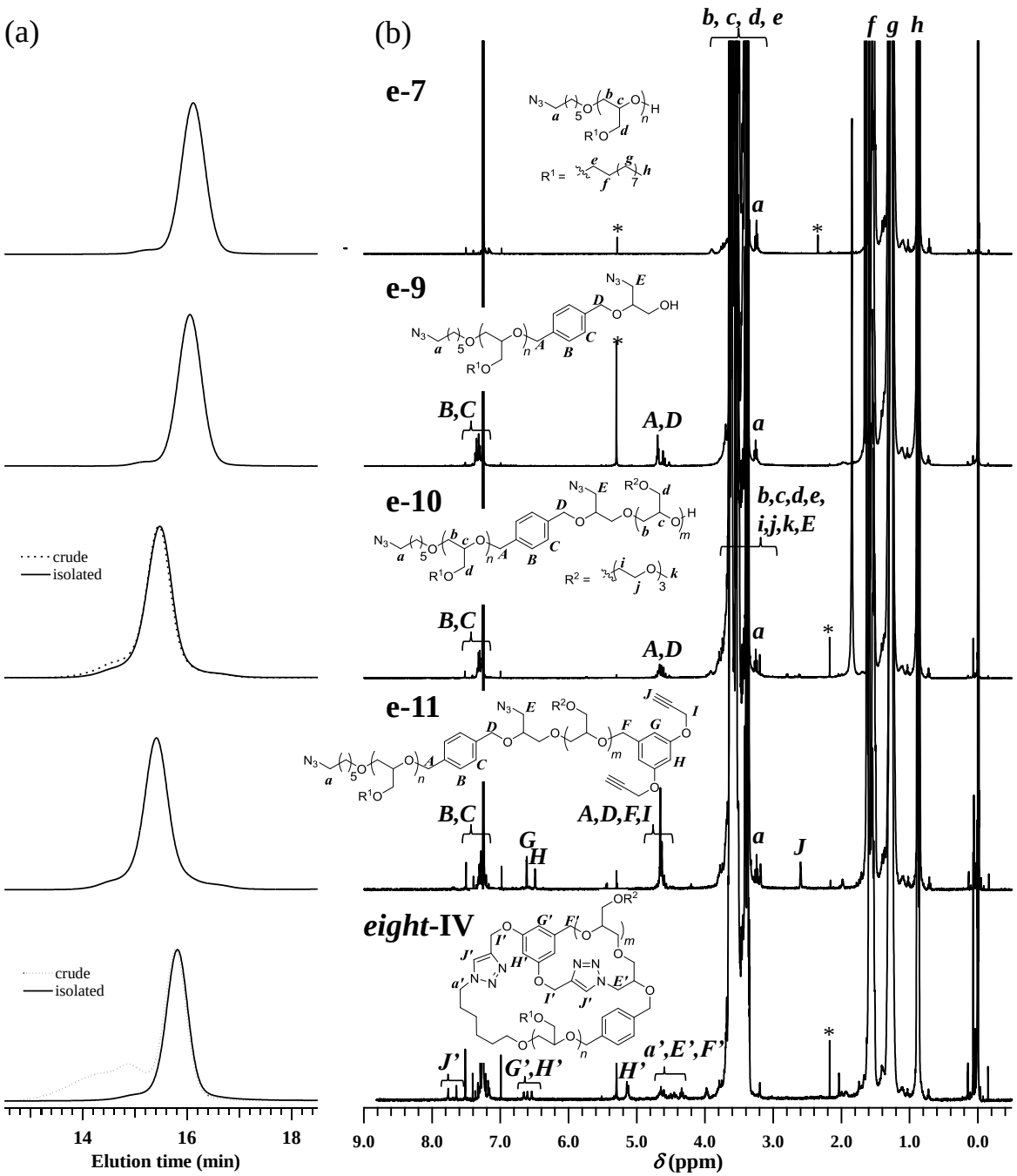

Figure 3-12. (a) SEC traces of **e-7**, **e-9**, **e-10** (dashed line, before purification; solid line, after the purification using preparative SEC), **e-11**, and ***eight*-IV** (dashed line, before purification; solid line, after the purification using preparative SEC). (b) ^{1}H NMR spectra of **e-7**, **e-9**, **e-10**, **e-11**, and ***eight*-IV** in $CDCl_3$ (400 MHz).

3.2.3 Synthesis of Tadpole-Shaped Block Copolyethers

The synthesis of the tadpole-shaped block copolymers were attempted as illustrated in **Scheme 3-6**. Poly-**M1** having a 3-phenyl–1-propoxy α-chain end (**poly-M1**, $M_{n,NMR}$ = 11100 g mol^{-1}, $Đ$ = 1.05) was modified by the treatment with **t-I** and following deprotection of the ethoxyethyl group, providing ω-azido-ω-hydroxyl-functionalized poly-**M1**, **tp-1**. The *t*-Bu-P_4-catalyzed ROP of **M2** using **tp-1** as a macroinitiator followed by treatment with propargyl bromide led to the poly-**M1**-*block*-poly-**M2** with an ethynyl group at the ω-chain end and an azido group at the junction point between the two blocks, **tp-3** ($M_{n,NMR}$ = 22400 g mol^{-1}, $Đ$ = 1.05). An analog of **tp-3** with the opposite block sequence, **tp-6** ($M_{n,NMR}$ = 22100 g mol^{-1}, $Đ$ = 1.05), was prepared in a similar fashion, beginning with poly-**M2** having the 3-phenyl-1-propoxy α-chain end (**poly-M2**, $M_{n,NMR}$ = 10900 g mol^{-1}, $Đ$ = 1.06). The click cyclization of **tp-3** and following SEC fractionation gave the desired tadopole-shaped block copolymers consisting of a hydrophilic cyclic unit and a hydrophobic tail, ***tadpole*-I** ($M_{n,NMR}$ = 21900 g mol^{-1}, $Đ$ = 1.04), in 56.2% yield. In a similar fashion, the tadopole-shaped block copolymers consisted of a hydrophobic cyclic unit and a hydrophilic tail, ***tadpole*-II** ($M_{n,NMR}$ = 22400 g mol^{-1}, $Đ$ = 1.06), was obtained in 32.7% yield. Although 23% and 20% of byproducts were formed during the cyclization reaction of **tp-3** and **tp-6**, respectively, as indicated by the SEC traces of the crude products, these were removed through the SEC fractionation process. The chemical structures of ***tadpole*-I** and ***tadpole*-II** were confirmed

by IR and NMR analyses, in which the disappearances of the azido and ethynyl groups as well as the formation of the triazol ring were observed (**Figures 3-13b**, **3-14b**, **3-15**). The cyclized architectures for ***tadpole*-I** and ***tadpole*-II** were further verified by the ⟨*G*⟩ values (0.88 for ***tadpole*-I** and 0.91 for ***tadpole*-II**; **Figures 3-13a**, **3-14a**, and **Table 3-4**) as well as the *g*' values (0.88 for ***tadpole*-I** and 0.68 for ***tadpole*-II**, **Table 3-4**).

Scheme 3-6. Synthesis of tadpole-shaped amphiphilic block copolyethers

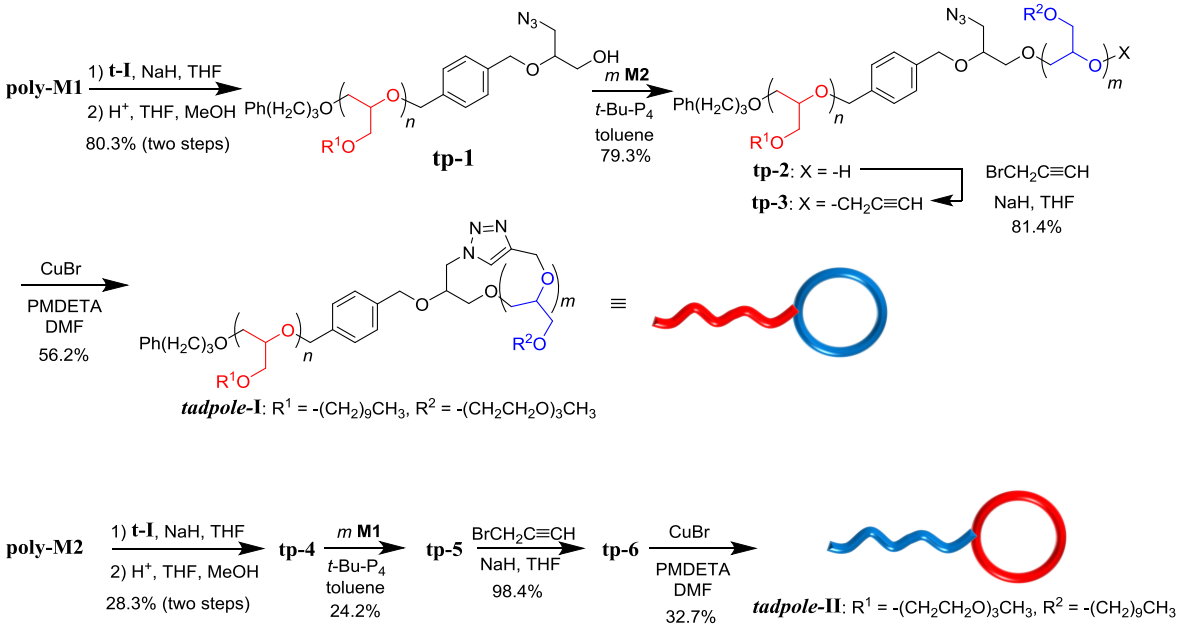

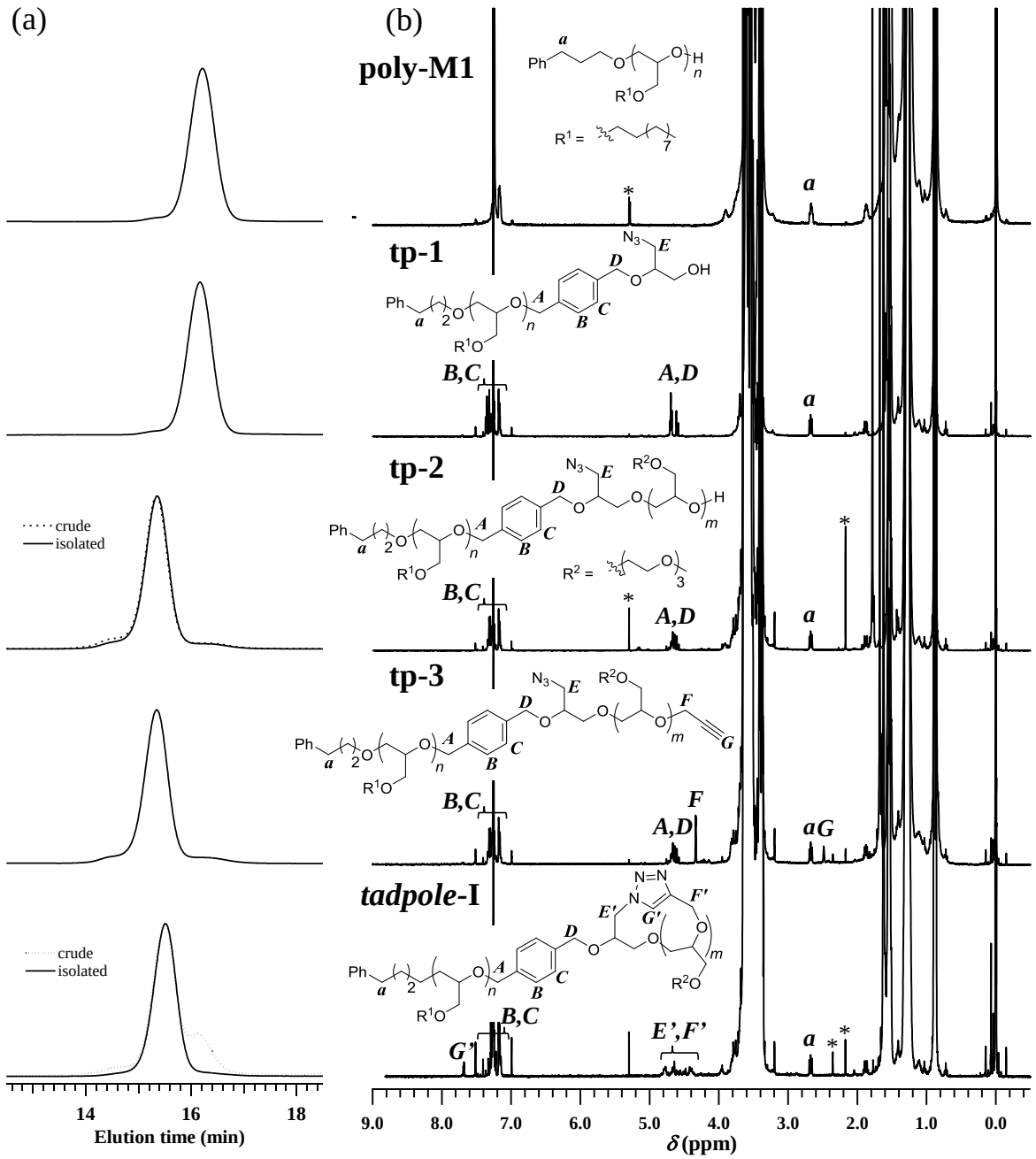

Figure 3-13. (a) SEC traces of **poly-M1**, **tp-1**, **tp-2** (dashed line, before purification; solid line, after the purification using preparative SEC), **tp-3**, and ***tadpole*-I** (dashed line, before purification; solid line, after the purification using preparative SEC). (b) ^{1}H NMR spectra of **poly-M1**, **tp-1**, **tp-2**, **tp-3**, and ***tadpole*-I** in $CDCl_3$ (400 MHz).

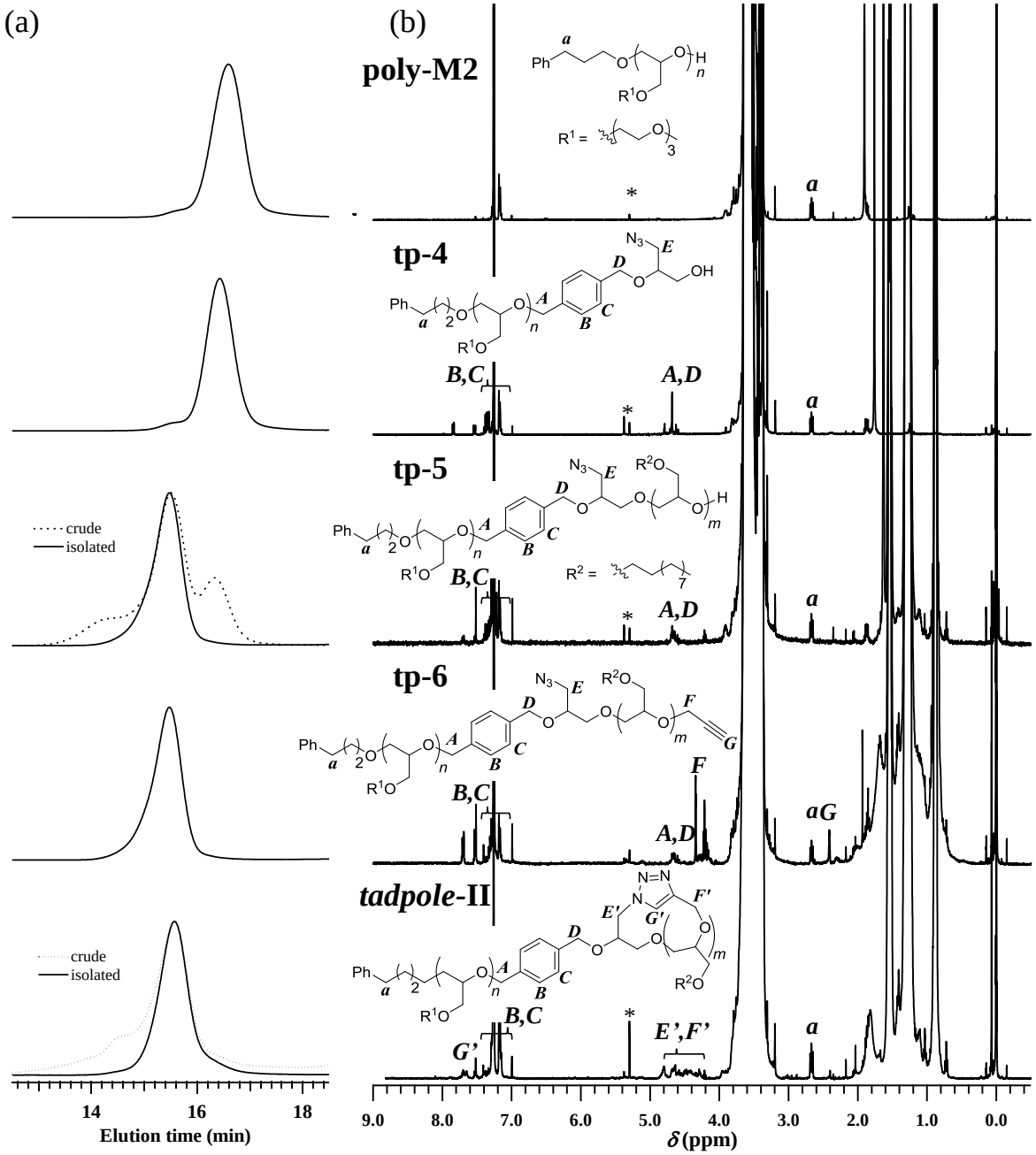

Figure 3-14. (a) SEC traces of **poly-M2**, **tp-4**, **tp-5** (dashed line, before purification; solid line, after the purification using preparative SEC), **tp-6**, and ***tadpole*-II** (dashed line, before purification; solid line, after the purification using preparative SEC). (b) ^{1}H NMR spectra of **poly-M2**, **tp-4**, **tp-5**, **tp-6**, and ***tadpole*-II** in $CDCl_3$ (400 MHz).

Table 3-4. Molecular Characteristics and Intrinsic Viscosities ([η]) of the Tadpole-shaped Block Copolyether and the Precursors

sample	$M_{n,NMR}$ [a] [g mol^{-1}]	$M_{p,sec}$ [b] [g mol^{-1}]	$\langle G \rangle$	$Đ$ [c]	DP_1/DP_2 [d]	$[\eta]$ [e] [mL g^{-1}]	g'	yield [%]
tp-3	22,500	16,400	0.88	1.06	51/49	9.7	0.88	53.0
***tadpole*-I**	21,900	14,500		1.04		8.5		
tp-6	22,100	16,000	0.91	1.05	51/50	10.3	0.68	32.7
***tadpole*-II**	22,400	14,600		1.06		7.0		

[a] Determined by ^{1}H NMR. [b] Determined by the peak top of SEC trace in THF using polystyrene standerds. [c] Determined by SEC in THF. [d] Number-average degree of polymerizations of decyl glycidyl ether (DP_1) and 2-(2-(2-methoxyethoxy)ethoxy)ethyl glycidyl ether (DP_2) in the copolymer were determined by ^{1}H NMR. [e] Determined by SEC-MALS in THF (0.3 mg mL^{-1}).

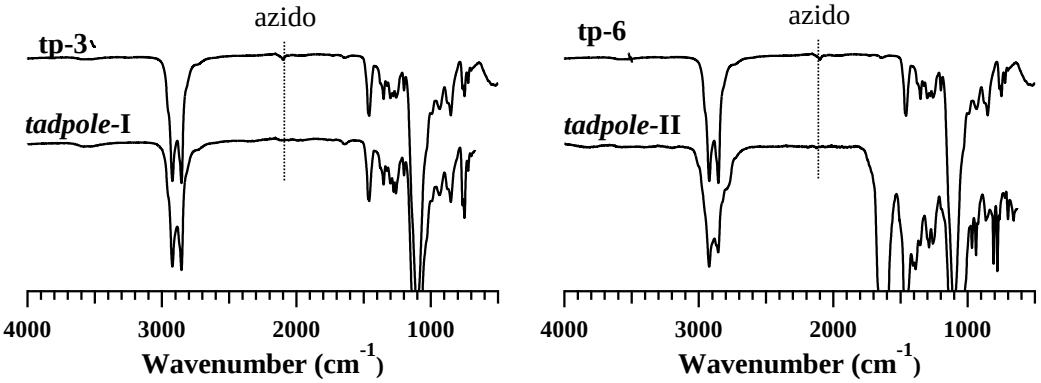

Figure 3-15. FT-IR spectra of **tp-3**, **tp-6**, ***tadpole*-I**, and ***tadpole*-II**.

3.2.4 Self-assembly Properties of Cyclic, Figure-eight-shaped, and Tadpole-shaped Amphiphilic Block Copolyethers in Water

For the preliminary study on regarding effect of the cyclic architecture, the author investigated the self-assembly of the cyclic (***cyclic*-I**), figure-eight-shaped (***eight*-I**, ***eight*-II**, ***eight*-III**, and ***eight*-IV**), and tadpole-shaped (***tadpole*-I** and ***tadpole*-II**) amphiphilic block copolymers together with the linear block copolymer (***linear*-I**, as described in Chapter 2) in water. The micelle solutions (concentration, 0.50 g L^{-1}) were prepared by the direct dissolution of the block copolymers in pure water at room temperature by sonication. The dynamic light scattering (DLS) experiment was employed to investigate the size of the aggregates (**Figure 3-20**). The intensity-average size distribution of every block copolymer aqueous solution displayed a monomodal peak corresponding to the aggregates formed through the self-assembling process. Multi-angle DLS measurements for the solutions revealed the linear dependence of the relaxation frequency ($\Gamma = 1/\tau$) on the square of the wavevector (q^2), which clearly indicated the Brownian diffusive motion. The slope is equal to the diffusion coefficient (D) of the aggregates in water, from which the hydrodynamic radius (R_h) was calculated by the Stokes-Einstein relation and was in the range of 42 – 111 nm (**Table 3-5**). The R_h values of the block copolymers were apparently greater than those of the fully-extended chain lengths (approximately 18 nm for cyclic and figure-eight-shaped block copolymers, 27 nm for tadpole-shaped block copolymers, in which the DP and molecular length of a monomer unit were assumed to be 100 and 0.358 nm,[43] respectively),

suggesting that the aggregates of every block copolymer were large compound micelles or vesicles. The actual morphologies of the aggregates were then confirmed by transmission electron microscopy (TEM), in which all of the samples were observed without staining. The TEM images revealed the presence of hard sphere-like nanoparticles or its agglomerates in all case (**Figure 3-21**), leading to the conclusion that all of the aggregates consisted of large compound micelles. Therefore, the cyclic architecture of the block copolymer as well as the block arrangement would have a small impact on the morphology of the aggregate in water.

Table 3-5. Molecular Characteristic, Critical Micelle Concentration (CMC), Hydrodynamic Radius (R_h), and Cloud Point ($T_{c.d.}$) of Cyclic (***cyclic*-I**), Figure-eight-shaped (***eight*-I**, ***eight*-II**, ***eight*-III**, and ***eight*-IV**), and Tadpole-shaped Block Copolymers (***tadpole*-I** and ***tadpole*-II**)

sample	$M_{n,NMR}$ [a] (g mol^{-1})	$Đ$ [b]	DP_a/DP_b [c]	CMC [d] (mg L^{-1})	R_h [e] (nm)	$T_{c.d.}$ [f] (°C)
***cyclic*-I**	22,300	1.04	51/50	1.8	83	87
***eight*-I**	21,800	1.06	50/48	1.5	69	75
***eight*-II**	22,300	1.03	52/48	1.0	90	80
***eight*-III**	22,200	1.03	50/50	1.4	86	67
***eight*-IV**	22,200	1.04	50/50	1.2	111	85
***tadpole*-I**	21,900	1.04	51/49	1.4	42	n.d. [g]
***tadpole*-II**	22,400	1.06	51/50	3.4	85	59
***linear*-I** [h]	21,900	1.04	50/51	1.4	62	83

[a] Determined by ^{1}H NMR. [b] Determined by SEC in THF. [c] Number-average degree of polymerizations of decyl glycidyl ether (DP_a) and triethyleneglycol methyl glycidyl ether (DP_b) in the copolymer were determined by ^{1}H NMR. [d] Determined by steady-state fluorescence method using pyrene as a prove at 25 °C. [e] Determined based on multi-angle DLS measurements (concentration, 0.50 g L^{-1}; temperature, 25 °C). [f] Determined by turbidimetric analysis (concentration, 0.50 g L^{-1}). $T_{c.d.}$ was defined by the temperature at which the transmittance of sample solution reached 50%. [g] $T_{c.d.}$ was not observed upon the heating up to 90 °C. [h] Detail data were described in Chapter 2.

The critical micelle concentrations (CMC) for the block copolymers in water were determined by a fluorescence technique using pyrene as the fluorescence probe at 25 °C (**Figure 3-22**). There is no distinctive difference in the CMC values among the block copolymers (1.0 – 3.4 mg L^{-1}, **Table 3-5**), indicating that the CMC value is not significantly affected by the cyclic topology as well as the block arrangement. Booth et al. reported the similar results which were determined by using the linear and cyclic poly(ethylene oxide)-*b*-poly(propylene oxide).[34]

The cloud point ($T_{c.d.}$) for the aggregates, that is a measure of their structural stability,[42] were determined by the variable-temperature UV-Vis absorption measurements of the aqueous block copolymer solutions (**Figure 3-16** and **3-23**). The transmittance at 300 nm was monitored during the continuous heating at the 1.0 °C min^{-1} heating ratio, and $T_{c.d.}$ was defined as the temperature at which the transmittance of the sample solution reached 50%.

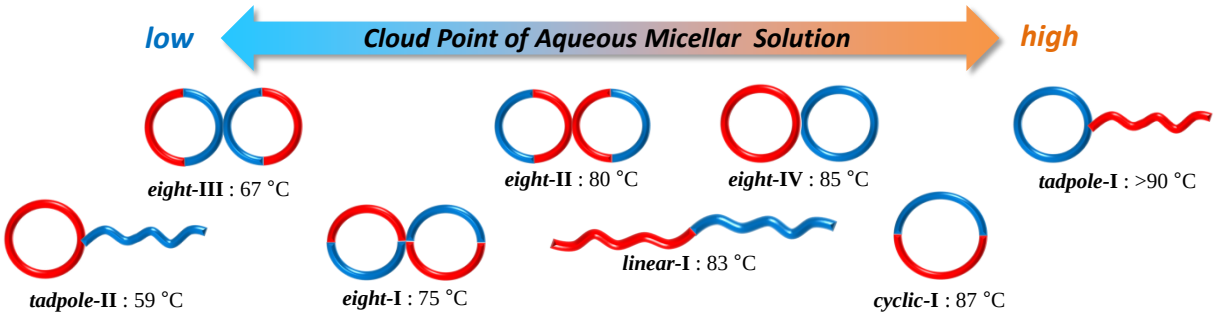

Figure 3-16. Schematic representation of $T_{c.d.}$ values of the amphiphilic cyclic-containing block copolyethers.

Every block copolymer, except for ***tadpole*-I**, exhibited the characteristic phase transition phenomenon at the $T_{c.d.}$ ranging from 59 – 87 °C, whereas ***tadpole*-I** exhibited no such phase transition up to 90 °C. Although the difference in the polymer structures among the block copolymers is only the macromolecular architecture, a significant variation in $T_{c.d.}$ was observed, which should provide an interesting insight into the thermal stabilities of the aggregates depending on the cyclic architecture. The cyclic amphiphilic block copolymer ***cyclic*-I** showed a $T_{c.d.}$ at 87 °C, which was 4 °C higher than that of the linear counterpart ***linear*-I** ($T_{c.d.}$ = 83 °C in Chapter 2). The increased $T_{c.d.}$ value of ***cyclic*-I** with respect to ***linear*-I** should be ascribed to the restricted inter-micelle linking due to the looped conformation of the hydrophilic block at the shell region. A significant difference in the $T_{c.d.}$ was observed between ***tadpole*-I** ($T_{c.d.}$ >90 °C) and ***tadpole*-II** ($T_{c.d.}$ = 59 °C), though both of them were categorized as having a tadpole-shaped architecture. Given that the aggregate of ***tadpole*-I** and ***tadpole*-II** is surrounded by the shell of hydrophilic cyclic or linear poly-**M2**, respectively, these results suggest that the cyclic architecture of the shell-forming block contributes to the increase in the $T_{c.d.}$ by reducing the inter-micelle linking as a consequence of their restricted chain mobility and lower entanglement nature. These results also implied that the cyclic architecture of the core-forming block led to a decrease in the $T_{c.d.}$ with respect to the corresponding linear diblock counterpart. It should be noted that a similar tendency

was observed for the amphiphilic miktoarm star copolyethers (***star*-VI** and ***star*-VII** in Chapter 2) as shown in **Figure 3-17**.

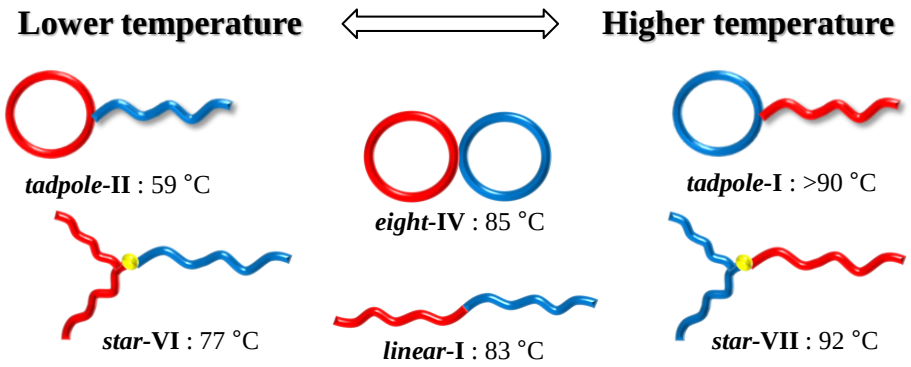

Figure 3-17. The correlation in $T_{c.d.}$ values between the cyclic-containing block copolyethers and the miktoarm star copolyethers.

On the other hand, the lower $T_{c.d.}$ values for the figure-eight-shaped block copolymers, ***eight*-I**, ***eight*-II**, and ***eight*-III**, than that of ***linear*-I** could not be explained by such effects due to their complicated chain packing at the interface of the micelle core and shell. Given that ***eight*-II** and ***eight*-III** are regarded as the analogs of the poly-**M2**-*block*-poly-**M1**-*block*-poly-**M2** and poly-**M1**-*block*-poly-**M2**-*block*-poly-**M1** triblock copolymers, respectively, an interesting comparison can be made between their $T_{c.d.}$ values. The relatively low $T_{c.d.}$ values of the triblock copolymers with hydrophobic end blocks with respect to those of the opposite block arrangement were reported for the poly(ethylene oxide)/poly(propyrene oxide) and poly(ethylene oxide)/poly(butylene oxide)

triblock copolymer systems.[27] In fact, the author could find similar results from the synthesized poly(**M1**)-*b*-poly(**M2**)-*b*-poly(**M1**) (*linear*-**III**, $T_{c.d.}$ = <30 °C) and poly(**M2**)-*b*-poly(**M1**)-*b*-poly(**M2**) (*linear*-**IV**, $T_{c.d.}$ = 54 °C) triblock copolyethers (**Figure 3-18**). This effect is related to the inter-micelle linking through the hydrophobic end blocks (**Figure 3-19**).[32] Therefore, the low $T_{c.d.}$ value of ***eight*-III** should be ascribed to the enhanced inter-micelle linking due to the hydrophobic end block. Similar trends were also provided from the star-block copolymers in Chapter 2, as shown in **Figure 3-18**. In addition, ***eight*-III** showed the $T_{c.d.}$ at 67 °C, though ***star*-II** and ***linear*-III** had already clouded at room temperature. These results suggested that the cyclic architecture may prevent an inter-micelle linking. On the other hand, the higher $T_{c.d.}$ values of ***eight*-III** and ***star*-I** compared to ***linear*-IV** suggested that the cyclic and branched architectures of the triblock copolymers with hydrophilic end blocks may increase the structural stability of their micellar aggregations.

In this study, the author determined the systematic relationship of the aqueous self-assembly behavior between the star-shaped and cyclic-cntaining block copolymers for the first time.

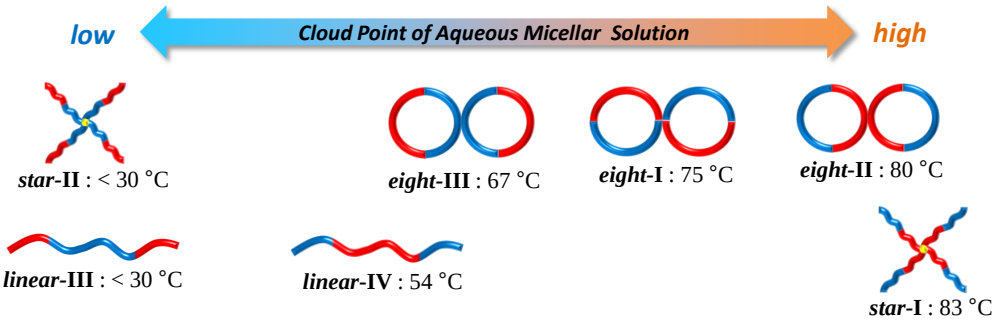

Figure 3-18. Schematic representation of the correlation in $T_{c.d.}$ values between the figure-eight-shaped block copolyethers and the star-block copolyethers.

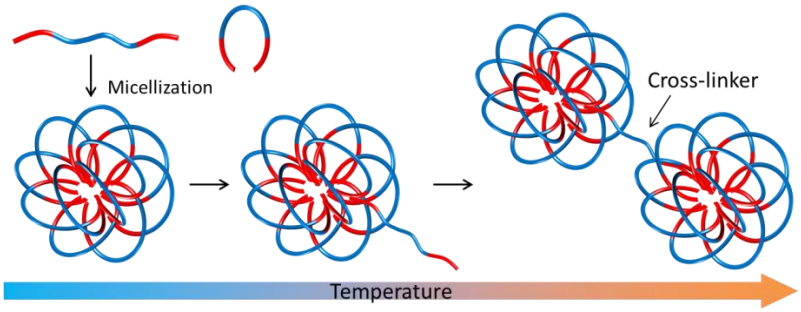

Figure 3-19. Schematic representation of proposed mechanism for the inter-micelle linking.

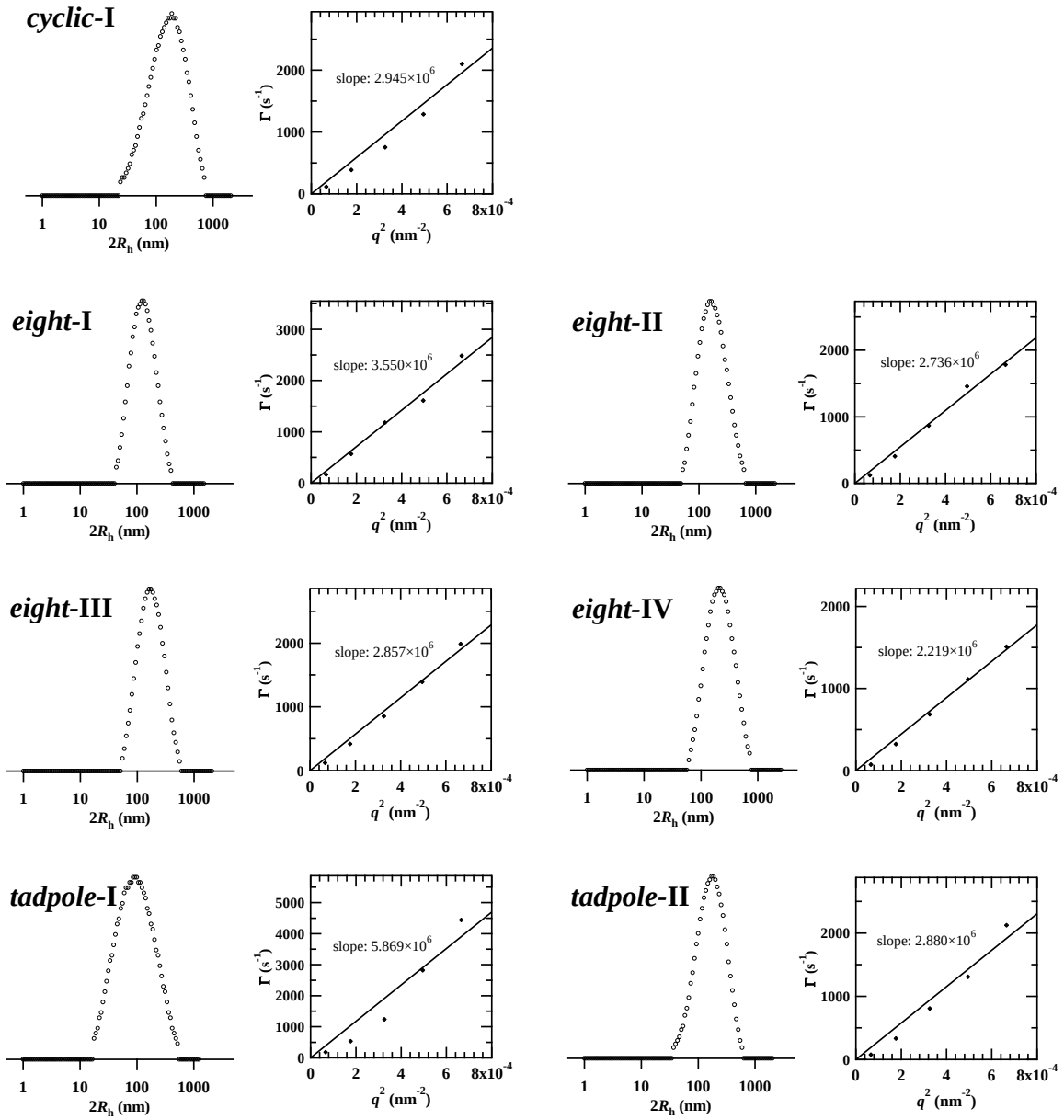

Figure 3-20. Intensity-average particle size distribution (measured at scattering angle of 90 °; left) and dependence of relaxation frequency (Γ) on squared wave vector (q^2) (right) for the micellar solution of ***cyclic*-I**, ***eight*-I**, ***eight*-II**, ***eight*-III**, ***eight*-IV**, ***tadpole*-I**, and ***tadpole*-II** (0.50 g L^{-1}, 25 °C). The $2R_h$ value (hydrodynamic radius) was calculated based on Stokes-Einstein relation using the slope of the Γ v.s. q^2 plot.

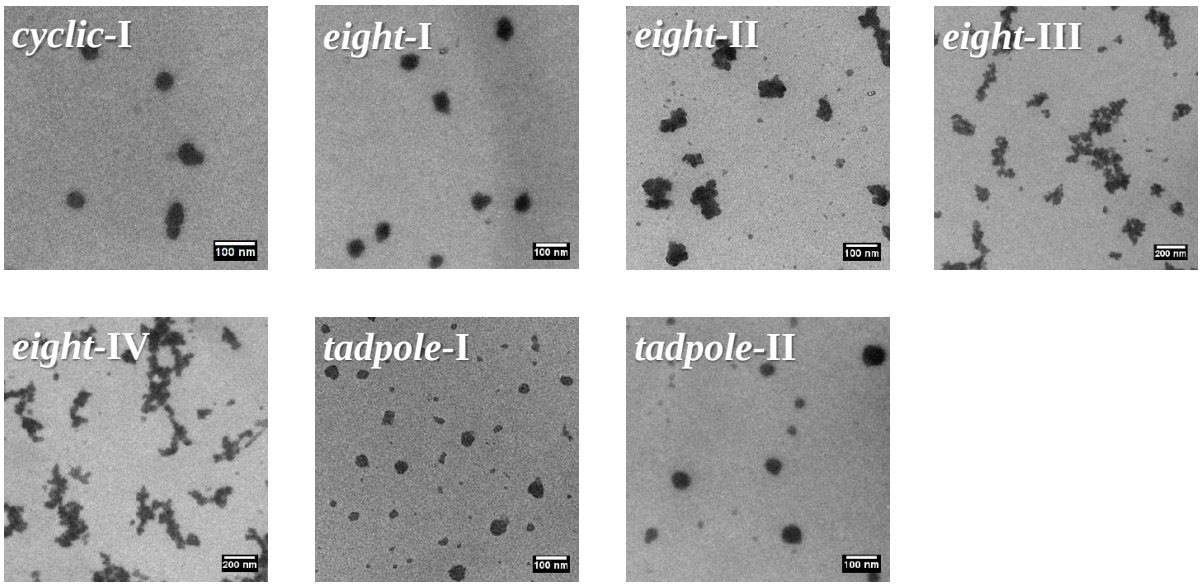

Figure 3-21. TEM images of BCP aggregates formed from ***cyclic*-I**, ***eight*-I**, ***eight*-II**, ***eight*-III**, ***eight*-IV**, ***tadpole*-I**, and ***tadpole*-II** (polymer concentration, 0.50 g L^{-1}).

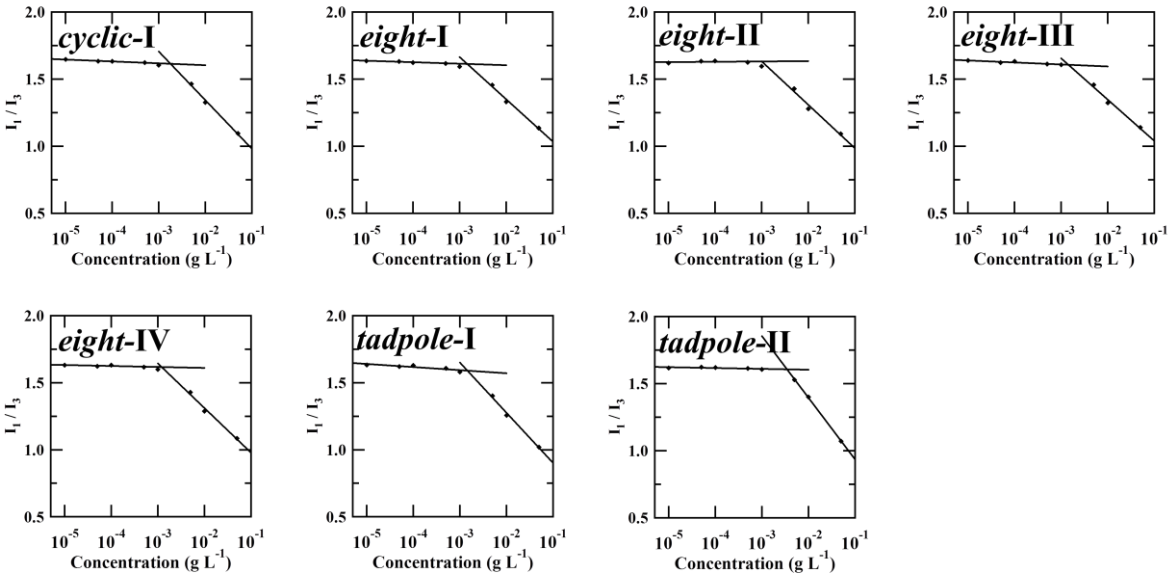

Figure 3-22. Variation in I_1/I_3 of pyrene emission spectra for ***cyclic*-I**, ***eight*-I**, ***eight*-II**, ***eight*-III**, ***eight*-IV**, ***tadpole*-I**, and ***tadpole*-II** as a function of polymer concentrations (measured at 25 °C).

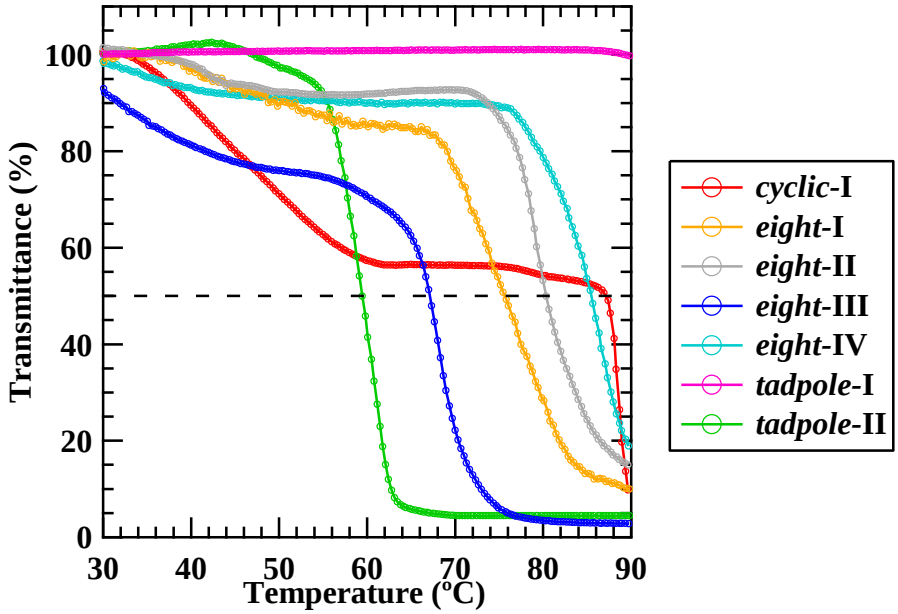

Figure 3-23. Temperature dependence of optical transmittance at 300 nm obtained for 0.50 g L^{-1} aqueous solution of ***cyclic*-I**, ***eight*-I**, ***eight*-II**, ***eight*-III**, ***eight*-IV**, ***tadpole*-I**, and ***tadpole*-II**.

3.3 Conclusion

The author have demonstrated the synthesis of systematic sets of cyclic, figure-eight-, and tadpole-shaped amphiphilic block copolymers via the combination of the *t*-Bu-P_4-catalyzed ROP of hydrophobic and hydrophilic glycidyl ethers and the click cyclization. The well-controlled nature of the ROP system allowed us to attain a series of azido- and ethynyl-functionalized di-, tri-, and multi-block copolymers with a predicted molecular weight, monomer composition, and narrow dispersity, which led to produce the corresponding cyclic-containing amphiphilic block copolymers via the intramolecular click cyclization. Preliminary studies on the self-assembly of the cyclic, figure-eight-shaped, and tadpole-shaped amphiphilic block copolymers in water revealed the significant variation in the $T_{c.d.}$ values depending on the cyclic topology. In addition, by comparing with the obtained results in Chapter 2, the author provided the systematic relationship of the structural stability of micellar aggregates based on the branched and cyclic architectures. Considering the capability of the functional groups in the glycidyl ether-based block copolymers, the present synthetic strategy provides a wide array of block copolymer systems with cyclic-containing architectures, which would be used as a model system for investigating the topological effect of the block copolymer self-assembly in both the solution and bulk states.

3.4 Experimental Section

Materials. 6-Azido-1-hexanol (**i-VI**),[44] ethoxyethyl glycidyl ether,[45] 1-bromomethyl-3,5-bis(2-propynyloxy)benzene (**t-II**),[44] and propargyl-functionalized Wang resin (PSt-C≡CH)[46] were prepared according to previously reported methods. 2,2-bis((6-azidohexyloxy)methy)propane-1,3-diol (**i-III**), decyl glycidyl ether (**M1**) and 2-(2-(2-methoxyethoxy)ethoxy)ethyl glycidyl ether (**M2**) were described in chapter 2, purified by distillation under vacuum over calcium hydride, and stored under an argon atmosphere. 60% NaH, sodium azide, α,α'-dibromo-*p*-xylene, propargyl bromide, and *N,N,N',N'',N''*-pentamethyldiethylenetriamine (PMDETA) were purchased from Tokyo Chemical Industry Co., Ltd. (TCI), and used as received. 3-Phenyl-1-propanol (**i-IV**) was purchased from TCI and purified by distillation under vacuum over calcium hydride. *t*-Bu-P_4 (in *n*-hexane as 1.0 mol L^{-1} solution), copper(I) bromide, and Dowex 50WX2 were purchased from the Sigma-Aldrich Chemicals Co., and used as received. Dry dimethylformamide (DMF; >99.5%; water content, <0.005%), dry toluene (>99.5%; water content, <0.001%), and dry tetrahydrofuran (THF; >99.5%; water content, <0.001%) were purchased from Kanto Chemical Co., Inc., and used as received.

Instruments. The instruments used in this study, such as the glovebox, size exclusion chromatography (SEC), NMR, FT-IR, and matrix-assisted laser desorption/ionization time-of-flight mass spectrometry (MALDI-TOF MS), are the same as Chapter 2.

Synthesis of Poly(butylene oxide) with Two Azido Groups at Chain Center ($(N_3)_2$-$(PBO)_2$). A typical polymerization procedure is as follows (Procedure A): **BO** (1.20 mL, 13.8 mmol) was added to a stirred solution of **i-III** (460 μL as 1.0 mol·L^{-1} stock solution in toluene, 460 μmol) and *t*-Bu-P_4 (230 μL as 1.0 mol·L^{-1} stock solution in *n*-hexane, 230 μmol) in toluene (873 μL), and the mixture was stirred at room temperature for 20 h. An excess of benzoic acid was then added to the mixture to terminate the polymerization, and the polymer was then purified by passing through a pad of alumina with THF to give $(N_3)_2$-$(PBO)_2$ as a colorless viscous liquid (1.03 g). Yield: 87.5%. ^{1}H NMR (400 MHz, $CDCl_3$): δ (ppm) 3.29−3.75 ($N_3(CH_2)_5CH_2O$−, $N_3(CH_2)_6OCH_2$−, −CH_2−O−PBO, −$OCH_2CH(CH_2CH_3)O$−, −$OCH_2CH(CH_2CH_3)O$−), 3.26 (N_3CH_2−), 1.36−1.69 ($N_3CH_2(CH_2)_4CH_2O$−, −$OCH_2CH(CH_2CH_3)O$−), 0.92 (−$OCH_2CH(CH_2CH_3)O$−). $M_{n,NMR}$ = 2480 g mol^{-1}; $M_{n,SEC}$ = 3020 g mol^{-1}; $Đ$ = 1.06.

Synthesis of *ω,ω′*-Diethynyl Poly(butylene oxide) with Two Azido Groups ($(N_3)_2$-$(PBO\text{-}C{\equiv}CH)_2$). The typical procedure for the ω-chain end ethynylation is as follows (Procedure B): To a stirred solution of $(N_3)_2$-$(PBO)_2$ ($M_{n,NMR}$ = 2480 g mol^{-1}, 147 mg) in THF

(3.95 mL) was added NaH (16.0 mg, 355 μmol; 60 % in mineral oil), then the solution was stirred at 40 °C for 1 h. After cooling to room temperature, propargyl bromide (26.8 μL, 355 μmol) was then added to the solution, and the entire mixture was stirred at room temperature for 48 h. The polymer was purified by passing through a pad of alumina to give $(N_3)_2$-(PBO-C≡CH)$_2$ as a pale yellow viscous liquid (140 mg). Yield: 94.8%. ^{1}H NMR (400 MHz, $CDCl_3$): δ (ppm) 4.30 (−OC*H*$_2$C≡CH), 3.29−3.75 ($N_3(CH_2)_5CH_2O$−, $N_3(CH_2)_6OCH_2$−, −C*H*$_2$−O−PBO, −OC*H*$_2$CH(CH_2CH_3)O−, −OCH$_2$C*H*(CH_2CH_3)O−), 3.26 (N_3CH_2−), 2.39 (−C≡C*H*), 1.36−1.69 ($N_3CH_2(CH_2)_4CH_2O$−, −OCH$_2$CH(C*H*$_2$CH$_3$)O−), 0.92 (−OCH$_2$CH(CH_2CH_3)O−). $M_{n,NMR}$ = 2560 g mol^{-1}; $M_{n,SEC}$ = 2800 g mol^{-1}; $Đ$ = 1.07.

Synthesis of Figure-Eight-Shaped Poly(butylene oxide) (*eight*-PBO). The typical click cyclization procedure is as follows (Procedure C): A solution of $(N_3)_2$-(PBO-C≡CH)$_2$ ($M_{n,NMR}$ = 2560 g mol^{-1}, 40.3 mg) in a degassed DMF (7.9 mL) was added to a stirred solution of CuBr (229 mg, 1.58 mmol) and PMDETA (658 μL, 3.15 mmol) in degassed DMF (100 mL) using a syringe pump at the rate of 0.3 mL·h^{-1} at 100 °C under an argon atmosphere. After completing the addition, PSt-C≡CH (185 mg), CuBr (48.5 mg, 3.15 mmol), and PMDETA (132 μL, 6.30 mmol) were added to the reaction mixture. After stirring at 120 °C for 24 h, the solvent was removed by evaporation, and the residue was purified by passing through a pad of alumina followed by preparative SEC to give *eight*-PBO as a light brown viscous liquid (30.0 mg). Yield: 74.4%. ^{1}H NMR (400 MHz, $CDCl_3$): δ (ppm) 7.56 (triazole

methine), 4.79 (−OCH_2−triazole ring), 4.33 (triazole ring−CH_2(CH_2)$_5$O−), 3.29−3.75 (triazole ring−(CH_2)$_5$CH_2O−, triazole ring−(CH_2)$_6$OCH_2−, −CH_2−O−PBO, −OCH_2CH(CH_2CH_3)O−, −OCH_2CH(CH_2CH_3)O−), 1.36−1.69 (triazole ring−CH_2(CH_2)$_4$$CH_2$O−, −OC$H_2$CH(C$H_2CH_3$)O−), 0.92 (−OC$H_2$CH($CH_2CH_3$)O−). $M_{n,NMR}$ = 2700 g mol^{-1}; $M_{n,SEC}$ = 2330 g mol^{-1}; $Đ$ = 1.06.

Synthesis of c-1. Procedure A was used for the polymerization of **M1** (276 µL, 1.17 mmol, first monomer, polymerization time = 20 h) and **M2** (241 µL, 1.17 mmol, second monomer, polymerization time = 20 h) with **i-VI** (23.3 µL as 1.0 mol L^{-1} stock solution in toluene, 23.3 µmol) and *t*-Bu-P_4 (23.3 µL as 1.0 mol L^{-1} stock solution in *n*-hexane, 23.3 µmol) in toluene (370 µL) to give **c-1** as a colorless waxy solid (450 mg). Yield: 88.8%. ^{1}H NMR (400 MHz, $CDCl_3$): δ (ppm) 3.29–3.75 (N_3(CH_2)$_5$CH_2OCH_2−, −OCH_2CH(CH_2OCH_2(CH_2)$_8$$CH_3$)O−, −OC$H_2CH$(C$H_2$O(C$H_2CH_2$O)$_3CH_3$)O−), 3.26 ($N_3CH_2$–), 1.10−1.69 ($N_3$$CH_2$(C$H_2$)$_4$$CH_2$O−, −OC$H_2$CH($CH_2OCH_2CH_2$(C$H_2$)$_7$$CH_3$)O−), 0.78−0.95 (−OC$H_2$CH($CH_2OCH_2$($CH_2$)$_8CH_3$)O−). $M_{n,NMR}$ = 22000 g mol^{-1}; $M_{n,SEC}$ = 16900 g mol^{-1}; $Đ$ = 1.05.

Synthesis of c-2. Procedure B was used for the propargylation of **c-1** (300 mg, 15.0 µmol) with NaH (6.00 mg, 150 µmol; 60% in mineral oil) and propargyl bromide (11.3 µL, 150 µmol) in THF (3 mL) to give **c-2** as a pale yellow waxy solid (261 mg). Yield: 87.0%. ^{1}H NMR (400 MHz, $CDCl_3$): δ (ppm) 4.40 (-OCH_2C≡CH), 3.29−3.75 (N_3(CH_2)$_5$CH_2OCH_2−,

−OC*H*$_2$C*H*(C*H*$_2$OC*H*$_2$(CH$_2$)$_8$CH$_3$)O−, −OC*H*$_2$C*H*(C*H*$_2$O(C*H*$_2$C*H*$_2$O)$_3$C*H*$_3$)O−), 3.26 (N$_3$C*H*$_2$–), 2.39 (–C≡C*H*), 1.10−1.69 (N$_3$CH$_2$(C*H*$_2$)$_4$CH$_2$O−, −OCH$_2$CH(CH$_2$OCH$_2$C*H*$_2$(C*H*$_2$)$_7$CH$_3$)O−), 0.78−0.95 (−OCH$_2$CH(CH$_2$OCH$_2$(CH$_2$)$_8$C*H*$_3$)O−). $M_{n,NMR}$ = 21900 g mol^{-1}; $M_{n,SEC}$ = 15900 g mol^{-1}; $Đ$ = 1.04.

Synthesis of *cyclic*-I. Procedure C was used for the click cyclization of **c-2** (100 mg, 4.50 μmol in degassed DMF (2.5 mL)) with a solution of CuBr (64.6 mg, 450 μmol) and PMDETA (181 μL, 900 μmol) in degassed DMF (27.5 mL) to give ***cyclic*-I** as a light brown waxy solid (37.0 mg). Yield: 37.0%. ^{1}H NMR (400 MHz, CDCl$_3$): δ (ppm) 7.56 (triazole methine), 4.79 (–OC*H*$_2$−triazole ring), 4.33 (triazole ring−C*H*$_2$(CH$_2$)$_5$O−), 3.29−3.75 (triazole ring−(CH$_2$)$_5$C*H*$_2$OC*H*$_2$−, −OC*H*$_2$C*H*(C*H*$_2$OC*H*$_2$(CH$_2$)$_8$CH$_3$)O−, −OC*H*$_2$C*H*(C*H*$_2$O(C*H*$_2$C*H*$_2$O)$_3$C*H*$_3$)O−), 1.10−1.69 (triazole ring−CH$_2$(C*H*$_2$)$_4$CH$_2$O−, −OCH$_2$CH(CH$_2$OCH$_2$C*H*$_2$(C*H*$_2$)$_7$CH$_3$)O−), 0.78−0.95 (−OCH$_2$CH(CH$_2$OCH$_2$(CH$_2$)$_8$C*H*$_3$)O−). $M_{n,NMR}$ = 22300 g mol^{-1}; $M_{n,SEC}$ = 13300 g mol^{-1}; $Đ$ = 1.04.

Synthesis of e-1. Procedure A was used for the block copolymerization of **M1** (276 μL, 1.17 mmol, first monomer, polymerization time = 20 h) and **M2** (241 μL, 1.17 mmol, second monomer, polymerization time = 20 h) with **i-III** (23.3 μL as 1.0 mol L^{-1} stock solution in toluene, 23.3 μmol) and *t*-Bu-P$_4$ (23.3 μL as 1.0 mol L^{-1} stock solution in *n*-hexane, 23.3 μmol) in toluene (370 μL) to give **e-1** as a colorless waxy solid (466 mg). Yield: 92.0%. ^{1}H NMR (400 MHz, CDCl$_3$): δ (ppm) 3.29–3.75 (N$_3$(CH$_2$)$_5$C*H*$_2$OC*H*$_2$−,

−OCH_2CH(CH_2OCH_2(CH_2)$_8$$CH_3$)O−, −OC$H_2CH$(C$H_2$O(C$H_2CH_2$O)$_3CH_3$)O−), 3.26 ($N_3CH_2$−), 1.10−1.69 ($N_3$$CH_2$(C$H_2$)$_4$$CH_2$O−, −OC$H_2$CH($CH_2OCH_2CH_2$(C$H_2$)$_7$$CH_3$)O−), 0.78−0.95 (−OC$H_2$CH($CH_2OCH_2$($CH_2$)$_8CH_3$)O−). $M_{n,NMR}$ = 21800 g mol^{-1}; $M_{n,SEC}$ = 14000 g mol^{-1}; $Đ$ = 1.04.

Synthesis of e-2. Procedure B was used for the propargylation of **e-1** (300 mg) with NaH (6.00 mg, 150 μmol; 60% in mineral oil) and propargyl bromide (11.3 μL, 150 μmol) in THF (4 mL) to give **e-2** as a pale yellow waxy solid (282 mg). Yield: 94.0%. ^{1}H NMR (400 MHz, $CDCl_3$): δ (ppm) 4.40 (−OCH_2C≡CH), 3.29−3.75 (N_3(CH_2)$_5$CH_2OCH_2−, −OCH_2CH(CH_2OCH_2(CH_2)$_8$$CH_3$)O−, −OC$H_2CH$(C$H_2$O(C$H_2CH_2$O)$_3CH_3$)O−), 3.26 ($N_3CH_2$−), 2.39 (–C≡C$H$), 1.10−1.69 ($N_3$$CH_2$(C$H_2$)$_4$$CH_2$O−, −OC$H_2$CH($CH_2OCH_2CH_2$(C$H_2$)$_7$$CH_3$)O−), 0.78−0.95 (−OC$H_2$CH($CH_2OCH_2$($CH_2$)$_8CH_3$)O−). $M_{n,NMR}$ = 21900 g mol^{-1}; $M_{n,SEC}$ = 14000 g mol^{-1}; $Đ$ = 1.04.

Synthesis of *eight*-I. Procedure C was used for the click cyclization of **e-2** (100 mg, 4.50 μmol in degassed DMF (2.5 mL)) with a solution of CuBr (64.6 mg, 450 μmol) and PMDETA (181 μL, 900 μmol) in degassed DMF (27.5 mL) to give ***eight*-I** as a light brown waxy solid (46.0 mg). Yield: 46.0%. ^{1}H NMR (400 MHz, $CDCl_3$): δ (ppm) 7.56 (triazole methine), 4.79 (–OCH_2−triazole ring), 4.33 (triazole ring−CH_2(CH_2)$_5$O–), 3.29−3.75 (triazole ring−(CH_2)$_5$CH_2OCH_2−, −OCH_2CH(CH_2OCH_2(CH_2)$_8$$CH_3$)O−, −OC$H_2CH$(C$H_2$O(C$H_2CH_2$O)$_3CH_3$)O−), 1.10−1.69 (triazole ring−CH_2(CH_2)$_4$$CH_2$O−,

−$OCH_2CH(CH_2OCH_2CH_2(CH_2)_7CH_3)O$−), 0.78−0.95 (−$OCH_2CH(CH_2OCH_2(CH_2)_8CH_3)O$−). $M_{n,NMR}$ = 21800 g mol^{-1}; $M_{n,SEC}$ = 11300 g mol^{-1}; $Đ$ = 1.06.

Synthesis of e-3. Procedure A was used for the triblock copolymerization of **M1** (166 µL, 700 µmol, first monomer, polymerization time = 20 h), **M2** (301 µL, 1.46 mmol, second monomer, polymerization time = 20 h), and **M1** (180 µL, 758 µmol, third monomer, polymerization time = 20 h) with **i-III** (29.2 µL as 1.0 mol L^{-1} stock solution in toluene, 29.2 µmol) and *t*-Bu-P_4 (23.3 µL as 1.0 mol L^{-1} stock solution in *n*-hexane, 23.3 µmol) in toluene (641 µL) to give **e-3** as a colorless waxy solid (491 mg). Yield: 77.5%. ^{1}H NMR (400 MHz, $CDCl_3$): δ (ppm) 3.29–3.75 ($N_3(CH_2)_5CH_2OCH_2$−, −$OCH_2CH(CH_2OCH_2(CH_2)_8CH_3)O$−, −$OCH_2CH(CH_2O(CH_2CH_2O)_3CH_3)O$−), 3.26 ($N_3CH_2$–), 1.10−1.69 ($N_3CH_2(CH_2)_4CH_2O$−, −$OCH_2CH(CH_2OCH_2CH_2(CH_2)_7CH_3)O$−), 0.78−0.95 (−$OCH_2CH(CH_2OCH_2(CH_2)_8CH_3)O$−). $M_{n,NMR}$ = 22100 g mol^{-1}; $M_{n,SEC}$ = 14300 g mol^{-1}; $Đ$ = 1.06.

Synthesis of e-4. Procedure B was used for the propargylation of **e-3** (300 mg, 15.0 µmol) with NaH (6.00 mg, 150 µmol; 60% in mineral oil) and propargyl bromide (11.3 µL, 150 µmol) in THF (4 mL) to give **e-4** as a pale yellow waxy solid (295 mg). Yield: 98.4%. ^{1}H NMR (400 MHz, $CDCl_3$): δ (ppm) 4.40 (–$OCH_2C{\equiv}CH$), 3.29−3.75 ($N_3(CH_2)_5CH_2OCH_2$−, −$OCH_2CH(CH_2OCH_2(CH_2)_8CH_3)O$−, −$OCH_2CH(CH_2O(CH_2CH_2O)_3CH_3)O$−), 3.26 ($N_3CH_2$–), 2.39 (–$C{\equiv}CH$), 1.10−1.69 ($N_3CH_2(CH_2)_4CH_2O$–,

−$OCH_2CH(CH_2OCH_2CH_2(CH_2)_7CH_3)O$−), 0.78−0.95 (−$OCH_2CH(CH_2OCH_2(CH_2)_8CH_3)O$−). $M_{n,NMR}$ = 22100 g mol^{-1}; $M_{n,SEC}$ = 14300 g mol^{-1}; $Đ$ = 1.06.

Synthesis of *eight*-II. Procedure C was used for the click cyclization of **e-4** (150 mg, 6.79 μmol in degassed DMF (3.4 mL)) with a solution of CuBr (96.9 mg, 676 μmol) and PMDETA (282 μL, 1.35 mmol) in degassed DMF (41.6 mL) to give ***eight*-II** as a light brown waxy solid (63.1 mg). Yield: 42.1%. ^{1}H NMR (400 MHz, $CDCl_3$): δ (ppm) 7.56 (triazole methine), 4.79 (−OCH_2−triazole ring), 4.33 (triazole ring−C$H_2(CH_2)_5O$–), 3.29−3.75 (triazole ring− $(CH_2)_5CH_2OCH_2$−, −OCH_2CH(CH_2O$CH_2(CH_2)_8CH_3$)O−, −OCH_2CH(CH_2O(CH_2CH_2O)$_3$CH_3)O−), 1.10−1.69 (triazole ring−$CH_2(CH_2)_4CH_2O$−, −$OCH_2CH(CH_2OCH_2CH_2(CH_2)_7CH_3)O$−), 0.78−0.95 (−$OCH_2CH(CH_2OCH_2(CH_2)_8CH_3)O$−). $M_{n,NMR}$ = 22300 g mol^{-1}; $M_{n,SEC}$ = 12900 g mol^{-1}; $Đ$ = 1.03.

Synthesis of e-5. Procedure A was used for the triblock copolymerization of **M2** (141 μL, 681 μmol, first monomer, polymerization time = 20 h), **M1** (336 μL, 1.42 mmol, second monomer, polymerization time = 20 h), and **M2** (152 μL, 738 μmol, third monomer, polymerization time = 20 h) with **i-III** (28.4 μL as 1.0 mol L^{-1} stock solution in toluene, 28.4 μmol) and *t*-Bu-P_4 (28.4 μL as 1.0 mol L^{-1} stock solution in *n*-hexane, 28.4 μmol) in toluene (602 μL) to give **e-5** as a colorless waxy solid (496 mg). Yield: 80.3%. ^{1}H NMR (400 MHz, $CDCl_3$): δ (ppm) 3.29–3.75 ($N_3(CH_2)_5CH_2OCH_2$−, −OCH_2CH(CH_2O$CH_2(CH_2)_8CH_3$)O−, −OCH_2CH(CH_2O(CH_2CH_2O)$_3$CH_3)O−), 3.26 (N_3CH_2–), 1.10−1.69 ($N_3CH_2(CH_2)_4CH_2O$–,

−$OCH_2CH(CH_2OCH_2CH_2(CH_2)_7CH_3)O$−), 0.78−0.95 (−$OCH_2CH(CH_2OCH_2(CH_2)_8CH_3)O$−). $M_{n,NMR}$ = 22000 g mol^{-1}; $M_{n,SEC}$ = 14300 g mol^{-1}; $Đ$ = 1.08.

Synthesis of e-6. Procedure B was used for the propargylation of **e-5** (300 mg, 15.0 µmol) with NaH (6.00 mg, 150 µmol; 60 % in mineral oil) and propargyl bromide (11.3 µL, 150 µmol) in THF (4 mL) to give **e-6** as a pale yellow waxy solid (293 mg). Yield: 97.6%. ^{1}H NMR (400 MHz, $CDCl_3$): δ (ppm) 4.40 (–OCH_2C≡CH), 3.29−3.75 ($N_3(CH_2)_5CH_2OCH_2$−, −O$CH_2CH(CH_2OCH_2(CH_2)_8CH_3)O$−, −O$CH_2CH(CH_2O(CH_2CH_2O)_3CH_3)O$−), 3.26 ($N_3CH_2$−), 2.39 (−C≡C*H*), 1.10−1.69 ($N_3CH_2(CH_2)_4CH_2O$−, −$OCH_2CH(CH_2OCH_2CH_2(CH_2)_7CH_3)O$−), 0.78−0.95 (−$OCH_2CH(CH_2OCH_2(CH_2)_8CH_3)O$−). $M_{n,NMR}$ = 22100 g mol^{-1}; $M_{n,SEC}$ = 14300 g mol^{-1}; $Đ$ = 1.08.

Synthesis of *eight*-III. Procedure C was used for the click cyclization of **e-6** (150 mg, 6.79 µmol in degassed DMF (3.4 mL)) with a solution of CuBr (96.9 mg, 676 µmol) and PMDETA (282 µL, 1.35 mmol) in degassed DMF (41.6 mL) to give ***eight*-III** as a light brown waxy solid (59.4 mg). Yield: 39.6%. ^{1}H NMR (400 MHz, $CDCl_3$): δ (ppm) 7.56 (triazole methine), 4.79 (−OCH_2−triazole ring), 4.33 (triazole ring−$CH_2(CH_2)_5O$−), 3.29−3.75 (triazole ring−$(CH_2)_5CH_2OCH_2$−, −O$CH_2CH(CH_2OCH_2(CH_2)_8CH_3)O$−, −O$CH_2CH(CH_2O(CH_2CH_2O)_3CH_3)O$−), 1.10−1.69 (triazole ring−$CH_2(CH_2)_4CH_2O$−, −$OCH_2CH(CH_2OCH_2CH_2(CH_2)_7CH_3)O$−), 0.78−0.95 (−$OCH_2CH(CH_2OCH_2(CH_2)_8CH_3)O$−). $M_{n,NMR}$ = 22200 g mol^{-1}; $M_{n,SEC}$ = 13300 g mol^{-1}; $Đ$ = 1.03.

Synthesis of 1-azido-3-(1-ethoxyethoxy)propan-2-ol. NaN_3 (41.5 g, 639 mmol) and NH_4Cl (17.1 g, 320 mmol) were added to a stirred solution of ethoxyethyl glycidyl ether (31.2 g, 213mmol) in a water/isopropanol mixed solvent (1/6, 300 mL), and the entire mixture was stirred at 80 ºC for 4 h. After removing the solvent by evaporation, the obtained residue was dissolved in AcOEt and washed three times with water. The combined organic layer was dried over anhydrous $MgSO_4$ and then concentrated. The residue was purified by silica gel column chromatography (*n*-hexane/AcOEt = 3/1 (v/v), R_f = 0.33) to give titled compound (17.8 g) as a colorless liquid. Yield: 44.0%. ^{1}H NMR (400 MHz, $CDCl_3$): δ (ppm) 4.71 (m, 1H, –OC*H*(CH_3)O–), 3.91 (m, 1H, N_3CH_2CH(OH)CH_2–), 3.45–3.66 (m, 4H, –CH_2OCH(CH_3)OCH_2–), 3.37 (m, 2H, N_3CH_2–), 2.86 (m, 1H, –O*H*), 1.33 (d, 3H, –OCH(CH_3)O–), 1.22 (t, 3H, –OCH_2CH_3). ^{13}C NMR (100 MHz, $CDCl_3$): δ (ppm) 100.4 (–O*C*H(CH_3)O–), 69.9 (N_3CH_2*C*H(OH)CH_2–), 67.1 (–CH(OH)*C*H_2O–), 61.5 (–O*C*H_2CH_3), 53.5 (N_3*C*H_2–), 19.8 (–OCH(*C*H_3)O–), 15.3 (–OCH_2*C*H_3). Anal. calcd for $C_7H_{15}N_3O_3$: C, 44.43; H, 7.99; N, 22.21. Found: C, 44.13; H, 8.00; N, 21.40.

Synthesis of 1-(((1-azido-3-(1-ethoxyethoxy)propan-2-yl)oxy)methyl)-4-(bromomethyl)benzene (t-I). Under a nitrogen atmosphere, NaH (4.23 g, 105.7 mmol; 60% in mineral oil) was added to a stirred solution of 1-azido-3-(1-ethoxyethoxy)propan-2-ol (10 g, 52.85 mmol), and then the solution was stirred at 40 ºC for 1 h. After cooling to room temperature, the solution was

dropwise added to a stirred solution of α,α'-dibromo-*p*-xylene (27.9 g, 105 mmol) in dry THF (200 mL) and stirred at room temperature for 5 h under a N_2 atmosphere. After removing the solvent by evaporation, the obtained residue was dissolved in AcOEt and washed three times with water. The combined organic layer was dried over anhydrous $MgSO_4$ and then concentrated. The residue was purified by silica gel column chromatography (*n*-hexane/AcOEt = 8/1 (v/v), R_f = 0.30) to give **t-I** (12.60 g) as a colorless liquid. Yield: 64.1%. ^{1}H NMR (400 MHz, $CDCl_3$): δ (ppm) 7.36 (q, 4H, aromatic), 4.71 (m, 1H, –OC*H*(CH_3)O–), 4.66 (s, 2H, –C*H*$_2$PhCH_2Br), 4.49 (s, 2H, –C*H*$_2$Br), 3.80−3.41 (m, 5H, N_3CH_2CH(O–)CH_2–, –C*H*$_2$OCH(CH_3)OC*H*$_2CH_3$), 3.40 (m, 2H, N_3C*H*$_2$–), 1.30 (d, 3H, –OCH(C*H*$_3$)O–), 1.19 (t, 3H, –OCH_2C*H*$_3$). ^{13}C NMR (100MHz, $CDCl_3$): δ (ppm) 138.4, 137.4, 129.3, 128.2 (aromatic), 99.9 (− O*C*H(CH_3)O–), 76.8 (–O*C*H_2PhCH_2Br), 72.0 (N_3CH_2*C*H(O–)CH_2–), 64.1 (–CH(O–)*C*H_2O–), 61.5 (−O*C*H_2CH_3), 52.2 (N_3*C*H_2–), 33.4 (–*C*H_2Br), 19.8 (−OCH(*C*H_3)O–), 15.3 (–OCH_2*C*H_3). Anal. calcd for $C_7H_{15}N_3O_3$: C, 48.40; H, 5.96; N, 11.29. Found: C, 48.21; H, 5.91; N, 11.59.

Synthesis of e-7. Procedure A was used for the polymerization of **M1** (1.11 mL, 4.67 mmol) with **i-VI** (93.3 μL as 1.0 mol L^{-1} stock solution in toluene, 93.3 μmol) and *t*-Bu-P_4 (93.3 μL as 1.0 mol L^{-1} stock solution in *n*-hexane, 93.3 μmol) in toluene (575 μL) to give **e-7** as a colorless viscous liquid (619 mg). Yield: 61.9%. ^{1}H NMR (400 MHz, $CDCl_3$): δ (ppm) 3.29–3.75 ($N_3(CH_2)_5$C*H*$_2$OCH_2–, $N_3(CH_2)_6$OC*H*$_2$–, −OC*H*$_2$C*H*(C*H*$_2$OC*H*$_2$$(CH_2)_8CH_3$)O−),

3.26 (N_3CH_2−), 1.10−1.69 ($N_3CH_2(CH_2)_4CH_2O$−, −$OCH_2CH(CH_2OCH_2CH_2(CH_2)_7CH_3)O$−), 0.78−0.95 (−$OCH_2CH(CH_2OCH_2(CH_2)_8CH_3)O$−). $M_{n,NMR}$ = 10900 g mol^{-1}; $M_{n,SEC}$ = 9990 g mol^{-1}; $Đ$ = 1.02.

Synthesis of e-8. A typical procedure for the ω-end functionalization is as follows (Procedure D): Under a nitrogen atmosphere, NaH (25.4 mg, 635 μmol; 60 % in mineral oil) was added to a stirred solution of **e-7** (690 mg, 63.5 μmol) in THF (4 ml), and the solution was stirred at 40 ºC for 30 min. After cooling to room temperature, **t-I** (236 mg, 635 μmol) was then added to the solution, and the entire mixture was stirred at room temperature for 48 h. The polymer was purified by dialysis against MeOH (molecular weight cut-off, MWCO 5000 Da) to give **e-8** as a pale yellow viscous liquid (572 mg). Yield: 82.9%. ^{1}H NMR (400 MHz, $CDCl_3$): δ (ppm) 7.36 (aromatic), 4.70 (−poly-**M1**−CH_2PhCH_2O−), 4.64 (−$OCH(CH_3)O$−), 3.29–3.75 ($N_3(CH_2)_5CH_2OCH_2$−, −$OCH_2CH(CH_2OCH_2(CH_2)_8CH_3)O$−, $N_3CH_2CH(O$−$)CH_2$−, −$CH_2OCH(CH_3)OCH_2CH_3$), 3.26 ($N_3CH_2CH_2$−), 1.10−1.69 ($N_3CH_2(CH_2)_4CH_2O$−, −$OCH_2CH(CH_2OCH_2CH_2(CH_2)_7CH_3)O$−), 0.78−0.95 (−$OCH_2CH(CH_2OCH_2(CH_2)_8CH_3)O$−). $M_{n,NMR}$ = 11200 g mol^{-1}; $M_{n,SEC}$ = 11000 g mol^{-1}; $Đ$ = 1.03.

Synthesis of e-9. A typical procedure for the deprotection of the ethoxyethyl group is as follows (Procedure E): Cation-exchange resin (100 mg; Dowex 50WX2) was added to a stirred solution of **e-8** (572 mg, 51.1 μmol) in a mixed solvent of CH_2Cl_2 : MeOH = 4:1 (10

mL), then the solution was stirred at room temperature for 48 h. The polymer was purified by passing through a pad of alumina to give **e-9** as a colorless viscous liquid (572 mg). Yield: 87.0%. ^{1}H NMR (400 MHz, $CDCl_3$): δ (ppm) 7.36 (aromatic), 4.70 (−poly-**M1**−CH_2PhCH_2O–), 3.29–3.75 ($N_3(CH_2)_5CH_2OCH_2$−, −OCH_2CH(CH_2OC$H_2(CH_2)_8CH_3$)O−, N_3CH_2CH(O−)CH_2−, −CH_2OH), 3.26 (N_3CH_2–), 1.10−1.69 ($N_3CH_2(CH_2)_4CH_2O$−, −OCH_2CH(CH_2OCH_2C$H_2(CH_2)_7CH_3$)O−), 0.78−0.95 (−OCH_2CH(CH_2OC$H_2(CH_2)_8CH_3$)O−). $M_{n,NMR}$ = 11100 g mol^{-1}; $M_{n,SEC}$ = 11000 g mol^{-1}; $Đ$ = 1.03

Synthesis of e-10. Procedure A was used for the polymerization of **M2** (267 µL, 1.29 mmol) with the **e-9** macroinitiator (288 mg, 25.9 µmol; dehydrated by lyophilization using dry benzene) and *t*-Bu-P_4 (25.9 µL as 1.0 mol L^{-1} stock solution in *n*-hexane, 25.9 µmol) in toluene (435 µL) to give **e-10** as a colorless waxy solid (445 mg). Yield: 77.7%. ^{1}H NMR (400 MHz, $CDCl_3$): δ (ppm) 7.36 (aromatic), 4.70 (−poly-**M1**−CH_2PhCH_2O−), 3.29–3.75 ($N_3(CH_2)_5CH_2OCH_2$−, −OCH_2CH(CH_2OC$H_2(CH_2)_8CH_3$)O−, −OCH_2CH(CH_2O(CH_2CH_2O)$_3$CH_3)O−, N_3CH_2CH(O−)CH_2−, −CH_2O−poly-**M2**−), 3.26 (N_3CH_2–), 1.10−1.69 ($N_3CH_2(CH_2)_4CH_2O$–, −OCH_2CH(CH_2OCH_2C$H_2(CH_2)_7CH_3$)O−), 0.78−0.95 (−OCH_2CH(CH_2OC$H_2(CH_2)_8CH_3$)O−). $M_{n,NMR}$ = 22000 g mol^{-1}; $M_{n,SEC}$ = 15500 g mol^{-1}; $Đ$ = 1.06.

Synthesis of e-11. Procedure D was used for the ω-end functionalization of **e-10** (273 mg, 12.4 μmol) with NaH (5.44 mg, 136 μmol; 60% in mineral oil) and **t-II** (38.0 mg, 136 μmol) in THF (4 mL) to give **e-11** as a pale yellow waxy solid (268 mg). Yield: 98.0%. ^{1}H NMR (400 MHz, $CDCl_3$): δ (ppm) 7.36 (aromatic), 6.60 (aromatic), 6.50 (aromatic), 4.70 (−poly-**M1**−CH_2PhCH_2O−, −poly-**M2**−CH_2Ph−), 4.65 (−OCH_2C≡CH), 3.29–3.75 ($N_3(CH_2)_5CH_2OCH_2$−, −OCH_2CH(CH_2OC$H_2(CH_2)_8CH_3$)O−, −OCH_2CH(CH_2O(CH_2CH_2O)$_3$CH_3)O−, N_3CH_2CH(O−)CH_2−, –CH_2O−poly-**M2**−), 3.26 (N_3CH_2−), 2.60 (−CH_2C≡CH), 1.10−1.69 (N_3CH_2(CH_2)$_4$CH_2O−, −OCH$_2$CH(CH$_2$OCH$_2$CH_2(CH_2)$_7$CH$_3$)O−), 0.78−0.95 (−OCH$_2$CH(CH$_2$OCH$_2$(CH$_2$)$_8$CH_3)O−). $M_{n,NMR}$ = 22100 g mol^{-1}; $M_{n,SEC}$ = 16000 g mol^{-1}; $Đ$ = 1.05.

Synthesis of *eight*-IV. Procedure C was used for the click cyclization of **e-11** (150 mg, 6.75 μmol in degassed DMF (5.0 mL)) with a solution of CuBr (96.8 mg, 675 μmol) and PMDETA (281 μL, 1.35 mmol) in degassed DMF (40 mL) to give ***eight*-IV** as a light brown waxy solid (58.0 mg). Yield: 38.7%. ^{1}H NMR (400 MHz, $CDCl_3$): δ (ppm) 7.76, 7.64 (triazole methine), 6.60 (aromatic), 6.50 (aromatic), 5.15 (–OCH_2−triazole ring), 4.70 (−poly-**M1**−CH_2PhCH_2O−, −poly-**M2**−CH_2Ph−), 4.45 (triazole ring−CH_2CH–), 4.35 (triazole ring−CH_2(CH$_2$)$_5$O–), 3.29−3.75 (triazole ring−(CH$_2$)$_5$CH_2OCH_2−, −OCH_2CH(CH_2OCH_2(CH$_2$)$_8$CH$_3$)O−, −OCH_2CH(CH_2O(CH_2CH_2O)$_3$CH_3)O−), 1.10−1.69 (triazole ring−CH$_2$(CH_2)$_4$CH$_2$O−, −OCH$_2$CH(CH$_2$OCH$_2$CH_2(CH_2)$_7$CH$_3$)O−), 0.78−0.95

(−$OCH_2CH(CH_2OCH_2(CH_2)_8CH_3)O$−). $M_{n,NMR}$ = 22200 g mol^{-1}; $M_{n,SEC}$ = 12400 g mol^{-1}; $Đ$ = 1.04.

Synthesis of tp-1. Procedure D was used for the ω-end functionalization of **poly-M1** (500 mg, 45.6 μmol; $M_{n,NMR}$ = 11000 g mol^{-1}, $M_{n,SEC}$ = 9840 g mol^{-1}, $Đ$ = 1.05) with NaH (18.2 mg, 456 μmol; 60% in mineral oil) and **t-I** (170 mg, 456 μmol) in THF (4 mL) to give a pale yellow viscous solid (442 mg). Yield: 88.3%. ^{1}H NMR (400 MHz, $CDCl_3$): δ (ppm) 7.36 (aromatic), 7.17 (aromatic), 4.70 (−poly-**M1**−CH_2PhCH_2O−), 4.64 (–$OCH(CH_3)O$–), 3.29−3.75 ($Ph(CH_2)_2CH_2OCH_2$−, −$OCH_2CH(CH_2OCH_2(CH_2)_8CH_3)O$−, $N_3CH_2CH(O-)CH_2$−, −$CH_2OCH(CH_3)OCH_2CH_3$), 2.68 ($PhCH_2CH_2CH_2$–), 1.10−1.69 ($PhCH_2CH_2CH_2O$–, −$OCH_2CH(CH_2OCH_2CH_2(CH_2)_7CH_3)O$−), 0.78−0.95 (−$OCH_2CH(CH_2OCH_2(CH_2)_8CH_3)O$−). $M_{n,NMR}$ = 11300 g mol^{-1}; $M_{n,SEC}$ = 9940 g mol^{-1}; $Đ$ = 1.05. Procedure E was used for the deprotection of the product (441 mg, 39.2 μmol) with a cation-exchange resin (100 mg; Dowex 50WX2) in a mixed solvent of CH_2Cl_2:MeOH = 4:1 (10 mL) to give **tp-1** as a colorless viscous liquid (401 mg). Yield: 90.9%. ^{1}H NMR (400 MHz, $CDCl_3$): δ (ppm) 7.36 (aromatic), 7.17 (aromatic), 4.70 (−poly-**M1**−CH_2PhCH_2O−), 3.29−3.75 ($Ph(CH_2)_2CH_2OCH_2$−, −$OCH_2CH(CH_2OCH_2(CH_2)_8CH_3)O$−, $N_3CH_2CH(O-)CH_2$−, −CH_2OH), 2.68 ($PhCH_2CH_2CH_2$–), 1.10−1.69 ($PhCH_2CH_2CH_2O$–, −$OCH_2CH(CH_2OCH_2CH_2(CH_2)_7CH_3)O$−), 0.78−0.95 (−$OCH_2CH(CH_2OCH_2(CH_2)_8CH_3)O$−). $M_{n,NMR}$ = 11300 g mol^{-1}; $M_{n,SEC}$ = 10100 g mol^{-1}; $Đ$ = 1.03.

Synthesis of tp-2. Procedure A was used for the polymerization of **M2** (199 μL, 212 μmol) with the **tp-1** macroinitiator (215 mg, 19.2 μmol) and *t*-Bu-P_4 (19.2 μL as 1.0 mol L^{-1} stock solution in *n*-hexane, 19.2 μmol) in toluene (344 μL) to give **tp-2** as a colorless waxy solid (339 mg). Yield: 79.3%. ^{1}H NMR (400 MHz, $CDCl_3$): δ (ppm) 7.36 (aromatic), 7.17 (aromatic), 4.70 (−poly-**M1**−CH_2PhCH_2O−), 3.29−3.75 (Ph$(CH_2)_2$CH_2OCH_2−, −OCH_2CH(CH_2OC$H_2$$(CH_2)_8CH_3$)O−, −OC$H_2CH$(C$H_2$O(C$H_2CH_2$O)$_3CH_3$)O−, N_3CH_2CH(O–)CH_2–, –CH_2O−poly-**M2**−), 2.68 (PhC$H_2$$CH_2CH_2$–), 1.10−1.69 (Ph$CH_2CH_2$$CH_2$O–, −O$CH_2$CH($CH_2OCH_2CH_2$$(CH_2)_7CH_3$)O−), 0.78−0.95 (−O$CH_2$CH($CH_2OCH_2$$(CH_2)_8CH_3$)O−). $M_{n,NMR}$ = 22400 g mol^{-1}; $M_{n,SEC}$ = 16400 g mol^{-1}; $Đ$ = 1.05.

Synthesis of tp-3. Procedure B was used for the propargylation of **tp-2** (230 mg, 10.4 μmol) with NaH (4.40 mg, 110 μmol; 60% in mineral oil) and propargyl bromide (8.26 μL, 110 μmol) in THF (4.0 mL) to give **tp-3** as a pale yellow waxy solid (187 mg). Yield: 81.4%. ^{1}H NMR (400 MHz, $CDCl_3$): δ (ppm) 7.36 (aromatic), 7.17 (aromatic), 4.70 (−poly-**M1**−CH_2PhCH_2O−), 4.30 (−OCH_2C≡CH), 3.29−3.75 (Ph$(CH_2)_2$CH_2OCH_2−, −OCH_2CH(CH_2OC$H_2$$(CH_2)_8CH_3$)O−, −OC$H_2CH$(C$H_2$O(C$H_2CH_2$O)$_3CH_3$)O−, N_3CH_2CH(O−)CH_2−, −CH_2O−poly-**M2**), 2.68 (PhC$H_2$$CH_2CH_2$–), 2.39 (–C≡C$H$), 1.10−1.69 (Ph$CH_2CH_2$$CH_2$O–, −O$CH_2$CH($CH_2OCH_2CH_2$$(CH_2)_7CH_3$)O−), 0.78−0.95

(−$OCH_2CH(CH_2OCH_2(CH_2)_8CH_3)O$−). $M_{n,NMR}$ = 22500 g mol^{-1}; $M_{n,SEC}$ = 16400 g mol^{-1}; $Đ$ = 1.06.

Synthesis of *tadpole*-I. Procedure C was used for the click cyclization of **tp-3** (150 mg, 6.75 μmol in degassed DMF (5.0 mL)) with a solution of CuBr (96.8 mg, 675 μmol) and PMDETA (281 μL, 1.35 mmol) in degassed DMF (40 mL) to give **tadpole-I** as a light brown waxy solid (84.3 mg). Yield: 56.2%. ^{1}H NMR (400 MHz, $CDCl_3$): δ (ppm) 7.70 (triazole methine), 7.36 (aromatic), 7.17 (aromatic), 4.78 (−OCH_2-triazole ring), 4.50–4.70 (−poly-**M1**−CH_2PhCH_2O−), 4.40 (−$CHCH_2$−triazole ring), 3.29−3.75 ($Ph(CH_2)_2CH_2OCH_2$−, −$OCH_2CH(CH_2OCH_2(CH_2)_8CH_3)O$−, −$OCH_2CH(CH_2O(CH_2CH_2O)_3CH_3)O$−), 2.68 ($PhCH_2CH_2CH_2$–), 1.10−1.69 ($PhCH_2CH_2CH_2O$–, −$OCH_2CH(CH_2OCH_2CH_2(CH_2)_7CH_3)O$−), 0.78−0.95 (−$OCH_2CH(CH_2OCH_2(CH_2)_8CH_3)O$−). $M_{n,NMR}$ = 21900 g mol^{-1}; $M_{n,SEC}$ = 14600 g mol^{-1}; $Đ$ = 1.04.

Synthesis of tp-4. Procedure D was used for the ω-end functionalization of **poly-M2** (1.10 g, 100 μmol; $M_{n,NMR}$ = 10900, $M_{n,SEC}$ = 7030, $Đ$ = 1.06) with NaH (39.8 mg, 996 μmol; 60% in mineral oil) and **t-I** (371 mg, 996 μmol) in THF (4.0 mL) to give a pale yellow viscous liquid (581 mg). Yield: 53.0%. ^{1}H NMR (400 MHz, $CDCl_3$): δ (ppm) 7.36 (aromatic), 7.17 (aromatic), 4.70 (−poly-**2**−CH_2PhCH_2O−), 4.64 (−$OCH(CH_3)O$−), 3.29−3.75 ($Ph(CH_2)_2CH_2OCH_2$−, −$OCH_2CH(CH_2O(CH_2CH_2O)_3CH_3)O$−, $N_3CH_2CH(O-)CH_2$−, −$CH_2OCH(CH_3)OCH_2$−), 2.68 ($PhCH_2CH_2CH_2$−), 1.85 ($PhCH_2CH_2CH_2$−), 1.30

(−OCH(CH_3)O−), 1.19 (−OCH$_2$CH_3). $M_{n,NMR}$ = 11300 g mol^{-1}; $M_{n,SEC}$ = 9040 g mol^{-1}; $Đ$ = 1.04. Procedure E was used for the deprotection of the product (580 mg, 51.1 µmol) with a cation-exchange resin (100 mg; Dowex 50WX2) in MeOH (10 mL) to give **tp-4** as a colorless viscous liquid (310 mg). Yield: 53.4%. ^{1}H NMR (400 MHz, $CDCl_3$): δ (ppm) 7.36 (aromatic), 7.17 (aromatic), 4.70 (−poly-**M2**−CH_2PhCH_2O−), 3.29−3.75 (Ph(CH$_2$)$_2$CH_2OCH_2−, −OCH_2CH(CH_2O(CH_2CH_2O)$_3$CH_3)O−, N$_3$CH_2CH(O−)CH$_2$−, −CH_2OH), 2.68 (PhCH_2CH$_2$CH$_2$–), 1.85 (PhCH$_2$CH_2CH$_2$–). $M_{n,NMR}$ = 11300 g mol^{-1}; $M_{n,SEC}$ = 8660 g mol^{-1}; $Đ$ = 1.05.

Synthesis of tp-5. Procedure A was used for the polymerization of **M1** (292 µL, 1.36 mmol) with the **tp-4** macroinitiator (307 mg, 27.2 µmol) and *t*-Bu-P$_4$ (13.6 µL as 1.0 mol L^{-1} stock solution in *n*-hexane, 13.6 µmol) in toluene (730 µL) to give the crude **tp-5**, which was further purified by preparative SEC to give **tp-5** as a colorless waxy solid (74.2 mg). Yield: 24.2%. ^{1}H NMR (400 MHz, $CDCl_3$): δ (ppm) 7.36 (aromatic), 7.17 (aromatic), 4.70 (−poly-**M2**−CH_2PhCH_2O−), 3.29−3.75 (Ph(CH$_2$)$_2$CH_2OCH_2−, −OCH_2CH(CH_2OCH_2(CH$_2$)$_8$CH$_3$)O−, −OCH_2CH(CH_2O(CH_2CH_2O)$_3$CH_3)O−, N$_3$CH_2CH(O–)CH$_2$−, −CH_2O−poly-**M1**), 2.68 (PhCH_2CH$_2$CH$_2$−), 1.10−1.69 (PhCH$_2$CH_2CH$_2$O−, −OCH$_2$CH(CH$_2$OCH$_2$CH_2(CH_2)$_7$CH$_3$)O−), 0.78−0.95 (−OCH$_2$CH(CH$_2$OCH$_2$(CH$_2$)$_8$CH_3)O−). $M_{n,NMR}$ = 22100 g mol^{-1}; $M_{n,SEC}$ = 16800 g mol^{-1}; $Đ$ = 1.05.

Synthesis of tp-6. Procedure B was used for the propargylation of **tp-5** (74.2 mg, 3.37 μmol) with NaH (1.35 mg, 33.7 μmol; 60% in mineral oil) and propargyl bromide (2.53 μL, 33.7 μmol) in THF (4.0 mL) to give **tp-6** as a pale yellow waxy solid (73.0 mg). Yield: 98.4%. ^{1}H NMR (400 MHz, $CDCl_3$): δ (ppm) 7.36 (aromatic), 7.17 (aromatic), 4.70 (−poly-**M2**−CH_2PhCH_2O−), 4.30 (−OCH_2C≡CH), 3.29−3.75 (Ph(CH_2)$_2$CH_2OCH_2−, −OCH_2CH(CH_2OCH_2(CH_2)$_8$CH_3)O−, −OCH_2CH(CH_2O(CH_2CH_2O)$_3$CH_3)O−, N_3CH_2CH(O−)CH_2−, –CH_2O−poly-**M1**), 2.68 (PhCH_2CH_2CH_2−), 2.39 (−C≡CH), 1.10−1.69 (PhCH_2CH_2CH_2O−, −OCH_2CH(CH_2OCH_2CH_2(CH_2)$_7$CH_3)O−), 0.78−0.95 (−OCH_2CH(CH_2OCH_2(CH_2)$_8$CH_3)O−). $M_{n,NMR}$ = 22100 g mol^{-1}; $M_{n,SEC}$ = 16900 g mol^{-1}; $Đ$ = 1.05.

Synthesis of *tadpole*-II. Procedure C was used for the click cyclization of **tp-6** (70 mg, 3.17 μmol in degassed DMF (4.0 mL)) with a solution of CuBr (45.5 mg, 317 μmol) and PMDETA (132 μL, 634 μmol) in degassed DMF (20 mL) to give ***tadpole*-II** as a light brown waxy solid (22.9 mg). Yield: 32.7%. ^{1}H NMR (400 MHz, $CDCl_3$): δ (ppm) 7.70 (triazole methine), 7.36 (aromatic), 7.17 (aromatic), 4.78 (−OCH_2−triazole ring) 4.50–4.70 (−poly-**M2**−CH_2PhCH_2O−), 4.40 (−CHCH_2−triazole ring), 3.29−3.75 (Ph(CH_2)$_2$CH_2OCH_2−, −OCH_2CH(CH_2OCH_2(CH_2)$_8$CH_3)O−, −OCH_2CH(CH_2O(CH_2CH_2O)$_3$CH_3)O−), 2.68 (PhCH_2CH_2CH_2−), 1.10−1.69 (PhCH_2CH_2CH_2O−, −OCH_2CH(CH_2OCH_2CH_2(CH_2)$_7$CH_3)O−), 0.78−0.95

(−$OCH_2CH(CH_2OCH_2(CH_2)_8CH_3)O$−). $M_{n,NMR}$ = 22400 g mol^{-1}; $M_{n,SEC}$ = 13600 g mol^{-1}; $Đ$ = 1.06.

Synthesis of *linear*-III. Procedure A was used for the triblock copolymerization of **M1** (111 μL, 467 μmol, first monomer, polymerization time = 20 h), **M2** (193 μL, 933 mmol, second monomer, polymerization time = 20 h), and **M2** (111 μL, 467 μmol, third monomer, polymerization time = 20 h) with **i-IV** (18.7 μL as 1.0 mol L^{-1} stock solution in toluene, 18.7 μmol) and *t*-Bu-P_4 (18.7 μL as 1.0 mol L^{-1} stock solution in *n*-hexane, 18.7 μmol) in toluene (482 μL) to give ***linear*-III** as a colorless waxy solid (329 mg). Yield: 81.0%. ^{1}H NMR (400 MHz, $CDCl_3$): δ (ppm) 7.28, 7.18 (aromatic), 3.29−3.80 ($Ph(CH_2)_2CH_2OCH_2$−, −$OCH_2CH(CH_2OCH_2(CH_2)_8CH_3)O$−, −$OCH_2CH(CH_2O(CH_2CH_2O)_3CH_3)O$−), 2.68 ($PhCH_2CH_2CH_2$-), 1.88 ($PhCH_2CH_2CH_2O$−), 1.15−1.80 (−$OCH_2CH(CH_2OCH_2CH_2(CH_2)_7CH_3)O$−), 0.78−1.00 (−$OCH_2CH(CH_2OCH_2(CH_2)_8CH_3)O$−). $M_{n,NMR}$ = 21700 g mol^{-1}; $M_{n,SEC}$ = 16200 g mol^{-1}; $Đ$ = 1.03.

Synthesis of *linear*-IV. Procedure A was used for the triblock copolymerization of **M2** (187 μL, 908 μmol, first monomer, polymerization time = 20 h), **M1** (430 μL, 1.82 mmol, second monomer, polymerization time = 20 h), and **M2** (187 μL, 908 μmol, third monomer, polymerization time = 20 h) with **i-IV** (36.3 μL as 1.0 mol L^{-1} stock solution in toluene, 36.3 μmol) and *t*-Bu-P_4 (36.3 μL as 1.0 mol L^{-1} stock solution in *n*-hexane, 36.3 μmol) in toluene (763 μL) to give **II** as a colorless waxy solid (683 mg). Yield: 86.6%. ^{1}H NMR (400 MHz,

$CDCl_3$): δ (ppm) 7.28, 7.18 (aromatic), 3.29−3.80 ($Ph(CH_2)_2CH_2OCH_2$−, −$OCH_2CH(CH_2OCH_2(CH_2)_8CH_3)O$−, −$OCH_2CH(CH_2O(CH_2CH_2O)_3CH_3)O$−), 2.67 ($PhCH_2CH_2CH_2$-), 1.87 ($PhCH_2CH_2CH_2O$−), 1.15−1.80 (−$OCH_2CH(CH_2OCH_2CH_2(CH_2)_7CH_3)O$−), 0.78−1.00 (−$OCH_2CH(CH_2OCH_2(CH_2)_8CH_3)O$−). $M_{n,NMR}$ = 21800 g mol^{-1}; $M_{n,SEC}$ = 16400 g mol^{-1}; M_w/M_n = 1.03.

Self-assembly studies of the amphiphilic block copolymers. The experimental methods used for the investigation of the CMC, micelle morphology, and $T_{c.d.}$ in aqueous solutions are the same as Chapter 2.

3.5 References and Notes

1. Hadjichristidis, N.; Pitsikalis, M.; Pispas, S.; Iatrou, H. *Chem. Rev.* **2001**, *101*, 3747−3792.

2. Hadjichristidis, N.; Iatrou, H.; Pitsikalis, M.; Mays, J. *Prog. Polym Sci.* **2006**, *31*, 1068−1132.

3. Yamamoto, T.; Tezuka, Y. *Polym. Chem.* **2011**, *2*, 19301941.

4. Laurent, B. A.; Grayson, S. M. *Chem. Soc. Rev.* **2009**, *38*, 2202−2213.

5. Jia, Z.; Monteiro, M. J. *J. Polym. Chem. Part A: Polym. Chem.* **2012**, *50*, 2085−2097.

6. Kricheldorf, H. R. *J. Polym. Chem. Part A: Polym. Chem.* **2010**, *48*, 251−284.

7. Honda, S.; Yamamoto, T.; Tezuka, Y. *J. Am. Chem. Soc.* **2010**, *132*, 10251−10253.

8. Honda, S.; Yamamoto, T.; Tezuka, Y. *Nat. Commun.* **2013**, *4*, 1574.

9. Heo, K.; Kim, Y. Y.; Kitazawa, Y.; Kim, M.; Jin, K. S.; Yamamoto, T.; Ree, M. *ACS Macro Lett.* **2014**, *3*, 233−239.

10. Zhu, Y.; Gido, S. P.; Iatrou, H.; Hadjichristidis, N.; Mays, J. W. *Macromolecules* **2003**, *36*, 148−152.

11. Takano, A.; Kadoi, O.; Hirahara, K.; Kawahara, S.; Isono, Y.; Suzuki, J.; Matsushita, Y. *Macromolecules* **2003**, *36*, 3045−3050.

12. Poelma, J. E.; Ono K.; Miyama, D.; Aida, T.; Satoh, K.; Hawker, C. J. *ACS Nano* **2012**, *6*, 10845−10854.

13. Iatrou, H.; Hadjichristidis, N.; Meier, G.; Frielinghaus, H.; Monkenbusch, M. *Macromolecules* **2002**, *35*, 5426−5437.

14. Borsali, R.; Minatti, E.; Putaux, J.-L.; Schappacher, M.; Deffieux, A.; Viville, P.; Lazzaroni, R.; Narayanan, T. *Langmuir* **2003**, *19*, 6−9.

15. Minatti, E.; Viville, P.; Borsali, R.; Schappacher, M.; Deffieux, A.; Lazzaroni, R. *Macromolecules* **2003**, *36*, 4125−4133.

16. Beinat, S.; Schappacher, M.; Deffieux, A. *Macromolecules* **1996**, *29*, 6737−6743.

17. Dong, Y.-Q.; Tong, Y.-Y.; Dong, B.-T.; Di, F.-S.; Li, Z.-C. *Macromolecules* **2009**, *42*, 2940−2948.

18. Wang, G.; Hu, B.; Fan, X.; Zhang, Y.; Huang, J. *J. Polym. Chem. Part A: Polym. Chem.* **2012**, *50*, 2227−2235.

19. Wang, X.; Liu, T.; Liu, S. *Biomacromolecules* **2011**, *12*, 1146−1154.

20. Shi, G.-Y.; Sun, J.-T.; Pan, C.-Y. *Macromol. Chem. Phys.* **2011**, *212*, 1305−1315.

21. Hatakeyama, F.; Yamamoto, T.; Tezuka, Y. *ACS Macro Lett.* **2013**, *2*, 427−431.

22. Fan, X.; Huang, B.; Wang, G.; Huang, J. *Macromolecules* **2012**, *45*, 3779−3786.

23. Lonsdale, D. E.; Monteiro, M. J. *J. Polym. Chem. Part A: Polym. Chem.* **2011**, *49*, 4603−4612.

24. Mark, H. F.; Bikales, N. M.; Overberger, C. G.; Menges, G; Kroschwitz, J. I., Eds. *Encyclopedia of Polymer Science and Engineering*, vol. 6; John Wiley & Sons, Inc., **1985**.

25. Schmolka, I. R. *J. Am. Oil Chem. Soc.* **1977**, *54*, 110−116.

26. Gupta, S.; Tyagi, R.; Parmar, V. S.; Sharma, S. K.; Haag, R. *Polymer* **2012**, *53*, 3053−3078.

27. Booth, C.; Attwood, D. *Macromol. Rapid Commun.* **2000**, *21*, 501−527.

28. Brocas, A.-L.; Gervais, M.; Carlotti, S.; Pispas, S. *Polym. Chem.* **2012**, *3*, 2148−2155.

29. Mai, S.-M.; Fairclough, J. P. A.; Terrill, N. J.; Turner, S. C.; Hamley, I. W.; Matsen, M. W.; Ryan, A. J.; Booth, C. *Macromolecules* **1998**, *31*, 8110−8116.

30. Halacheva, S.; Rangelov, S.; Tsvetanov, C. *Macromolecules* **2006**, *39*, 6845−6852.

31. Yu, G.-E.; Yang, Y.-W.; Yang, Z.; Attwood, D.; Booth, C. *Langmuir* **1996**, *12*, 3404−3412.

32. Altinok, H.; Yu, G.-E.; Nixon, S. K.; Gorry, P. A.; Attwood, D.; Booth, C. *Langmuir* **1997**, *13*, 5837−5848.

33. Yu, G.-E.; Yang, Z.; Attwood, D.; Price, C.; Booth, C. *Macromolecules* **1996**, *29*, 8479−8486.

34. Yu, G.-E.; Garrett, C. A.; Mai, S.-M.; Altinok, H.; Attwood, D.; Price, C.; Booth, C. *Langmuir* **1998**, *14*, 2278−2285.

35. Laurent, B. A.; Grayson, S. M. *J. Am. Chem. Soc.* **2006**, *128*, 4238−4239.

36. Lansdale, D. E.; Bell, C. A.; Monteiro, M. J. *Macromolecules* **2010**, *43*, 3331−3339.

37. Misaka, H.; Sakai, R.; Satoh, T.; Kakuchi, T. *Macromolecules* **2011**, *44*, 9099−9107.

38. Misaka, H.; Tamura, E.; Makiguchi, K.; Kamoshida, K.; Sakai, R.; Satoh, T.; Kakuchi, T. *J. Polym. Sci. Part A: Polym. Chem.* **2012**, *50*, 1941−1952.

39. Kwon, W.; Roh, Y.; Kamoshida, K.; Kwon, K. H.; Jeong, Y. C.; Kim, J.; Misaka, H.; Shin, T. J.; Kim, J.; Kim, K.-W.; Jin, K. S.; Chang, T.; Kim, H.; Satoh, T.; Kakuchi, T.; Ree, M. *Adv. Funct. Mater.* **2012**, *22*, 5194−5208.

40. Laurent, B. A.; Grayson, S. M. *J. Am. Chem. Soc.* **2006**, *128*, 4238−4239.

41. Shi, G.-Y.; Pan, C.-Y. *Macromol. Rapid Commun.* **2008**, *29*,1672−1678.

42. Schappacher, M.; Deffieux, A. *Macromolecules* **1995**, *28*, 2629−2636.

43. Rixman, M. A.; Dean, D.; Ortiz, C. *Langmuir* **2003**, *19*, 9357−9372.

44. Malkoch, M.; Schleicher, K.; Drockenmuller, E.; Hawker, C. J.; Russell, T. P.; Fokin, V. V. *Macromolecules* **2005**, *38*, 3663−3678.

45. Toy, A. A.; Reinicke, S.; Mueller, A. H. E.; Schmalz, H. *Macromolecules* **2007**, *40*, 5241−5244.

46. Rao, J.; Zhang, Y.; Zhang, J.; Liu, S. *Biomacromolecules* **2008**, *9*, 2586−2593.

Chapter 4

Synthesis of Well-Defined Three- and Four-armed Cage-shaped Polyethers via "Topological Conversion" from Trefoil- and Quatrefoil-shaped Polyethers

4.1 Introduction

Constructing various macromolecular architectures, such as cyclic, star, and brush polymers, has been one of the central subjects in the polymer chemistry field over the past few decades.[1–6] Such considerable synthetic efforts have revealed a variety of existing properties coming from the non-linear architecture, which, in turn, offered a huge opportunity to design novel functional polymers based on topological effects. Among the various macromolecular architectures, cyclic architectures have attracted particular attention for a long time due not only to their fascinating structures, but also to their distinctive physical properties originating from the absence of chain ends.[7–12] To date, a number of efficient synthetic methodologies for cyclic polymers and related architectures like figure-eight-shaped and tadpole-shaped polymers has been demonstrated.[13–17] Some of the most successful synthetic approaches were the ring-expansion polymerization,[18, 19] ring-closing metathesis,[20–22] and click cyclization,[23–25] by which cyclic polymers with a variety of main chain and side chain structures were prepared.

Meanwhile, only a little attention has been paid to the polymers with a cage-shaped architecture, which is a special class of cyclic architectures, such as theta-shape and delta-graph, in spite of its intriguing structural characteristic due to the three-dimensional cavity. Such cage-shaped polymers can be regarded as a macromolecular analog of cryptand. Thus, it is highly expected that the cage-shaped polymers show an ability to encapsulate

relatively large molecules in their cavities, leading to a range of applications such as size-selective molecular recognition,[25, 26] stabilization of unstable molecules,[27] and nano-reactors.[28] However, the basic properties as well as molecular functions due to the cage-shaped architectures have not been investigated because of the inherent synthetic difficulties.

The first efficient synthesis of a cage-shaped polymer was achieved by Tezuka et al., in which the "electrostatic self-assembly and covalent fixation" (ESA-CF) method was applied to build the three-armed cage-shaped (theta-shaped) poly(THF) from the combination of the three-armed star poly(THF) possessing a quaternary ammonium cation moiety at each arm end with a tricarboxylate molecule (**Scheme 4-1a**).[29, 30] The ESA-CF process to produce a figure-eight-shaped poly(THF) possessing two olefin groups followed by its intramolecular olefin metathesis led to formation of the four-armed cage-shaped (delta-graph) poly(THF) (**Scheme 4-1b**).[31] On the other hand, Paik et al. reported the synthesis of three- and four-armed cage-shaped polystyrenes by the click coupling reaction of the ω-azido functionalized star-shaped polystyrenes using multiple alkynyl coupling agents (**Scheme 4-1a**).[32, 33] Such "intermolecular cyclization" approaches are useful and straightforward for the synthesis of a series of cage-shaped polymers. However, exact stoichiometric amount of the functional star-shaped polymer precursor and coupling agent have to be used to implement the cyclization. The inexact stoichiometry can result in forming byproducts, such as

oligomeric products and non-cyclized products. In addition, an appreciable polymer concentration is typically required for the intermolecular cyclization, which causes the pronounced formation of the oligomeric products. Therefore, of particular interest is to develop an efficient route to high purity and narrowly-dispersed cage-shaped polymers by "intramolecular cyclization" approach. The intramolecular cyclization approach is advantageous over the intermolecular cyclization for the effective preparation of cage-shaped polymers with high purity because the problem stem from the inexact stoichiometry of the complementary reactive functionalities can be eliminated. Furthermore, the high dilution condition is applicable for this approach and therefore the formation of the intermolecular coupling byproduct can be minimized. Despite its potential, however, there has been only one example of the cage-shaped polymer synthesis through the intramolecular cyclization[34] (**Scheme 4-1c**)

The author now propose a novel synthetic approach toward cage-shaped polymers, in which trefoil- and quatrefoil-shaped polymers were first synthesized as the precursor according to the intramolecular cyclization approach and were converted into three- and four-armed cage-shaped polymers, respectively, by cleaving the focal point. A schematic diagram for this "topological conversion" approach is described in **Scheme 4-1d**. The most important feature of the proposed approach is that byproduct formation can be avoided during the cage-shaped polymer formation step. This allows direct comparison of the polymer

properties between the trefoil/quatrefoil and cage-shaped polymers without changing the degree of polymerization and monomer composition, which could provide an insight into the structure-property relationship for the highly complexed topological polymers.

Scheme 4-1. Synthetic approaches of reported methods and present method for cage-shaped polymers.

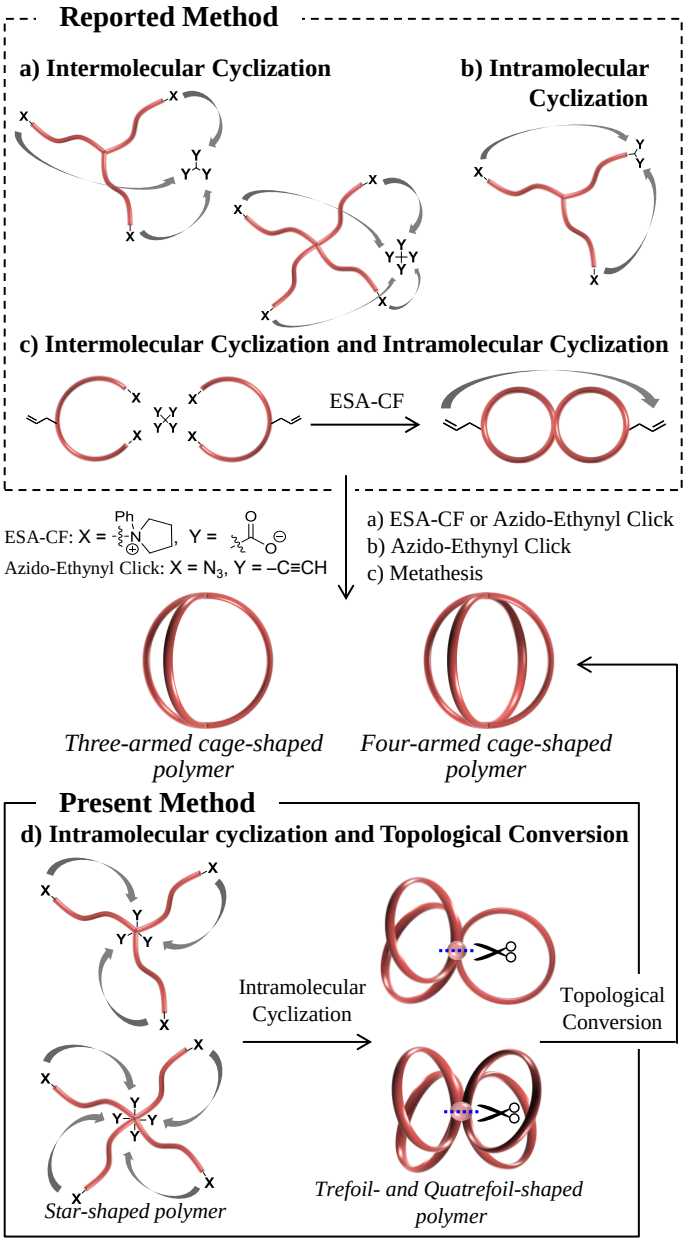

To realize such a synthetic approach, each polymer precursor has to be guaranteed a perfect chain end functionality; otherwise, inseparable byproducts would be generated during the cyclization step. For the synthesis of the trefoil- and quatrefoil-shaped polymer precursors, the author employed the combination of the *t*-Bu-P_4-catalyzed ring-opening polymerization of the epoxide with simultaneous click cyclizations. The methodology was verified to be effective for the synthesis of a series of cyclic, figure-eight-shaped, and tadpole-shaped polyethers with very narrow dispersities, as described in Chapter 3. **Scheme 4-2** describes a detailed synthetic scheme for constructing the three- and four-armed cage-shaped poly(butylene oxide)s (PBO) (***cage*$_3$-PBO** and ***cage*$_4$-PBO**, respectively). Thus, the author have prepared the trefoil- and quatrefoil-shaped PBOs (***trefoil*-PBO** and ***quatrefoil*-PBO**) having two benzyl ether linkages at the focal point by the intramolecular click cyclization of the clickable star-shaped precursors (**tf-2** and **qt-2**). The subsequent topological conversion from ***trefoil*-PBO** and ***quatrefoil*-PBO** was accomplished by removing the benzyl ether moiety to yield the three- and four-armed cage-shaped PBOs ***cage*$_3$-PBO** and ***cage*$_4$-PBO**. Although the polymer topological conversion from linear to single-cyclic and from cyclic to bicyclic (vice versa) had been reported,[21, 22, 35] this is the first example of the topological conversion from the trefoil/quatrefoil to cage-shaped architectures. This new approach was further extended for the synthesis of the trefoil/quatrefoil and cage-shaped amphiphilic block copolyethers, and the preliminary study of their aggregation behavior in

water was performed to demonstrate the polymer property change upon the topological conversion.

Scheme 4-2. Synthetic pathway for trefoil/quatrefoil and cage-shaped polybutylene oxides

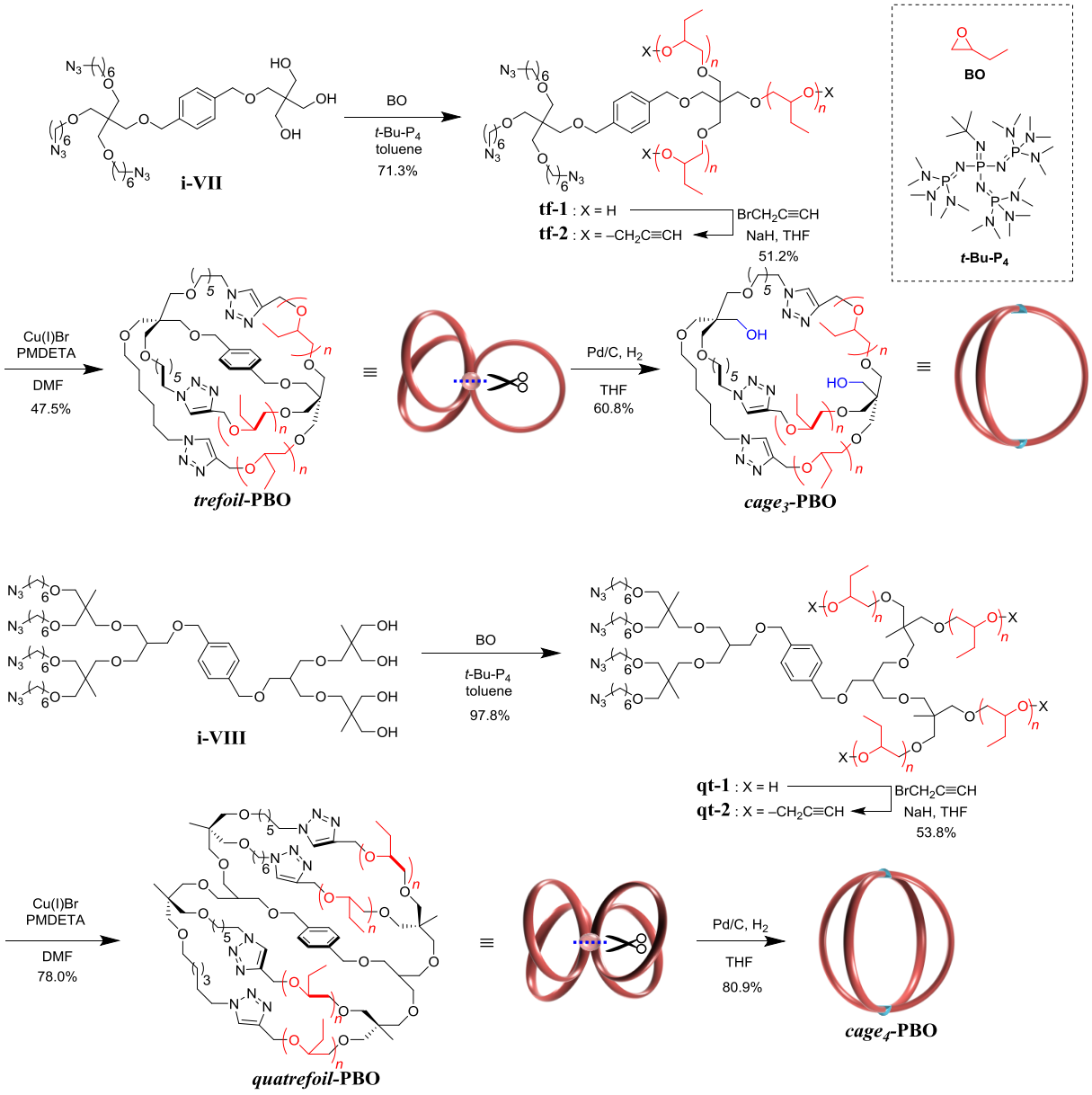

4.2 Results and Discussion

4.2.1 Design and Synthesis of Multifunctional Initiators

To realize the synthesis of the cage-shaped polymers via the topological conversion approach, the author newly designed multifunctional initiators (**i-VII** and **i-VIII**) consisting of multiple hydroxy- and azido-functionalized components tethered by a *p*-xylene moiety. The hydroxy functionality will serve as the initiating site of the *t*-Bu-P_4-catalyzed ring-opening polymerization (ROP), while the azido groups will act as reactive sites for the subsequent click cyclization. The key point of these initiator designs is the two benzyl ether linkages that tether the azido and hydroxy functionalities. The author envisaged that the benzyl ethers installed at the focal point of the trefoil- and quatrefoil-shaped polymers can be cleaved upon the catalytic hydrogenolysis, which would allow the topological conversion to the corresponding cage-shaped polymers.

The initiators **i-VII** and **i-VIII** were synthesized as shown in **Schemes 4-3** and **4-4**, respectively. For the synthesis of **i-VII**, the triazido-functionalized alcohol (**i1**) was first prepared starting from pentaerythritol in accordance with previous report.[36] The triazido-functionalized benzyl bromide **i2** was then synthesized by reacting the sodium alkoxide of **i1** with an excess amount of dibromo-*p*-xylene. The reaction of the potassium alkoxide of **i3** with **i2** followed by the deprotection of the orthoester yielded the desired **i-VII** as a colorless viscous liquid. For the synthesis of **i-VIII**, a dendron-like compound **i6** was

first prepared by the coupling of **i4** and 3-chloro-2-chloromethyl-1-propene followed by hydroboration-oxidation in two steps. The obtained **i6** was then derivatized into the benzyl bromide **i7** and the tetraazido-functionalized alcohol **i12**, then the two segments (**i7** and **i12**) were coupled by an etherification reaction. The desired **i-VIII** was finally obtained as a colorless viscous liquid after removal of the acetal protecting groups by acidic treatment. The obtained initiators **i-VII** and **i-VIII** were subjected to the polymerizations after careful purification by column chromatography and subsequent freeze-drying from a dry-benzene solution.

Scheme 4-3. Synthetic pathway for **i-VII**

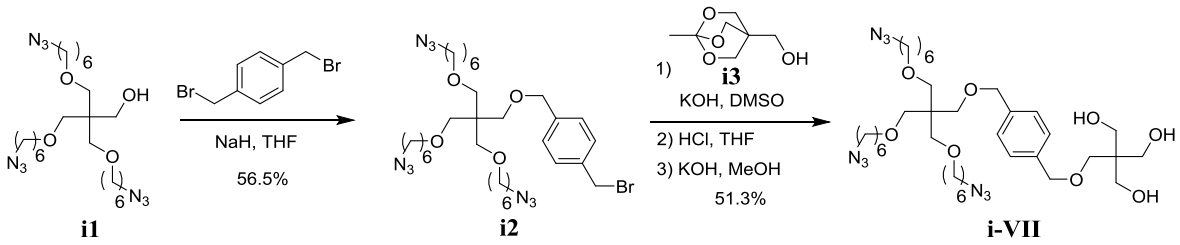

Scheme 4-4. Synthetic pathway for **i-VIII**

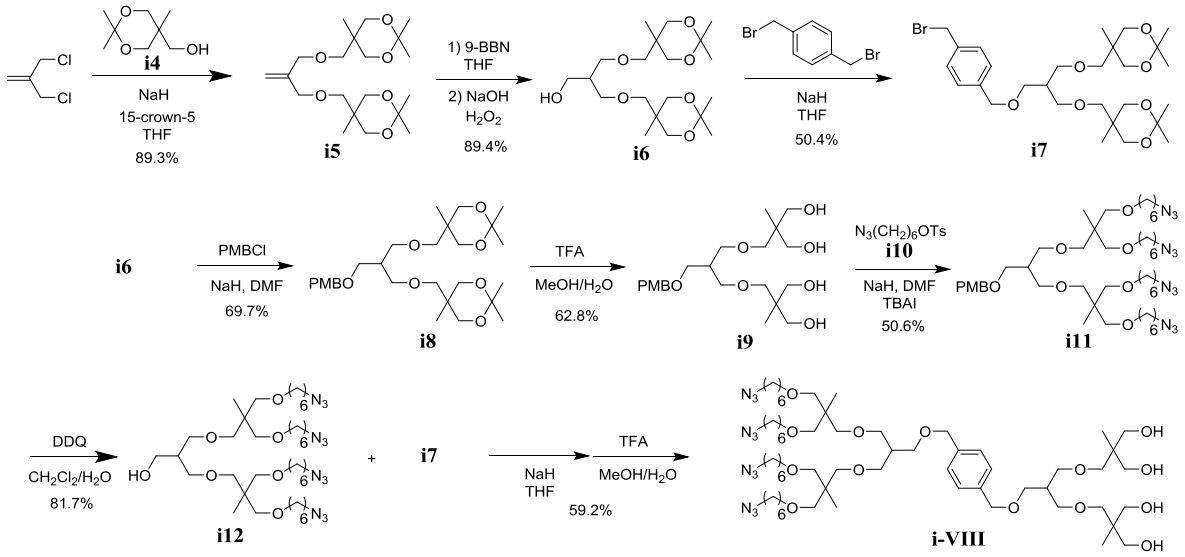

4.2.2 Synthesis of Three- and Four-armed Cage-shaped Poly(butylene oxide)s by the Topological Conversion from Trefoil- and Quatrefoil-shaped Precursors

With the specially designed initiators in hand, the author developed a feasibility study to demonstrate the principle of the topological conversion from the trefoil- and quatrefoil-shapes to cage-shaped architecture, i.e., trefoil to a three-armed cage-shape and quatrefoil to a four-armed cage shape.

The trefoil-shaped poly(butylene oxide) (PBO) (***trefoil*-PBO**) was synthesized in three steps involving the polymerization of butylene oxide (BO) with **i-VII**, end group modification with propargyl bromide, and intramolecular click cyclization (**Scheme 4-2**). According to Chapter 3,[26] the *t*-Bu-P_4-catalyzed ROP of BO using **i-VII** as an initiator was carried out at the $[BO]_0/[\textbf{i-VII}]_0/[t\text{-Bu-P}_4]_0$ ratio of 30/1/1 to produce the three-armed star-shaped PBO having three azido groups at the focal point (**tf-1**; $M_{n,NMR}$ = 3180 g mol^{-1}, DP = 34, $Đ$ = 1.07) in 71.3% isolated yield. The ^{1}H NMR spectrum showed the characteristic signals due to the PBO backbone along with the minor signals due to the initiator residue, such as the methylene adjacent to the azido group (*A*: 3.26 ppm in **Figure 4-1d**) and the benzyl group (*B*: 4.45 ppm), verifying that the ROP of BO was initiated from **i-VII**. Note that the obtained **tf-1** should fairly possess three arms with uniform length, as indicated by Chapter 2 based on the arm cleavage experiments. Next, **tf-1** was treated with an excess amount of propargyl bromide in the presence of sodium hydride to give the three-armed star-shaped PBO having three azido groups at the focal point and three propargyl

groups at the ω-ends (**tf-2**; $M_{n,NMR}$ = 3300 g mol^{-1}, DP = 34, $Đ$ = 1.06). No significant difference was observed between the SEC trace of the **tf-1** and **tf-2**, suggesting the absence of any side reactions (**Figures 4-1a** and **4-1b**). The proton signal due to the terminal alkyne (proton *D*) was observed at 2.39 ppm in **Figure 4-1e**, and the quantitative introduction of the propargyl groups was verified by comparing the peak areas of the ethynyl proton *D* (2.39 ppm) and benzyl proton *B* (4.45 ppm).

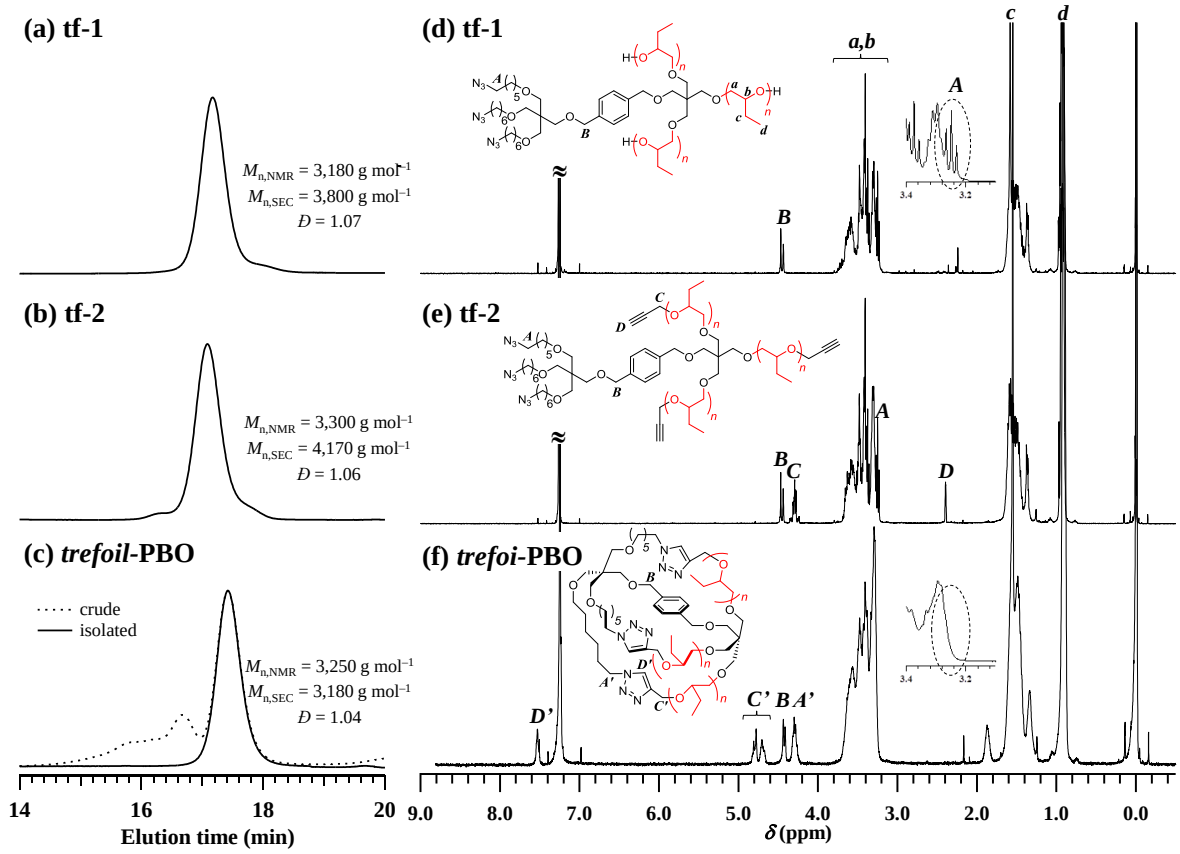

Figure 4-1. (a–c) SEC traces of **tf-1**, **tf-2**, and ***trefoil*-PBO** (dotted line, before purification; solid line, after purification using preparative SEC). The $M_{n,NMR}$s, $M_{n,SEC}$s, and $Đ$s were determined from the respective isolated polymers. (d–f) ^{1}H NMR spectra of **tf-1**, **tf-2**, and ***trefoil*-PBO** in $CDCl_3$ (400 MHz). The insets show the expanded ^{1}H NMR spectra which indicated the disappearance of the azido groups after the intramolecular click cyclization.

The intramolecular multiple click cyclization of **tf-2** was next performed to obtain the trefoil-shaped PBO ***trefoil*-PBO** under a high dilution condition using the CuBr/*N*,*N*,*N*′,*N*″,*N*″-pentamethyldiethylenetriamine (PMDETA) catalyst system in DMF at 90 °C. After the purification using an alumina column, the complete disappearance of the azido groups was confirmed by an FT-IR analysis (**Figure 4-2a**). The obtained crude product was subjected to an SEC analysis to confirm the progress of the cyclization reaction, as shown in **Figure 4-1c**. The elution peak maximum of the product was observed in the lower molecular weight region as compared to the star-shaped precursor **tf-2**, which strongly supported the decrease in the hydrodynamic volume by the intramolecular cyclization reaction. On the other hand, broad peaks were visible in the higher molecular weight region, which could be attributed to the oligomeric byproducts formed by the intermolecular click reaction. Further purification was performed by the preparative SEC to remove the high molecular weight byproducts, giving an analytically pure product in 47.5% yield. The isolated product displayed a unimodal SEC trace with the $Đ$ value of 1.04 (**Figure 4-1c**). The ratio between the $M_{n,SEC}$s at the SEC peak top of the cyclized ***trefoil*-PBO** and **tf-2**, i.e., $M_{n,p(\textbf{\textit{trefoil}-PBO})}/M_{n,p(\textbf{tf-2})} = \langle G \rangle$, was calculated to be 0.76 (**Table 4-1**). The new signals (*A'*: 4.30 ppm, *C'*: 4.66-4.86 ppm, *D'*: 7.54 ppm in **Figure 4-1f**) assignable to the triazole rings formed by the click reaction appeared in the ^{1}H NMR spectrum, while the signals due to the ethynyl groups and the methylene adjacent to the azido groups completely disappeared.

Based on the end group analysis by ^{1}H NMR, the $M_{n,NMR}$ and DP were calculated to be 3250 g mol^{-1} and 34, respectively. Furthermore, a matrix-assisted laser desorption/ionization time-of-flight mass spectrometry (MALDI-TOF MS) measurement was performed to identify the chemical structure of the isolated product. Note that the MALDI-TOF MS spectrum of the star-shaped precursor **tf-2** showed several set of peaks other than the predicted molar mass of **tf-2**, which can be assigned to the fragment peaks due to the decomposition of the azido groups during the ionization process of the measurement (**Figure 4-3**). In contrast, the MALDI-TOF MS spectrum of the cyclized product showed only one set of peaks having a regular interval of 72.05 Da for the molar mass of a BO unit, which indicated the absence of the unreacted azido group. More importantly, the peak observed at *m*/*z* of 3049.92 Da well agreed with the calculated molar mass for the 30-mer of the trefoil-shaped PBO (3049.25 Da, calculated for $[M+Na]^+$) (**Figure 4-4**). Based on the SEC, FT-IR, NMR, and MALDI-TOF MS analyses, the obtained product was assigned to the desired trefoil-shaped PBO, ***trefoil*-PBO**.

Table 4-1. Synthesis of trefoil/quatrefoil and cage-shaped PBOs and the corresponding precursors

polymer	$M_{n,NMR}$ [a] [g mol^{-1}]	DP [a]	$M_{n,SEC}$ [b] [g mol^{-1}]	$Đ$ [b]	$M_{n,p}$ [b] [g mol^{-1}]	$\langle G \rangle$
tf-2	3,300		4,170	1.06	4,380	0.76
***trefoil*-PBO**	3,250	34	3,180	1.06	3,310	
***cage*$_3$-PBO**	3,150		3,260	1.05	3,370	
qt-2	3,780		4,770	1.02	4,830	0.73
***quatrefoil*-PBO**	3,770	33	3,460	1.02	3,520	
***cage*$_4$-PBO**	3,660		3,550	1.02	3,600	

[a] Determined by ^{1}H NMR in $CDCl_3$. [b] Determined by SEC in THF using polystyrene standards.

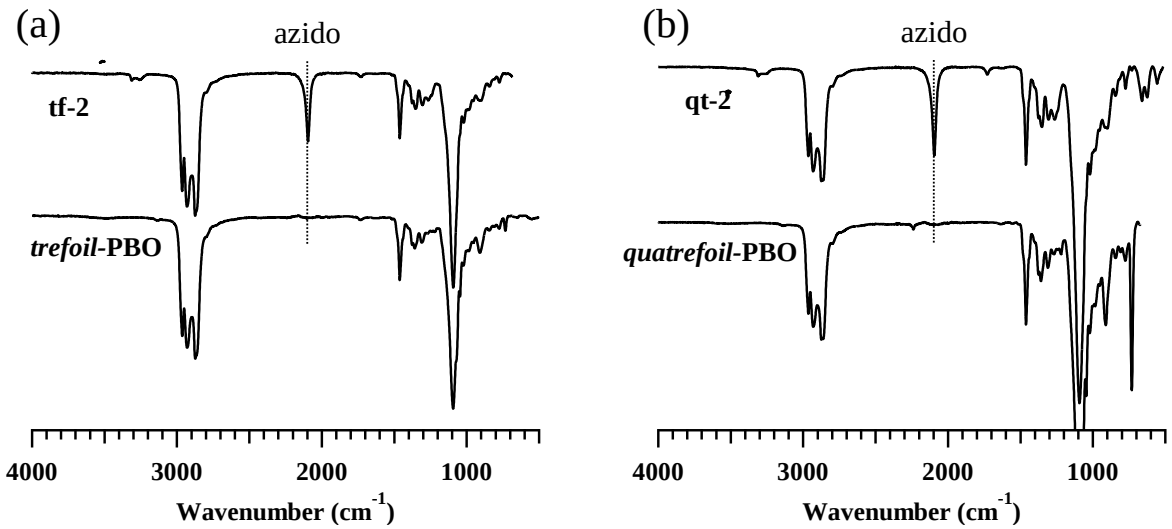

Figure 4-2. FT-IR spectra of the PBOs. (a) **tf-2** (upper) and *trefoil*-**I** (lower). (b) **qt-2** (upper) and ***quatrefoil*-PBO** (lower).

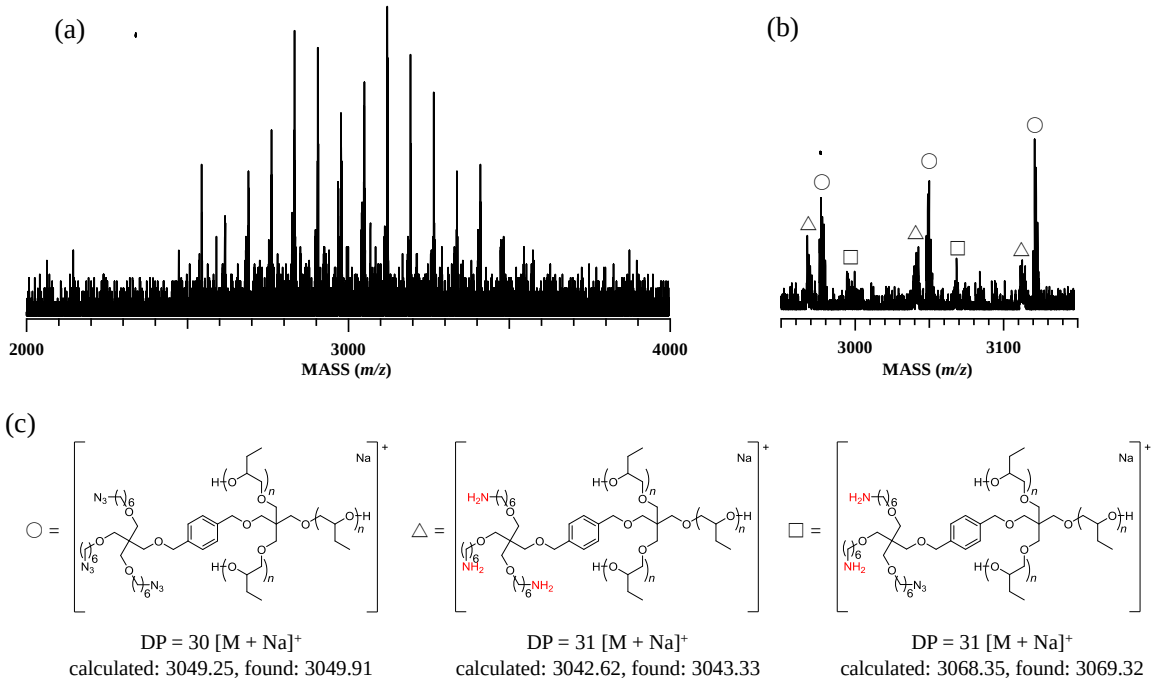

Figure 4-3. (a) MALDI-TOF MS spectrum of **tf-2**, (b) the expanded spectrum from 2950 to 3150 Da, and (c) the predicted polymer structure and calculated molecular weight.

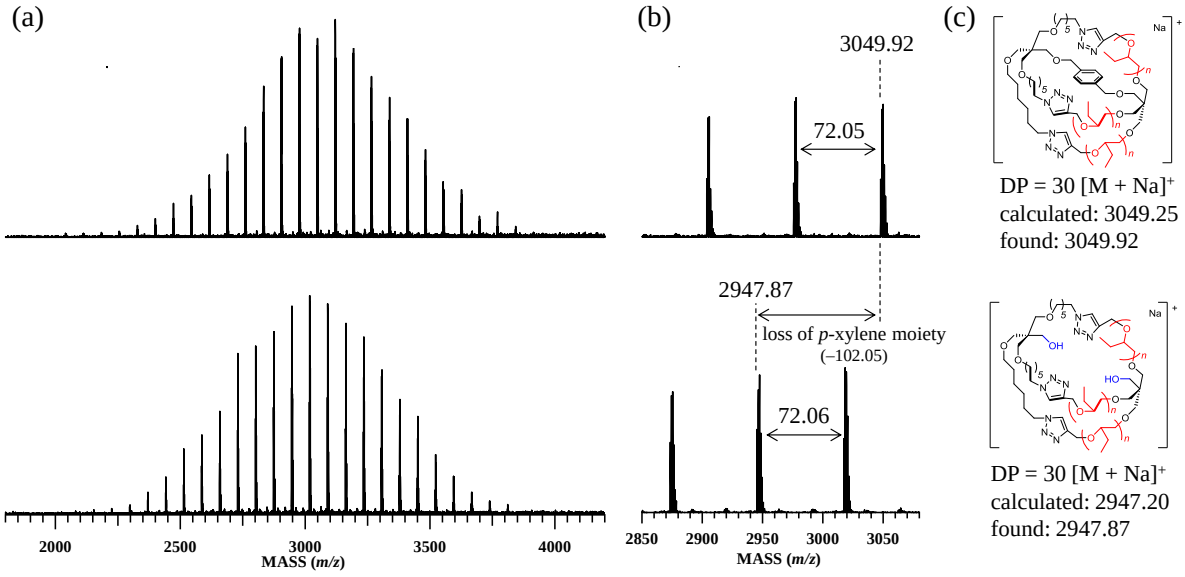

Figure 4-4. (a) MALDI-TOF MS spectrum of ***trefoil*-PBO** (upper) and ***cage*$_3$-PBO** (lower), (b) the expanded spectra from 2850 to 3080 Da, and (c) the predicted polymer structure and calculated molecular weight.

In a similar fashion, the quatrefoil-shaped PBO (***quatrefoil*-PBO**) was synthesized in three steps, beginning with **i-VIII** as the initiator (**Scheme 4-2**). The *t*-Bu-P_4-catalyzed ROP of BO using **i-VIII** ($[BO]_0/[\textbf{i-VIII}]_0/[t\text{-Bu-P}_4]_0$ ratio of 30/1/1) followed by the end group modification with propargyl bromide afforded the four-armed star-shaped PBO having four azido groups at the focal point and four propargyl groups at the ω-chain ends (**qt-2**). It should be noted that a non-negligible amount of a high molecular weight byproduct was observed in the SEC trace of the crude **qt-2** (**Figure 4-5b**). According to the recent report by Grayson, such a byproduct should be attributed to the oligomers produced by the uncatalyzed dimarization.[37] Thus, the crude product was purified by the preparative SEC to give the pure **qt-2** in 53.8% isolated yield ($M_{n,NMR}$ = 3780 g mol^{-1}, DP = 33, $Đ$ = 1.02). The precursor polymer **qt-2** was then subjected to the intramolecular multiple click cyclization. Although the SEC trace of the crude product indicated the formation of high molecular weight byproducts, the analytically pure quatrefoil-shaped PBO ***quatrefoil*-PBO** ($M_{n,NMR}$ = 3770 g mol^{-1}, DP = 33, $Đ$ = 1.02) was isolated in 78.0% yield by SEC fractionation (**Figure 4-5c**). The ^{1}H NMR, FT-IR, and MALDI-TOF MS analyses also identified the predicted structure of ***quatrefoil*-PBO** (**Figure 4-2b**, **Figure 4-5f**, and **Figure 4-6**). The $\langle G \rangle$ value of 0.73 ($M_{n,p(\textbf{\textit{quatrefoil}-PBO})}$ = 3520 g mol^{-1} and $M_{n,p(\textbf{qt-2})}$ = 4830 g mol^{-1}) was lower than that of the trefoil-shaped PBO, indicating the formation of a more compact cyclized architecture.

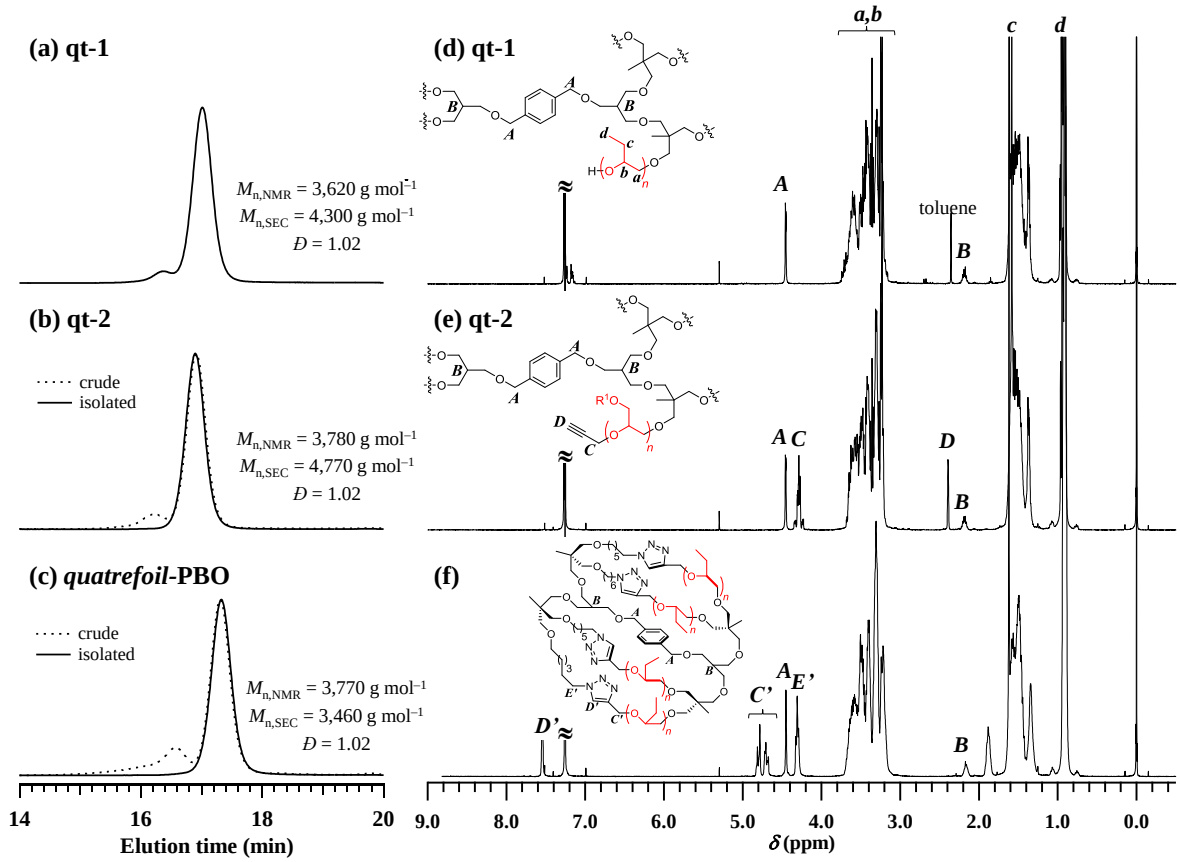

Figure 4-5. (a–c) SEC traces of **qt-1**, **qt-2**, and ***quatrefoil*-PBO** (dotted line, before purification; solid line, after the purification using preparative SEC). The $M_{n,NMR}$s, $M_{n,SEC}$s, and $Đ$s were determined from the respective isolated polymers. (d–f) ^{1}H NMR spectra of **qt-1**, **qt-2**, and ***quatrefoil*-PBO** in $CDCl_3$ (400 MHz).

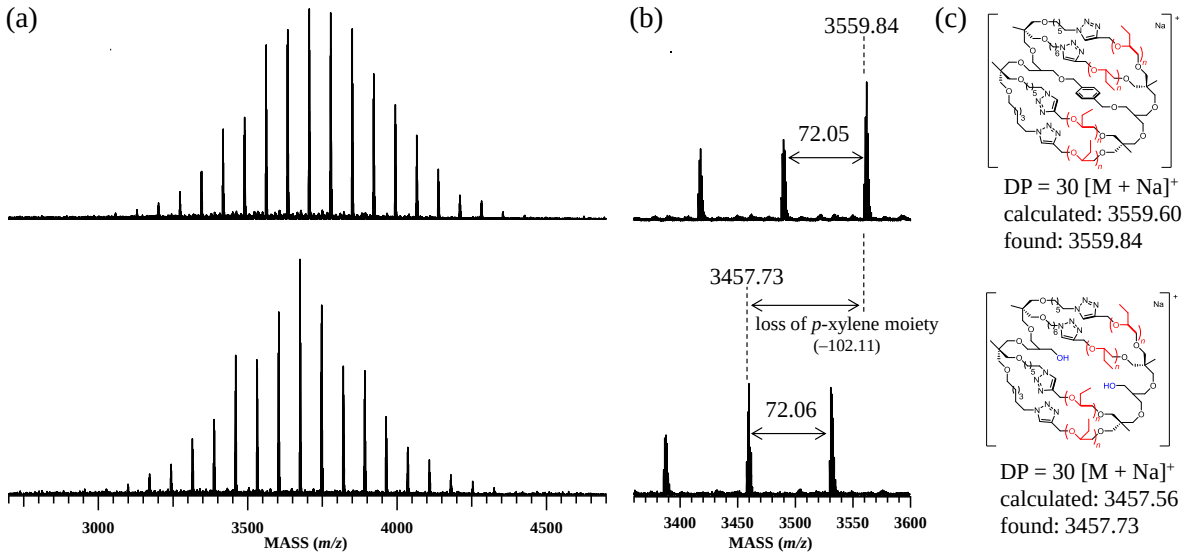

Figure 4-6. (a) MALDI-TOF MS spectrum of ***quatrefoil*-PBO** (upper) and ***cage*$_3$-PBO** (lower), (b) the expanded spectra from 3360 to 3600 Da, and (c) the predicted polymer structure and calculated molecular weight.

Finally, the author attempted to synthesize the cage-shaped PBOs (***cage*$_3$-PBO** and ***cage*$_4$-PBO**) by the topological conversion from the trefoil- and quatrefoil-shaped PBO precursors ***trefoil*-PBO** and ***quatrefoil*-PBO**, respectively. The topological conversion was achieved by cleaving the two benzyl ether linkages located at the focal point of the trefoil and quatrefoil structures. Thus, the author first performed the catalytic hydrogenolysis reaction on ***trefoil*-PBO** in the presence of Pd/C under a hydrogen atmosphere (1 atm) at room temperature. The extent of the hydrogenolysis was monitored by ^{1}H NMR, and the complete disappearance of the signals due to benzyl ether linkage was observed in 24 h. After a thorough purification to remove any metal residue by washing with a NaCN aqueous solution,

a product was obtained in 60.8% yield which was subjected to NMR, MALDI-TOF MS, and SEC analyses. In the NMR spectrum, the signal due to the benzyl group (*B*; 4.45 ppm in **Figure 4-7b**) completely disappeared, while the other signals were intact. Indeed, the $M_{n,NMR}$ (3150 g mol^{-1}) of the cleaved product well agreed with the expected M_n value ($M_{n,calc.}$ = 2930 g mol^{-1}). The unimodal SEC elution peak with a narrow $Đ$ value also guaranteed the absence of any undesirable side reactions like a main chain scission (**Figure 4-7a**).

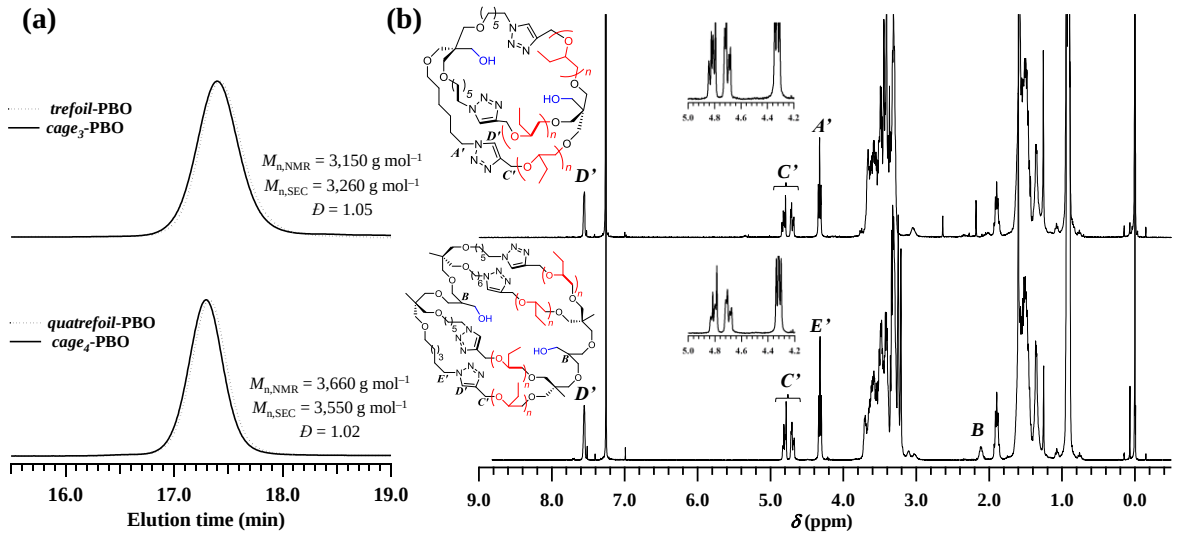

Figure 4-7. (a) SEC traces of ***cage*$_3$-PBO** (upper) and ***cage*$_4$-PBO** (lower; dotted line, before the cleavage reaction). (b) ^{1}H NMR spectra of ***cage*$_3$-PBO** (upper) and ***cage*$_4$-PBO** (lower) in $CDCl_3$ (400 MHz). The insets show the expanded ^{1}H NMR spectra which indicated the absence of the *p*-xylene group.

The MALDI-TOF MS spectrum exhibited only one series of peaks as shown in **Figure 4-4a**, even after the hydrogenolysis reaction. Most importantly, one of the peaks observed at *m*/*z* of 2947.87 Da well agreed with the calculated mass for the expected chemical structure of

30-mer of ***cage*$_3$-PBO** (2947.20 Da), unambiguously indicating the loss of the *p*-xylene moiety without any side reaction (**Figure 4-4b**). These spectroscopic data provided compelling evidence of forming the three-armed cage-shaped PBO ***cage*$_3$-PBO** via the topological conversion upon the catalytic hydrogenolysis of the benzyl ethers at the focal point of ***trefoil*-PBO**. In a similar manner, the topological conversion was also performed on ***quatrefoil*-PBO** to produce the four-armed cage-shaped PBO ***cage*$_4$-PBO** ($M_{n,NMR}$ = 3660 g mol^{-1}, DP = 33, $Đ$ = 1.02, 80.9% yield), which was fully characterized by ^{1}H NMR and MALDI-TOF MS spectroscopic analyses (**Figure 4-7** and **Figure 4-6**). Interestingly, the SEC elution peaks of ***cage*$_3$-PBO** and ***cage*$_4$-PBO** ($M_{n,SEC}$ = 3260 g mol^{-1} and 3550 g mol^{-1}, respectively) slightly shifted to the high molecular weight region as compared to their trefoil- and quatrefoil-shaped precursors ***trefoil*-PBO** and ***quatrefoil*-PBO** ($M_{n,SEC}$ = 3180 g mol^{-1} and 3460 g mol^{-1}, respectively), while keeping the unimodal and symmetric peak shape. This observation was most likely due to the increase in the hydrodynamic volume of the polymers via the topological conversion from the trefoil/quatrefoil to cage-shaped architectures. Thus, cage-shaped polymers with a very narrow dispersity are now accessible in a well-defined fashion via the intramolecular multiple click cyclization of the star-shaped precursor to form trefoil- and quatrefoil-shaped polymers followed by the topological conversion.

4.2.3 Synthesis of Amphiphilic Trefoil/Quatrefoil and Cage-shaped Block Copolyethers

Encouraged by the promising results, the author next targeted the amphiphilic caged-shaped polyethers (***cage*$_3$-I** and ***cage*$_4$-I**) as shown in **Scheme 4-5**. It has been reported that cyclic amphiphilic block copolymers exhibited peculiar self-assembly properties, which are unattainable from the linear counterparts, both in the solution and solid states. Thus, of particular interest is to understand the effect of the macromolecular architecture on the self-assembly properties based on a series of architecturally complex amphiphilic block copolyethers with a fixed molecular weight and monomer composition. The author envisaged that ***cage*$_3$-I** and ***cage*$_4$-I** as well as their trefoil/quatrefoil-shaped precursors ***trefoil*-I** and ***quatrefoil*-I** should be of interest as the model system for such an architecture–property relationship study. The decyl glycidyl ether (**M1**) and 2-(2-(2-methoxyethoxy)ethoxy)ethyl glycidyl ether (**M2**) were then employed as hydrophobic and hydrophilic monomers, respectively, and the DP of each monomer in the copolymer was adjusted to approximately 50. Note that the *t*-Bu-P$_4$-catalyzed sequential block copolymerization of these monomers, leading to linear, star, cyclic, tadpole, and figure-eight-shaped amphiphilic block copolyethers, was successfully achieved in Chapter 2 and 3.

Scheme 4-5. Synthetic pathway for trefoil/quatrefoil and cage-shaped block copolyethers (***trefoil*-I**, ***cage*$_3$-I**, ***quatrefoil*-I**, and ***cage*$_4$-I**)

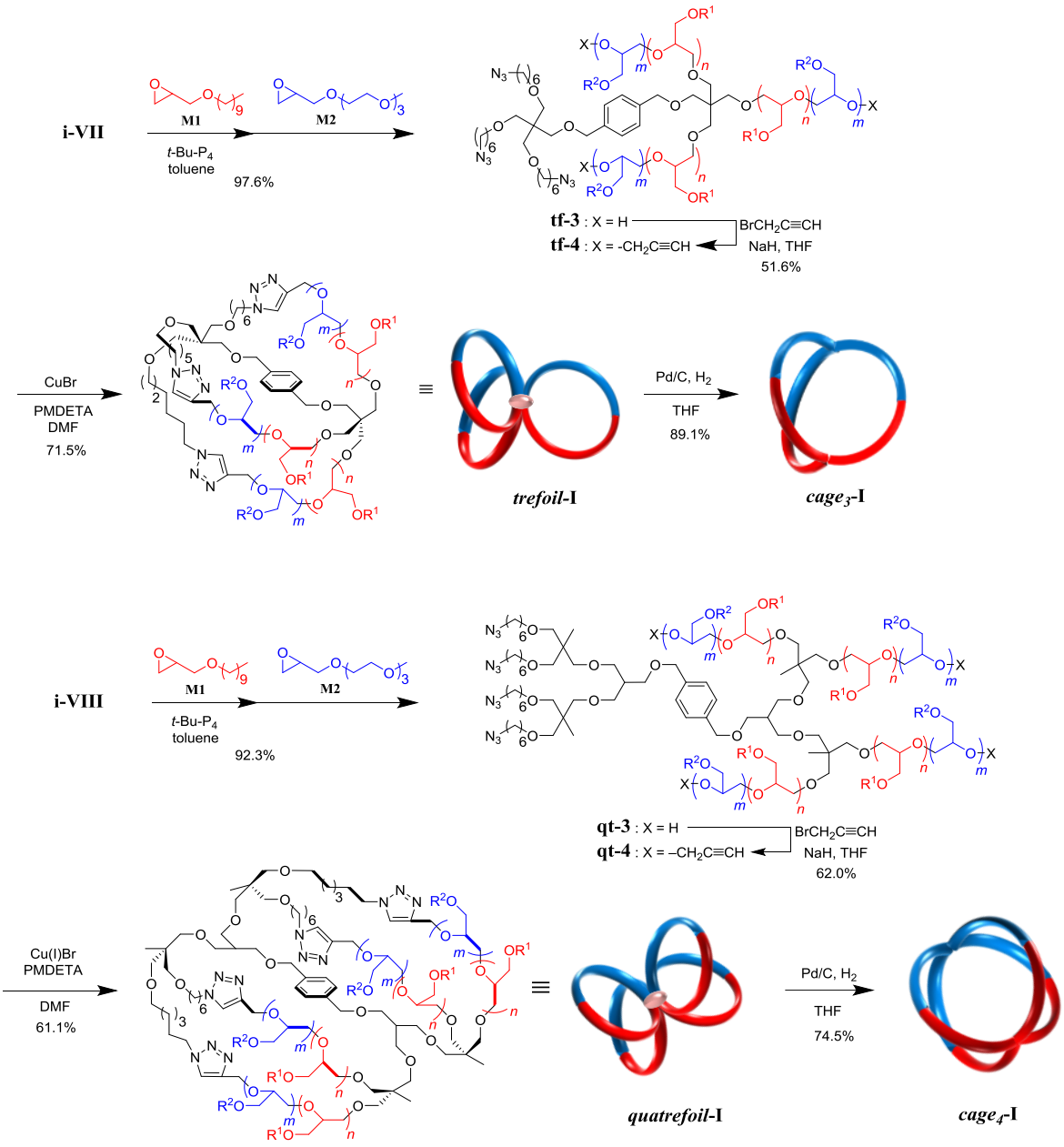

First, the three-armed star-block copolyether having three azido groups at the focal point and three propargyl groups at the ω-ends **tf-4** ($M_{n,NMR}$ = 22700 g mol^{-1}, DP$_{\mathbf{M1}}$/DP$_{\mathbf{M2}}$ = 51/51, $Đ$ = 1.04) was synthesized by the *t*-Bu-P$_4$-catalyzed block copolymerization using

i-VII as an initiator at the $[\mathbf{M1}]_0/[\mathbf{M2}]_0/[\mathbf{i\text{-}VII}]_0$ ratio of 50/50/1 followed by the ω-end ethynylation. The SEC trace of poly(**M1**) obtained by the first polymerization completely shifted to the high molecular weight region after the second polymerization of **M2** while retaining a narrow $Đ$ (1.04), which is convincing evidence of the successful block copolymerization (**Figure 4-8a**). In the ^{1}H NMR spectrum of **tf-4**, the signals due to the poly(**M1**) and poly(**M2**) backbone were observed together with the minor signals due to the initiator residue (proton *B* in **Figure 4-8f**) and the ethynyl groups (protons *C* and *D*). Next, the author performed the intramolecular click cyclization of the precursor polymer **tf-4** to obtain the trefoil-shaped block copolyethers ***trefoil*-I**. The SEC analysis confirmed the clear shift of the elution peak into the lower molecular weight region (**Figure 4-8c**). Thus, the established cyclization conditions were found to work well to produce the intramolecularly cyclized product, though ca. 8% of the high molecular weight byproduct formed by the intermolecular click reaction was observed. After removing the byproduct by preparative SEC purification, the narrowly-dispersed ***trefoil*-I** with the $M_{n,NMR}$ of 22900 g mol^{-1} (DP_1 = 51, DP_2 = 51) was isolated in 71.5% yield. The $\langle G \rangle$ value was calculated to be 0.78, which well agreed with that for the trefoil-shaped PBO (**Table 1**). The ^{1}H NMR and FT-IR spectra were reasonably assigned to the expected chemical structure of ***trefoil*-I** (**Figure 4-8g** and **Figure 4-9a**), which definitely confirmed the successful formation of the trefoil-shaped architecture via the intramolecular click cyclization. In a similar fashion, the amphiphilic

quatrefoil-shaped block copolyethers ***quatrefoil*-I** ($M_{n,NMR}$ = 23400 g mol^{-1}, DP_{M1}/DP_{M2} = 50/50, $Đ$ = 1.02) was obtained in 61.1% isolated yield, beginning from the $\omega,\omega',\omega'',\omega'''$-tetraethynyl four-armed star-block precursor with four azido groups at the focal point **qt-4** ($M_{n,NMR}$ = 23300 g mol^{-1}, DP_{M1}/DP_{M2} = 50/50, $Đ$ = 1.03) (**Table 2**, **Figure 4-9b** and **Figure 4-10**).

Table 4-2. Molecular Characteristics and Intrinsic Viscosities ($[\eta]_w$) of the Trefoil/quatrefoil and Cage-shaped Block Copolyethers together with the Star-shaped Precursors

sample	$M_{n,NMR}$ [a] [g mol^{-1}]	DP_1/DP_2 [b]	$M_{n,SEC}$ [c] [g mol^{-1}]	$Đ$ [c]	$M_{n,p}$ [c] [g mol^{-1}]	$\langle G \rangle$	$[\eta]_w$ [d] [mL g^{-1}]
tf-4	22,700	51/51	16,400	1.04	16,500	0.78	11.4
***trefoil*-I**	22,900		13,000	1.03	12,900		5.9
***cage*$_3$-I**	22,500		14,500	1.03	14,000	1.09	6.5
qt-4	23,300	50/50	15,400	1.03	15,100	0.77	7.2
***quatrefoil*-I**	23,400		11,600	1.02	11,600		5.1
***cage*$_4$-I**	23,200		12,400	1.02	12,200	1.05	5.6

[a] Determined by ^{1}H NMR. [b] Number-average degree of polymerizations of decyl glycidyl ether (DP_1) and 2-(2-(2-methoxyethoxy)ethoxy)ethyl glycidyl ether (DP_2) in the copolymer were determined by ^{1}H NMR. [c] Determined by SEC in THF. [d] Determined by SEC equipped with viscometer in THF (0.3 mg mL^{-1}).

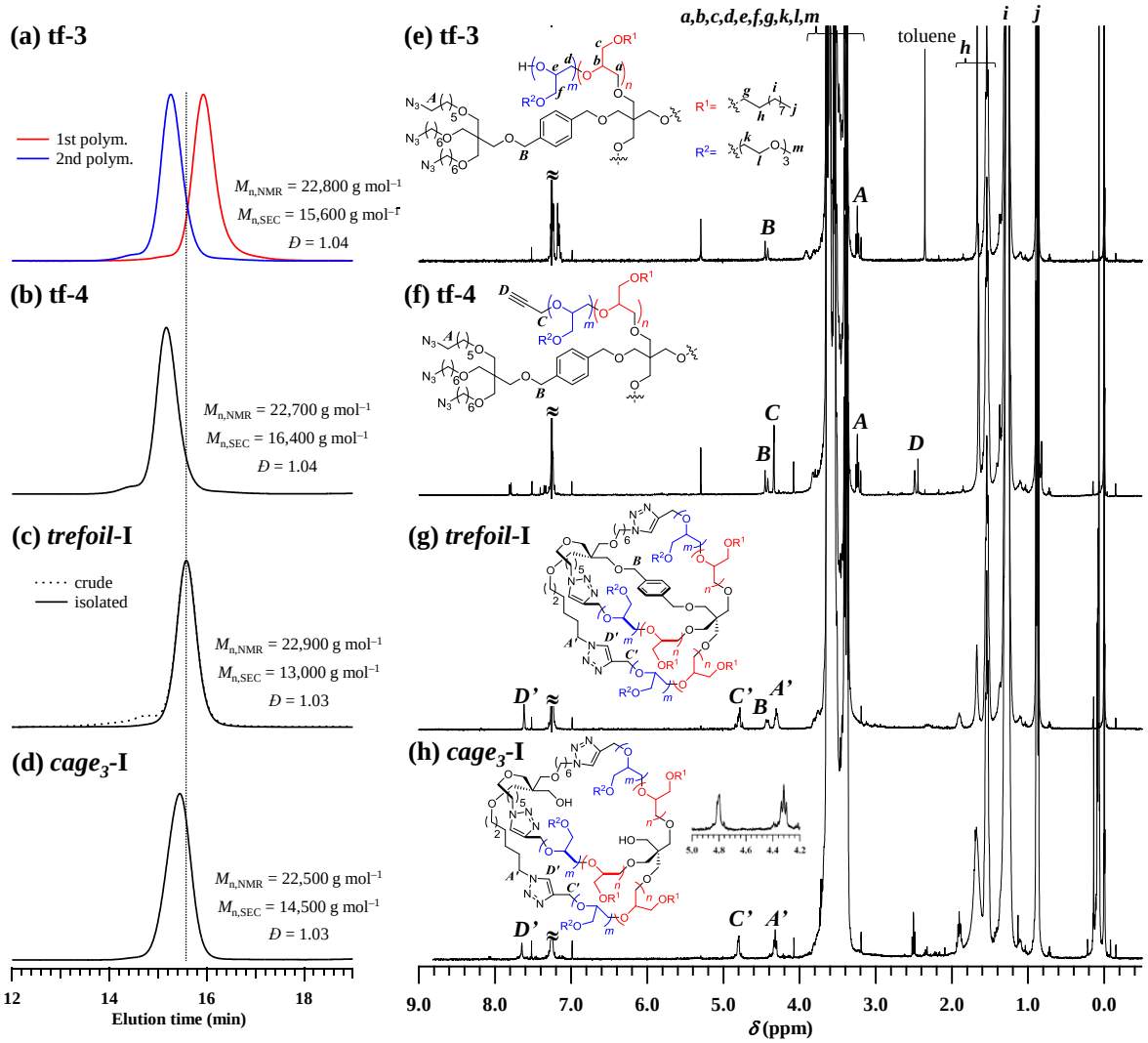

Figure 4-8. (a–d) SEC traces of **tf-3** (red line, 1st polymerization of **M1**; blue line block copolymerization of **M2**), **tf-4**, ***trefoil*-I** (dotted line, before purification; solid line, after the purification using preparative SEC), and ***cage*$_3$-I**. The $M_{n,NMR}$s, $M_{n,SEC}$s, and $Đ$s were determined from the respective isolated polymers. (e–h) ^{1}H NMR spectra of **tf-3**, **tf-4**, ***trefoil*-I**, and ***cage*$_3$-I** in $CDCl_3$ (400 MHz). The insets show the expanded ^{1}H NMR spectra.

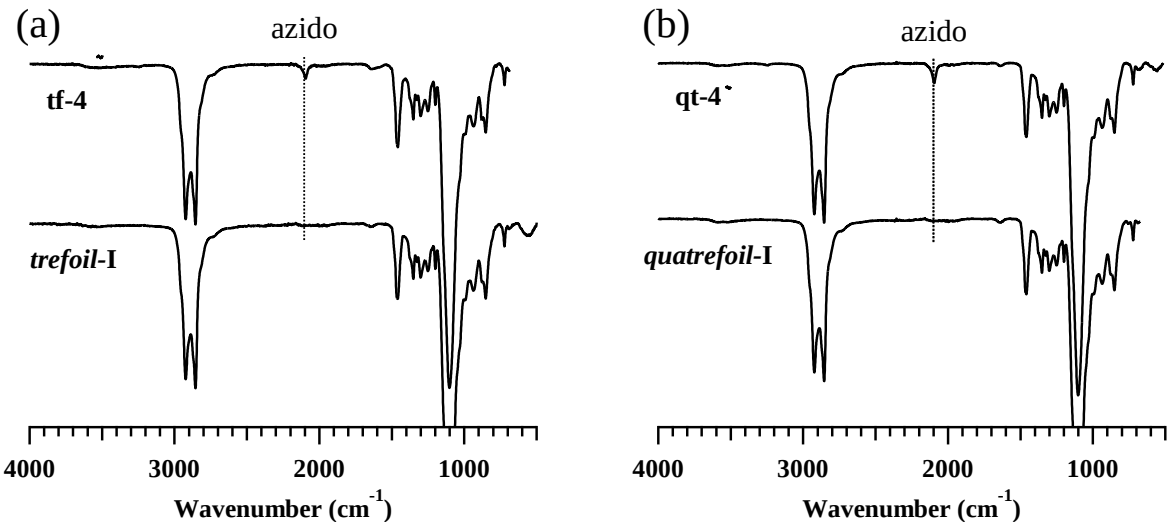

Figure 4-9. FT-IR spectra of the amphiphilic block copolyethers. (a) **tf-4** (upper) and ***trefoil*-I** (lower). (b) **qt-4** (upper) and ***quatrefoil*-I** (lower).

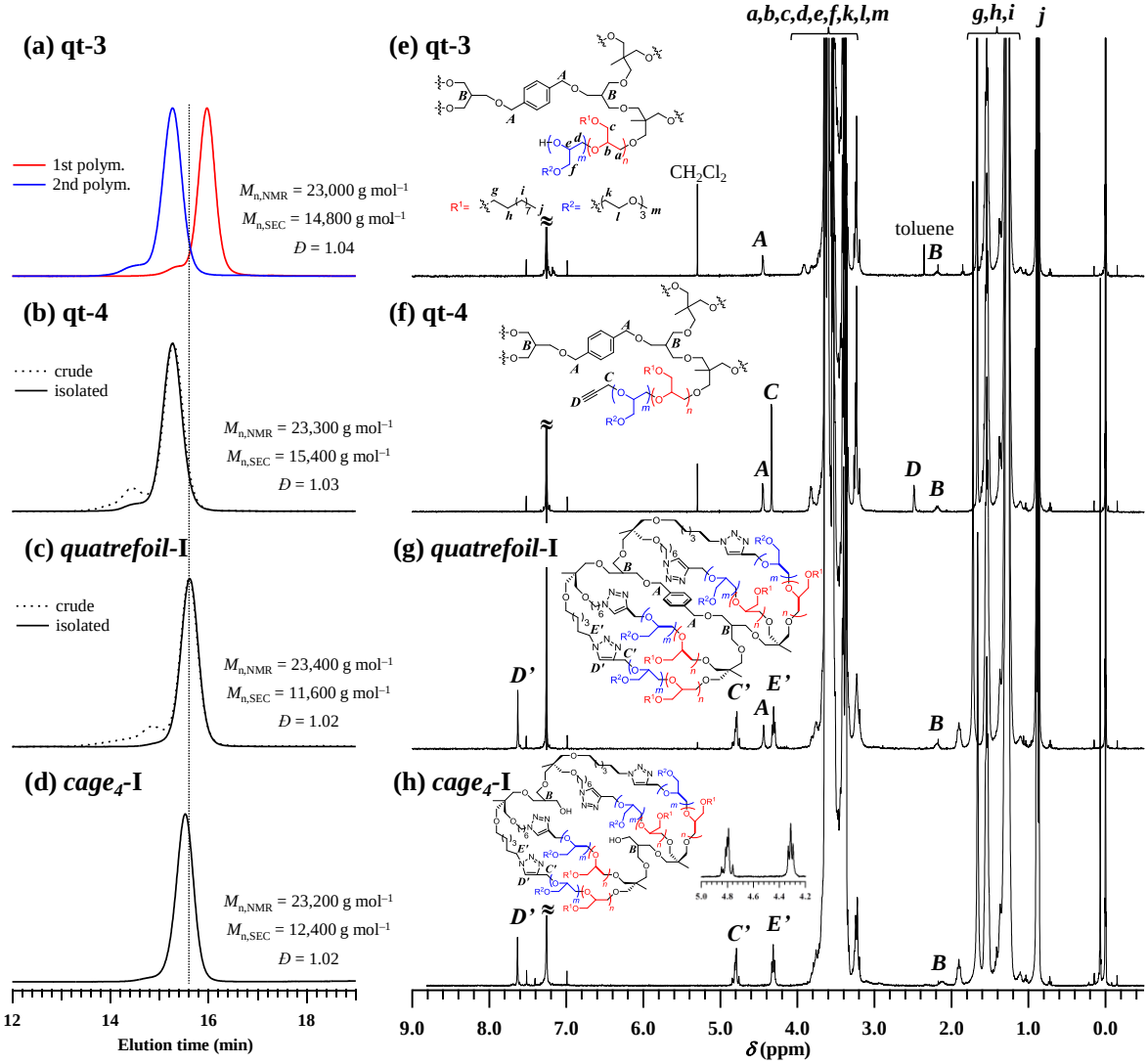

Figure 4-10. (a–d) SEC traces of **qt-3** (red line, 1st polymerization of **M1**; blue line block copolymerization of **M2**), **qt-4**, ***quatrefoil*-I** (dotted line, before purification; solid line, after the purification using preparative SEC), and ***cage*$_4$-I**. The $M_{n,NMR}$s, $M_{n,SEC}$s, and $Đ$s were determined from the respective isolated polymers. (e–h) ^{1}H NMR spectra of **qt-3**, **qt-4**, ***quatrefoil*-I**, and ***cage*$_4$-I** in $CDCl_3$ (400 MHz). The insets show the expanded ^{1}H NMR spectra.

The topological conversion from the trefoil-shaped to three-armed cage-shaped block copolyether via the hydrogenolysis reaction was then investigated. During the course of this reaction, the author found that the ordinary Pd/C catalyst did not work to completely remove the benzyl ether linkages from ***trefoil*-I**, even after three weeks. This is presumably due to the presence of long side chains, i.e., decyl and tetraethylene glycol bristles, along the polymer backbone, which may hamper the access of the benzyl ether moiety to the catalytic site. On the other hand, a highly active Pd/C catalyst "ASCA-2" was found to quantitatively cleave the benzyl ether linkages, affording the targeted ***cage*$_3$-I** ($M_{n,NMR}$ = 22500 g mol^{-1}, $Đ$ = 1.03) in 89.1% yield (**Figure 4-8h**). The SEC elution peak of ***cage*$_3$-I** ($M_{n,SEC}$ = 14500 g mol^{-1} in **Figure 4-8d**) clearly shifted to the higher molecular weight region as compared to ***trefoil*-I** ($M_{n,SEC}$ = 13000 g mol^{-1} in **Figure 4-8c**), which was consistent with that observed of the topological conversion from ***trefoil*-PBO** to ***cage*$_3$-PBO**. Likewise, the quatrefoil-shaped block copolyether ***quatrefoil*-I** was also subjected to the hydrogenolysis reaction to produce the four-armed cage-shaped block copolyether ***cage*$_4$-I** ($M_{n,NMR}$ = 23200 g mol^{-1}, $Đ$ = 1.02) in 74.5% isolated yield (**Figure 4-10**). Thus, our topological conversion approach was verified to be highly effective for the synthesis of the well-defined amphiphilic cage-shaped block copolyethers.

To further characterize the series of block copolyethers, an online SEC measurement conjugated with viscosity and RI detectors was performed in THF (**Table 4-2**). The

viscometic data provided valuable information about the macromolecular architecture of each block copolyether. The intrinsic viscosities ($[\eta]_w$s) of the trefoil- and quatrefoil-shaped polyethers (***trefoil*-I**; $[\eta]_w$ = 5.9 mL g^{-1} and ***quatrefoil*-I**; $[\eta]_w$ = 5.1 mL g^{-1}) were apparently lower than those of the star-shaped precursors (**tf-4**; $[\eta]_w$ = 11.4 mL g^{-1} and **qt-4**; $[\eta]_w$ = 7.2 mL g^{-1}). This observation can be interpreted as the decrease in the hydrodynamic volume via the intramolecular cyclization, which again confirmed the successful formation of the trefoil- and quatrefoil-shaped architectures. On the other hand, the cage-shaped polyethers showed a higher $[\eta]_w$ (***cage*$_3$-I**; $[\eta]_w$ = 6.5 mL g^{-1} and ***cage*$_4$-I**; $[\eta]_w$ = 5.6 mL g^{-1}) as compared to those of the trefoil- and quatrefoil-shaped precursors, indicating that the hydrodynamic volume of the block copolyether increased via the topological conversion from the trefoil/quatrefoil to the cage-shaped architecture. The $[\eta]_w$ value of the quatrefoil-shaped ***quatrefoil*-I** was lower than that for the trefoil-shaped ***trefoil*-I**, as can be expected by the number of cyclic units in the macromolecule. As a similar result, the four-armed cage-shaped ***cage*$_4$-I** was found to exhibit a lower $[\eta]_w$ value than that for the three-armed cage-shaped ***cage*$_3$-I**.

4.2.4 Self-assembly Properties of Amphiphilic Multicyclic Copolyethers in water

Our novel amphiphilic block copolyethers that had been synthesized as already described (***trefoil*-I**, ***cage*$_3$-I**, ***quatrefoil*-I**, and ***cage*$_4$-I**) are highly expected to self-assemble into a certain morphology of a micellar aggregate in water. Before starting the investigation into the micellar morphology of the trefoil-, quatrefoil- (***trefoil*-I** and ***quatrefoil*-I**), and cage-shaped block copolyethers (***cage*$_3$-I** and ***cage*$_4$-I**), the critical micelle concentration (CMC) of each polymer was determined by the standard fluorescence technique and was observed in the range of 0.80–1.8 mg L^{-1} (**Figure 4-11**). Interestingly, the cage-shaped polyethers ***cage*$_3$-I** and ***cage*$_4$-I** exhibited higher CMC values (1.8 and 1.7 mg L^{-1}, respectively) than those of the trefoil- and quatrefoil-shaped polyethers ***trefoil*-I** and ***quatrefoil*-I** (0.83 and 0.80 mg L^{-1}, respectively), which implied the change in the hydrophilic character of the polymer by the topological conversion.

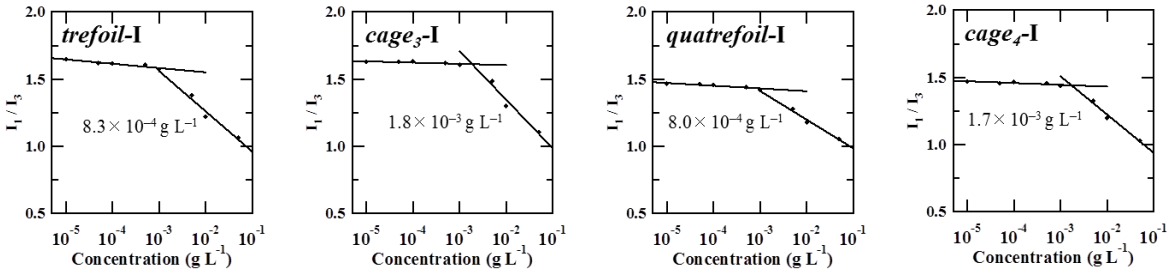

Figure 4-11. Variation in I_1/I_3 of pyrene emission spectra for ***trefoil*-I**, ***quatrefoil*-I**, ***cage*$_3$-I**, and ***cage*$_4$-I** as a function of the polymer concentrations (25 °C, λ_{ex} = 337 nm, 2.0 nm excitation bandwidth, and 2.0 nm emission bandwidth). The ratio of the emission intensities of I_1 (at 373 nm) and I_3 (at 384 nm) was plotted versus the polymer concentrations and the CMC was determined from the inflection point of the graph.

The DLS and TEM measurements were then performed on the micellar solutions of ***trefoil*-I**, ***cage*$_3$-I**, ***quatrefoil*-I**, and ***cage*$_4$-I** in pure water with the polymer concentrations well-above the CMC (0.50 g L^{-1}). For the micellar solutions of ***trefoil*-I** and ***cage*$_3$-I**, the monomodal particle size distributions were observed by DLS, and the number average hydrodynamics diameter ($2R_h$) was determined to be 60 nm for ***trefoil*-I** and 48 nm for ***cage*$_3$-I** (**Figure 4-12**). The TEM images exhibited the presence of spherical or rather irregular shaped aggregates, whose number average diameter was determined to be 77 nm for ***trefoil*-I** and 60 nm for ***cage*$_3$-I** which was essentially consistent with the DLS data (**Figure 4-12**). For the micellar solutions of the quatrefoil- and four-armed cage-shaped block copolyethers ***quatrefoil*-I** and ***cage*$_4$-I**, the DLS analysis proved the bimodal particle size distribution. The $2R_h$ value of the major population was 20 nm for ***quatrefoil*-I** and 17 nm for ***cage*$_4$-I**. The TEM images for the micellar solutions of ***quatrefoil*-I** and ***cage*$_4$-I** clearly displayed the coexistence of small spherical nanoparticles as the major component and large irregular-shaped particles as the minor component. This observation is consistent with the DLS analysis. The large particles seem to be formed by agglomeration of the smaller spherical nanoparticles. Although the detailed micellar morphology and molecular packing geometry in the micelle are unclear at this time, the significant difference in the micellar size between ***trefoil*-I**/***cage*$_3$-I** and ***quatrefoil*-I**/***cage*$_4$-I** could be due to the hydrodynamic volume or the architecture of each polymer. On the other hand, the slight decrease in the $2R_h$ value

by the topological conversion from the trefoil/quatrefoil (***trefoil*-I** and ***quatrefoil*-I**) to cage-shaped architectures (***cage*$_3$-I** and ***cage*$_4$-I**) would be attributed to the change in the molecular packing geometry in the micelle.

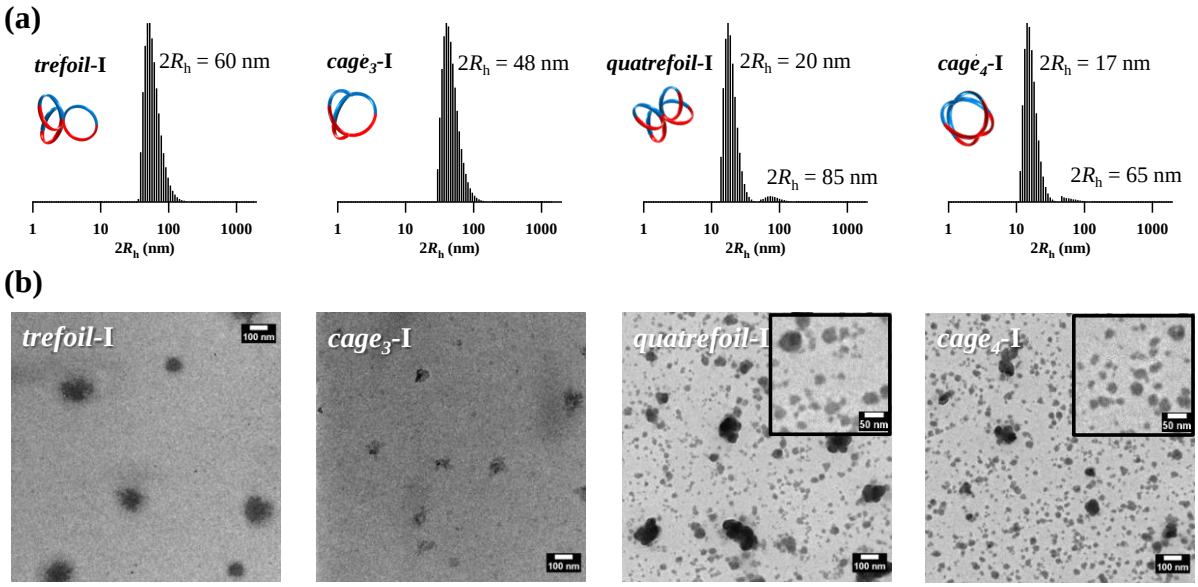

Figure 4-12. (a) Number average particle size distribution for the micellar solutions (measured by DLS at the scattering angle of 90°, 0.50 g L^{-1}, 25 °C). (b) TEM images of micellar aggregates of ***trefoil*-I**, ***quatrefoil*-I**, ***cage*$_3$-I**, and ***cage*$_4$-I**. The insets are the expanded TEM images.

To investigate the structural stability of the micellar aggregates as the cloud point ($T_{c.d.}$), we performed the turbidimetric measurement for the micellar solutions (**Figure 4-13**). The $T_{c.d.}$s of the ***trefoil*-I** (69 °C) and ***quatrefoil*-I** (64 °C) were lower than that of the corresponding cage-shaped polyether (***cage*$_3$-I**; $T_{c.d.}$ = 78 °C and ***cage*$_4$-I**; $T_{c.d.}$ = 67 °C). These results also suggested that the packing structure in the micellar aggregates was changed after the

topological conversion. Interestingly, we could find the correlationship between the amphiphilic cyclic-containing polyethers as shown in **Figure 4-14**. The $T_{c.d.}$s were decreased depending on the increase of cyclic units, which indicated the structural stability of the micellar aggregates was affected by the number of cyclic units. Although several previous studies reported that the monocyclic architecture increase the structural stability of their micelles, the author revealed for the first time the excessive numbers of cyclic architecture in a molecule lead the decreasing of their structural stability of micelles.

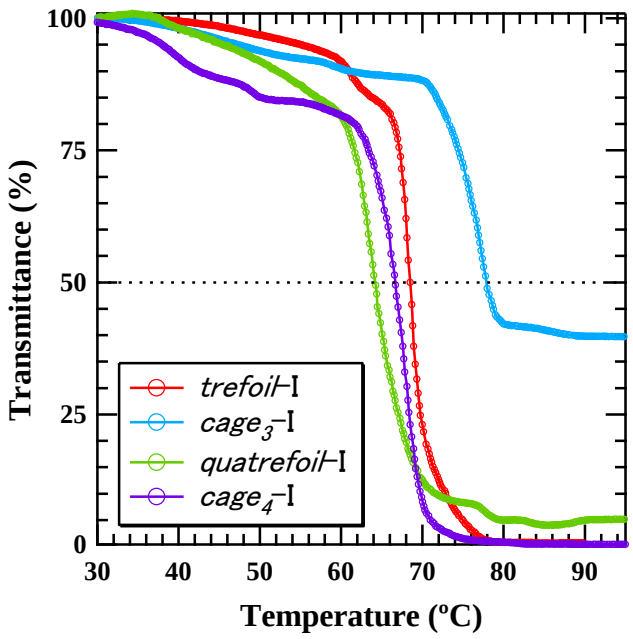

Figure 4-13. Temperature dependence of optical transmittance at 300 nm obtained for 0.50 g L^{-1} aqueous solution of ***trefoil*-I**, ***quatrefoil*-I**, ***cage*$_3$-I**, and ***cage*$_4$-I**.

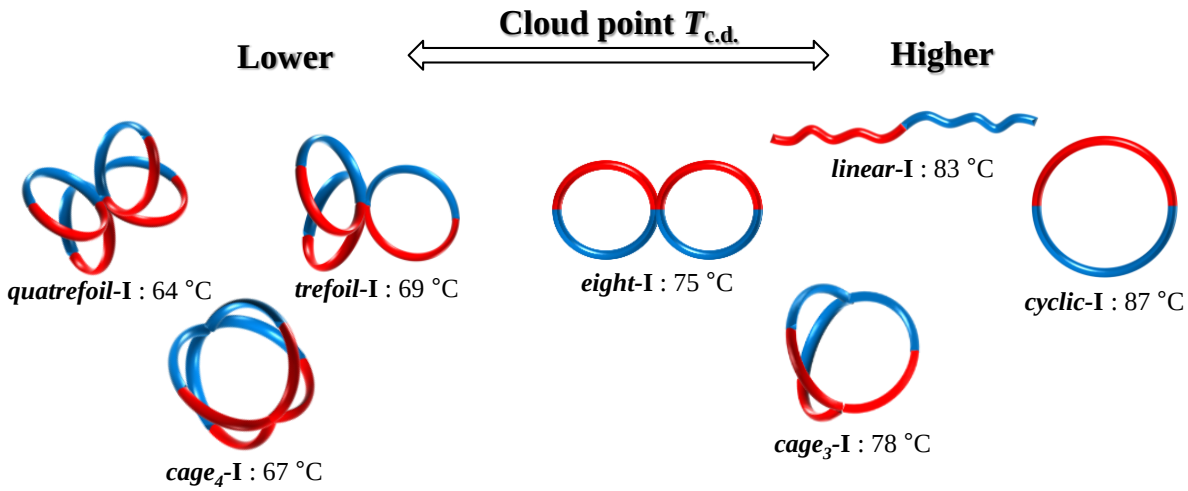

Figure 4-14. Schematic representation of the correlation in $T_{c.d.}$ values between the cyclic-containing block copolyethers.

4.3 Conclusion

The author has demonstrated the synthesis of cage-shaped polyethers via the topological conversion from the trefoil- and quatrefoil-shaped polyethers. The well-defined trefoil- and quatrefoil-shaped polyethers were synthesized by the intramolecular multiple click cyclization of the clickable star-shaped precursors that had been prepared by the *t*-Bu-P_4 catalyzed ROP of BO using the specially-designed multifunctional initiators **i-VII** and **i-VIII**. The hydrogenolysis of the benzyl ether linkages installed at the focal point of the trefoil- and quatrefoil-shaped polyethers successfully produced the corresponding cage-shaped polyethers without any undesired side reaction. Moreover, the author succeeded in the preparation of a series of trefoil/quatrefoil and cage-shaped amphiphilic block copolyethers according to the established procedure, which made it possible to directly compare the aggregation properties in water before and after the topological conversion. The author investigated for the first time the aggregation properties of amphiphilic multicyclic polyethers and revealed that the numbers of cyclic units in amphiphilic block copolyethers directly affect to the hydrodynamic size and structural stability of their aggregates. It is envisaged that the topological conversion approach will provide concise access to the trefoil/quatrefoil and cage-shaped polyethers with various main chain and side chain structures as well as contributing to a greater understanding of the properties and functions due to the complexed macromolecular architectures.

4.4 Experimental Section

Materials. Decyl glycidyl ether (**M1**)[38] and 2-(2-(2-methoxyethoxy)ethoxy)ethyl glycidyl ether (**M2**)[39] were synthesized according to reported methods, purified by distillation under vacuum over calcium hydride, and stored under an argon atmosphere. 1-(6-Azidohexyloxy)-2,2-bis((6-azidohexyloxy)methyl)-3-propanol (**i1**),[36] 4-(hydroxymethyl)–2,6,7-trioxa-bicyclo[2.2.2]octyl methane (**i3**),[40] 5-(hydroxymethyl)-2,2,5-trimethyl-1,3-dioxane (**i4**),[41] 6-azidohexyl tosylate (**i10**),[42] and propargyl-functionalized Wang resin (PSt-C≡CH)[43] were synthesized according to reported methods. *p*-Methoxy benzyl chloride was purchased from Kanto Chemical Co., Ltd., and used as received. Pentaerythritol, 60% NaH, tetrabutylammonium iodide (TBAI), trifluoroacetic acid (TFA) 2,3-dichloro-5,6-dicyano-1,4-benzoquinone (DDQ), α,α'-dibromo-*p*-xylene, propargyl bromide, *N,N,N',N'',N''*-pentamethyldiethylenetriamine (PMDETA), and 10% palladium on carbon (Pd/C; wetted with ca. 55% water) were purchased from Tokyo Chemical Industry Co., Ltd. (TCI), and used as received. ASCA-2 (wetted with ca. 50% water) was purchased from Wako Pure Chemical Industry Co., Ltd. (Wako), and used as received. 1,2-Butylene oxide (BO) was purchased from TCI, and purified by distillation over CaH_2. *t*-Bu-P_4 (in *n*-hexane as 1.0 mol L^{-1} solution), copper(*trefoil-PBO*) bromide (CuBr), aluminum oxide (alumina), 9-borabicyclo[3.3.1]nonane (in THF as 0.5 mol L^{-1} solution), dithranol, and sodium trifluoroacetate were purchased from the Sigma-Aldrich Chemicals Co.,

and used as received. Dry dimethylformamide (DMF; >99.5%; water content, <0.005%), dry toluene (>99.5%; water content, <0.001%), dry tetrahydrofuran (THF; >99.5%; water content, <0.001%), and dimethyl sulfoxide (DMSO; >98.0%) were purchased from Kanto Chemical Co., Inc., and used as received.

Instruments. The instruments used in this study, such as the glovebox, size exclusion chromatography (SEC), NMR, FT-IR, and matrix-assisted laser desorption/ionization time-of-flight mass spectrometry (MALDI-TOF MS), are the same as Chapter 2 and 3.

Synthesis of 1-(6-azidohexyloxy)-2,2-bis((6-azidohexyloxy)methyl)-3–(4-bromomethylbenzoxy)propane (i2). Under a nitrogen atmosphere, **i1** (7.72 g, 15.1 mmol) was treated with NaH (3.62 g, 90.5 mmol; 60% in mineral oil) in THF (200 mL) at r.t. for 1 h to prepare the corresponding sodium alkoxide. The alkoxide solution was slowly transferred to a stirred solution of *α,α'*-dibromo-*p*-xylene (12.0 g, 45.3 mmol) in THF (100 mL) via a cannula, and the entire mixture was stirred at 60 °C for 3 days under a nitrogen atmosphere. After removing the solvent by evaporation, the resulting residue was dissolved in cold Et_2O, and the insoluble part was removed by celite filtration. The filtrate was concentrated to dryness, and the residue was purified by silica gel column chromatography (*n*-hexane/EtOAc = 9/1, R_f = 0.18) to give **i2** (5.93 g, 8.53 mmol) as a colorless liquid. Yield: 56.5%. ^{1}H NMR (400 MHz, $CDCl_3$): δ (ppm) 7.35 (d, J = 8.0 Hz, 2H, aromatic), 7.28 (d, J =

8.0 Hz, 2H, aromatic), 4.50 (s, 2H, –OCH_2Ph–), 4.47 (s, 2H, –OCH_2Br), 3.46 (s, 2H, –CCH_2OCH$_2$Ph–), 3.42–3.32 (m, 12H, –CH$_2$CH_2OCH$_2$C–, –CH$_2$CH$_2$OCH_2C–), 3.25 (t, J = 7.2 Hz, 6H, N$_3$CH_2–), 1.62–1.48 (m, 12H, N$_3$CH$_2$CH_2(CH$_2$)$_4$O–, N$_3$(CH$_2$)$_4$CH_2CH$_2$O–), 1.42–1.32 (m, 12H, N$_3$(CH$_2$)$_2$(CH_2)$_2$(CH$_2$)$_2$O–). ^{13}C NMR (100MHz, CDCl$_3$): δ (ppm) 139.5, 136.8, 129.1, 127.6 (aromatic), 72.9 (–CCH$_2$O–), 71.4 (–CH$_2$$CH_2OCH_2$C–), 70.0 (–CH$_2OCH_2$C–), 69.8 (–O$CH_2$Ph–), 51.5 (N$_3$$CH_2$–), 45.6 ((–$CH_2$)(–$CH_2$)(–$CH_2$)(–$CH_2$)$C$), 33.6 (–Ph$CH_2$Br), 29.6, 29.0 (N$_3CH_2$$CH_2$(CH$_2$)$_4$O–, N$_3$(CH$_2$)$_4$$CH_2CH_2$O–), 26.7, 26.0 (N$_3$(CH$_2$)$_2$$CH_2$(CH$_2$)$_3$O–, N$_3$(CH$_2$)$_3$$CH_2$(CH$_2$)$_2$O–). HRMS-FD (*m/z*): [M + H]$^+$ calcd for C$_{31}$H$_5$BrN$_9$O$_4$, 694.3404; Found, 694.3409.

Synthesis of *α*-(1-(6-azidohexyloxy)-2,2-bis((6-azidohexyloxy)methyl)–3-propoxy)*α*'-(1,1,1-tris(hydroxymethyl)-2-ethoxy)-*p*-xylene (i-VII). **i2** (1.2 g, 1.73 mmol) was added to a stirred solution of KOH (1.46 g, 26.0 mmol) and **i3** in DMSO (15 mL), and the entire mixture was stirred at r.t. for 10 h. The stirred solution was diluted with water and extracted with Et$_2$O. The combined organic layers were concentrated. The residue was dissolved in THF, then 1N-HCl (5 mL) was added to the solution. After stirring at r.t. for 24 h, KOH (1.00 g, 17.8 mmol) and MeOH (5 mL) were added to the stirred solution, and the solution was again stirred at r.t. for 24 h. After removing the solvent by evaporation, the resulting residue was dissolved in EtOAc and washed with water. The organic layer was dried over anhydrous MgSO$_4$, then concentrated. The residue was purified by silica gel column

chromatography (*n*-hexane/EtOAc = 1/3, R_f = 0.37) to give **i-VII** (666 mg, 888 μmol) as a colorless viscous liquid. Yield: 51.3%. ^{1}H NMR (400 MHz, $CDCl_3$): δ (ppm) 7.32–7.23 (m, 4H, aromatic), 4.51, 4.49 (s, 4H, –OC*H*$_2$Ph), 3.73 (s, 6H, –C(C*H*$_2$OH)$_3$), 3.53 (s, 2H, –C*H*$_2$C(CH$_2$OH)$_3$), 3.47 (s, 2H, –CC*H*$_2$OCH$_2$Ph–), 3.42–3.34 (m, 12H, –CH$_2$C*H*$_2$OCH$_2$C–, –CH$_2$CH$_2$OC*H*$_2$C–), 3.25 (t, *J* = 7.2 Hz, 6H, N$_3$C*H*$_2$–), 2.47 (s, 3H, –O*H*), 1.66–1.48 (m, 12H, N$_3$CH$_2$C*H*$_2$(CH$_2$)$_4$O–, N$_3$(CH$_2$)$_4$C*H*$_2$CH$_2$O–), 1.42–1.32 (m, 12H, N$_3$(CH$_2$)$_2$(C*H*$_2$)$_2$(CH$_2$)$_2$O–). ^{13}C NMR (100MHz, $CDCl_3$): δ (ppm) 139.4, 137.0, 128.0, 127.8 (aromatic), 74.1, 73.4 (–PhCH$_2$OCH$_2$C–), 72.8 (–PhCH$_2$O–), 71.7 (–CH$_2$CH$_2$OCH$_2$C–), 70.3 (–PhCH$_2$O–), 70.2 (–CH$_2$CH$_2$OCH$_2$C–), 65.4 (–C(CH$_2$OH)$_3$), 51.9 (N$_3$CH$_2$–), 45.9, 45.4 ((–CH$_2$)(–CH$_2$)(–CH$_2$)(–CH$_2$)C), 29.9, 29.3 (N$_3$CH$_2$CH$_2$(CH$_2$)$_4$O–, N$_3$(CH$_2$)$_4$CH$_2$CH$_2$O–), 27.1, 26.3 (N$_3$(CH$_2$)$_2$CH$_2$(CH$_2$)$_3$O–, N$_3$(CH$_2$)$_3$CH$_2$(CH$_2$)$_2$O–). Anal. calcd. for $C_{36}H_{63}N_9O_8$: C, 57.66; H, 8.47; N, 16.81. Found: C, 57.58; H, 8.37; N, 16.63.

Synthesis of 1,1-bis(((2,2,5-trimethyl-1,3-dioxan-5-yl)methoxy)methyl)ethylene (i5). Under a nitrogen atmosphere, **i4** (38.5 g, 240 mmol) was added to a stirred solution of 3-chloro-2-chloro propene (10.0 g, 80.0 mmol), NaH (14.4 g, 360 mmol; 60% in mineral oil), and 15-crown-5 (3.17 mL, 16.0 mmol) in THF (400 mL), then the solution was stirred at 60 °C for 24 h. After removing the solvent by evaporation, the obtained residue was dissolved in EtOAc and washed three times with water. The organic layer was dried over anhydrous $MgSO_4$, then concentrated. The residue was purified by silica gel column chromatography

(*n*-hexane/EtOAc = 5/1, R_f = 0.27) to give **i5** (26.6 g, 71.4 mmol) as a white solid. Yield: 89.3%. ^{1}H NMR (400 MHz, $CDCl_3$): δ (ppm) 5.15 (s, 2H, CH_2=C–), 3.99 (s, 4H, CH_2=C(CH_2O–)$_2$), 3.73–3.53 (m, 8H, –CCH_2OC–), 3.41 (s, 4H, CH_2=CCH_2OCH_2C–), 1.43, 1.39 (s, 12H, –OC(CH_3)$_2$), 0.89 (s, 6H, –CH_2C(CH_3)(CH_2–)$_2$). ^{13}C NMR (100MHz, $CDCl_3$): δ (ppm) 113.2 (CH_2=*C*–), 98.0 (–O*C*(CH_3)$_2$), 73.3, 72.2 (CH_2=C*C*H_2O–, –O*C*H_2C(CH_3)(CH_2–)$_2$), 66.7 (–C(CH_3)(*C*H_2O–)$_2$), 34.5 (–OCH_2*C*(CH_3)(CH_2–)$_2$), 26.5, 21.4 (–C(*C*H_3)$_2$), 18.5 (–C(*C*H_3)(CH_2–)$_3$). Anal. calcd for $C_{20}H_{36}O_6$: C, 64.49; H, 9.74. Found: C, 64.12; H, 9.57. HRMS-ESI (*m/z*): $[M + Na]^+$ calcd for $C_{20}H_{36}O_6Na$, 395.2410; Found, 395.2402.

Synthesis of 1,3-bis((2,2,5-trimethyl-1,3-dioxan-5-yl)methoxy)–2-hydroxymethylpropane (i6). 9-BBN (0.5 M in THF, 100 mL, 50 mmol) was dropwise added to a stirred solution of **i5** (12.0 g, 32.2 mmol) in dry-THF (300 mL) at -10 °C under a N_2 atmosphere. The mixture was stirred at 0 °C for 2h, then stirred overnight at 25 °C. An aqueous NaOH solution (6.0 g of NaOH in distilled water) and H_2O_2 (30% in water, 100 mL) were slowly added to the reaction mixture at 0 °C. After stirring overnight at 50 °C, the mixture was extracted three times with AcOEt. The combined organic layers were washed three times with brine, dried over anhydrous $MgSO_4$, and concentrated. The residue was purified by silica gel column chromatography (*n*-hexane/acetone = 2/1, R_f = 0.35) to give **i6** (11.3 g, 28.8 mmol) as a colorless liquid. Yield: 89.4%. ^{1}H NMR (400 MHz, $CDCl_3$): δ (ppm)

3.76 (t, J = 7.2 Hz, 2H, HOCH_2–), 3.70–3.50 (m, 12H, –OCH_2C(CH_3)(CH_2O–)$_2$), 3.43 (m, 4H, HOCH_2CH(CH_2O–)$_2$), 2.59 (t, J = 7.2 Hz, 1H, –OH), 2.16 (m, 1H, HOCH_2CH(CH_2O–)$_2$), 1.43, 1.39 (s, 12H, –OC(CH_3)$_2$), 0.85 (s, 6H, –CH_2C(CH_3)(CH_2–)$_2$). ^{13}C NMR (100MHz, $CDCl_3$): δ (ppm) 98.0 (–OC(CH_3)$_2$), 73.3, 72.2 (–CH(CH_2O–)$_2$, –OCH_2C(CH_3)(CH_2–)$_2$), 66.7 (–C(CH_3)(CH_2O–)$_2$), 64.5 (HOCH_2–), 41.6 (HOCH_2CH–) 34.6 (–OCH_2C(CH_3)(CH_2–)$_2$), 26.8, 21.0 (–C(CH_3)$_2$), 18.4 (–C(CH_3)(CH_2–)$_3$). Anal. calcd for $C_{20}H_{38}O_7$: C, 61.51; H, 9.81. Found: C, 61.15; H, 9.81. HRMS-ESI (*m/z*): $[M + Na]^+$ calcd for $C_{20}H_{38}O_7Na$, 413.2515; Found, 413.2504.

Synthesis of 1,3-bis((2,2,5-trimethyl-1,3-dioxan-5-yl)methoxy)–2-((4-bromomethylbenzoxy)methyl)propane (i7). Under a nitrogen atmosphere, **i6** (11.1 g, 28.4 mmol) was added to a stirred solution of NaH (3.0 g, 75.0 mmol; 60% in mineral oil) in THF (300 mL), then the solution was stirred at 50 °C for 1 h. A solution of α,α'-dibromo-*p*-xylene (22.5 g, 85.2 mmol) in THF (100 mL) was added to the reacting mixture, and the entire mixture was stirred under reflux condition for 3 days. After removing the solvent by evaporation, the obtained residue was dissolved in cold Et_2O, and the insoluble part was removed by celite filtration. The filtrate was concentrated to dryness, and the residue was purified by silica gel column chromatography (*n*-hexane/acetone = 8/1, R_f = 0.29) to give **i7** (8.22 g, 14.3 mmol) as a pale yellow liquid. Yield: 50.4%. ^{1}H NMR (400 MHz, $CDCl_3$): δ (ppm) 7.37–7.26 (m, 4H, aromatic), 4.49, 4.48 (s, 4H, –PhCH_2–), 3.70–3.50, 3.37 (m, 18H,

–OC*H*$_2$C(CH$_3$)(C*H*$_2$O–)$_2$, –OC*H*$_2$CH(C*H*$_2$O–)$_2$), 2.59 (t, *J* = 7.2 Hz, 1H, –O*H*), 2.23 (m, 1H, –OCH$_2$C*H*(CH$_2$O–)$_2$), 1.42, 1.39 (s, 12H, –OC(C*H*$_3$)$_2$), 0.85 (s, 6H, –CH$_2$C(C*H*$_3$)(CH$_2$–)$_2$). ^{13}C NMR (100MHz, CDCl$_3$): δ (ppm) 139.2, 137.0, 129.2, 128.0 (aromatic), 97.9 (–O*C*(CH$_3$)$_2$), 74.1 (–O*C*H$_2$C(CH$_3$)(CH$_2$–)$_2$), 72.8 (–Ph*C*H$_2$O–), 69.9 (–CH(*C*H$_2$O–)$_2$), 69.0 (–PhCH$_2$O*C*H$_2$CH–), 66.7 (–C(CH$_3$)(*C*H$_2$O–)$_2$), 40.6 (–OCH$_2$*C*H–) 34.6 (–OCH$_2$*C*(CH$_3$)(CH$_2$–)$_2$), 33.6 (Br*C*H$_2$–), 26.8, 21.0 (–C(*C*H$_3$)$_2$), 18.4 (–C(*C*H$_3$)(CH$_2$–)$_3$). HRMS-ESI (*m/z*): [M + Na]$^+$ calcd for C$_{28}$H$_{45}$O$_7$BrNa, 595.2246; Found, 595.2241.

Synthesis of 1,3-bis((2,2,5-trimethyl-1,3-dioxan-5-yl)methoxy)-2-((*p*-methoxy–benzoxy)methyl)propane (i8). Under a nitrogen atmosphere, **i6** (11.3 g, 28.8 mmol) was added to a stirred solution of NaH (2.30 g, 57.6 mmol; 60% in mineral oil) and TBAI (1.06 g, 2.88 mmol) in DMF (300 mL), then the solution was stirred at 45 °C for 30 min. A solution of *p*-methoxybenzyl chloride (5.86 mL, 43.2 mmol) in DMF (10 mL) was dropwise added to the reacting mixture, and the entire mixture was stirred at 80 °C for 17 h under a nitrogen atmosphere. After removing the solvent by evaporation, the obtained residue was dissolved in AcOEt, and washed with water and brine. The organic layer was dried over anhydrous MgSO$_4$, then concentrated. The residue was purified by silica gel column chromatography (*n*-hexane/AcOEt/acetone = 10/1/1, R_f = 0.34) to give **i8** (10.3 g, 20.1 mmol) as a colorless liquid. Yield: 69.7%. ^{1}H NMR (400 MHz, CDCl$_3$): δ (ppm) 7.24, 6.86 (d, *J* = 8.0 Hz, 4H, aromatic), 4.41 (s, 2H, –PhC*H*$_2$–), 3.80 (s, 3H, C*H*$_3$OPh–), 3.70–3.46 (m, 14H,

–$PhCH_2OCH_2$–, –$OCH_2C(CH_3)(CH_2O–)_2$), 3.35 (s, 4H, –$OCH_2CH(CH_2O–)_2$), 2.20 (m, 1H, –$OCH_2CH(CH_2O–)_2$), 1.42, 1.38 (s, 12H, –$OC(CH_3)_2$), 0.86 (s, 6H, –$CH_2C(CH_3)(CH_2–)_2$). ^{13}C NMR (100MHz, $CDCl_3$): δ (ppm) 159.2, 130.8, 129.3, 113.8 (aromatic) 97.9 (–$OC(CH_3)_2$), 74.1 (–$OCH_2C(CH_3)(CH_2–)_2$), 73.0 (–$PhCH_2O–$), 69.9 (–$CH(CH_2O–)_2$), 68.6 (–$PhCH_2OCH_2CH–$), 66.7 (–$C(CH_3)(CH_2O–)_2$), 55.4 ($CH_3OPh–$), 40.5 (–$OCH_2CH–$) 34.6 (–$OCH_2C(CH_3)(CH_2–)_2$), 26.1, 21.7 (–$C(CH_3)_2$), 18.5 (–$C(CH_3)(CH_2–)_3$). Anal. calcd for $C_{28}H_{46}O_8$: C, 65.86; H, 9.08. Found: C, 65.47; H, 8.86. HRMS-ESI (*m/z*): $[M + Na]^+$ calcd for $C_{28}H_{46}O_8Na$, 533.3090; Found, 533.3076.

Synthesis of 1,3-bis((1-methyl-1,1-bis(hydroxymethyl))-2-ethoxy)–2-((*p*-methoxybenzoxy)methyl)propane (i9). TFA (1.0 mL, 13.1 mmol) was added to a stirred solution of **i8** (10.0 g, 19.6 mmol) and water (2 mL) in MeOH (50 mL), then the mixture was stirred at r.t. for 4 h. After removing the solvent by evaporation, the residue was purified by silica gel column chromatography (EtOAc to AcOEt/MeOH (5/1)) to give **i9** (5.30 g, 12.3 mmol) as a white solid. Yield: 62.8%. ^{1}H NMR (400 MHz, $CDCl_3$): δ (ppm) 7.24, 6.88 (d, J = 8.0 Hz, 4H, aromatic), 4.41 (s, 2H, –$PhCH_2$–), 3.81 (s, 3H, $CH_3OPh–$), 3.61 (s, 8H, –CH_2OH), 3.58–3.40 (m, 10H, –$PhCH_2OCH_2$–, –$CH_2OCH_2C(CH_3)$–), 3.16 (b, J = 8.0 Hz, 4H, –OH), 2.19 (m, 1H, –$OCH_2CH(CH_2O–)_2$), 0.77 (s, 6H, –$CH_2C(CH_3)(CH_2–)_2$). ^{13}C NMR (100MHz, $CDCl_3$): δ (ppm) 159.3, 130.3, 129.5, 113.9 (aromatic), 76.2 (–$OCH_2C(CH_3)(CH_2OH)_2$), 73.0 (–$PhCH_2O–$), 70.4 (–$CH(CH_2O–)_2$), 68.8

(–PhCH$_2$O*C*H$_2$CH–), 68.1 (–*C*H$_2$OH), 55.4 (*C*H$_3$OPh–), 40.9 (–OCH$_2$*C*(CH$_3$)(CH$_2$OH)$_2$), 40.1 (–OCH$_2$*C*H–), 17.3 (–C(*C*H$_3$)(CH$_2$–)$_3$). Anal. calcd for $C_{22}H_{38}O_8$: C, 61.37; H, 8.90. Found: C, 60.52; H, 8.47.HRMS-ESI (*m/z*): $[M + Na]^+$ calcd for $C_{22}H_{38}O_8Na$, 453.2464; Found, 453.2459.

Synthesis of 1,3-bis((1-methyl-1,1-bis(6-azidohexyloxymethyl))-2-ethoxy)–-2-((*p*-methoxybenzoxy)methyl)propane (i11). Under a nitrogen atmosphere, **i9** (4.00 g, 11.3 mmol) was added to a stirred solution of NaH (1.78 g, 44.6 mmol; 60% in mineral oil) in DMF (300 mL), then the solution was stirred at 50 °C for 1 h. **i10** (13.2 g, 44.6 mmol) and TBAI (857 mg, 2.32 mmol) were added to the reacting mixture, and the entire mixture was stirred at 50 °C for 24 h under a nitrogen atmosphere. After removing the solvent by evaporation, the obtained residue was dissolved in *n*-hexane and washed three times with water. The combined organic layers were dried over anhydrous $MgSO_4$, then concentrated. The residue was purified by silica gel column chromatography (*n*-hexane/EtOAc = 7/1, R_f = 0.26) to give **i11** (4.38 g, 4.70 mmol) as a colorless liquid. Yield: 50.6%. ^{1}H NMR (400 MHz, $CDCl_3$): δ (ppm) 7.23, 6.86 (d, *J* = 8.0 Hz, 4H, aromatic), 4.41 (s, 2H, –PhC*H*$_2$–), 3.80 (s, 3H, C*H*$_3$OPh–), 3.48 (d, *J* = 8.0 Hz, 2H, –PhCH$_2$OC*H*$_2$–), 3.41 (d, *J* = 8.0 Hz, 4H, –CH$_2$OC*H*$_2$C(CH$_3$)–), 3.35 (t, *J* = 7.2 Hz, 8H, –C(CH$_3$)C*H*$_2$OCH$_2$CH$_2$–), 3.25 (t, *J* = 7.2 Hz, 8H, –C(CH$_3$)CH$_2$OC*H*$_2$CH$_2$–), 3.24–3.21 (m, 4H, –CHC*H*$_2$OCH$_2$C(CH$_3$)–), 3.22 (s, 8H, –C*H*$_2$N$_3$), 2.17 (m, 1H, –OCH$_2$C*H*(CH$_2$O–)$_2$), 1.64–1.50 (m, 16H,

–$OCH_2CH_2(CH_2)_2CH_2CH_2N_3$), 1.40–1.32 (m, 16H, –$OCH_2CH_2(CH_2)_2CH_2CH_2N_3$), 0.90 (s, 6H, –$CH_2C(CH_3)(CH_2–)_2$). ^{13}C NMR (100MHz, $CDCl_3$): δ (ppm) 159.1, 130.9, 129.2, 113.8 (aromatic), 74.0 (–$OCH_2C(CH_3)(CH_2–)_2$), 73.7 (–$CH_2OCH_2CH_2$–), 72.9 (–PhCH_2O–), 71.4 (–$CH_2OCH_2CH_2$–) 70.0 (–$CH(CH_2O–)_2$), 68.8 (–$PhCH_2OCH_2CH$–), 55.4 (CH_3OPh–), 51.6 (–CH_2N_3), 41.1 (–$OCH_2C(CH_3)(CH_2OH)_2$), 40.5 (–OCH_2CH–), 29.6 (–$O(CH_2)_4CH_2CH_2N_3$), 29.0 (–$OCH_2CH_2(CH_2)_4N_3$), 26.7 (–$O(CH_2)_3CH_2(CH_2)_2N_3$), 26.0 (–$O(CH_2)_2CH_2(CH_2)_3N_3$), 17.6 (–$C(CH_3)(CH_2–)_3$). Anal. calcd for $C_{46}H_{82}N_{12}O_8$: C, 59.33; H, 8.88; N, 18.05. Found: C, 59.43; H, 9.01; N, 17.69. HRMS-ESI (*m/z*): $[M + Na]^+$ calcd for $C_{46}H_{82}N_{12}O_8Na$, 953.6276; Found, 953.6274.

Synthesis of 1,1-bis(((1-methyl-1,1-bis(6-azidohexyloxymethyl))-2-ethoxy)–methyl)-2-ethanol (i12). DDQ (2.10 g, 9.24 mmol) was added to the stirred solution of **i11** (4.30g, 4.62 mmol) in CH_2Cl_2/water (150 mL, v/v = 2/1), and the entire mixture was stirred at r.t. for 4 h. The reaction was quenched by adding a saturated solution of $NaHCO_3$, and the organic layer was washed three times with water. The organic layer was dried over anhydrous $MgSO_4$, then concentrated. The residue was purified by silica gel column chromatography (CH_2Cl_2 , R_f = 0.01 → CH_2Cl_2/MeOH = 5/1, R_f = 1.0) to give **i12** (3.06 g, 3.77 mmol) as a pale orange liquid. Yield: 81.7%. ^{1}H NMR (400 MHz, $CDCl_3$): δ (ppm) 3.74 (t, J = 7.2 Hz, 2H, $HOCH_2$–), 3.51–3.41 (m, 4H, –$CH_2OCH_2C(CH_3)$–), 3.37 (t, J = 7.2 Hz, 8H, –$C(CH_3)CH_2OCH_2CH_2$–), 3.28–3.24 (m, 12H, –$C(CH_3)CH_2OCH_2CH_2$–,

–CHC*H*$_2$OCH$_2$C(CH$_3$)–), 3.23 (s, 8H, –C*H*$_2$N$_3$), 2.14 (m, 1H, –OCH$_2$C*H*(CH$_2$O–)$_2$), 1.64–1.50 (m, 16H, –OCH$_2$C*H*$_2$(CH$_2$)$_2$C*H*$_2$CH$_2$N$_3$), 1.40–1.32 (m, 16H, –OCH$_2$CH$_2$(C*H*$_2$)$_2$CH$_2$CH$_2$N$_3$), 0.91 (s, 6H, –CH$_2$C(C*H*$_3$)(CH$_2$–)$_2$). ^{13}C NMR (100MHz, CDCl$_3$): δ (ppm) 74.6 (–O*C*H$_2$C(CH$_3$)(CH$_2$–)$_2$), 73.7 (–*C*H$_2$OCH$_2$CH$_2$–), 71.9 (–CH(*C*H$_2$O–)$_2$), 71.4 (–CH$_2$O*C*H$_2$CH$_2$–) 65.0 (–*C*H$_2$OH), 51.5 (–*C*H$_2$N$_3$), 41.3 (–OCH$_2$*C*(CH$_3$)(CH$_2$O–)$_2$), 41.0 (–OCH$_2$*C*H–), 29.6 (–O(C*H*$_2$)$_4$*C*H$_2$CH$_2$N$_3$), 29.0 (–OCH$_2$*C*H$_2$(C*H*$_2$)$_4$N$_3$), 26.7 (–O(CH$_2$)$_3$*C*H$_2$(C*H*$_2$)$_2$N$_3$), 25.9 (–O(CH$_2$)$_2$*C*H$_2$(C*H*$_2$)$_3$N$_3$), 17.7 (–C(*C*H$_3$)(CH$_2$–)$_3$). Anal. calcd for C$_{38}$H$_{74}$N$_{12}$O$_7$: C, 56.27; H, 9.20; N, 20.72. Found: C, 56.26; H, 9.31; N, 20.33. HRMS-ESI (*m/z*): [M + Na]$^+$ calcd for C$_{38}$H$_{74}$N$_{12}$O$_7$Na, 833.5701; Found, 833.5694.

Synthesis of *α*-(1,1-bis(((1-methyl-1,1-bis(6-azidohexyloxymethyl))-2-ethoxy)–methyl)-2-ethoxy)-*α*'-(1,1-bis(((1-methyl-1,1-bis(hydroxymethyl))-2-ethoxy)methyl)-2–ethoxy)-*p*-xylene (i-VIII). **i12** (1.99 g, 2.45 mmol) was added to a stirred solution of NaH (294 mg, 7.35 mmol) in THF (50 mL), then the solution was stirred at 50 °C for 1 h. A solution of **i7** (2.11 g, 3.68 mmol) in THF (10 mL) was added to the stirred solution, and the entire mixture was stirred under reflux for 2 days. After removing the solvent by evaporation, the residue was purified by silica gel column chromatography (*n*-hexane/AcOEt = 4/1, R_f = 0.32) to give the liquid mixture. The mixture was dissolved in MeOH (50 mL), then TFA (500 μL) and distilled water (2 mL) were added to the solution. After stirring at r.t. for 5 h, the

solvent was removed by evaporation. The residue was purified by silica gel column chromatography (*n*-hexane/EtOAc/MeOH = 7/3/1, R_f = 0.42) to give **i-VIII** (1.78 g, 1.45 mmol) as a colorless viscous liquid. Yield: 59.2%. ^{1}H NMR (400 MHz, $CDCl_3$): δ (ppm) 7.29 (d, J = 8.0 Hz, 4H, aromatic), 4.47 (s, 4H, –PhCH_2–), 3.59 (s, 8H, HOCH_2–), 3.55–3.40 (m, 20H, –CH_2OCH_2C(CH_3)–, –PhCH_2OCH_2–, –C(CH_3)CH_2OCH_2CH_2–), 3.36 (t, J = 7.2 Hz, 8H, –CH_2OCH_2CH_2–) 3.28–3.24 (m, 16H, –CHCH_2OCH_2C(CH_3)–, –CH_2N_3), 2.20 (m, 2H, –OCH_2CH(CH_2O–)$_2$), 1.64–1.50 (m, 16H, –OCH_2CH_2(CH_2)$_2$C$H_2CH_2N_3$), 1.40–1.32 (m, 16H, –OCH_2CH_2(CH_2)$_2CH_2CH_2N_3$), 0.91 (s, 6H, –CH_2C(CH_3)(CH_2OH)$_2$), 0.77 (s, 6H, –CH_2C(CH_3)(CH_2OCH_2–)$_2$). ^{13}C NMR (100MHz, $CDCl_3$): δ (ppm) 138.3, 137.4, 127.9, 127.7 (aromatic), 76.2 (–OCH_2C(CH_3)(CH_2OH)$_2$), 74.1 (–OCH_2C(CH_3)(CH_2–)$_2$), 73.6 (–CH_2OCH_2CH_2–), 73.1 (–PhCH_2O–), 71.4 (–CH_2OCH_2CH_2–) 70.3, 69.9 (–PhCH_2OCH_2CH(CH_2O–)$_2$), 69.3, 68.9 (–PhCH_2OCH_2CH–), 68.3 (–CH_2OH), 51.5 (–CH_2N_3), 41.1 (–OCH_2C(CH_3)($CH_2OCH_2CH_2$–)$_2$), 40.9 (–OCH_2C(CH_3)(CH_2OH)$_2$), 40.5, 40.1 (–OCH_2CH–), 29.6 (–O(CH_2)$_4$C$H_2CH_2N_3$), 29.0 (–OCH_2CH_2(CH_2)$_4N_3$), 26.7 (–O(CH_2)$_3$CH_2(CH_2)$_2N_3$), 25.9 (–O(CH_2)$_2$CH_2(CH_2)$_3N_3$), 17.6, 17.3 (–C(CH_3)(CH_2–)$_3$). Anal. calcd for $C_{60}H_{110}N_{12}O_{14}$: C, 58.90; H, 9.06; N, 13.74. Found: C, 58.60; H, 9.12; N, 13.20. HRMS-ESI (*m/z*): $[M + Na]^+$ calcd for $C_{38}H_{74}N_{12}O_7Na$, 1245.8162; Found, 1245.8144.

Synthesis of three-armed poly(butylene oxide) with three azido groups at the chain center (tf-1). A typical polymerization procedure is as follows (method A): BO (864

μL, 10.0 mmol) was added to a stirred solution of **i-VII** (251 mg, 334 μmol) and *t*-Bu-P_4 (167 μL as 1.0 mol L^{-1} stock solution in *n*-hexane, 167 μmol) in toluene (2.06 mL), then the entire mixture was stirred at room temperature for 40 h. An excess of benzoic acid was then added to the mixture to terminate the polymerization, and the product was purified by passing it through a pad of alumina using THF to give **tf-1** as a colorless viscous liquid (413 mg). Yield: 71.3%. ^{1}H NMR (400 MHz, $CDCl_3$): δ (ppm) 7.26 (aromatic), 4.45 (–PhCH_2–), 3.70–3.20 (N_3CH_2–, $N_3(CH_2)_5CH_2$–, $N_3(CH_2)_6OCH_2$–, –$PhCH_2OCH_2$–, PBO–OCH_2–, –OCH_2CH(CH_2CH_3)O–, –OCH_2CH(CH_2CH_3)O–), 1.66–1.34 ($N_3CH_2(CH_2)_4CH_2O$–, –$OCH_2CH(CH_2CH_3)O$–), 0.92 (–$OCH_2CH(CH_2CH_3)$O–). $M_{n,NMR}$ = 3180 g mol^{-1} ($CDCl_3$); $M_{n,SEC}$ = 3800 g mol^{-1} (THF); $Đ$ = 1.07.

Synthesis of *ω,ω′,ω″*-triethynyl three-armed poly(butylene oxide) with three azido groups at the chain center (tf-2). A typical procedure for the *ω*-chain end ethynylation is as follows (method B): NaH (58.9 mg, 1.47 mmol) was added to a stirred solution of **tf-1** ($M_{n,NMR}$ = 3180 g mol^{-1}, 442 mg) in THF (5 mL), then the entire mixture was stirred at room temperature for 30 min. Propargyl bromide (160 μL, 1.47 mmol) was then added to this mixture, and the entire mixture was stirred at room temperature for 48 h. The product was purified by passing it through a pad of alumina to give **tf-2** as a pale yellow viscous liquid (227 mg). Yield: 51.2%. ^{1}H NMR (400 MHz, $CDCl_3$): δ (ppm) 7.26 (aromatic), 4.45 (–Ph–CH_2–), 4.32–4.26 (HC≡CCH_2O–), 3.70–3.20 (N_3CH_2–, $N_3(CH_2)_5CH_2$–,

$N_3(CH_2)_6OCH_2$–, –Ph–CH_2OCH_2–, PBO–OCH_2–, –$OCH_2CH(CH_2CH_3)O$–, –$OCH_2CH(CH_2CH_3)O$–), 2.39 (*H*C≡C–), 1.66–1.34 ($N_3CH_2(CH_2)_4CH_2O$–, –$OCH_2CH(CH_2CH_3)O$–), 0.92 (–$OCH_2CH(CH_2CH_3)O$–). $M_{n,NMR}$ = 3300 g mol^{-1} ($CDCl_3$); $M_{n,SEC}$ = 4170 g mol^{-1} (THF); $Đ$ = 1.06.

Synthesis of trefoil-shaped poly(butylene oxide) (*trefoil*-PBO). A typical procedure for the intramolecular click cyclization is as follows (method C): A solution of **tf-2** ($M_{n,NMR}$ = 3300 g mol^{-1}, 165 mg) in degassed DMF (25 mL) was added to a stirred solution of CuBr (731 mg, 5.10 mmol) and PMDETA (2.10 mL, 10.2 mmol) in degassed DMF (300 mL) using a syringe pump at the rate of 0.3 mL h^{-1} at 90 °C under a nitrogen atmosphere. After completing the addition, PSt-C≡CH (30 mg), CuBr (146 mg, 1.02 mmol), and PMDETA (420 μL, 2.03 mmol) were added to the reaction mixture. After stirring at 90 °C for 24 h, the solvent was removed by evaporation, and the residue was purified by passing it through a pad of alumina followed by preparative SEC to give ***trefoil*-PBO** as a pale yellow viscous liquid (78.3 mg). Yield: 47.5%. ^{1}H NMR (400 MHz, $CDCl_3$): δ (ppm) 7.54 (m, triazole ring), 7.25 (aromatic), 4.86–4.66 (–triazole ring–CH_2O–), 4.45 (–Ph–CH_2–), 4.30 (–$O(CH_2)_5CH_2$–triazole ring–), 3.70–3.20 (–triazole ring–$(CH_2)_5CH_2OCH_2$–, –Ph–CH_2OCH_2–, PBO–OCH_2–, –$OCH_2CH(CH_2CH_3)O$–, –$OCH_2CH(CH_2CH_3)O$–), 1.66–1.34 (–triazole ring–$CH_2(CH_2)_4CH_2O$–, –$OCH_2CH(CH_2CH_3)O$–), 0.92 (–$OCH_2CH(CH_2CH_3)O$–). $M_{n,NMR}$ = 3250 g mol^{-1} ($CDCl_3$); $M_{n,SEC}$ = 3180 g mol^{-1} (THF); $Đ$ = 1.04.

Synthesis of three-armed cage-shaped poly(butylene oxide) (*cage*$_3$-PBO). A typical procedure for the cleavage reaction is as follows (method D): A mixture of ***trefoil*-PBO** ($M_{n,NMR}$ = 3250 g mol^{-1}, 74.3 mg) and the Pd/C (149 mg) in THF (3.0 mL) was stirred under a hydrogen atmosphere at room temperature for 24h. After filtration of the reaction mixture, the solvent was removed by evaporation. The resulting residue was dissolved in $CHCl_3$ and washed three times with a NaCN aqueous solution to remove the metal residue. The combined organic layers were dried over anhydrous $MgSO_4$ and concentrated to give the ***cage*$_3$-PBO** as a pale yellow viscous liquid (45.2 mg). Yield: 60.8%. ^{1}H NMR (400 MHz, $CDCl_3$): δ (ppm) 7.54 (triazole ring), 4.86–4.66 (–triazole ring–CH_2O–), 4.30 (–O(CH$_2$)$_5$CH_2–triazole ring–), 3.70–3.20 (–triazole ring–CH_2–, –triazole ring–(CH$_2$)$_5$CH_2–, –triazole ring–(CH$_2$)$_6$OCH_2–, –Ph-CH$_2$OCH_2–, PBO–OCH_2–, –OCH_2CH(CH$_2$CH$_3$)O–, –OCH$_2$CH(CH$_2$CH$_3$)O–), 1.66–1.34 (–triazole ring–CH$_2$(CH_2)$_4$CH$_2$O–, –OCH$_2$CH(CH_2CH$_3$)O–), 0.92 (–OCH$_2$CH(CH$_2$CH_3)O–). $M_{n,NMR}$ = 3150 g mol^{-1} ($CDCl_3$); $M_{n,SEC}$ = 3260 g mol^{-1} (THF); $Đ$ = 1.05.

Synthesis of four-armed star-shaped poly(butylene oxide) with four azido groups at the chain center (qt-1). Method A was used for the polymerization of BO (717 μL, 8.32 mmol) with **i-VIII** (1.06 mL as 0.26 mol L^{-1} stock solution in toluene, 277 μmol) and *t*-Bu-P$_4$ (277 μL as 1.0 mol L^{-1} stock solution in *n*-hexane, 277 μmol) in toluene (1.27 mL) to give **qt-1** as a colorless viscous liquid (918 mg). Yield: 97.8%. ^{1}H NMR (400 MHz,

$CDCl_3$): δ (ppm) 7.27 (aromatic), 4.45 (–PhCH_2–), 3.77–3.15 (–OCH_2C(CH_3)(CH_2OCH_2(CH_2)$_4$C$H_2$$N_3$)$_2$, –OC$H_2$C($CH_3$)(C$H_2$O–PBO)$_2$, –PhC$H_2OCH_2$CH(C$H_2$O–)$_2$, –OC$H_2CH$($CH_2CH_3$)O–), 2.18 (–OC$H_2CH$($CH_2$O–)$_2$), 1.68–1.28 (–OC$H_2CH_2$($CH_2$)$_2CH_2$$CH_2$$N_3$, –OC$H_2$CH(C$H_2$$CH_3$)O–), 1.04–0.81 (–OC$H_2$CH($CH_2CH_3$)O–, –C$H_2$C(C$H_3$)($CH_2$O–PBO)$_2$, –C$H_2$C(C$H_3$)($CH_2OCH_2$–)$_2$). $M_{n,NMR}$ = 3620 g mol^{-1} ($CDCl_3$); $M_{n,SEC}$ = 4300 g mol^{-1} (THF); $Đ$ = 1.02.

Synthesis of *ω,ω′,ω″,ω‴*-tetraethynyl four-armed star-shaped poly(butylene oxide) with four azido groups at the chain center (qt-2). Method B was used for the *ω*-chain end ethynylation of **qt-1** ($M_{n,NMR}$ = 3620 g mol^{-1}, 918 mg) with NaH (203 mg, 5.07 mmol) and propargyl bromide (380 μL, 5.07 mmol) in THF (10 mL). The residue was purified by preparative SEC to give **qt-2** as a pale yellow viscous liquid (516 mg). Yield: 53.8%. ^{1}H NMR (400 MHz, $CDCl_3$): δ (ppm) 7.27 (aromatic), 4.45 (–PhCH_2–), 4.29 (–OCH_2C≡CH), 3.77–3.15 (–OCH_2C(CH_3)(CH_2OCH_2(CH_2)$_4$C$H_2$$N_3$)$_2$, –OC$H_2$C($CH_3$)(C$H_2$O–PBO)$_2$, –PhC$H_2OCH_2$CH(C$H_2$O–)$_2$, –OC$H_2CH$($CH_2CH_3$)O–), 2.39 ($H$C≡C–), 2.18 (–OC$H_2CH$($CH_2$O–)$_2$), 1.68–1.28 (–OC$H_2CH_2$($CH_2$)$_2CH_2$$CH_2$$N_3$, –OC$H_2$CH(C$H_2$$CH_3$)O–), 1.04–0.81 (–OC$H_2$CH($CH_2CH_3$)O–, –C$H_2$C(C$H_3$)($CH_2$O–PBO)$_2$, –C$H_2$C(C$H_3$)($CH_2OCH_2$–)$_2$). $M_{n,NMR}$ = 3780 g mol^{-1} ($CDCl_3$); $M_{n,SEC}$ = 4770 g mol^{-1} (THF); $Đ$ = 1.02.

Synthesis of quatrefoil-shaped poly(butylene oxide) (*quatrefoil*-PBO). Method

C was used for the intramolecular click cyclization of **qt-2** ($M_{n,NMR}$ = 3780 g mol^{-1}, 460 mg) with CuBr (2.10 g, 14.6 mmol), PMDETA (6.11 mL, 29.3 mmol), and PSt-C≡CH (500 mg) in degassed DMF (874 mL) to give ***quatrefoil*-PBO** as a light brown waxy solid (359 mg). Yield: 78.0%. ^{1}H NMR (400 MHz, $CDCl_3$): δ (ppm) 7.54 (triazole ring), 7.27 (aromatic), 4.85–4.65 (–triazole ring–CH_2O–), 4.45 (–PhCH_2–), 4.31 (–O$(CH_2)_5$CH_2–triazole ring–), 3.73–3.10 (–OCH_2C(CH_3)(CH_2OC$H_2(CH_2)_4$–)$_2$, –OCH_2C(CH_3)(CH_2O–PBO)$_2$, –PhCH_2OCH_2CH(CH_2O–)$_2$, –OCH_2C$H(CH_2CH_3)$O–), 2.17 (–OCH_2C$H(CH_2O–)_2$), 1.98–1.28 (–OCH_2C$H_2(CH_2)_2$CH_2CH_2–triazole ring–, –OCH_2CH(CH_2CH_3)O–), 1.10–0.71 (–OCH_2CH(CH_2CH_3)O–, –CH_2C(CH_3)(CH_2O–PBO)$_2$, –CH_2C(CH_3)(CH_2OCH_2–)$_2$). $M_{n,NMR}$ = 3770 g mol^{-1} ($CDCl_3$); $M_{n,SEC}$ = 3460 g mol^{-1} (THF); $Đ$ = 1.02.

Synthesis of four-armed cage-shaped poly(butylene oxide) (*cage$_4$*-PBO). Method D was used for the hydrogenolysis of ***quatrefoil*-PBO** ($M_{n,NMR}$ = 3770 g mol^{-1}, 150 mg) with Pd/C (300 mg) in dry THF (5 mL) for 24 h to give ***cage$_4$*-PBO** as a colorless viscous liquid (118 mg). Yield: 80.9%. ^{1}H NMR (400 MHz, $CDCl_3$): δ (ppm) 7.54 (triazole ring), 7.27 (aromatic), 4.85–4.65 (–triazole ring–CH_2O–), 4.31 (–O$(CH_2)_5$CH_2–triazole ring–), 3.73–3.10 (–OCH_2C(CH_3)(CH_2OC$H_2(CH_2)_4$–)$_2$, –OCH_2C(CH_3)(CH_2O–PBO)$_2$, HOCH_2CH(CH_2O–)$_2$, –OCH_2C$H(CH_2CH_3)$O–), 2.17 (–OCH_2C$H(CH_2O–)_2$), 1.98–1.28 (–OCH_2C$H_2(CH_2)_2$CH_2CH_2–triazole ring–, –OCH_2CH(CH_2CH_3)O–), 1.10–0.71 (–OCH_2CH(CH_2CH_3)O–, –CH_2C(CH_3)(CH_2O–PBO)$_2$, –CH_2C(CH_3)(CH_2OCH_2–)$_2$). $M_{n,NMR}$ =

3660 g mol^{-1} ($CDCl_3$); $M_{n,SEC}$ = 3550 g mol^{-1} (THF); $Đ$ = 1.02.

Synthesis of three-armed star-block copolyether having three azido groups at the chain center (tf-3). A typical procedure for the block copolymerization is as follows (method E): **M1** (774 μL, 3.27 mmol) was added to a stirred solution of **i-VII** (49.0 mg, 65.3 μmol) and *t*-Bu-P_4 (65.3 μL as a 1.0 mol L^{-1} stock solution in *n*-hexane, 65.3 μmol) in toluene (467 μL), and the mixture was stirred at room temperature for 20 h. **M2** (674 μL, 3.27 mmol) and toluene (1.29 mL) were added to the stirred mixture, which was stirred at room temperature for 20 h. An excess of benzoic acid was then added to the mixture to terminate the polymerization, and the product was purified by passing it through a pad of alumina using THF to give **tf-3** as a colorless waxy solid (1.39 g). Yield: 97.6%. ^{1}H NMR (400 MHz, $CDCl_3$): δ (ppm) 7.25 (aromatic), 4.44 (–PhCH_2–), 3.84–3.29 ($N_3(CH_2)_5CH_2OCH_2$–, –$PhCH_2OCH_2C(CH_2$–polymer$)_3$, –$OCH_2CH(CH_2OCH_2(CH_2)_8CH_3)O$–, –$OCH_2CH(CH_2O(CH_2CH_2O)_3CH_3)O$–), 3.24 ($N_3CH_2$–), 1.75–1.07 ($N_3CH_2(CH_2)_4CH_2O$–, –$OCH_2CH(CH_2OCH_2CH_2(CH_2)_7CH_3)O$–), 0.95–0.78 (–$OCH_2CH(CH_2OCH_2(CH_2)_8CH_3)O$–). $M_{n,NMR}$ = 22800 g mol^{-1} ($CDCl_3$); $M_{n,SEC}$ = 15600 g mol^{-1} (THF); $Đ$ = 1.04.

Synthesis of *ω*,*ω′*,*ω″*-triethynyl three-armed star-block copolyether having three azido groups at the chain center (tf-4). Method B was used for the *ω*-chain end ethynylation of **tf-3** ($M_{n,NMR}$ = 22800 g mol^{-1}, 1.38 g) with NaH (24.4 mg, 609 μmol; 60% in mineral oil) and propargyl bromide (45.7 μL, 609 μmol) in THF (5 mL) to give **tf-4** as a pale

yellow waxy solid (946 mg). Yield: 51.6%. ^{1}H NMR (400 MHz, $CDCl_3$): δ (ppm) 7.25 (aromatic), 4.44 (–PhCH_2–), 4.34 (–OCH_2C≡CH), 3.84–3.29 ($N_3(CH_2)_5CH_2OCH_2$–, –CCH_2OCH_2Ph–, –OCH_2CH($CH_2OCH_2(CH_2)_8CH_3$)O–, –OCH_2CH($CH_2O(CH_2CH_2O)_3CH_3$)O–), 3.24 (N_3CH_2–), 2.49 (–C≡CH), 1.75–1.07 ($N_3CH_2(CH_2)_4CH_2O$–, –$OCH_2CH(CH_2OCH_2CH_2(CH_2)_7CH_3)O$–), 0.95–0.78 (–$OCH_2CH(CH_2OCH_2(CH_2)_8CH_3)O$–). $M_{n,NMR}$ = 22700 g mol^{-1} ($CDCl_3$); $M_{n,SEC}$ = 16400 g mol^{-1} (THF); $Đ$ = 1.04.

Synthesis of trefoil-shaped block copolyether (*trefoil*-I). Method C was used for the intramolecular click cyclization of **tf-4** ($M_{n,NMR}$ = 22700 g mol^{-1}, 715 mg) with CuBr (542 mg, 3.78 mmol), PMDETA (1.58 mL, 7.56 mmol), and PSt-C≡CH (220 mg) in degassed DMF (226 mL) to give ***trefoil*-I** as a light brown waxy solid (511 mg). Yield: 71.5%. ^{1}H NMR (400 MHz, $CDCl_3$): δ (ppm) 7.63 (triazole methine), 7.25 (aromatic), 4.79 (–OCH_2–triazole ring–), 4.43 (–PhCH_2–), 4.31 (–triazole ring–C$H_2(CH_2)_5$O–), 3.84–3.29 (–$(CH_2)_5CH_2OCH_2$–, –CCH_2OCH_2Ph–, –OCH_2CH($CH_2OCH_2(CH_2)_8CH_3$)O–, –OCH_2CH($CH_2O(CH_2CH_2O)_3CH_3$)O–), 1.75–1.07 (–triazole ring–$CH_2(CH_2)_4CH_2O$–, –$OCH_2CH(CH_2OCH_2CH_2(CH_2)_7CH_3)O$–), 0.95–0.78 (–$OCH_2CH(CH_2OCH_2(CH_2)_8CH_3)O$–). $M_{n,NMR}$ = 22900 g mol^{-1} ($CDCl_3$); $M_{n,SEC}$ = 13000 g mol^{-1} (THF); $Đ$ = 1.03.

Synthesis of three-armed cage-shaped block copolyether (*cage*$_3$-I). Method D was used for the hydrogenolysis of ***trefoil*-I** ($M_{n,NMR}$ = 22900 g mol^{-1}, 82 mg) with ASCA-2 (400

mg) in dry THF (5 mL) for 3 weeks to give ***cage*$_3$-I** as a colorless waxy solid (71.7 mg). Yield: 89.1%. ^{1}H NMR (400 MHz, $CDCl_3$): δ (ppm) 7.63 (triazole methine), 4.79 (–OC*H*$_2$– triazole ring–), 4.31 (–triazole ring–C*H*$_2$(CH$_2$)$_5$O–), 3.84–3.29 (–(CH$_2$)$_5$C*H*$_2$OC*H*$_2$–, –CC*H*$_2$OCH$_2$Ph–, *H*OC*H*$_2$C–, –OC*H*$_2$C*H*(C*H*$_2$OC*H*$_2$(CH$_2$)$_8$CH$_3$)O–, –OC*H*$_2$C*H*(C*H*$_2$O(C*H*$_2$C*H*$_2$O)$_3$C*H*$_3$)O–), 1.75–1.07 (–triazole ring–CH$_2$(C*H*$_2$)$_4$CH$_2$O–, –OCH$_2$CH(CH$_2$OCH$_2$C*H*$_2$(C*H*$_2$)$_7$CH$_3$)O–), 0.95–0.78 (–OCH$_2$CH(CH$_2$OCH$_2$(CH$_2$)$_8$C*H*$_3$)O–). $M_{n,NMR}$ = 22,500 g mol^{-1} ($CDCl_3$); $M_{n,SEC}$ = 14,500 g mol^{-1} (THF); $Đ$ = 1.03.

Synthesis of four-armed star-block copolyether having four azido groups at the chain center (qt-3). Method E was used for the block copolymerization of **M1** (553 μL, 2.33 mmol, first monomer, polymerization time = 24 h) and **M2** (482 μL, 2.33 mmol, second monomer, polymerization time = 24 h) with **i-VIII** (179 μL as a 0.26 mol L^{-1} stock solution in toluene, 46.7 μmol) and *t*-Bu-P$_4$ (46.7 μL as a 1.0 mol L^{-1} stock solution in *n*-hexane, 46.7 μmol) in toluene (1.10 mL), to give **qt-3** as a colorless waxy solid (992 mg). Yield: 92.3%. ^{1}H NMR (400 MHz, $CDCl_3$): δ (ppm) 7.26 (aromatic), 4.45 (–C*H*$_2$PhC*H*$_2$–), 3.98–3.11 (–OC*H*$_2$C(CH$_3$)(C*H*$_2$OC*H*$_2$(CH$_2$)$_4$C*H*$_2$N$_3$)$_2$, –OC*H*$_2$C(CH$_3$)(C*H*$_2$O–polymer)$_2$, –PhCH$_2$OC*H*$_2$CH(C*H*$_2$O–)$_2$, –OC*H*$_2$C*H*(C*H*$_2$OC*H*$_2$(CH$_2$)$_8$CH$_3$)O–, –OC*H*$_2$C*H*(C*H*$_2$O(C*H*$_2$C*H*$_2$O)$_3$C*H*$_3$)O–), 2.18 (–OCH$_2$C*H*(CH$_2$O–)$_2$), 1.75–1.06 (–OCH$_2$C*H*$_2$(CH$_2$)$_2$C*H*$_2$CH$_2$N$_3$, –OCH$_2$CH(CH$_2$OCH$_2$C*H*$_2$(C*H*$_2$)$_7$CH$_3$)O–), 1.05–0.78 (–CH$_2$C(C*H*$_3$)(CH$_2$O–polymer)$_2$, –CH$_2$C(C*H*$_3$)(CH$_2$OCH$_2$–)$_2$,

–$OCH_2CH(CH_2OCH_2(CH_2)_8CH_3)O$–). $M_{n,NMR}$ = 23000 g mol^{-1} ($CDCl_3$); $M_{n,SEC}$ = 14800 g mol^{-1} (THF); $Đ$ = 1.04.

Synthesis of *ω,ω′,ω″,ω‴*-tetraethynyl four-armed star-block copolyether having four azido groups at the chain center (qt-4). Method B was used for the *ω*-chain end ethynylation of **qt-3** ($M_{n,NMR}$ = 23000 g mol^{-1}, 982 mg) with NaH (34.1 mg, 852 μmol; 60% in mineral oil) and propargyl bromide (63.9 μL, 852 μmol) in THF (5 mL). The residue was purified by preparative SEC to give **qt-4** as a pale yellow waxy solid (616 mg). Yield: 62.0%. ^{1}H NMR (400 MHz, $CDCl_3$): δ (ppm) 7.26 (aromatic), 4.45 (–CH_2PhCH_2–), 4.34 (–OCH_2C≡CH), 3.98–3.11 (–OCH_2C(CH_3)(CH_2OCH_2(CH_2)$_4$C$H_2$$N_3$)$_2$, –OC$H_2$C($CH_3$)(C$H_2$O–polymer)$_2$, –Ph$CH_2OCH_2$CH(C$H_2$O–)$_2$, –OC$H_2$CH(C$H_2OCH_2$($CH_2$)$_8$$CH_3$)O–, –OC$H_2$CH(C$H_2$O(C$H_2CH_2$O)$_3CH_3$)O–), 2.49 (–C≡C*H*), 2.18 (–OCH_2CH(CH_2O–)$_2$), 1.75–1.06 (–OCH_2CH_2(CH_2)$_2$C$H_2$$CH_2N_3$, –$OCH_2CH(CH_2OCH_2CH_2(CH_2)_7CH_3)O$–), 1.05–0.78 (–$CH_2$C(C$H_3$)($CH_2$O–polymer)$_2$, –$CH_2$C(C$H_3$)($CH_2OCH_2$–)$_2$, –$OCH_2CH(CH_2OCH_2(CH_2)_8CH_3)O$–). $M_{n,NMR}$ = 23300 g mol^{-1} ($CDCl_3$); $M_{n,SEC}$ = 15400 g mol^{-1} (THF); $Đ$ = 1.03.

Synthesis of quatrefoil-shaped block copolyether (*quatrefoil*-I). Method C was used for the intramolecular click cyclization of **qt-4** ($M_{n,NMR}$ = 23300 g mol^{-1}, 550 mg) with CuBr (407 mg, 2.83 mmol), PMDETA (1.18 mL, 5.66 mmol), and PSt-C≡CH (150 mg) in degassed DMF (172 mL) to give ***quatrefoil*-I** as a light brown waxy solid (336 mg). Yield:

61.1%. ^{1}H NMR (400 MHz, $CDCl_3$): δ (ppm) 7.63 (triazole methine), 7.26 (aromatic), 4.79 (−OC*H*$_2$−triazole ring), 4.44 (–C*H*$_2$PhC*H*$_2$–), 4.31 (–triazole ring−C*H*$_2$(CH$_2$)$_5$O−), 3.98–3.11 (–OC*H*$_2$C(CH$_3$)(C*H*$_2$OC*H*$_2$(CH$_2$)$_4$C*H*$_2$–)$_2$, –OC*H*$_2$C(CH$_3$)(C*H*$_2$O–polymer)$_2$, –PhCH$_2$OC*H*$_2$CH(C*H*$_2$O–)$_2$, –OC*H*$_2$C*H*(C*H*$_2$OC*H*$_2$(CH$_2$)$_8$CH$_3$)O–, –OC*H*$_2$C*H*(C*H*$_2$O(C*H*$_2$C*H*$_2$O)$_3$C*H*$_3$)O–), 2.19 (–OCH$_2$C*H*(CH$_2$O–)$_2$), 1.75–1.06 (–OCH$_2$C*H*$_2$(CH$_2$)$_2$C*H*$_2$CH$_2$–, –OCH$_2$CH(CH$_2$OCH$_2$C*H*$_2$(C*H*$_2$)$_7$CH$_3$)O–), 1.05–0.78 (–CH$_2$C(C*H*$_3$)(CH$_2$O–polymer)$_2$, –CH$_2$C(C*H*$_3$)(CH$_2$OCH$_2$–)$_2$, –OCH$_2$CH(CH$_2$OCH$_2$(CH$_2$)$_8$C*H*$_3$)O–). $M_{n,NMR}$ = 23400 g mol^{-1} ($CDCl_3$); $M_{n,SEC}$ = 11600 g mol^{-1} (THF); $Đ$ = 1.02.

Synthesis of four-armed cage-shaped block copolyether (*cage*$_4$-I). Method D was used for the hydrogenolysis of ***quatrefoil*-I** ($M_{n,NMR}$ = 23400 g mol^{-1}, 150 mg) with ASCA-2 (450 mg) in dry THF (5 mL) for 3 weeks to give ***cage*$_4$-I** as a colorless waxy solid (111 mg). Yield: 74.5%. ^{1}H NMR (400 MHz, $CDCl_3$): δ (ppm) 7.64 (triazole methine), 4.79 (−OC*H*$_2$−triazole ring), 4.31 (–triazole ring−C*H*$_2$(CH$_2$)$_5$O−), 3.98–3.11 (–OC*H*$_2$C(CH$_3$)(C*H*$_2$OC*H*$_2$(CH$_2$)$_4$C*H*$_2$–)$_2$, –OC*H*$_2$C(CH$_3$)(C*H*$_2$O–polymer)$_2$, HOC*H*$_2$CH(C*H*$_2$O–)$_2$, –OC*H*$_2$C*H*(C*H*$_2$OC*H*$_2$(CH$_2$)$_8$CH$_3$)O–, –OC*H*$_2$C*H*(C*H*$_2$O(C*H*$_2$C*H*$_2$O)$_3$C*H*$_3$)O–), 2.19 (–OCH$_2$C*H*(CH$_2$O–)$_2$), 1.75–1.06 (–OCH$_2$C*H*$_2$(CH$_2$)$_2$C*H*$_2$CH$_2$–, –OCH$_2$CH(CH$_2$OCH$_2$C*H*$_2$(C*H*$_2$)$_7$CH$_3$)O–), 1.05–0.78 (–CH$_2$C(C*H*$_3$)(CH$_2$O–polymer)$_2$, –CH$_2$C(C*H*$_3$)(CH$_2$OCH$_2$–)$_2$,

–$OCH_2CH(CH_2OCH_2(CH_2)_8CH_3)O$–). $M_{n,NMR}$ = 23200 g mol^{-1} ($CDCl_3$); $M_{n,SEC}$ = 12400 g mol^{-1} (THF); $Đ$ = 1.02.

Self-assembly studies of the amphiphilic block copolyethers. The experimental methods used for the investigation of the CMC, micelle morphology, and $T_{c.d.}$ in aqueous solutions are the same as Chapter 2 and 3.

4.5 References and Notes

1. Pispas, S.; Hadjichristidis, N.; Potemkin, I.; Khokhlov, A. *Macromolecules* **2000**, *33*, 1741−1746.
2. Ishizu, K.; Uchida, S. *Prog. Polym. Sci.* **1999**, *24*, 1439−1480.
3. Hadjichristidis, N.; Pitsikalis, M.; Pispas, S.; Iatrou, H. *Chem. Rev.* **2001**, *101*, 3747−3792.
4. Jia, Z.; Monteiro, M. J. *J. Polym. Sci. Part A: Polym. Chem.* **2012**, *50*, 2085−2097.
5. Yamamoto, T.; Tezuka, Y. *Polym. Chem.* **2011**, *2*, 1930−1941.
6. Deng, Y.; Zhang, S.; Lu, G.; Huang, X. *Polym. Chem.* **2013**, *4*, 1289−1299.
7. Honda, S.; Yamamoto, T.; Tezuka, Y. *J. Am. Chem. Soc.* **2010**, *132*, 10251−10253.
8. Heo, K.; Kim, Y. Y.; Kitazawa, Y.; Kim, M.; Jin, K. S.; Yamamoto, T.; Ree, M. *ACS Macro Lett.* **2014**, *3*, 233−239.
9. Poelma, J. E.; Ono K.; Miyama, D.; Aida, T.; Satoh, K.; Hawker, C. J. *ACS Nano* **2012**, *6*, 10845−10854.
10. Borsali, R.; Minatti, E.; Putaux, J.-L.; Schappacher, M.; Deffieux, A.; Viville, P.; Lazzaroni, R.; Narayanan, T. *Langmuir* **2003**, *19*, 6−9.
11. Iatrou, H.; Hadjichristidis, N.; Meier, G.; Frielinghaus, H.; Monkenbusch, M. *Macromolecules* **2002**, *35*, 5426−5437.
12. Honda, S.; Yamamoto, T.; Tezuka, Y. *Nat. Commun.* **2013**, *4*, 1574.
13. Beinat, S.; Schappacher, M.; Deffieux, A. *Macromolecules* **1996**, *29*, 6737−6743.
14. Dong, Y.-Q.; Tong, Y.-Y.; Dong, B.-T.; Di, F.-S.; Li, Z.-C. *Macromolecules* **2009**, *42*, 2940−2948.
15. Wang, X.; Liu, T.; Liu, S. *Biomacromolecules* **2011**, *12*, 1146−1154.
16. Hatakeyama, F.; Yamamoto, T.; Tezuka, Y. *ACS Macro Lett.* **2013**, *2*, 427−431.
17. Lonsdale, D. E.; Monteiro, M. J. *J. Polym. Chem. Part A: Polym. Chem.* **2011**, *49*, 4603−4612.

18. Bielawski, C. W.; Benitez, D.; Grubbs, R. H. *Science* **2002**, *297*, 2041−2044.
19. Ryner, M.; Finne, A.; Albertsson, A. C.; Kricheldorf, H. R. *Macromolecules* **2001**, *34*, 7281−7287.
20. Quirk, R. P.; Wang, S. F.; Foster, M. D.; Wesdemiotis, C.; Yol, A. M. *Macromolecules* **2011**, *44*, 7538−7545.
21. Hayashi, S.; Adachi, K.; Tezuka, Y. *Polym. J.* **2008**, *40*, 572−576.
22. Tezuka, Y.; Komiya, R.; Washizuka, M. *Macromolecules* **2003**, *36*, 12−17.
23. Lonsdale, D. E.; Bell, C. A.; Monteiro, M. J. *Macromolecules* **2010**, *43*, 3331−3339.
24. Laurent, B. A.; Grayson, S. M. *J. Am. Chem. Soc.* **2006**, *128*, 4238−4239.
25. Staats, H.; Lützen, A. *Beilstein J. Org. Chem.* **2010**, *6*, No. 10.
26. Xu, D.; Warmuth, R. *J. Am. Chem. Soc.* **2008**, *130*, 7520−7521.
27. Galan, A.; Ballester, P. *Chem. Soc. Rev.* **2016**, *45*, 1720−1737.
28. Liu, A.; Traulsen, C. H.-H.; Cornelissen, J. J. L. M. *ACS Catal.* **2016**, *6*, 3084−3091.
29. Oike, H.; Imaizumi H.; Mouri, T.; Yoshioka, Y.; Uchibori, A.; Tezuka, Y. *J. Am. Chem. Soc.* **2000**, *122*, 9592−9599.
30. Tezuka, Y.; Tsuchitani, A.; Yoshioka, Y.; Oike, H. *Macromolecules* **2003**, *36*, 65−70.
31. Tezuka, Y.; Fujiyama, K. *J. Am. Chem. Soc.* **2005**, *127*, 6266−6270.
32. Jeong, J.; Kim, K.; Lee, R.; Lee, S.; Kim, H.; Jung, H.; Kadir, M. A.; Jang, Y.; Jeon, H. B.; Matyjaszewski, K.; Chang, T.; Paik, H.-j. *Macromolecules* **2014**, *47*, 3791−3796.
33. Lee, T.; Oh, J.; Jeong, J.; June, H.; Chang, T.; Paik, H.-j. *Macromolecules* **2016**, *49*, 3672−3680.
34. Shi, G.-Y.; Pan, C.-Y. *J. Polym. Sci. Part A: Polym. Chem.* **2009**, *47*, 2620−2630.
35. Quirk, R. P.; Wang, S. F.; Foster, M. D.; Wesdemiotis, C.; Yol, A. M. *Macromolecules* **2011**, *44*, 7538−7545.
36. Isono, T.; Miyachi, K.; Satoh, Y.; Nakamura, R.; Zhang, Y.; Otsuka, I.; Tajima, K.; Kakuchi, T.; Borsali, R.; Satoh, T. *Macromolecules* **2016**, *49*, 4178−4194.

37. Elupula, R.; Oh, J.; Haque, F. M.; Chang, T.; Grayson, S. M. *Macromolecules* **2016**, *49*, 4369−4372.
38. Karuna, M. S. L.; Devi, B. L. A. P.; Prasad, P. S. S.; Prasad, R. B. N. *J. Surfact. Deterg.* **2009**, *12*, 117−123.
39. Diaz-Quijada, G. A.; Farrahi, S.; Clarke, J.; Tonary, A. M.; Pezacki, J. P. *J. Biomater. Appl.* **2007**, *21*, 235−249.
40. Dunn, T. J.; Neumannn, W. L.; Rogic, M. M.; Woulfe, S. R. *J. Org. Chem.* **1990**, 55, 6368−6373.
41. Ouchi, M.; Inoue, Y.; Wada, K.; Iketani, S. I.; Hakushi, T.; Weber, E. *J. Org. Chem.* **1987**, *52*, 2420−2427.
42. Goldup, S. M.; Leigh, D. A.; Long, T.; McGonigal, P. R.; Symes, M. D.; Wu, J. *J. Am. Chem. Soc.* **2009**, *131*, 15924−15929.
43. Rao, J.; Zhang, Y.; Zhang, J.; Liu, S. F. *Biomacromolecules* **2008**, *9*, 2586−2593.

Chapter 5

Conclusions

In this thesis, the author described the precise synthesis and self-assembly properties of the polyether-based star-shaped, tadpole-shaped, and multicyclic block copolyethers. These block copolyethers were synthesized by combining the *t*-Bu-P_4-catalyzed ring-opening polymerization (ROP) of glycidyl ethers and the CuAAC click reaction. The well-controlled nature of the ROP enabled the production of the well-defined block copolyethers with a perfect end-functionality and allowed us to construct the complex macromolecular architectures. In addition, the characterization of the self-assembly properties for a comprehensive set of block copolyethers provided systematic information about the relationship between the macromolecular architectures and the self-assembly behaviors in water.

A summary of this thesis is as follows:

Chapter 2 "Synthesis of Well-Defined Amphiphilic Star-block and Miktoarm Star Copolyethers"

The synthesis of a systematic set of amphiphilic star-shaped block copolyethers, i.e., the $(AB)_3$-, $(BA)_3$-, $(AB)_4$-, and $(BA)_4$-type star-block copolyethers and A_2B_2-, AB_2-, and A_2B-type miktoarm star copolyethers, with comparable molecular weights and monomer conpositions were achieved. The star-block copolyethers were synthesized according to the core-first approach, and the predicted arm number and the uniform arm length of these

polyethers were identified by the cleavage of the initiator residue. The miktoarm star copolyethers were synthesized using the coupling-onto approach, in which the azido or ethtnyl end-functionalized precursors were used. The investigation of the aqueous self-assembly behavior of the obtained amphiphilic block copolyethers revealed that the branched architecture affected the structure of the resultant micelles and the cloud points ($T_{c.d.}$s) value of the aqueous solution. In particular, the comparison of the self-assembly behavior of the miktoarm star polyethers provided unique insights into the effect of the branched architecture in the amphiphilic block copolymers. The presented synthetic strategies provided easy access to well-defined block copolyethers with various branched architectures and might be useful as a model system for investigating the essential effect of the branched architecture on the self-assembly properties.

Chapter 3 "Synthesis of Cyclic, Figure-Eight-Shaped, and Tadpole-Shaped Amphiphilic Block Copolyethers"

The synthesis of systematic sets of cyclic, figure-eight-, and tadpole-shaped amphiphilic block copolyethers was achieved by the combination of the *t*-Bu-P_4-catalyzed block copolymerization and the intramolecular click cyclization. A series of well-defined azido- and ethynyl-functionalized di-, tri-, and penta-block linear precursors were prepared by the sequential post-polymerization and the end-functionalization techniques. The intramolecular click cyclization of these precursors provided the well-defined

cyclic-containing amphiphilic block copolyethers with predicted molecular weights, monomer compositions, and narrow dispersities. The topological effect of the cyclic architecture on the self-assembly properties was revealed by the investigation of the hydrodynamic radii and $T_{c.d.}$ values of the micellar solutions. Interestingly, the $T_{c.d.}$s of the tadpole-shaped block copolyethers showed significantly different values depending on their block arrangements. These results indicated that the cyclic architecture directly affected their self-assembly behavior. The present synthetic strategies provide a wide array of block copolymer systems with cyclic-containing architectures, and would be used as a model system for investigating the topological effect of the block copolymer self-assembly in both the solution and bulk states.

Chapter 4 "Synthesis of Well-Defined Three- and Four-armed Cage-shaped Polyethers via "Topological Conversion" from Trefoil- and Quatrefoil-shaped Polyethers"

The synthesis of cage-shaped amphiphilic block copolyethers was achieved via the topological conversion from the well-defined trefoil- and quatrefoil-shaped block copolyethers which were synthesized by the intramolecular multiple click cyclization of the clickable star-shaped precursors. The topological conversion was accomplished by the hydrogenolysis of the focal point of the trefoil- and quatrefoil-shaped polyethers without any undesirable side reaction. The significant difference in the micellar sizes and the $T_{c.d.}$ values between the amphiphilic trefoil/quatrefoil- and cage-shaped block copolyethers were observed

during the aqueous self-assembly study. This is the first example of the investigation of the self-assembly behaviors of cage-shaped block copolyethers. It is envisaged that the topological conversion approach will provide concise access to the trefoil/quatrefoil and cage-shaped polymers with various main chain and side chain structures as well as contributing to a greater understanding of the properties and functions due to the complex macromolecular architectures.

In conclusion, the author established the synthetic methods for the polyether-based star-shaped, tadpole-shaped, and multicyclic block copolyethers using the *t*-Bu-P_4-catalyzed ROP system and click reaction. These methods make it possible to obtain a systematic set of architecturally complex block copolyethers with highly-controlled molecular weights, monomer compositions, and quite narrow dispersities, which is suitable for studying the novel insight into the relationship between the macromolecular architecture and the polymer properties such as the self-assembly behavior. In fact, the author investigated the micellization properties of the amphiphilic block copolyethers possessing various architectures, and revealed that the branched and cyclic architectures significantly affect the self-assembly behavior of the block copolymers. The author expects that the presented synthetic approaches will contribute to the synthesis and characterization of architecturally complex block copolymers, leading to the creation of novel advanced polymer materials.